

Structural and functional characterisation of peptide inhibitors of voltage-gated sodium channels from piscivorous cone snails

A thesis submitted in fulfilment of the requirements for the degree of

DOCTOR OF PHILOSOPHY

By

Brad Reed Green

Bachelor of Science – Microbiology (Weber State University, USA)

Masters of Science – Medicinal Chemistry (University of Utah, USA)



Medicinal Chemistry

Monash Institute of Pharmaceutical Sciences

Faculty of Pharmacy and Pharmaceutical Sciences

Monash University

Melbourne, Victoria, Australia

January 2016

Copyright notice

© The author (2016). Except as provided in the Copyright Act 1968, this thesis may not be reproduced in any form without the written permission of the author.

I certify that I have made all reasonable efforts to secure copyright permissions for third-party content included in this thesis and have not knowingly added copyright content to my work without the owner's permission.

“But to be learned is good if they hearken unto the counsels of God.”

2 Nephi 9:29

Table of Contents

General Declaration	1
Acknowledgments	3
Abbreviations	5
List of Figures	8
List of Tables	10
Abstract	11
Chapter 1: Introduction	13
1.1 Chronic pain: A persistent problem.....	14
1.2 The numerous aetiologies of chronic pain.....	14
1.3 Voltage-gated sodium channels as targets for the treatment of pain.....	15
1.4 Voltage-gated sodium channel inhibitors.....	17
1.4.1 Small molecule inhibitors of VGSC function.....	17
1.4.2 Naturally occurring inhibitors of VGSCs.....	18
1.4.3 Peptide inhibitors of VGSC function.....	19
1.5 Identification and characterisation of VGSC-modulating peptides.....	20
1.5.1 Synthesis of biologically-active VGSC blocking peptides.....	20
1.5.2 Oxidative folding of disulfide-rich peptides.....	22
1.5.3 Structure determination by nuclear magnetic resonance spectroscopy.....	24
1.5.4 Assessment of activity by two-electrode voltage-clamp electrophysiology.....	25
1.6 Scope of the thesis.....	25
Chapter 2: Materials and Methods	27
2.1 Recombinant expression of VGSC-blocking peptides.....	28
2.2 Synthesis, cleavage and oxidative folding of synthetic VGSC-blocking conotoxins.....	29
2.2.1 Solid phase peptide synthesis.....	29
2.2.2 Peptide cleavage from solid support resin.....	30

2.2.3 Purification of peptides by reversed phase high performance liquid chromatography (RP-HPLC)	32
2.2.4 Oxidative folding of disulfide-rich conotoxins	32
2.3 Determination of disulfide connectivity by CID-MS/MS	34
2.4 Two-electrode voltage-clamp electrophysiology	34
2.5 Nuclear magnetic resonance (NMR) spectroscopy	36
2.5.1 One-dimensional ¹ H NMR experiments	37
2.5.2 Two-dimensional ¹ H NMR experiments	38
2.5.2.1 Correlation spectroscopy (COSY)	39
2.5.2.2 Total-correlation spectroscopy (TOCSY)	40
2.5.2.3 Nuclear Overhauser effect spectroscopy (NOESY)	40
2.5.3 Structural calculations	40
2.6 Summary	41

Chapter 3: Structure and Function of μ -Conotoxins, Peptide-based Sodium Channel

Blockers with Analgesic Activity	42
3.1 Declaration for thesis Chapter 3	43
3.1.1 Declaration by candidate	43
3.2 Journal article	44

Chapter 4: Correlation of Activity with Disulfide-bridging Pattern in μ -Conotoxin

BuIIIIB	66
4.1 Declaration for thesis Chapter 4	67
4.1.1 Declaration by candidate	67
4.2 Abstract	69
4.3 Introduction	69
4.4 Materials and Methods	71
4.4.1 Construction of the expression plasmid Trx-BuIIIIB	71
4.4.2 Fusion protein expression and purification	71
4.4.3 Purification of rBuIIIIB [^] from fusion protein	72
4.4.4 Screening of rBuIIIIB [^] folding isoforms against rNav1.3	73

4.4.5 Determination of disulfide connectivity for rBuIIIB ^Δ isoforms	74
4.5 Results	74
4.6 Discussion	82
4.7 Acknowledgements	84
4.8 Supporting information	86

Chapter 5: Interactions of Disulfide-deficient Selenocysteine Analogues of μ -Conotoxin

BuIIIB with the α-subunit of the Voltage-gated Sodium Channel Subtype Nav1.3	94
5.1 Declaration for thesis Chapter 5	95
5.1.1 Declaration by candidate	95
5.2 Journal article	96
5.3 Supporting information	110

Chapter 6: Structural Basis for the Inhibition of Voltage-gated Sodium Channels by

Conotoxin μOξ-GVIIJ	113
6.1 Declaration for thesis Chapter 6	114
6.1.1 Declaration by candidate	114
6.2 Abstract	116
6.3 Introduction	116
6.4 Experimental procedures	120
6.4.1 Peptide synthesis, oxidative folding and purification	120
6.4.2 Nuclear magnetic resonance (NMR) spectroscopy	122
6.4.3 Structural constraints and calculations	123
6.4.4 Structure-activity studies on GVIIJ _{SSEA} and GVIIJ _{SSC} with rNav1.2 and competition experiments of μ - versus μ O ξ -conotoxins with rNav1.4	123
6.5 Results	124
6.6 Discussion	137
6.7 Acknowledgements	144
6.8 Conflict of interest	145
6.9 Author contribution	145

Chapter 7: Conclusions and Future Directions	146
Chapter 8: References	150
Appendix I: Distinct Disulfide Isomers of μ-Conotoxins KIIIA and KIIIB Block Voltage-gated Sodium Channels	160
Appendix II: A Disulfide Tether Stabilizes the Block of Sodium Channels by the Conotoxin μOδ-GVIIJ	187

General Declaration by Author

Monash University

Declaration for thesis based or partially based on conjointly published or unpublished work.

In accordance with Monash University Doctorate Regulation 17.2 Doctor of Philosophy and Research Master's regulations the following declarations are made:

I hereby declare that this thesis contains no material which has been accepted for the award of any other degree or diploma at any university or equivalent institution and that, to the best of my knowledge and belief, this thesis contains no material previously published or written by another person, except where due reference is made in the text of the thesis.

This thesis includes two original papers published in peer reviewed journals, one submitted manuscript and one manuscript in preparation. The core theme of the thesis is the structure-activity relationship studies of conotoxins, and conotoxin analogues that modulate voltage-gated sodium channel activity. The ideas, development and writing up of all the papers in the thesis were the principal responsibility of myself, the candidate, working within the Department of Medicinal Chemistry, Faculty of Pharmacy and Pharmaceutical Sciences under the supervision of Professor Raymond S. Norton. My contributions to the publications included as Appendices 1 and 2 were minor and consisted of the synthesis, purification and oxidation of analogues for the papers. Additionally, I contributed to the writing and editing of the manuscripts. These publications were included because of their high relevance to the thesis theme.

The inclusion of co-authors reflects the fact that the work came from active collaboration between researchers and acknowledges input into team-based research.

In the case of Chapters 3 - 6 my contribution to the work involved the following:

Thesis chapter	Publication title	Publication status*	Nature and extent of candidate's contribution
3	Structure and function of μ -conotoxins, peptide-based sodium channel blockers with analgesic activity	Published	BRG wrote the paper and is first and corresponding author.
4	Correlation of activity with disulfide-bridging pattern in μ -conotoxin BuIIIb	In preparation	BRG jointly conceived the study and wrote the paper. Designed and performed experiments, and analysed experiments data. BRG is joint first author.
5	Interactions of disulfide-deficient selenocysteine analogues of μ -conotoxin BuIIIb with the voltage-gated sodium channel $Na_v1.3$	Published	BRG jointly conceived the study and wrote the paper. Designed and performed experiments, and analysed experiments data. BRG is first author.
6	Structural basis for the inhibition of voltage-gated sodium channels by conotoxin μ O ξ -GVIIJ	Published	BRG jointly conceived the study and wrote the paper. Designed and performed experiments, and analysed experiments data. BRG is joint first author.

I have renumbered sections of submitted or published papers in order to generate a consistent presentation within the thesis.

**Candidate's
signature**



Date

22.01.16

Acknowledgements

The findings presented here can be attributed to those who freely gave of their own knowledge, time, patience and resources. Though the following list is by no means exhaustive, I would like to express my deepest gratitude to the following individuals for their valuable insight and contributions to this thesis, without whom none of this would have been possible.

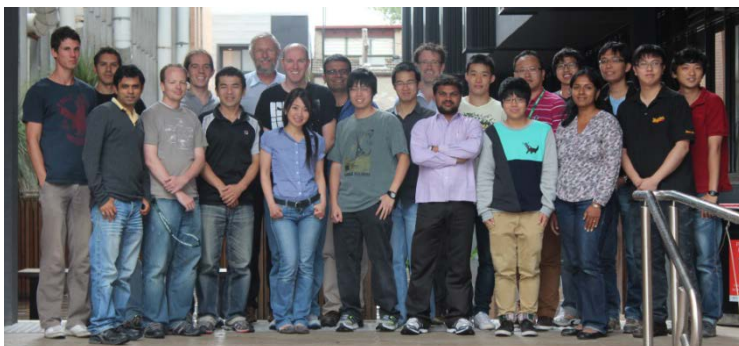
First and foremost I would like to thank my supervisor Prof. Raymond S. Norton for his guidance and direction over the course of my PhD studies. I am truly grateful for his willingness to take me into his lab and to allow me to conduct my research in a highly collaborative and multi-disciplinary environment. From the beginning Ray has always encouraged me to explore scientific methods and techniques beyond peptide chemistry. These opportunities have provided me with an increased skill set and have given me a greater appreciation and understanding of structural biology. I am particularly grateful for Ray's patience and ability to explain NMR concepts with patience and completeness. Ray has a high standard of excellence for members of his research group, and I feel that what I have learned from him will help me in future scientific endeavours. I appreciate that Ray has also provided me with the necessary flexibility and understanding to enable me to balance family responsibility with my scientific aspirations.

My gratitude is also extended to members of the Norton Research Group that have given of their time and talents to help me in my research endeavours. I am indebted to Drs. Sandeep Chhabra and Samuel D. Robinson for their friendship and for the countless hours of explaining even the most basic of NMR concepts to me. I am particularly grateful to Sam for always providing honest and unfiltered feedback even though it was sometimes difficult to hear. I would like to extend a heartfelt thanks to Dr. Eleanor W. W. Leung for all of her help with the recombinant expression of conotoxins. There were many days when things were not working out and Eleanor's cheerful disposition and 'can do' attitude were the only things that helped to get me through. Additionally, Dr. Rodrigo Morales has become a true friend. I am thankful for all of the times he would drag me away from the lab for a late meal and for all of the memorable adventures we had together. Numerous other members of Ray's group were also influential either scientifically or socially all of whom provided friendship and guidance throughout my PhD training at Monash. I am grateful to all of them.

I would also like to thank the numerous collaborators who have offered their facilities and expertise towards completion of the projects described in this thesis, especially those at the University of Utah in the lab of Prof. Baldomero ‘Toto’ Olivera. My sincere appreciation is given to Toto for allowing me access to his lab and for providing resources to synthesize and characterize the peptide analogues for SAR studies. I am thankful for his wealth of knowledge of all things *Conus*. I am grateful to several members of the Olivera lab that have provided assistance or who have been there to help me work these projects through to completion. Drs. Joanna Gajewiak (peptide synthesis), Pradip Bandyopadhyay (recombinant expression) and Min-Min Zhang (electrophysiology) have all given of their time to mentor me and help me to gain new skills to be a more capable scientist.

Also, I would like to thank Dr. Grzegorz Bulaj (University of Utah, Dept. of Medicinal Chemistry) for his oversight of projects related to this thesis and for his mentorship and friendship throughout my often non-linear scientific career. I am truly grateful for his understanding of my situation and his constant reminder to take care of my family first and to worry about the science after that.

Last, but certainly not least, I cannot express adequately the gratitude that I have for my family (Melissa, Gavin and Ryleigh). They have often taken a backseat to help me reach my scientific goals, and I am thankful for their repeated sacrifice and patience throughout my academic career. I appreciate their constant words of encouragement and support.



Norton Research Group



Green Family

Abbreviations

ACN	acetonitrile
BOC	t-butyloxycarbonyl
C ^α	carbon atom attached to the carboxylic carbon
C ^β	first carbon atom of an amino acid side chain
cDNA	complementary deoxyribonucleic acid
CID-MS/MS	collision-induced dissociation tandem mass spectrometry
Da	Dalton
Dab	L-2,4-diaminoutyric acid
Dap	L-2,3-diaminopropionic acid
ddSecBuIIIIB	disulfide-deficient, selenocysteine-containing BuIIIIB
DCM	dichloromethane
DIPEA	N,N-diisopropylethylamine
DMF	N,N-dimethylformamide
DRG	dorsal root ganglia
DTNP	2,2'-dithiobis(5-nitropyridine)
DTT	dithiothreitol
EDTA	ethylenediaminetetraacetic acid
ESI	electrospray ionisation
Fmoc	fluorenylmethyloxycarbonyl
FPLC	fast protein liquid chromatography
Gla	γ-carboxyglutamate
h	hour
H ^α	hydrogen atom attached to C ^α
H ^N	hydrogen atom attached to the backbone nitrogen atom
HPLC	high performance liquid chromatography
IC ₅₀	inhibitory concentration at 50% blockade
ICK	inhibitor cysteine knot motif
IPTG	isopropyl β-D-1-thiogalactopyranoside
K	degrees Kelvin

k_{on}	on-rate kinetics of blockade
k_{off}	off-rate kinetics of blockade
K_{d}	dissociation constant
kDa	kilodalton
MALDI-TOF	matrix-assisted laser desorption ionization time of flight
MBHA	4-methylbenzhydrylamine
min	minutes
MTBE	methyl-tert butyl ether
MS	mass spectrometry
MW	molecular weight
m/z	mass-to-charge ratio
Na^+	sodium ion
Nav1	α -subunit of the voltage-gated sodium channel
Nav β	β -subunit of the voltage-gated sodium channel
NMP	N-methyl-2-pyrrolidone
NMR	nuclear magnetic resonance
NOE	nuclear Overhauser effect
NOESY	nuclear Overhauser effect spectroscopy
PCR	polymerase chain reaction
PDB	protein data bank
PIP	piperidine
ppm	parts per million
PTM	posttranslational modification
PyBOP	benzotriazol-1-yl-oxytripyrrolidinophosphonium hexafluorophosphate
RACE-PCR	rapid amplification of cDNA ends polymerase chain reaction
rBuIII B	recombinantly expressed μ -conotoxin BuIII B
rBuIII B^{\wedge}	recombinantly expressed μ -conotoxin BuIII B with a free C-terminal carboxylate
RMSD	root mean square deviation
RP-HPLC	reversed phase high performance liquid chromatography
SAR	structure-activity relationship
SD	standard deviation

SDS-PAGE	sodium dodecyl sulphate polyacrylamide gel electrophoresis
Sec	Fmoc-selenocysteine-OH
SEM	standard error of the mean
SPPS	solid phase peptide synthesis
TFA	trifluoroacetic acid
TOCSY	two-dimensional nuclear magnetic resonance spectroscopy
Tris	tris(hydroxymethyl)aminomethane
Trx	thioredoxin
VGSC	voltage-gated sodium channel
1D	one-dimensional
2D	two-dimensional
¹ H	proton nuclear magnetic resonance
°C	degrees Celsius

- * The standard 1- and 3-letter codes will be used to represent amino acids in this thesis (e.g. Cysteine: Cys or C)

List of Figures

Figure 1.1 A brief history of the treatment of neuropathic pain.....	14
Figure 1.2 Crystal structure of the α -subunit of the bacterial sodium channel NaVA β from <i>Acrobacter butzleri</i>	15
Figure 1.3 Interaction of local anaesthetic drugs with the α -subunit of the VGSC.....	17
Figure 1.4 Selected VGSC inhibiting toxins from vertebrate and invertebrate sources.....	19
Figure 1.5 Photos of shells from <i>Conus bullatus</i> and <i>Conus geographus</i>	25
Figure 2.1 General approach to Fmoc solid-phase peptide synthesis.....	29
Figure 2.2 Removal of the synthesised peptide from the solid support resin.....	30
Figure 2.3 Exogenous methods of disulfide-bridge formation.....	32
Figure 2.4 Two electrode voltage-clamp electrophysiology.....	34
Figure 2.5 Spin system designations for the 20 common proteinogenic amino acids.....	36
Figure 2.6 Interactions measured by COSY, TOCSY and NOESY spectra.....	38
Figure 3.1 Voltage-gated sodium channel structure.....	44
Figure 3.2 Examples of small molecule inhibitors of voltage-gated sodium channels.....	46
Figure 3.3 The μ -conotoxins as an emerging class of sodium channel blocking peptides.....	47
Figure 3.4 Summary of identified μ -conotoxins from m4 and m5 branches of the M-superfamily.....	48
Figure 3.5 Selectivity profiles of μ -conotoxins against Nav1-subtypes.....	49
Figure 3.6 Structure-activity characterization of μ -conotoxins.....	50
Figure 3.7 Description of the ddSec strategy used to facilitate structure-activity relationship studies of μ -BuIII β	54
Figure 3.8 Conotoxins at various stages of preclinical and clinical development.....	57
Figure 4.1 The structure of μ -conotoxin BuIII β	69
Figure 4.2 Recombinant expression of the free acid form of μ -BuIII β	74
Figure 4.3 Characterization of rBuIII β ^ folding isoforms.....	76
Figure 4.4 Experimentally determined disulfide connectivity of rBuIII β ^ Isoform 4.....	79
Figure 4.5 Experimentally determined disulfide connectivity of rBuIII β ^ Isoform 5.....	80
Figure 5.1 Sequence alignment of μ -BuIII β with other μ -conotoxins.....	96

Figure 5.2 Comparison of wild-type μ -BuIIIIB with ddSecBuIIIIB	98
Figure 5.3 Optimization of NMR conditions for ddSecBuIIIIB	99
Figure 5.4 Structural comparisons of μ -BuIIIIB and ddSecBuIIIIB	100
Figure 5.5 Effects of Ala-substitution of non-cysteine residues in the ddSecBuIIIIB scaffold ..	102
Figure 5.6 Exploration of charge effects at position 3 using the ddSecBuIIIIB scaffold	103
Figure 5.7 Exploration of steric effects at position 3 in the ddSecBuIIIIB scaffold	104
Figure 6.1 Binding site of μ O \S -GVIIJ on the channel and its peptide sequence	116
Figure 6.2 Characterization of GVIIJ[C24S] by NMR spectroscopy	125
Figure 6.3 Deviation of backbone amide (H^N) and C^α proton (H^α) chemical shifts from random coil values at 25 °C	128
Figure 6.4 Structure of the μ O \S -GVIIJ analogue GVIIJ[C24S]	129
Figure 6.5 Characterization of the final 20 structures of GVIIJ[C24S]	131
Figure 6.6 Structure-activity relationship studies of residues in the Cys-24 containing loop 4 ..	133
Figure 6.7. Nav1.2 block by μ O \S -GVIIJ	135
Figure 6.8 Block of Nav1.4 by μ -PIIIA[R14Q], μ -GIIIA, μ O \S -GVIIJ or (μ O \S -GVIIJ) ₂ , alone or in binary combinations	137
Figure 6.9 Structural comparison of the GVIIJ[C24S] backbone with those of other ICK motif-containing peptides	139
Figure 6.10 ‘Functionally bipartite’ mechanism of action for μ O \S -GVIIJ	143
Figure 7.1 Diversity among <i>Conus</i> species	148

List of Tables

Table 3.1 Sodium channel subtypes and their distribution.....	45
Table 4.1 Kinetics of block of rNav1.3 by rBuIIIIB [^] isoforms.....	75
Table 5.1 Structural and pharmacological characterization of ddBuIIIIB and ddSecBuIIIIB scaffolds.....	97
Table 5.2 Summary of the ability of μ -BuIIIIB and Ala-scan analogues of ddSecBuIIIIB to block rNav1.3 and rNav1.4 expressed in <i>X. laevis</i> oocytes as determined by two-electrode voltage-clamp electrophysiology.....	101
Table 5.3 Contributions of individual amino acids to activity in μ -conotoxins possessing three disulfide bridges.....	105
Table 6.1 Characterization of μ O ξ -GVIII analogues by HPLC retention time, purity and molecular mass.....	119
Table 6.2 Structural statistics for GVIII[C24S].....	127
Table 6.3 Kinetics of block of rNav1.2 by μ O ξ -GVIII analogues.....	138
Table 6.4 Values of k_{obs} for the block by μ -GIIIA, μ O ξ -GVIII or (μ O ξ -GVIII) ₂ of control I _{Na} and of rI _{Na} in presence of 33 μ M μ -PIIIA[R14Q].....	141

Abstract

The venoms of piscivorous (fish-hunting) snails of the genus *Conus* contain a vast array of neuroactive peptides used to immobilize prey and for defence. The intrinsic specificity and potency of these components for certain molecular targets has attracted the interest of researchers as novel drug leads for a wide range of neurological disorders. Beyond their therapeutic potential, these compounds have been invaluable as pharmacological probes to better understand the structure and function of their respective targets.

Members of the M- and O1-conotoxin superfamilies are disulfide-rich neurotoxins characterised by the ability to potently and specifically inhibit voltage-gated sodium channels (VGSCs). As with other peptide-based therapeutics, issues of poor bioavailability, low metabolic stability and a general lack of VGSC subtype-selectivity have hindered the development of these toxins as viable therapeutic options. Structure-activity relationship (SAR) studies, such as those described here, have served as a basis from which important structural features of the peptide could be identified and peptide analogues with improved pharmacological profiles could be designed. The overall goal of this thesis is to identify the key structural components of two potent conotoxins, μ -conotoxin BuIIIb (M-superfamily) and μ O δ -conotoxin GVIIJ (O1-superfamily), that contribute to VGSC blockade.

Chapter 3 reviews the SAR studies of μ -conotoxins and summarizes efforts to identify the structural features that contribute to their biological activity. To date, over 20 members of this family have been described, many of which possess an innate preference for certain VGSC subtypes. This chapter discusses what is known about the interactions of μ -conotoxins with the channel and highlights their therapeutic potential for the treatment of neurological disorders and severe pain.

One member of the μ -conotoxin family, μ -BuIIIb, is of interest for its purported role in inhibiting the sodium channel subtype Nav1.3. Chapter 4 describes efforts to produce this peptide by recombinant expression and explores the importance of disulfide-connectivity for inhibition of Nav1.3. Chapter 5 details SAR studies of μ -BuIIIb against Nav1.3, using a disulfide-deficient, selenocysteine-containing analogue of μ -BuIIIb. This analogue simplified the oxidative folding of μ -BuIIIb and facilitated an alanine-scan of non-cysteine residues to identify amino acid residues critical for biological activity.

Chapter 6 explores a different class of VGSC-inhibiting peptides that exert their block by covalently linking to the channel at a recently identified site on the channel that is close to, but physically

distinct from, the site of interaction of the μ -conotoxins. In this chapter we solved the structure of the O1-superfamily toxin μ O ξ -GVIII by NMR and performed complimentary SAR studies to identify structural features that contribute to VGSC blockade.

Members of the M- and O1-superfamilies hold promise as therapeutic leads due to their intrinsic potency and specificity for VGSCs. SAR studies were performed to identify the structural features that are important for the biological activity of these two peptides. These studies identified structural components of μ -BuIIIB and μ O ξ -GVIII that could be replaced to alter potency against pain-relevant VGSC subtypes. Studies such as those described here are an important step in designing peptide analogues that improve upon the existing pharmacological properties of venom-derived peptides.

Chapter 1

Introduction

1.1 Chronic pain: A persistent problem

Alleviation of severe and persistent pain is an age old problem that has plagued civilizations, ancient and modern, for millennia (Figure 1.1). Conservative estimates place the number of individuals affected at over 20% of adults worldwide, with an additional 10% diagnosed annually (1). The earliest reports of chronic pain far predate any modern understanding of the underlying molecular mechanisms of pain. The first recorded description of chronic pain was made in the second century AD by Aretaeus of Cappadocia of what would later be defined as trigeminal neuralgia (2). Some reports suggest that the indigenous peoples of Central and South America may have topically applied coca plant to affected areas to alleviate pain over 3000 years ago (2). Even earlier than that (2838-2698 B.C.), in the first Chinese pharmacopeia *Pen-T'so Chin*, recommendation for the ingestion of puffer fish eggs to “arrest convulsive diseases” was made (3). Much later, it would be determined that the neuroactive component found in these eggs was tetrodotoxin (TTX), a naturally occurring alkaloid neurotoxin that potently blocks voltage-gated sodium channels (VGSCs). Throughout history a significant amount of time and energy has been devoted to the discovery and development of compounds that alleviate chronic pain. Early ‘discovery’ efforts emphasised the application of nature-derived compounds to block painful stimuli, an approach still employed today.

1.2 The numerous aetiologies of chronic pain

Modern medicine has yielded several compounds to alleviate the symptoms of pain; however the complexity of pain pathways has made it difficult to develop drugs that are both safe and efficacious for all major pain conditions. Furthermore, the molecular targets for pain modulation are numerous, encompassing all major classes of regulatory proteins (e.g. G-protein coupled receptors, ion channels, regulatory enzymes, neurotrophins, kinases and several others) (4). According to Woolf, pain can be broadly categorised into three major classes: *nociceptive pain* (the sensing of noxious stimuli), *inflammatory pain* (pain caused by the activation of the immune system due to injury or infection) and *pathological pain* (pain as a result of damage to (neuropathic pain) or dysfunction of (dysfunctional pain) of the nervous system) (5).

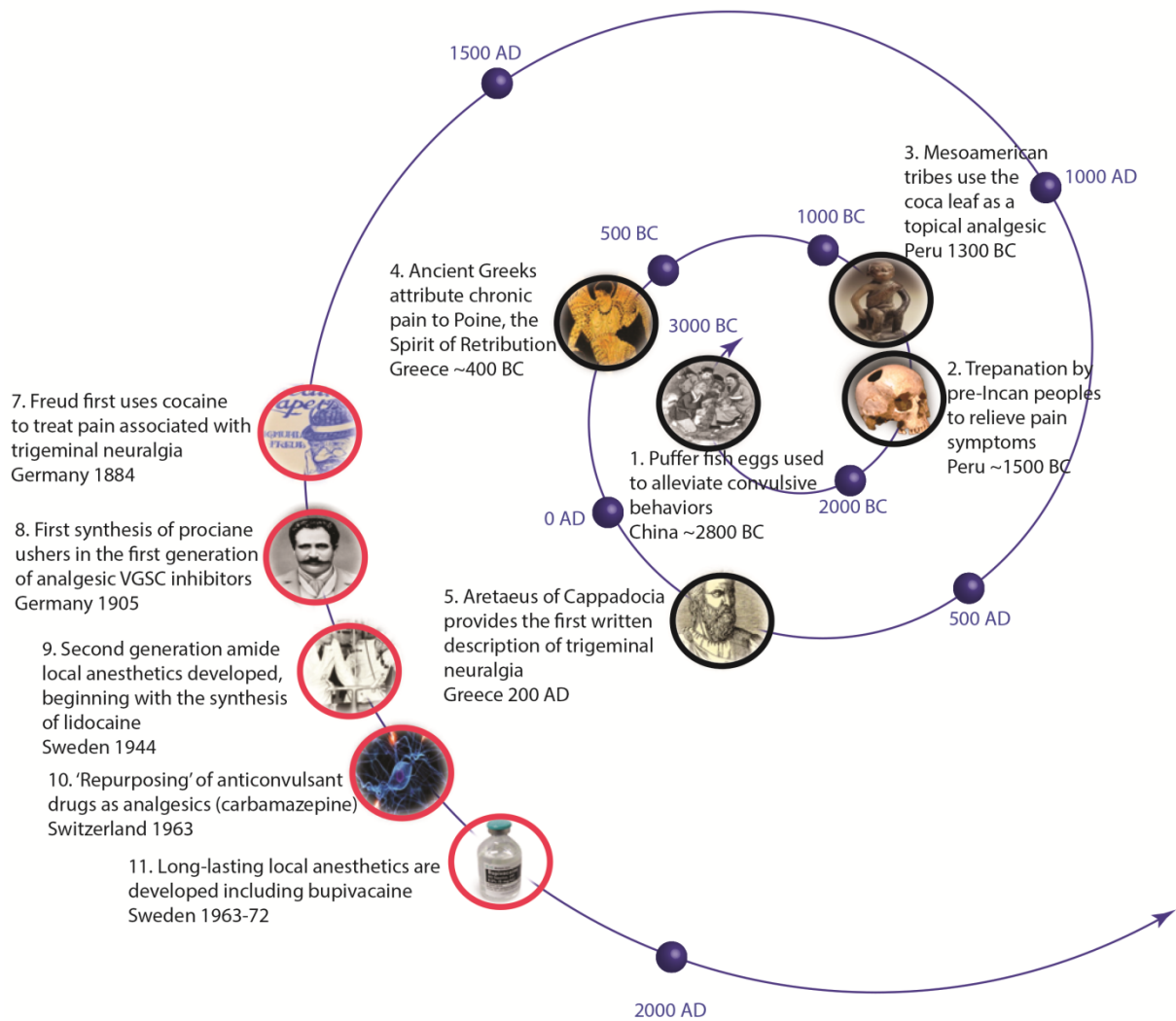


Figure 1.1. A brief history of the treatment of neuropathic pain. Timeline illustrates major developments in the treatment of severe pain ranging from 3000 BC to the present day. Early strategies focused on the use of compounds of plant or animal origin, without a clear understanding of the mechanisms of pain. The modern pharmaceutical era (Red circles) has focused more on the development of anaesthetic compounds based on preferred chemical scaffolds known to possess analgesic properties.

1.3 Voltage-gated sodium channels as targets for the treatment of pain

Neuropathic pain typically arises from damage, through illness or injury, to nerves or muscle tissues leading to rapid firing of sensory neurons, often referred to as *neuronal excitability* (6,7). Spontaneous and uncontrolled neuronal firing often stem from dysfunction of the transmembrane proteins responsible for the transport of materials across the cell membrane, particularly those involved in the influx or efflux of ions (e.g. Na⁺, K⁺ or Ca²⁺). Changes in the expression levels or nature of these channels can drastically affect excitability and pain (8).

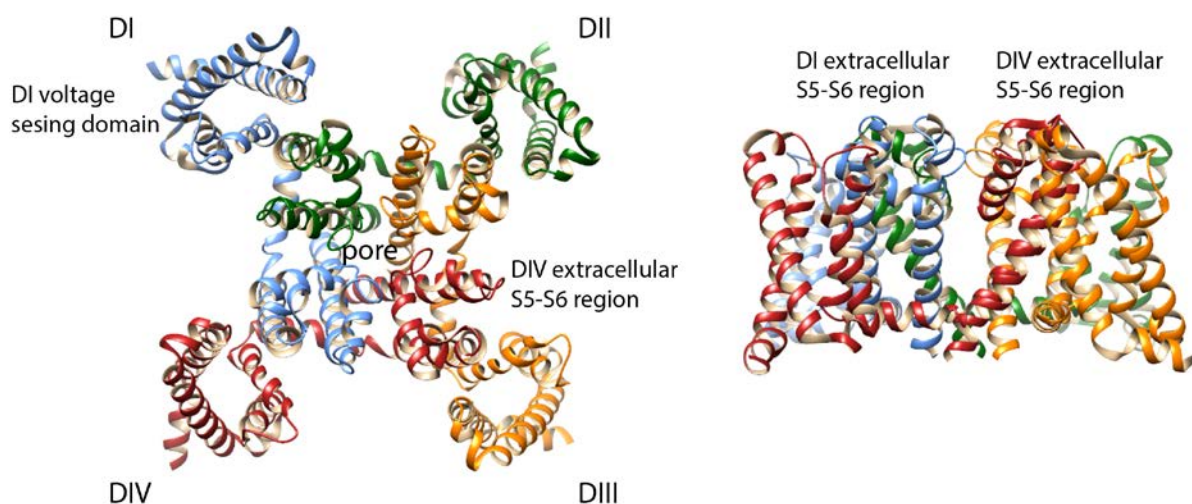


Figure 1.2. Crystal structure of the α -subunit of the bacterial sodium channel NavAb from *Acrobacter butzleri* (PDB ID 4EKW). The VGSC α -subunit is a pseudotetrameric transmembrane protein that regulates sodium channel conductance in excitable tissues. Four homologous domains (DI – DIV) are arranged about a central pore region through which Na⁺ ions flow across the cell membrane. Several compounds have been discovered that either bind deep within the sodium conductance pore, or interact at the extracellular surface with the so-called voltage-sensing domain. All structural images were prepared using UCSF Chimera.

Voltage-gated sodium channels (VGSCs) are found in excitable tissues throughout the central and peripheral nervous systems and are important for the initiation and propagation of action potentials (9). The role of the VGSC is to regulate the flow of sodium current across the cell membrane. To date, nine distinct sodium channel subtypes have been described (Nav1.1-1.9) (10). In general, the VGSC is comprised of a pseudotetrameric integral membrane protein called the α -subunit (Nav1) and one or more accessory β -subunits (Nav β) (Figure 1.2). The α -subunit by itself is capable of carrying out all of the physiological functions of a fully functional channel (11). Traditional pharmacological assays, including those described in this thesis, have therefore focussed on the effects of compounds against the α -subunit without the associated β -subunits. Only recently has the importance of the β -subunit, which was initially referred to as an ‘auxiliary’ protein, begun to be appreciated (12). Mutations to sodium channel genes coding for the α -subunit have been identified as the root causes of numerous clinical conditions including epilepsy (Nav1.1 and Nav1.2), primary periodic paralysis (Nav1.4), ataxia (Nav1.6) and neuropathic pain (Nav1.3, Nav1.7, Nav1.8 and Nav1.9) (13). Despite recent successes in crystallization of bacterial VGSCs (14,15), the crystal structure of the mammalian VGSC has not been solved. Homology models based on prokaryotic VGSCs have provided valuable information about sodium channel structure-function, and toxin binding, but have inherent limitations due to significant differences between bacterial and vertebrate channels (16). Thus, knowledge of VGSC structure and function has been almost entirely reliant on compounds (e.g. small molecules or peptides) that either promote or inhibit channel activity.

1.4 Voltage-gated sodium channel inhibitors

1.4.1 Small molecule inhibitors of VGSC function

In the modern era, efforts to inhibit VGSCs as a means of treating pain began in the mid- to late 19th century (Figure 1.1). Though not a VGSC blocker *per se*, the first clinical use of a compound capable of inhibiting VGSCs surfaced in 1884 when Freud and Koller reported the successful administration of cocaine to treat trigeminal neuralgia (2). Shortly thereafter, the toxicity of cocaine was realised and researchers began the search for safe and efficacious alternatives. Among the first generation VGSC inhibitors were those that bind to what would later be identified as the local anaesthetic binding site (17) deep within the α -subunit (Figure 1.3). Ester local anaesthetics such as benzocaine (1900) and procaine (1904) led these efforts and gained widespread popularity (18). Due to issues of low potency, slow onset and limited tissue penetration, a second generation of amide local anaesthetics was developed. The first of these compounds, lidocaine (1944) effectively blocked peripheral nerves and possessed superior tissue penetration (18). Lidocaine ushered in a new class of analgesic compounds, including mepivacaine and prilocaine. Unfortunately, issues of short duration-of-action still limited their use. Subsequently, so-called long acting local anaesthetics were developed, which included bupivacaine (1963) and etidocaine (1972) (18,19). Although improvements were observed with respect to duration-of action, serious motor toxicity issues arose, which severely limited the widespread use of these compounds. Beginning in the 1950s, anticonvulsant compounds such as phenytoin (1950) and carbamazepine (1962) gained traction as analgesics by demonstrating effectiveness in treating trigeminal neuralgia (18). The use of such compounds was based largely on the overlapping mechanisms of neuronal hyperexcitability common to both epileptic seizures and neuropathic pain (20). Issues of teratogenicity (phenytoin) and bone marrow suppression (carbamazepine) led to the development of compounds such as oxcarbazepine and lacosamide, which are still used in the clinic today. A major roadblock in the development of synthetic, small molecule VGSC inhibitors as effective analgesics continues to be a lack of target specificity (Figure 1.3) where promiscuity with other receptors or channels can lead to serious and sometimes deadly off-target effects.

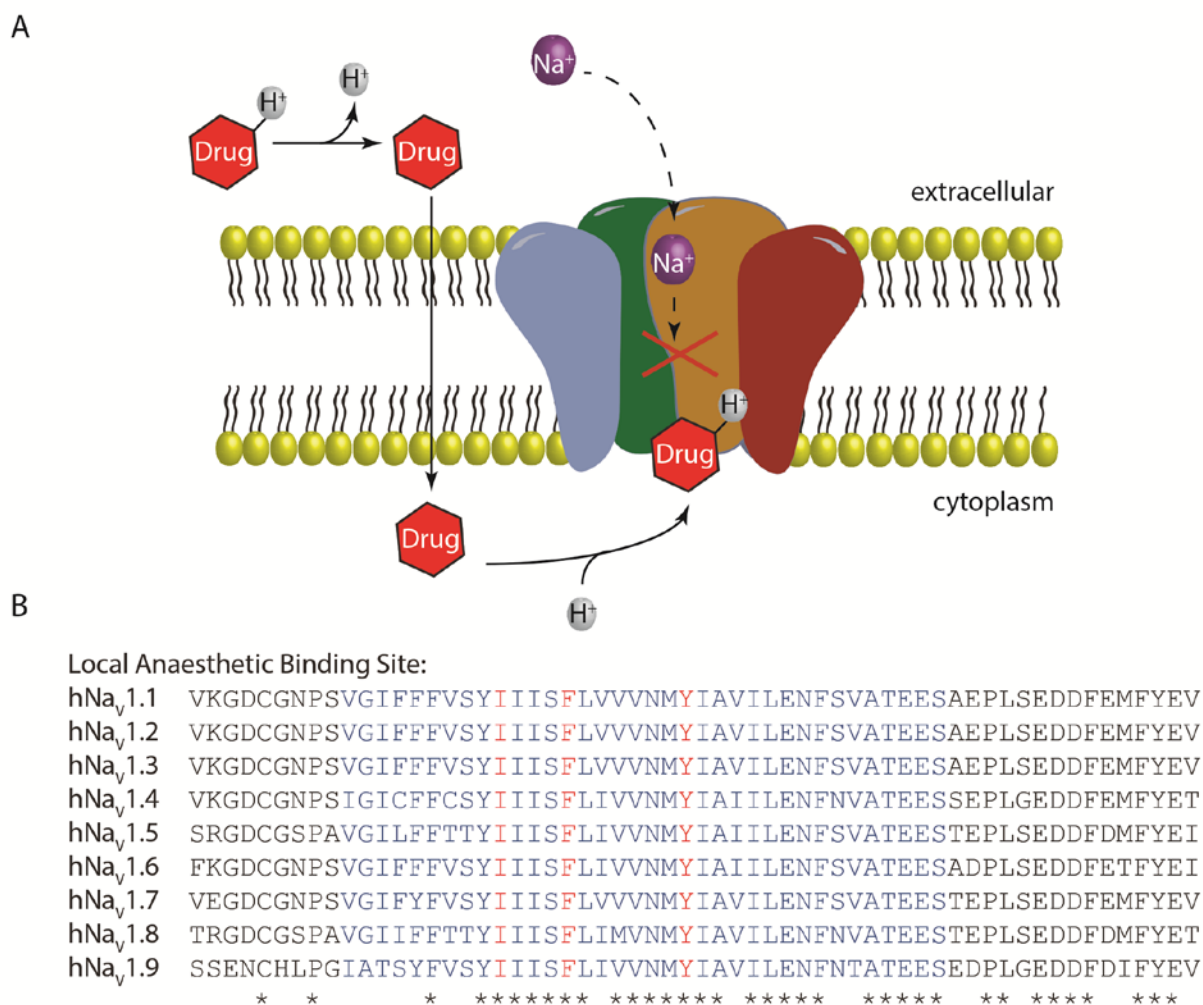


Figure 1.3. Interaction of local anaesthetic drugs with the α -subunit of the VGSC. (A) Mechanism of action of local amide or ester anaesthetics. These compounds cross the cell membrane and bind to the local anaesthetic binding site deep within the pore on the cytoplasmic side of Domain IV where they prevent Na^+ conductance. (B) Sequence alignment showing the similarities between Na_v1 -subtypes for the local anaesthetic binding site. The lack of subtype specificity of many small molecule VGSC inhibitors can be attributed to homology amongst VGSC subtypes at their site of action. Homologous residues within the binding site are shown in blue, important residues for interaction are shown in red.

1.4.2 Naturally occurring inhibitors of VGSCs

In continuing efforts to identify promising chemical entities for the treatment of neuropathic pain, while mitigating undesirable off-target effects, both academia and the pharmaceutical industry have again turned to nature (21). Numerous organisms produce toxins or secondary metabolites that demonstrate neuroactive properties, and many of these may have therapeutic potential. Such compounds may include small molecules, peptides or multi-domain proteins, each tailored for a specific subset of molecular targets such as ion channels, GPCRs or transporters.

Small-molecule inhibitors of VGSCs are abundant in nature and have been found in diverse species such as shellfish (saxitoxin –STX) (22), fish (tetrodotoxin –TTX) (23), amphibians (zetekitoxin

AB) (24) and numerous others (Figure 1.4) (25). A key feature of these potent neurotoxins is the presence of a guanidinium group that tightly binds to the channel and prevents sodium influx. In the early 1960s, Narahashi and co-workers described the ability of a small alkaloid component of puffer fish poison (TTX) to potently block sodium conductance across the cell membrane (23). Nanomolar concentrations of TTX irreversibly blocked six of the nine sodium channel subtypes (i.e. TTX-sensitive channels), whereas micromolar concentrations were required to block Nav1.5, 1.8 and 1.9 (i.e. TTX-resistant channels) (26,27). The lack of subtype specificity of synthetic and naturally-occurring VGSC inhibitors can be attributed to the architecture of the channel itself, the high levels of sequence homology or identity amongst important regions of the α -subunit and the similarities between VGSCs and other voltage-gated channels including potassium and calcium channels (13). Although some success has recently been achieved in generating TTX analogues with improved selectivity (28) the development of TTX as a viable drug has been severely hampered by the inability to discriminate between TTX-sensitive subtypes. The true value of TTX, and other alkaloid neurotoxins, can be found in the identification and characterization of the TTX binding site (Site 1), deep within the conductance pore, distinct from the site of interaction for the local anaesthetics (29).

1.4.3 Peptide inhibitors of VGSC function

Peptide-rich venom mixtures have evolved over millions of years as an efficient means to immobilize prey or to protect organisms against predation. These mixtures are observed in diverse phyla encompassing both invertebrate (insects, spiders and molluscs) and vertebrate (frogs, snakes and lizards) classes and may consist of several hundred individual bioactive compounds (Figure 1.4). Fractionation and isolation of the individual venom components is a promising means of identifying potent and selective analgesic compounds that could also be used as pharmacological tools to better understand pain signalling pathways. Similar to identification of the TTX binding site, venom-derived peptides that modulate VGSC activity have also been instrumental in identifying discrete sites of action on the channel. VGSC-inhibiting peptides selectively modulate sodium channel activity through either direct occlusion of the Na⁺ conductance pore at Site 1 (μ -conotoxins) or through interaction with the voltage-sensing domain of the α -subunit (Site 3: α -scorpion toxin and sea anemone toxins; Site 4: β -scorpion toxins, ProTxI/II and μ O-conotoxins; Site 8; μ O δ -conotoxins) (2). The advantage of peptidic inhibitors over their small-molecule counterparts is their innate specificity for certain VGSC subtypes and their amenability to modification to enhance existing pharmacological properties (e.g. potency or specificity). The focus

of this thesis will be the structure-activity relationship (SAR) studies of two functionally related peptides from the venoms of predatory marine snails of the genus *Conus*.

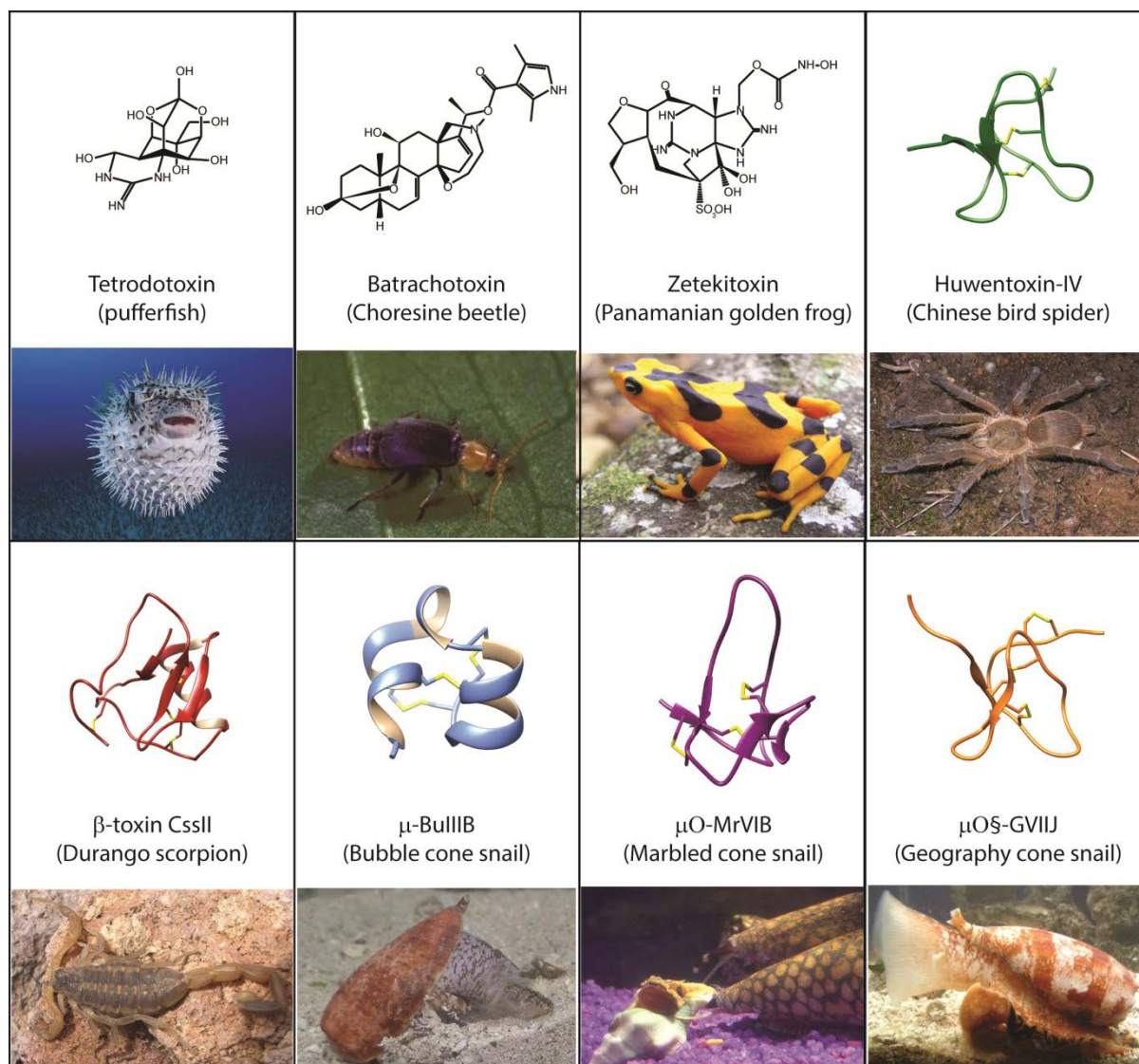


Figure 1.4. Selected VGSC inhibiting toxins from vertebrate and invertebrate sources. Small alkaloid neurotoxins inhibit the channel either directly through binding to neurotoxin binding site 1 within the sodium conductance pore (tetrodotoxin and zetekitoxin), or allosterically through interaction with site 2 on the surface of the channel (batrachotoxin). Similarly, peptide inhibitors of VGSC bind to specific sites on or within the channel. The μ -conotoxins bind to site 1 and physically occlude the channel, whereas gate-modifying spider, scorpion and μ O-conotoxins bind to the channel voltage-sensing domains located on the surface of the α -subunit of the VGSC. Huwentoxin-IV (1MB6), β -toxin Cssl (2LI7), μ O-MrVIB (1RMK), μ -BuIII B (2LO9) and μ O§-GVIIJ (2N8H). Photos reprinted with permission of: Jack Dumbacher (Choresine beetle), Jaime Garcia-Moreno (Panamanian golden frog) Kari McWest (Durango scorpion), Baldomero M. Olivera (cone snails).

1.5 Identification and characterisation of VGSC-modulating peptides

1.5.1 Identification of VGSC-modulating peptides

In the mid- to latter half of the 19th century, the French physiologist Claude Bernard described toxins (and venoms) as a means to ‘dissect’ the constitutive principles of physiological processes. It would take nearly a full century before separation methods were sufficiently advanced to isolate the individual components of complex venom mixtures (30). Identification of new neuroactive venom peptides has traditionally been driven by bioassay-guided discovery approaches (31,32). Crude, whole venoms are isolated and extracted from the venom apparatus (fangs, stingers or glands) and are then fractionated by chromatographic methods. These crude fractions, often containing numerous peptide components, are tested in animal models for activity. The fractions are further purified by repeated chromatography steps until a single product is finally obtained. The sequence of the active peptide can then be determined by Edman sequencing. In cases of partial sequence determination, cDNA libraries can be constructed through reverse transcription of venom gland RNA and oligonucleotide primers are constructed against specific toxin families for PCR amplification. One drawback to this method is the inability to confidently identify post-translational modifications (PTMs), which are common amongst these peptides (33). More recently, transcriptomic approaches, coupled with mass spectrometry matching, have been employed for sequencing and identification of post-translational modification of certain amino acids (34).

1.5.2 Synthesis of biologically-active VGSC blocking peptides

Frequently, only picomole or nanomole quantities of the bioactive peptide are obtained from the direct fractionation of complex venom mixtures. For further structural or functional characterization, much larger quantities are necessary. To accomplish this, researchers have typically relied on either chemical synthesis or recombinant peptide expression, both of which have their own individual merits and shortcomings.

Solid phase peptide synthesis (SPPS) provides a rapid and reliable method for construction of peptides on a solid support resin. Synthesis of the first tetrapeptide by SPPS was reported by Merrifield in 1963 (35). Within a decade of Merrifield’s report, over 500 papers had been published on the subject of SPPS (36). Since its inception, the process has involved the coupling of amino acid residues to a polystyrene bead where the polypeptide chain is grown through condensation reactions which form a peptide bond. The amino groups of each residue, in addition to reactive groups on the side chain, are commonly protected using a variety of groups that minimize unwanted side reactions (37).

Today, SPPS largely relies on either Boc (tert-butyloxycarbonyl) or Fmoc (9-fluorenylmethyloxycarbonyl) chemistries. Both methods involve repetitive deprotection and amino acid coupling steps to form the polypeptide chain. Although both methods have their individual

merits, Fmoc-protocols are often preferred to Boc-SPPS methods for a number of reasons. In Boc-protocols, deprotection of the N- α -amine group is performed by acidolysis and sensitive sequences may be modified or degraded by repeated treatment with trifluoroacetic acid (TFA). Moreover, removal of the crude peptide from the solid support requires HF cleavage from the resin. The requirement for HF poses serious health concerns, leading to the third drawback of this method, which is that Boc-syntheses are often costly and require specialised equipment to accommodate harsh cleavage conditions (38). In 1972, Carpino and co-workers developed a strategy that employed a base-labile N-terminal protecting group, 9-fluorenylmethyloxycarbonyl (Fmoc) and eventually gave way to what is now commonly referred to as Fmoc-synthesis (39). This method takes advantage of base-labile amino protecting groups, a welcome alternative to the use of HF. Fmoc-protocols also allowed for the production of freely soluble, easily purified peptides and have proven both efficient and versatile for the stepwise synthesis of polypeptides (40).

SPPS is often the method of choice for large scale production, given the unusually high frequency of post-translational modifications in venom-derived peptides (e.g. C-terminal amidation, hydroxyproline, pyroglutimation, glycosylation) (33). Synthetic approaches also offer an added advantage of incorporation of non-natural amino acids, which may improve bioactivity. Venom-derived peptides commonly possess several cysteine residues that oxidise to form disulfide bridges. Disulfide bridge formation between these residues acts to constrain the structure of the folded peptide and proper disulfide connectivity between cysteines may also be important for the function of neuroactive peptides. SPPS provides for the option of orthogonal protection of cysteine thiols for directed folding of cysteine-rich peptides to ensure the desired disulfide connectivity. The drawbacks to synthetic methods include the cost and time associated with producing large quantities of peptide, in addition to use of potentially hazardous reagents used in amino acid coupling and deprotection.

Recombinant prokaryotic or eukaryotic expression systems are currently of great interest as an alternative to chemical peptide synthesis (41,42). Such approaches are relatively cost effective and hold promise as a means of large-scale, rapid production of bioactive peptides. Expressed peptides can also be isotopically labelled, facilitating structural characterization by NMR. Unfortunately, these methods have been limited by the inability of commonly used expression systems to incorporate some PTMs. However, with the more recent discovery of enzymatic machinery involved in post-translational modification, recombinant expression of conotoxins may soon become a more viable alternative to SPPS (43,44).

1.5.3 Oxidative folding of disulfide-rich peptides

Generally speaking, venom-derived peptides are categorised as either disulfide-rich or disulfide-poor. Nearly 90% of the naturally-occurring peptides in the venoms of cone snails contain between four to six cysteine residues (45). These cysteine residues form disulfide bridges and restrict conformational flexibility. In principle, the number of different folding isoforms increases in proportion to the number of bridges according to the equation: $(2n)!/(2^n n!)$. As an example: for any three disulfide bridge containing peptide, up to 15 distinct folding isoforms are possible. Many of these isoforms are selected against based on energetics, and oxidative folding results in a single, major folding product. However, equally-favoured bridging patterns do arise and may have distinct activities when compared to the 'native' fold (See Chapter 4). Critical to the exploration, and potential development, of venom-derived peptides as drugs is the ability to produce these molecules in their biologically active forms.

In vivo, peptide toxins are produced ribosomally as part of a larger propeptide complex consisting of a signal sequence, a propeptide region and the mature toxin itself (46). Following secretion, this complex is processed and cleaved to reveal the bioactive peptide. However, the mechanisms by which the protoxins are processed into fully-functional mature toxins are not yet well understood. Following synthesis of these propeptide complexes, the signal sequence is cleaved and the propeptide-containing toxin is secreted to the endoplasmic reticulum where post-translational modification and oxidation of cysteine thiols is thought to occur (47). It is generally accepted that the propeptide region is recognised by a multi-enzyme complex consisting of protein disulfide isomerase (PDI), peptidyl-prolyl cis-trans isomerase, immunoglobulin-binding protein (BiP) and likely other enzymes that recognise the propeptide region and aid in proper folding (48,49). Without a complete understanding of *in vivo* oxidative folding pathways, researchers have been reliant on exogenous methods of synthesis and folding to produce and study these potentially useful compounds.

If the disulfide connectivity of a particular toxin is known, cysteine thiols can be orthogonally-protected using groups that allow for chemoselective deprotection and formation of the disulfide bonds between two identically-protected cysteine thiols (e.g. S-acetamidomethyl or Acm-protection) (47,50). In the absence of disulfide-shuffling, this approach allows for controlled disulfide-bridge formation. A disadvantage to this strategy is the requirement for additional purification steps, which may result in decreased yields after multiple oxidation steps. An alternative to this approach is the synthesis of peptides with cysteine-protecting groups that are removed concurrently with other side-chain protecting groups upon peptide cleavage (e.g. S-triphenylmethyl Trt-protection). The reduced (linear) peptide can then be folded in buffered solution using molecular oxygen (i.e. air oxidation) or in the presence of exogenous oxidizing

agents such as glutathione (GSH) guanidine hydrochloride (guanidine-HCl) or dimethyl sulfoxide (DMSO) (51). The advantage of these agents is that, although certain ‘misfolded’ folding species may be favoured kinetically, thermodynamically-favoured disulfide bridge patterns may be obtained upon reaching folding equilibrium. For the majority of the peptides described in this thesis, folding was performed in the presence of 1:1 mM reduced/oxidised glutathione.

Solid support oxidants such as Ekathiox, CLEAR-Ox and others have also gained popularity in recent years as efficient methods of disulfide-bridge formation (52). Solid support oxidants take advantage of so-called pseudodilution effects wherein high dilution conditions are mimicked using micro-porous resins that are selective for intramolecular disulfide-bridge formation. The major advantage of solid support folding is the ability to conduct folding reactions at higher concentrations than would typically be practical under solution folding conditions. Another approach that has recently gained favour amongst peptide chemists for the folding of disulfide-rich peptides is that of alternative cyclization methods such as diselenide (53), dicarba- (54), or thioether bridges (55). Such methods can often be performed on resin, prior to peptide cleavage, and offer the advantage of preferential formation of selected macrocyclizations independent of cysteine oxidation.

1.5.4 Structure determination by nuclear magnetic resonance spectroscopy

The three-dimensional structure of bioactive peptides or proteins is a key determinant of biological function. Determination of the solution structures of bioactive molecules has proven useful for the design of analogues with improved physicochemical or pharmacological properties. The inherent properties of peptide toxins (i.e. small size, solubility and relatively high stability) make them ideally suited for structural analysis by NMR methods (56,57).

A brief survey of VGSC-inhibiting conotoxins reveals some common features among the various classes in relation to their site-of-action. Pore-blocking μ -conotoxins all possess a helical region near the C-terminus (58-60) and SAR studies have revealed several key residues within this region that have important roles in either potency or selectivity of these peptides (61-63). The importance of this region was highlighted by Khoo and co-workers, who constructed lactam-stabilised analogues of the C-terminal residues of μ -KIIIA that potently blocked VGSC subtypes (64). In contrast, gate-modifying toxins of the μ O- and the recently described μ O δ -classes, act on the ectodomain of the α -subunit at the voltage-sensing domain. All members of these classes described, so far, possess an inhibitor cystine knot (ICK) motif (65). This motif is characterised by 2-3 β -strands and a knot-like connectivity of disulfide bridges in the core of the folded peptide (66). ICK

peptides are of current interest for pharmaceutical development given their high metabolic stability and amenability for modification. Structure elucidation of peptides is helpful in determining the relative positions of important residues and, when coupled with pharmacological assays, is a powerful approach for designing peptide analogues with enhanced activity.

1.5.5 Assessment of activity by two-electrode voltage-clamp electrophysiology

The initial assessment of toxin activity is typically undertaken using *in vivo* assays to determine broad pharmacological activity. Coupled with information about the primary structure (e.g. precursor sequence, disulfide connectivity and amino acid composition), one can speculate as to the peptide's molecular target. An important consideration when using such assays, however, is the often tissue-specific activity of many of these toxins. Nine different VGSC subtypes are currently known; these subtypes are localised to specific excitable tissues throughout the body and the differences in binding sites between individual subtypes are often very minor. *In vitro* pharmacological assays are a useful means to determine the specific activity of bioactive compounds for a given family of receptors or channels. A commonly employed method to assess activity for sodium channel-blocking conotoxins is two-electrode voltage-clamp electrophysiology. Two-electrode voltage-clamp electrophysiology is a proven and robust method for rapid screening of the activity of neuroactive peptides against sodium channel subtypes (67). In 1982, Barnard and co-workers reported first reported this method, which allowed for a higher throughput study of the physiology, pharmacology and biophysics of membrane-bound proteins including ion channels (68). This approach utilised membrane proteins heterologously expressed on the surface of *Xenopus laevis* oocytes and provided a number of advantages to direct electrophysiological assay of mammalian cells. One advantage lies in the large size of the oocyte which enables manipulation, culture and assay. Another advantage is the ability of the oocyte to synthesize nearly any protein following cRNA injection. Expression levels of endogenous ion channels, regulatory proteins, etc. on the surface of the oocyte are relatively low. As such, this system gives the added benefit of expression of one or more known membrane proteins with relatively low background interference.

1.6 Scope of the thesis

The peptide-rich venoms of predatory organisms, including those of cone snails, are a promising source of VGSC-blocking compounds. Such compounds are of interest not only as therapeutic leads, but also as pharmacological probes to better understand a potentially useful target for the treatment of neuropathic pain. The overarching goal of this thesis is to explore two classes of

peptides from *Conus* venoms with the aim of identifying the key structural features for VGSC inhibition (Figure 1.5). Chapter 2 presents an overview of all μ -conotoxins reported to date and summarizes the SAR work performed on this potentially useful class of peptides. Chapter 3 describes the recombinant expression of the free acid form of μ -BuIIIIB and includes studies to determine the importance of not only C-terminal modification, but also disulfide connectivity, for VGSC inhibition. Chapter 4 illustrates how the combination of disulfide-deficiency (i.e. selective removal of Cys-Cys pairings) and diselenide-bridge replacement could facilitate rapid electrophysiological screening of ‘poorly folding’ μ -BuIIIIB to identify key amino acid residues for activity. Finally, Chapter 5 details structural and functional studies of the recently identified gate-modifying toxin μ O ξ -GVIIIJ that elicits its biological activity through both covalent ‘tethering’ to the sodium channel surface and interactions of key residues located in a less well-defined looped region of the peptide. Detailed SAR studies such as those described here are important to identify key features of bioactive peptides and serve as the starting point for additional studies to improve upon the inherent activities of these nature-derived compounds.



Figure 1.5. Photos of shells from *Conus bullatus* (left) and *Conus geographus* (right). Potent VGSC blocking peptides from the μ -, μ O- and the newly described μ O ξ -conotoxin classes have been isolated from the peptide-rich venoms of fish-hunting *Conus* species.

Chapter 2

Materials and Methods

This chapter contains a description of the methods and materials employed in this thesis in sufficient detail to enable further studies of VGSC modulating peptides. Recombinant expression, solid phase peptide synthesis (SPPS), electrophysiology and NMR methods were used extensively throughout this thesis, and as such, these techniques are described in greater detail here.

2.1 Recombinant expression of VGSC-blocking peptides

Thorough chemical and pharmacological characterization of conotoxins often requires large quantities of pure peptide. One bottleneck in the studies of these molecules has been the production of such quantities by synthetic means. Recombinant expression systems offer an efficient and cost-effective means for producing large quantities of peptide. However, as mentioned in the previous chapter, the post-translational modifications common to conotoxins make such approaches challenging (47). Recent success has been observed in the production of disulfide-rich peptides as fusion proteins with thioredoxin (69,70), which catalyses disulfide bond formation, even under reducing conditions (71). We applied such a strategy for the synthesis of the free acid form of μ -conotoxin BuIIIb. Compared to other members of the μ -conotoxin family, μ -BuIIIb has relatively few modifications, and was therefore selected as a model system to explore recombinant expression in *E. coli*.

The BuIIIb gene was codon-optimised and synthesised by Genscript. The gene was digested with KpnI and NcoI and cloned into pET32a to form pET32-BuIIIb. The pET32-BuIIIb construct, which is an ampicillin resistant, contained a thioredoxin tag, an N-terminal hexahistidine affinity tag and an enterokinase cleavage site (DDDDK). The pET32-BuIIIb vector was transformed into Rosetta-gami (DE3) *Escherichia coli* competent cells (Novagen) and was grown overnight at 37 °C on a Luria Bertani (LB) agar plate that contained ampicillin (100 μ g/mL) and chloramphenicol (30 μ g/mL). A single colony was selected and was inoculated into 3 mL fresh LB medium, supplemented with ampicillin (100 μ g/mL) and chloramphenicol (30 μ g/mL), and was grown for 16 h at 37 °C. A 1 mL aliquot of this starter culture was transferred to 50 mL fresh LB medium and grown for an additional 3 h at 37 °C. The bacterial culture was then transferred into 1 L fresh LB medium and grown at 37 °C until the OD₆₀₀ reading reached between 0.5-0.7. The bacterial culture was allowed to cool to 25 °C prior to isopropyl β -D-1-thiogalactopyranoside (IPTG) induction at a final concentration of 1 mM, Induction was carried out for 16 h at 25 °C. Cells were pelleted by centrifugation at 5,000 g for 10 min at 4 °C. The cell pellet was resuspended to a concentration of 4 mL in Bug Buster master mix per 1 g of cells and was incubated for 1 h with gentle mixing. The crude lysate was centrifuged at 20,000 rpm for 30 min at 4°C. The thioredoxin-BuIIIb fusion protein was then purified from the clear lysate by subjecting it to Ni-NTA affinity chromatography (GE Healthcare). The bound thioredoxin-BuIIIb fusion protein was washed with 30 column volumes of 20 mM Tris-HCl, pH 8.0, 500 mM NaCl, 10 mM imidazole, and subsequently eluted with 20 mL of 20 mM Tris-HCl, pH 8.0, 500 mM NaCl, 500 mM Imidazole. Fractions containing thioredoxin-BuIIIb fusion protein were pooled and were buffer exchanged into enterokinase

cleavage buffer (20 mM Tris-HCl, pH 7.4, 50 mM NaCl and 2 mM CaCl₂) using a PD-10 desalting column (GE Healthcare). 20 U of enterokinase was used to cleave ~ 5 mg of fusion protein in 48 h at 20°C. Cleaved rBuIIIIB^Δ was then subjected to preparative RP-HPLC for further purification and the removal of thioredoxin. Recombinant expression of μ-BuIIIIB did not result in a single folded product. As such, the product was reduced and refolded *in vitro* (discussed later in this section) and the individual folding products were isolated by RP-HPLC for further characterisation.

2.2 Synthesis, cleavage and oxidative folding of synthetic VGSC-blocking conotoxins

2.2.1 Solid phase peptide synthesis

All analogues described in this thesis were produced using batch-wise Fmoc-chemistry protocols (Figure 2.1). Peptides were synthesised at 30 – 50 μmol scale using an Apex 396 automated peptide synthesiser (AAPPTec, Louisville, KY). Peptides were constructed using either pre-loaded Fmoc-Cys(Trt) Rink Amide MBHA resin (μ-conotoxins KIIIA and BuIIIIB) or Fmoc-L-Ala Wang resin (μO§-GVIII). Resin selection was based upon the requirement of the desired product for either C-terminal amidation or carboxylation. Prior to the first amino acid coupling, resins were swollen in dichloromethane (DCM) for at least 30 min to allow for sufficient exposure of the functional groups on the resin to reagents. Fmoc-deprotection was accomplished by 20 min treatment with 20% (vol/vol) piperidine (PIP) in dimethylformamide (DMF). Following deprotection, amino acid coupling was accomplished by addition of 1 equivalent 0.22 M benzotriazol-1-yl-oxytrypyrrolidino-phosphonium hexafluorophosphate (PyBOP) and 2 equivalents 2 M diisopropylethyl amine (DIPEA) in N-methyl-2-pyrrolidone (NMP). Standard amino acids were coupled for 60 min in 10-fold excess. Non-proteinogenic amino acids such as Fmoc-L-Sec(pMeOBzl)-OH, Fmoc-L-2,4-diaminobutyric acid-OH and Fmoc-L-gamma-carboxyglutamate were coupled for 90 min in 3-fold excess. Upon completion of each synthesis, a final deprotection step was performed to remove Fmoc-protection from the terminal amino acid residue.

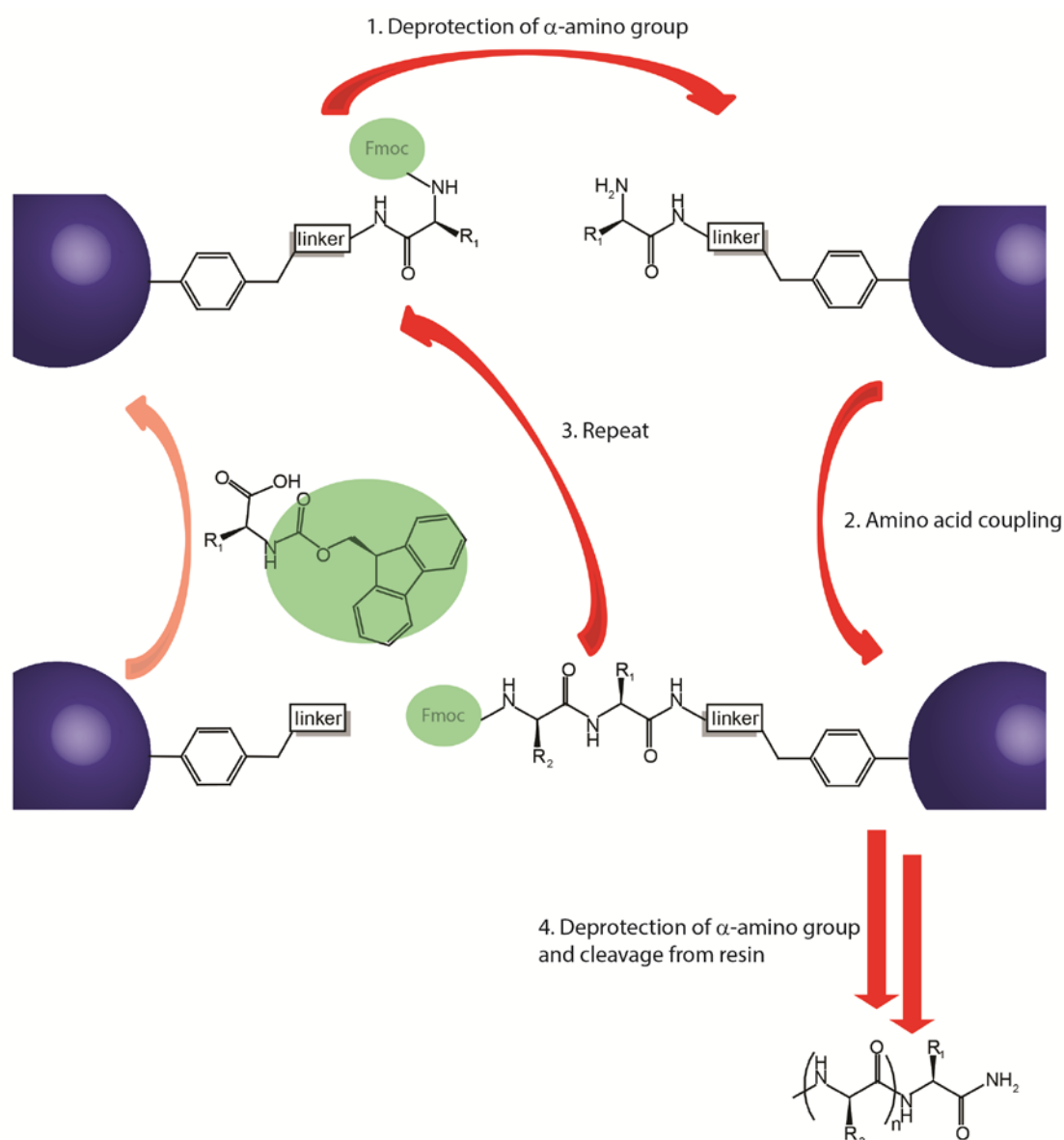


Figure 2.1. General approach to Fmoc solid-phase peptide synthesis. The Fmoc-protected C-terminal residue is attached to a functionalised solid support via linker molecules (e.g. rink amide or Wang linkers). The polypeptide chain is grown by repeated steps including: 1) removal of the Fmoc-protecting group from the N-terminal amine through treatment with a strong base such as piperidine, 2) coupling of subsequent amino acid residues through amide bond formation in the presence of phosphonium salt coupling reagents such as (benzotriazol-1-yloxy)tris(dimethylamino)phosphonium hexafluorophosphate (BOP) or (benzotriazol-1-yloxy)tris(pyrrolidino)phosphonium hexafluorophosphate (PyBOP), 3) repetition of steps 1 and 2 until the entire peptide has been synthesised and 4) deprotection of the final amino acid and removal from the solid support resin.

2.2.2 Peptide cleavage from solid support resin

Side chain deprotection was performed concomitantly with peptide cleavage from the solid support resin through acidolysis in the presence of scavengers using Reagent K (TFA/H₂O/phenol/thioanisole/1,2-ethanedithiol; 82.5/5/5/5/2.5 by volume) (Figure 2.2). This protocol was modified for analogues that incorporated Fmoc-L-Sec(pMeOBzl)-OH. For these

peptides, 1.3 equivalents 2,2'-dithiobis(5-nitropyridine) (DTNP) was added to the mixture to facilitate removal of Mob-protecting groups from selenocysteine side-chains (Reagent K[†]: trifluoroacetic acid (TFA)/thioanisole/phenol/nH₂O; 90:2.5:7.5:2.5 by volume). Peptides were cleaved for 2.5 h at room temperature with an additional 0.5 for each arginine residue in the sequence to ensure complete removal of Pbf-protecting groups from the side chain. Following cleavage, crude peptides were separated from resin by vacuum filtration. Peptides were precipitated using chilled methyl tert-butyl ether (MTBE) and crude material was concentrated by centrifugation. The crude pellet was then washed repeatedly with MTBE to remove excess TFA and scavengers.

For μ -BuIIIb analogues containing selenocysteine, the crude pellet was treated with 50 mM dithiothreitol (DTT) to remove 5-thionitropyridyl derivatives and allow for formation of the diselenide bridge (Figure 2.2). The product of this reaction was then purified by either solid phase extraction using a C18-bound silica resin or by preparative HPLC. For all other analogues, the crude precipitate was resuspended in 0.1% TFA in H₂O (Solvent A) and the linear peptide was directly purified by reversed phase HPLC.

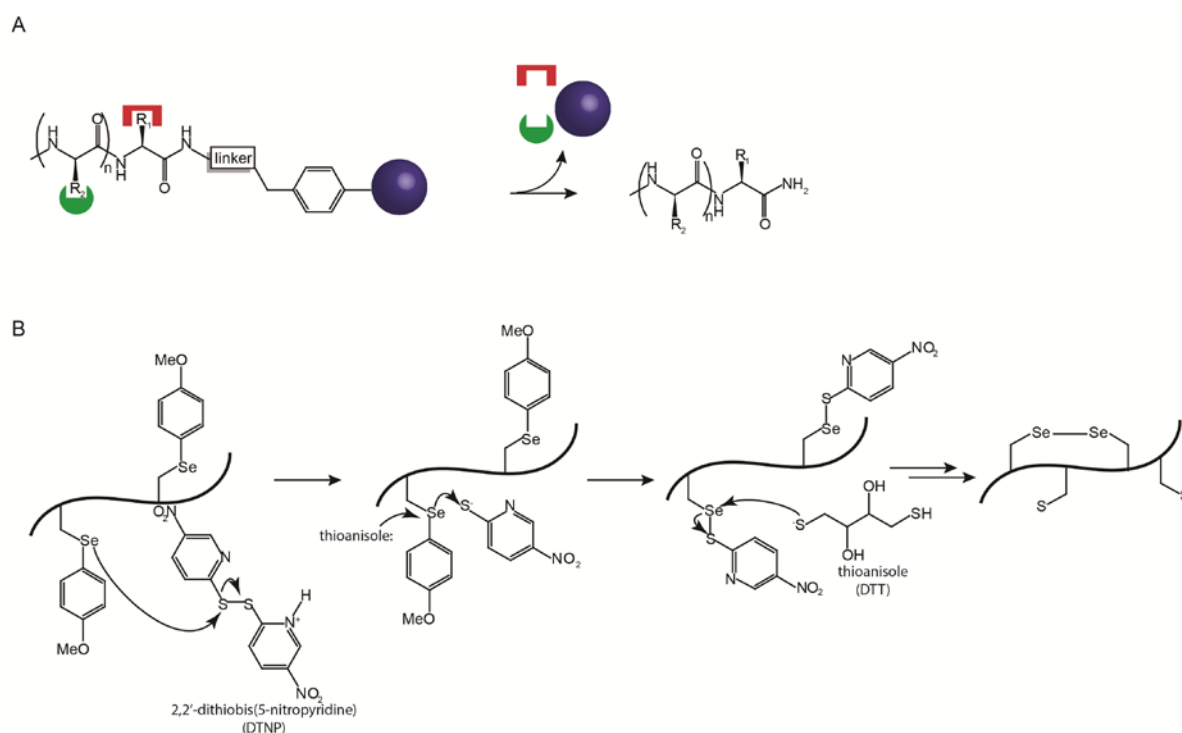


Figure 2.2. Removal of the synthesised peptide from the solid support resin. (A) Cartoon depicts removal of acid-labile protecting groups from reactive groups on the amino acid side chains. Upon treatment with Reagent K, the peptide is removed from the solid support resin. (B) Removal of Mob-protecting groups with concomitant formation of the diselenide bridge.

2.2.3 Purification of peptides by reversed phase high performance liquid chromatography (RP-HPLC)

Since its development in the 1970s, HPLC methods have emerged as one of the most widely used chromatographic techniques for analytical or preparative purification of biological compounds (72,73). Reversed-phase HPLC (RP-HPLC) effectively separates molecules based on polarity and their interactions with a hydrophobic matrix. Peptides bind to the column under aqueous conditions and are eluted with increasing concentrations of organic solvent. All peptides described here were purified by RP-HPLC where the mobile phase was 89.9% acetonitrile (ACN) 10% H₂O and 0.1% TFA (Solvent B₉₀). The stationary phase consisted of an octadecyl carbon chain (C18) covalently bound to a silica resin. Peptides were loaded onto a C18 RP-HPLC column (Vydac Protein & Peptide C18, 300 Å, 5 µm, 10 mm x 250 mm) and were purified over a linear gradient of increasing percentage of Solvent B₉₀. Peptides eluted from the column based on relative hydrophobicities, allowing for purification of the linear peptide. Individual fractions were checked for purity by analytical RP-HPLC and samples possessing greater than 90% purity were combined. Identities of all conotoxin analogues were confirmed either by MALDI-TOF or electrospray (ESI) mass spectrometry. Final peptide yields were determined by UV spectroscopy at wavelengths of 280 nm ($\epsilon_{\text{max}} = 5600$) or 275 nm ($\epsilon_{\text{max}} = 1420$) for peptides containing tryptophan or tyrosine residues, respectively (74). Finally, linear peptides were aliquotted and dried by lyophilization in preparation for oxidative folding.

2.2.4 Oxidative folding of disulfide-rich conotoxins

Folding of disulfide-rich peptides becomes increasingly more complex with increased numbers of cysteine residues. For the μ - or μ O-conotoxin families, which possess six cysteines resulting in three disulfide bridges, there is a possibility of formation of up to 15 different folding isoforms. Numerous exogenous methods have been developed to improve *in vitro* oxidative folding, and to minimize the number of folding isoforms. Traditionally, these methods have relied on either air oxidation of deprotected cysteine thiols or formation of disulfide bridges via addition of exogenous oxidants such as glutathione (75). Oxidative refolding of the analogues described here employed either direct oxidation in the presence of a mixture of reduced/oxidised glutathione or an immobilised disulfide reagent (Figure 2.3).

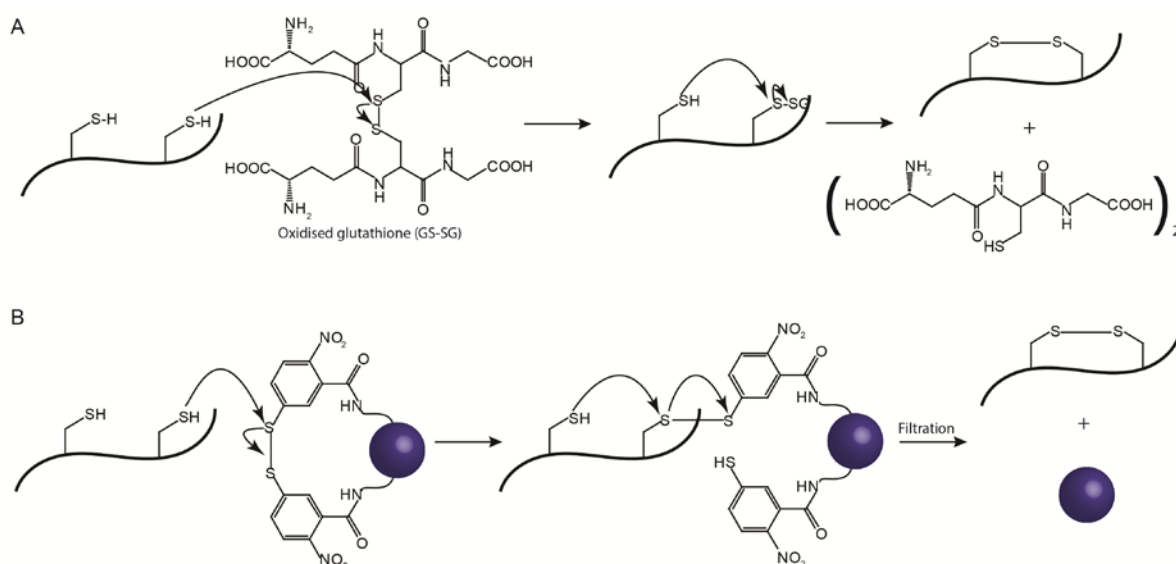


Figure 2.3. Exogenous methods of disulfide-bridge formation. Oxidative folding mechanisms for direct oxidative methods using oxidised glutathione (A) and use of a resin-bound oxidant such as Ellman's reagent (B).

Direct oxidative folding methods shown to be effective for the folding of similar VGSC-blocking peptides were also applied here: 20 μM final peptide, 0.1 M Tris-HCl, pH 7.5, 1 mM ethylenediaminetetraacetic acid (EDTA) and 1:1 mM oxidised/reduced glutathione (GSSG/GSH) (76). However, it was observed that folding yields for $\mu\text{-BuIII B}$ analogues could be further improved through modification of these conditions by addition of 1 M NaCl (76). Peptides were generally folded at room temperature with gentle agitation of the folding mixture. Once folding equilibrium had been reached, reactions were quenched by acidification through addition of 8% v/v formic acid.

Solid support oxidants take advantage of so-called pseudo-dilution effects that mitigate formation of non-productive disulfide-bridging patterns and increase the overall yield of the desired product. One example of this is the resin-bound Ellman's reagent commercially known as CLEAR-OXTM (52). For disulfide-deficient, diselenide-bridge containing analogues of $\mu\text{-BuIII B}$, one of the disulfide pairs was removed and another was replaced by a diselenide bridge that formed spontaneously following deprotection. Therefore, a single pair of cysteines remained which presented an opportunity to use such an approach to form the final disulfide bridge. Resin was prepared by swelling 48 molar equivalents CLEAR-OXTM (1 equivalent = 2.768 μg resin/nmol linear peptide) in dichloromethane (DCM) for 30 min. The resin was then washed with 0.5 mL of the following: dimethylformamide (DMF), methanol, 50% acetonitrile in H₂O and folding buffer (0.05 M Tris-HCl; 75% acetonitrile, pH 8.7). Peptides were added to a final concentration of 3 mM to resin and allowed to react for 2 h at 25 °C. Folding was quenched by 100-fold dilution of the peptide with

Solvent A (0.1% TFA in H₂O). Folded peptides were then removed from the CLEAR-OX™ resin by centrifugation or vacuum filtration and the mixture was purified by RP-HPLC.

2.3 Determination of disulfide connectivity by CID-MS/MS

Determination or confirmation of disulfide connectivities in disulfide-rich peptides can be challenging and time consuming. Furthermore, identification of disulfide pairings by NMR is often reliant on inferences made from the three dimensional structure based on inter-proton distance constraints from NOE data (77). Biochemical methods for determining the disulfide bridging patterns in conotoxins were pioneered by Gray and co-workers (78,79) and typically involve selective reduction and alkylation of cysteines, followed by peptide sequencing. These methods are often very labour-intensive and have the added disadvantage of consuming large quantities of peptide just to establish the optimal reduction/alkylation conditions.

Collision-induced dissociation mass spectrometry (CID-MS/MS) is a method that has recently gained favour for assignment of disulfide connectivity in conotoxins (80). The major advantages of this approach are the efficiency of the analysis, the ability to work with disulfide intact peptides and a requirement for only small amounts of material for analysis. CID-MS/MS capitalizes on the different modes of disulfide bond cleavage under ion trap mass spectrometric conditions (81). Peptides were first digested by combining 5 µL of 100 ammonium bicarbonate buffer, pH 7.8, containing trypsin at a 100:1 (peptide:protease) ratio. Proteolysis was allowed to proceed for 15 min at 37 °C after which the digested peptides were analysed by LC-MS analysis using a Bruker Q-ToF mass spectrometer coupled to an Agilent 1100 HPLC (Agilent C18 column, 4.6 x 150 mm). Spectra were averaged over four scans with the dry gas and nebulizer set to 10 L·min⁻¹ and 30 psi, respectively. Samples were infused at a flow rate of 2 µL·min⁻¹. CID experiments were performed by collision with He (g) and the amplitude of fragmentation varied from 1-3. The structures of the major fragment ions were obtained using the program *DisConnect* which was developed for analysis of CID MS/MS data for the 'native' disulfide bonded peptides (81).

2.4 Two-electrode voltage-clamp electrophysiology

All analogues were screened against α -subunits voltage-gated sodium channels expressed in *Xenopus laevis* oocytes by two-electrode voltage clamp electrophysiology (Figure 2.4). Peptide analogues were screened against α -subunits alone to facilitate comparison with previously published results. *Xenopus laevis* oocytes were micro-injected with 30-50 nL (approximately 5 ng) of the appropriate Nav1 subtype (BuIIIIB analogues: Nav1.3 or Nav1.4; GVIII analogues: Nav1.2)

dissolved in RNase-free water. Nav1 clones were provided by Professor Alan Goldin (University of California, Irvine) and cRNA was

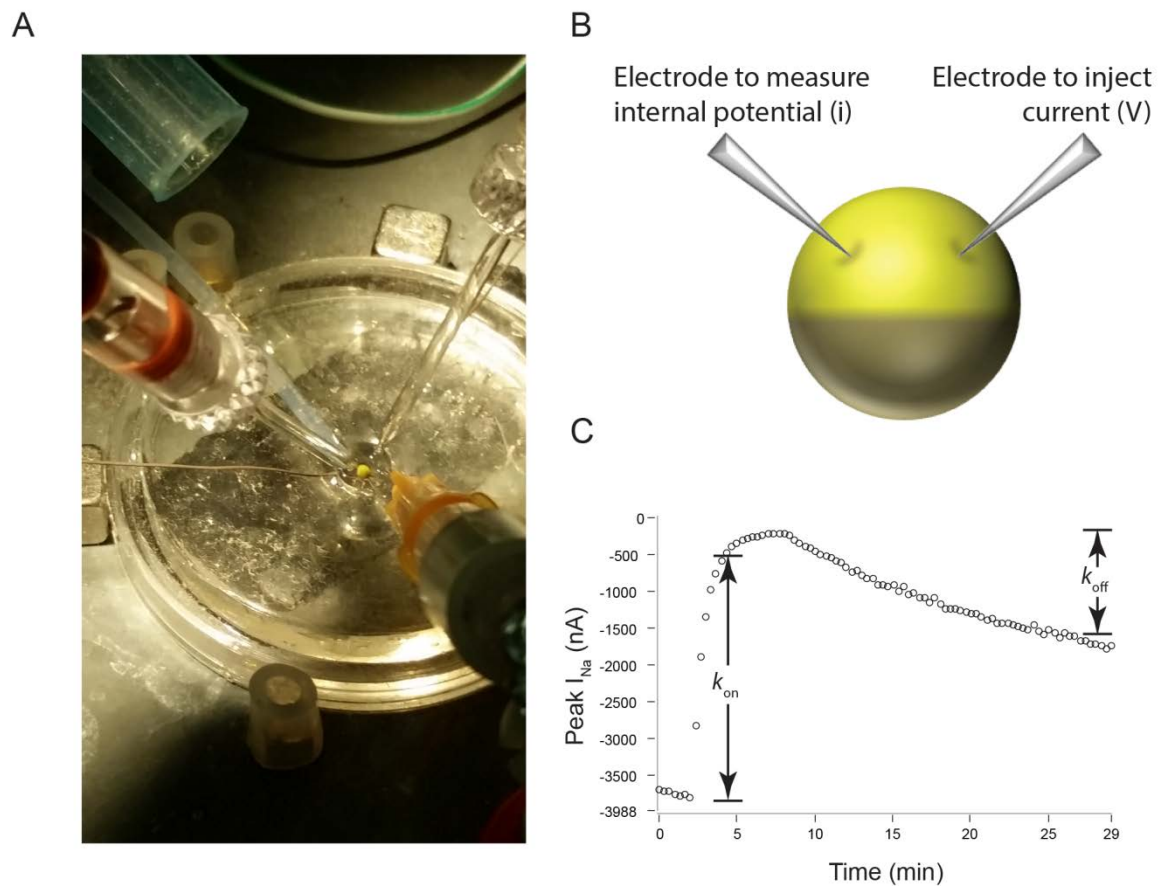


Figure 2.4. Two electrode voltage-clamp electrophysiology. (A) Oocytes expressing Nav1-subtypes are placed in a 30 μ L well. Toxin is applied to the well at 10X concentration and inhibition is measured under static bath conditions to conserve limited quantities of peptide. (B) Cartoon depiction of a clamped oocyte. Two KCl-filled electrodes are used to impale the oocyte. As shown, one electrode measures the internal potential (i), while the other delivers current (V). (C) Example of a I_{Na} curve for a slowly reversible toxin applied to an oocyte expressing Nav1.2. On-rate constants (k_{on}) are determined as the onset of block at a given concentration which is then fit to a single-exponential function to yield the observed rate constant (k_{obs}). On-rates are then obtained from the linear-regression slope of k_{obs} versus concentration. This is performed for three different peptide concentrations on at least 3 oocytes per concentration. If off-rates are slow ($k_{off} < 50\%$ recovery after 20 min), these values are estimated assuming that recovery followed as single-exponential time-course.

prepared by Dr. Layla Azam (University of Utah). Injected oocytes were incubated for 24-48 h (depending on injection volume) at 16 $^{\circ}$ C in ND96 buffer (96 nM NaCl, 2 mM KCl, 1.8 mM CaCl₂, and 5 mM HEPES, pH 7.5), supplemented with antibiotics (100 units/mL penicillin, 0.1 mg/mL streptomycin).

Voltage-clamping was performed with a Warner OC-725C amplifier (Warner Instruments) using 3 M KCl-filled microelectrodes (resistance < 0.5 M Ω) (62). An oocyte was placed in a 4 mm diameter well (30 μ L volume) filled with ND96 and clamped at a -80 mV holding potential.

Voltage-gated sodium currents (I_{Na}) were induced at 20 s intervals with a 50 ms depolarizing pulse to -10 mV. The peptides to be tested were dissolved in ND96 at 10X the desired final concentration and applied in 3 μ L volumes to the static bath containing the voltage-clamped oocyte. A static bath was used to conserve the limited quantities of the peptide analogues. Immediately following peptide application, the solution in the well was gently mixed through repeated pipetting of the bath solution. All experiments were performed at room temperature.

The time-course of peak I_{Na} was plotted before and during toxin exposure as well as following toxin washout. The observed rate constants (k_{obs}) were determined by fitting the onset of block to a single-exponential function for ≥ 3 oocytes at each of three different peptide concentrations. Since most of the analogues tested were very slowly reversible (i.e. $< 50\%$ recovery after 20 min washout or $k_{off} < 0.035 \text{ min}^{-1}$), off rates (k_{offs}) were estimated from the level of recovery after 20 min washout for ≥ 9 oocytes and assuming a single-exponential time-course (62). To minimize effects of baseline drift, times longer than 20 min were not used. Values of k_{obs} were plotted against [peptide], and k_{on} values were obtained from the slope of the linear regression line assuming the equation, $k_{obs} = k_{on}[\text{peptide}] + k_{off}$ (82). Electrophysiology data are presented as the mean \pm SD and statistical significance was determined using the two-tailed unpaired t test in GraphPad Prism.

2.5 Nuclear magnetic resonance (NMR) spectroscopy

At the most basic level, NMR looks at the properties of individual atomic nuclei when placed in a strong magnetic field. Interactions between nuclei can occur via either through-bond interactions (scalar coupling) or through-space interactions (dipolar interaction) and these interactions are used to construct three-dimensional models of bioactive molecules such as conotoxins (Figure 2.5). For the purposes of this thesis, NMR was utilised for secondary structural analysis of μ -BuIII B and structure determination of μ O \S -GIII J and their analogues. The details of individual experiments used in these studies can be found in Chapters 4 and 5, respectively.

To obtain good quality NMR spectra, relatively pure samples are required. For NMR analyses, peptides were rigorously purified to greater than 95%, as determined by RP-HPLC peak area. The lyophilised peptide was dissolved in either a mixture of 90% H_2O :10% $^2\text{H}_2\text{O}$ or in 100% $^2\text{H}_2\text{O}$ to concentrations ranging from 0.16 to 1.4 mM and pH was adjusted accordingly. A sufficiently low concentration of $^2\text{H}_2\text{O}$ was added to the solvent to facilitate lock of the field (typically 10% $^2\text{H}_2\text{O}$), while minimizing the loss of signal by deuterium exchange for rapidly exchanging protons. Spectra were acquired using either a Varian Inova 600 MHz or Bruker DRX-600 MHz spectrometer.

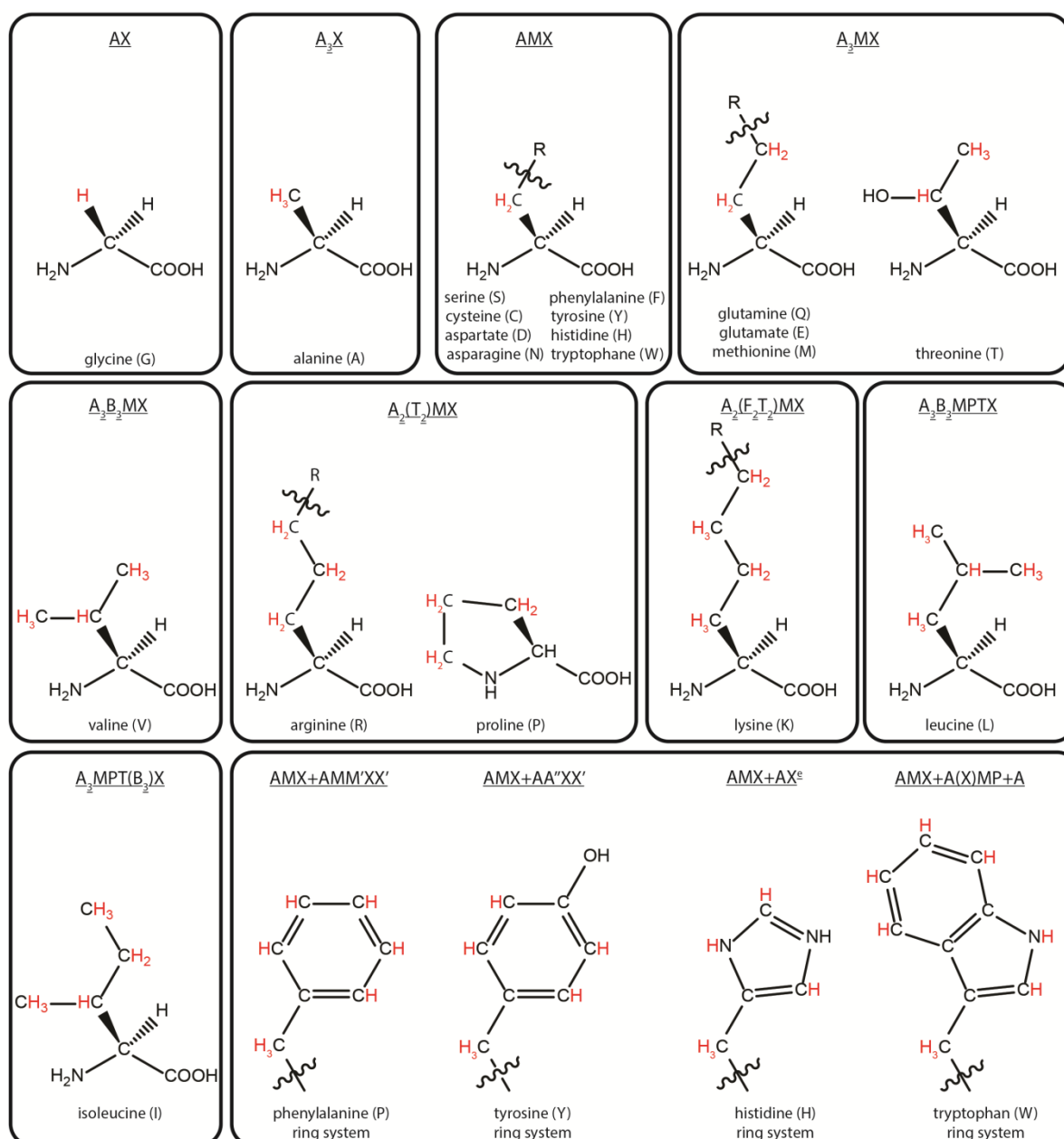


Figure 2.5. Spin system designations for the 20 common proteinogenic amino acids. Hydrogen atoms listed in red are those that may give rise to cross-peaks in NMR spectra.

2.5.1 One-dimensional ¹H NMR experiments

One-dimensional (1D) NMR experiments provide information about chemical shifts and ³J-coupling (spin-spin coupling) for individual resonances in an NMR spectrum (83). These spectra also provide a glimpse of the quality of the sample as well as a general assessment of the structure of the peptide (folded *versus* unstructured). In this thesis, one-dimensional NMR was used for temperature titration, hydrogen-deuterium exchange, and pH titration experiments. Amide

temperature coefficients were obtained from a series of one-dimensional ^1H spectra acquired over the temperature range of 283 – 313 K, in 5 K increments. Chemical shift differences were plotted and those that displayed backbone amide chemical shift differences ($\Delta\delta/\Delta t$) lower than 4 ppb/K were suggested to either be buried within the peptide, or to participate in H-bonding (84). These studies also helped to determine the optimal temperature under which subsequent NMR experiments should be performed.

Hydrogen-deuterium exchange experiments were performed to identify rapidly and slowly exchanging backbone amide protons (85). These experiments give some indication of the solvent accessibility of backbone amides for certain residues. For these experiments, lyophilised samples were dissolved in 100% $^2\text{H}_2\text{O}$ and one-dimensional spectra were acquired over 0 – 14 h. Deuteron exchange was assessed by the disappearance or persistence of signals. Rapidly exchanging protons were categorised as those which had completely disappeared from the one-dimensional spectra within 1 h and slowly exchanging protons were those which were still present after 4 h. Experiments were performed at 298 K using a 600 MHz spectrometer.

pH titration experiments were also performed to 1) identify appropriate conditions under which two-dimensional experiments should be conducted, and 2) to identify titratable amino acids based on amide proton chemical shift differences over a range of pH values (pH 2.8 – 8) (86). Lyophilised peptides were dissolved in 90% H_2O :10% $^2\text{H}_2\text{O}$. The pH of the sample was adjusted to the appropriate value directly in the NMR tube using deuterium chloride (^2HCl) or sodium deuterioxide (NaO^2H). Experiments were performed at 298 K using a 600 MHz spectrometer.

2.5.2 Two-dimensional ^1H NMR experiments

Given the limitations of one-dimensional NMR spectra for structural assignment (83), additional experiments are required for structural characterisation of peptides. Two-dimensional homonuclear (^1H - ^1H) experiments monitor the interaction of two ^1H nuclei along two axes, thereby overcoming the problem of signal overlap in one-dimensional NMR spectra (83). For the purposes of this thesis, two-dimensional ^1H - ^1H experiments such as correlated spectroscopy (COSY), total-correlation spectroscopy (TOCSY) and nuclear Overhauser effect spectroscopy (NOESY) experiments were performed to obtain chemical shifts and assignments for backbone and side-chain proton resonances (Figure 2.6).

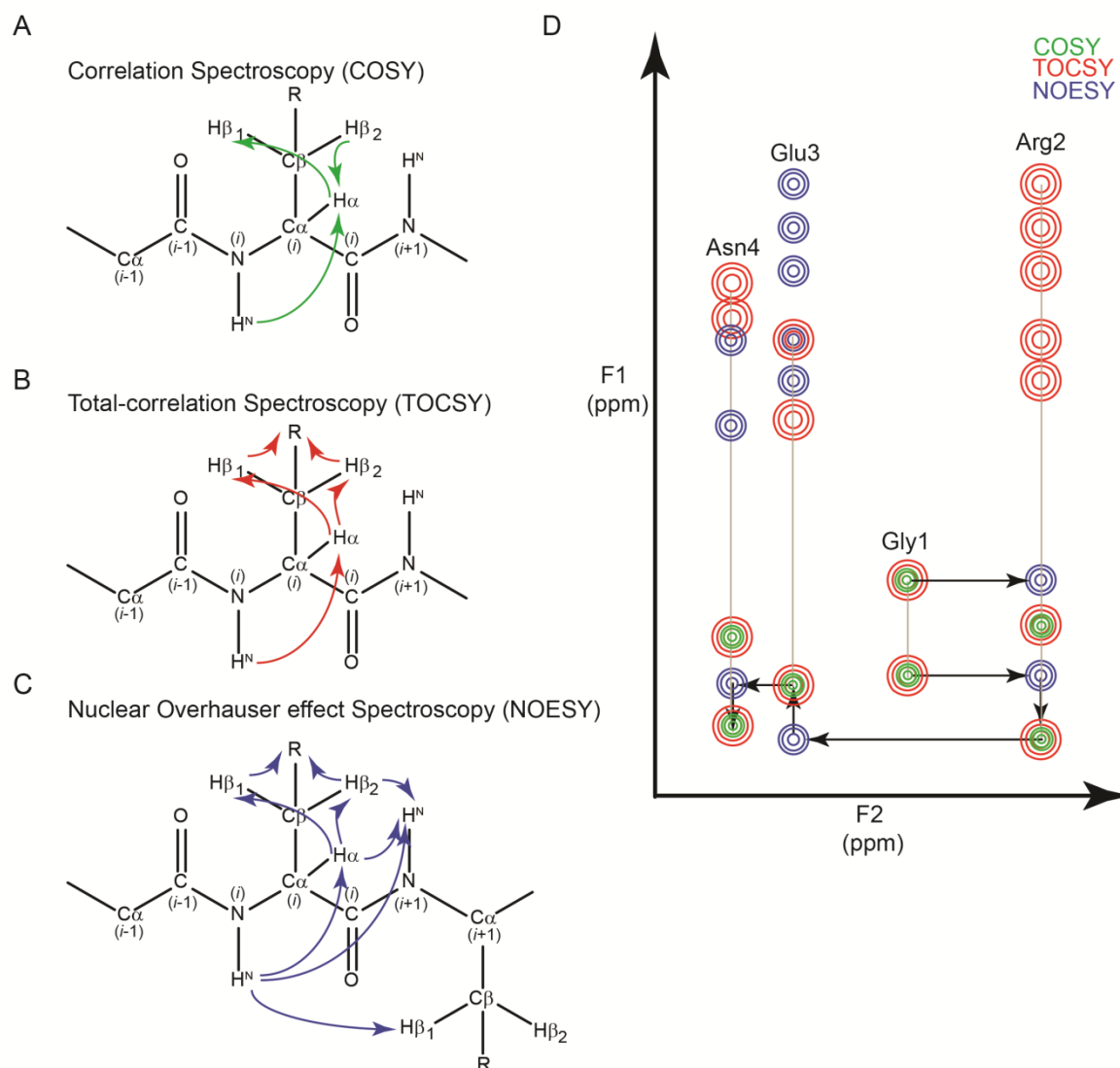


Figure 2.6. Interactions measured by COSY, TOCSY and NOESY spectra. (A) COSY spectra measure ^1H - ^1H interactions through scalar coupling. (B) TOCSY spectra also measure three-bond interactions, but are capable of reaching remote protons in the amino acid side chains by increasing spin-lock times. (C) NOESY spectra enable measurement of inter-residue interactions through spatial interactions between protons. (D) Representation of the fingerprint region of the hypothetical peptide Gly-Arg-Glu-Asn. Individual spin systems for each amino acid are denoted by gray lines.

2.5.2.1 Correlation spectroscopy (COSY)

^1H nuclei in individual amino acids are coupled to one other by interactions through chemical bonds (^3J scalar coupling) and are collectively referred as *spin systems* (83). COSY spectra measure the interactions between protons through scalar couplings within a spin system. For the experiments described in this thesis, COSY experiments were used infrequently, as similar information could be obtained by using total-correlation spectroscopy experiments with shorter mixing times (see section 2.5.2.2).

2.5.2.2 Total-correlation spectroscopy (TOCSY)

Total-correlation spectroscopy (TOCSY) identifies ^1H resonances in a given spin system, irrespective of the distance from the backbone amide proton. The magnetization of the amide proton (H^{N}) is transferred to other protons in the spin system through three-bond scalar coupling. This magnetization transfer can be extended to protons further along the side chain by increasing the spin lock times. In the studies described in this thesis, spin lock times of 30 ms were used to study ^1H nuclei near the backbone and were increased to either 70 or 100 ms to study more distant side chain protons. TOCSY experiments were also used in $^2\text{H}_2\text{O}$ exchange experiments, as well as temperature and pH titration experiments, because of the ability of these experiments to detect interactions between H^{N} with H^{α} , H^{β} and H^{γ} within a given spin system. The application of TOCSY spectra for these purposes is illustrated in Chapters 4 and 5.

2.5.2.3 Nuclear Overhauser effect spectroscopy (NOESY)

COSY and TOCSY spectra are useful for identifying nuclei within a single spin system. A NOESY spectrum not only provides information about coupled nuclei within a single spin system (intra-residue NOEs), but also yields cross-peaks between nuclei of different spin systems that are in close proximity ($<5 \text{ \AA}$ apart) to one another (inter-residue NOEs) (87). NOESY spectra are also important for generating distance restraints for generating a structure. An initial series of NOESY spectra, with varying mixing times (30 – 200 ms), was acquired to determine the optimal mixing time to maximize cross-peak intensity (or volume), while minimizing spin diffusion effects (87). In our studies, mixing times of 150 ms ($\mu\text{O}\S\text{-GVIIIJ}$) and 200 ms ($\mu\text{-BuIIIIB}$) were selected. The NOESY spectra were overlaid with TOCSY spectra, to make chemical shift assignments using either Sparky v. 3.114 (88) or CcpNmr Analysis (89). Following the complete assignment of the peptides, chemical shift data were used to construct plots to show deviations from random coil values for backbone amide (H^{N}) and C^{α} proton (H^{α}) (90). These data provide an initial idea of regions of ordered secondary structure in the peptide.

2.5.3 Structural calculations

The calculation of a peptide structure based on NMR data is reliant on the generation of a number of restraints as input for structure generation programs (chemical shifts, dihedral angles and hydrogen bonds) (91). Distance constraints for structural calculations were generated from assigned cross-peaks in NOESY spectra (150 ms mixing time) acquired at 298 K, pH 3.2. Dihedral angle constraints (ϕ and ψ) were generated from TALOS-N predictions (92) and from $^3J_{\text{HN-H}\alpha}$ coupling

constants according to the following: ${}^3J_{\text{HN-H}\alpha} > 8 \text{ Hz}$, $\Phi = -120 \pm 40^\circ$; ${}^3J_{\text{HN-H}\alpha} < 6 \text{ Hz}$, $\Phi = -60 \pm 40^\circ$. Disulfide bond constraints were added according to the previous experimentally determined connectivity (93). The ${}^2\text{H}$ exchange rates and temperature coefficients were used to identify H-bonded backbone amides; where H-bond acceptors could be identified from initial rounds of structural calculation (present and consistent in $\geq 80\%$ of structures), and were included in subsequent structural calculations. Initial structure calculations were optimised for a low target function using the noeassign macro in CYANA 3.0 (94). Structures generated by CYANA were then used to resolve the assignment of any remaining ambiguous inter-residue NOEs. Following optimization, the final set of constraints was entered into CNS version 1.3 (95), and an ensemble of 100 structures was generated. Of these, the 20 lowest energy structures without violations were selected to represent the solution structure of GVIIJ[C24S]. Validation of the final calculated structures was accomplished using PROCHECK-NMR (96). Secondary structure prediction was performed using DSSP (97) and PROMOTIF (98) based on the closest-to-average structure of GVIIJ[C24S]. Classification of β -turns was based on the criteria reported in (99). Structures were analysed using MOLMOL (100), and structural representations were constructed using either PyMOL (<http://www.pymol.org>) (101) or UCSF Chimera (<http://www.cgl.ucsf.edu/chimera>) (102).

2.6 Summary

The purpose of this chapter was to provide descriptions of the techniques applied to studies in this thesis. The following chapters will illustrate more specifically how these methods were applied towards identifying the important structural features that contribute to the biological activities of two classes of VGSC-blocking peptides, namely the μ - and $\mu\text{O}\delta$ -conotoxins.

Chapter 3

Structure and Function of μ -Conotoxins, Peptide-based Sodium Channel Blockers with Analgesic Activity

This chapter provides a detailed description of SAR studies of the μ -conotoxins from fish-hunting cone snails. Chapter 3 sets the scene for subsequent chapters in this thesis focussing on SAR studies of peptides from this family (Chapters 4 - 5, Appendix I).

This chapter consists of the following publication:

Green, B. R.; Bulaj, G.; Norton, R. S. Structure and function of μ -conotoxins, peptide-based sodium channel blockers with analgesic activity. *Future Med. Chem.*, 2014, 6(15): 1677-1698.

3.1 Declaration for Thesis Chapter 3

3.1.1 Declaration by candidate

In the case of Chapter 3, the nature and extent of my contribution to the work was the following:

Nature of contribution	Contribution (%)
Jointly conceived and wrote the paper. First and corresponding author	80%

The following co-authors contributed to the work. If co-authors are students at Monash University, the extent of their contribution in percentage terms must be stated:

Name	Nature of contribution	Contribution (%)
Grzegorz Bulaj	Assisted with manuscript preparation and intellectual input.	
Raymond S. Norton	Assisted with manuscript preparation and intellectual input.	

The undersigned hereby certify that the above declaration correctly reflects the nature and extent of the candidate's and co-authors' contributions to this work*.

**Candidate's
signature**



**Date
22.01.16**

**Main
supervisor's
signature**



**Date
22.01.16**

For reprint orders, please contact reprints@future-science.com

Structure and function of μ -conotoxins, peptide-based sodium channel blockers with analgesic activity

μ -Conotoxins block voltage-gated sodium channels (VGSCs) and compete with tetrodotoxin for binding to the sodium conductance pore. Early efforts identified μ -conotoxins that preferentially blocked the skeletal muscle subtype ($\text{Na}_v1.4$). However, the last decade witnessed a significant increase in the number of μ -conotoxins and the range of VGSC subtypes inhibited ($\text{Na}_v1.2$, $\text{Na}_v1.3$ or $\text{Na}_v1.7$). Twenty μ -conotoxin sequences have been identified to date and structure–activity relationship studies of several of these identified key residues responsible for interactions with VGSC subtypes. Efforts to engineer-in subtype specificity are driven by *in vivo* analgesic and neuromuscular blocking activities. This review summarizes structural and pharmacological studies of μ -conotoxins, which show promise for development of selective blockers of $\text{Na}_v1.2$, and perhaps also $\text{Na}_v1.1,1.3$ or 1.7.

Currently, there are approximately 128 peptide-derived drugs in various stages of clinical development [1]. In 2012 alone, six peptide drugs received FDA approval, making this class of compounds second only to small-molecule drugs in approvals granted during a given year [1]. Biologics such as peptides are rapidly gaining acceptance as viable therapeutic entities and, as the search to identify new drug leads continues [2], one source of bioactive peptides that has shown particular promise is the complex venom mixtures of predatory organisms. Venoms have evolved over millions of years as efficient mediators of defense, predation and competition. They are of interest to the pharmaceutical industry for their potential therapeutic benefits, resulting largely from the fact that the individual constituents are often highly potent ligands for specific subsets of key therapeutic targets (e.g., cell-surface receptors, ion channels and transporters). Out of the six FDA-approved drugs derived from venoms, four are of peptide origin: eptifibatid [3], bivalirudin [4], ziconotide [5] and exenatide [6]. Furthermore, approximately 20 additional venom-derived peptides are currently at various stages of clinical/preclinical development [7].

The venoms of marine snails of the genus *Conus* constitute an abundant source of neuroactive peptides [8–10]. Cone snails hunt by injection of a venom cocktail containing at least 100–200 bioactive peptides designed to rapidly immobilize prey or defend against predators [11,12]. The complexity of these venoms, combined with the large number of identified *Conus* species so far (500–700 species) [13], highlights the tremendous potential of these venoms as a source of pharmacological tools for the study or even treatment of numerous neurological disorders [14].

Conotoxins are broadly classified into 16 gene ‘superfamilies’ based on the endoplasmic reticulum (ER) signal peptide sequence [15]. Each superfamily is further subdivided according to disulfide bridging framework and/or pharmacological target [15]. The M-superfamily encompasses 10 distinct cysteine frameworks and at least four distinct molecular targets. Within this superfamily are two classes of peptides that inhibit **voltage-gated sodium channels** (VGSCs): the μ -conotoxins, which block Na^+ conductance by direct occlusion of the VGSC pore [16], and the μO -conotoxins, which act as gating modifiers by binding

Brad R Green^{*1,2},
Grzegorz Bulaj² &
Raymond S Norton¹

¹Medicinal Chemistry, Monash Institute of Pharmaceutical Sciences, Monash University, 381 Royal Parade, Parkville VIC 3052, Australia

²Department of Medicinal Chemistry, L. S. Skaggs Pharmacy Institute, University of Utah, Salt Lake City, UT 84112, USA

*Author for correspondence:
brad.green@monash.edu

to sites on the voltage-sensing domain on the extracellular surface of the VGSC [17,18]. This review will focus on the μ -conotoxins, thus far identified only in the venoms of piscivorous members of *Conus*. They are characterized by a Type III cysteine framework (i.e., CysI-CysIV, CysII-CysV, CysIII-CysVI) [16,19].

The sodium channel α -subunit (Na_v1) is a large pore-forming protein complex comprised of four homologous domains arranged about a central pore region (DI–D4) [20]. Each domain comprises six membrane-spanning segments (S1–S6) with an extended extracellular looped region (P-loop) connecting segments 5 and 6 (Figure 1) [21]. To date, nine distinct isoforms of the α -subunit (Na_v1.1 – Na_v1.9) have been described in various excitable tissues of the CNS or PNS, where they have been shown to modulate signal transduction in neuronal, cardiac or skeletal muscle cell types (Table 1) [22]. The flux of sodium ions

through VGSCs is responsible for both the initiation of action potentials and propagation of these signals along the length of the axon. Abnormal sodium conductance, through illness or injury, can lead to spontaneous firing of neurons and hyperexcitability, resulting in channelopathies associated with neuropathic pain [23] or other neurological disorders [24]. Channelopathies can also have the opposite effect and result in the inability to perceive painful stimuli in humans [25]. A 2006 *Nature* paper first described how a congenital loss-of-function mutation (i.e., nonsense-codon mutation) in the SCN9A gene that codes for the Na_v1.7 VGSC subtype resulted in an individual's inability to perceive pain [25].

Three VGSC subtypes have demonstrated roles in the transmission of pain signals: Na_v1.3, Na_v1.7 and Na_v1.8 (Table 1) [28,29]. Na_v1.3 expression is significantly increased in various neuropathic pain

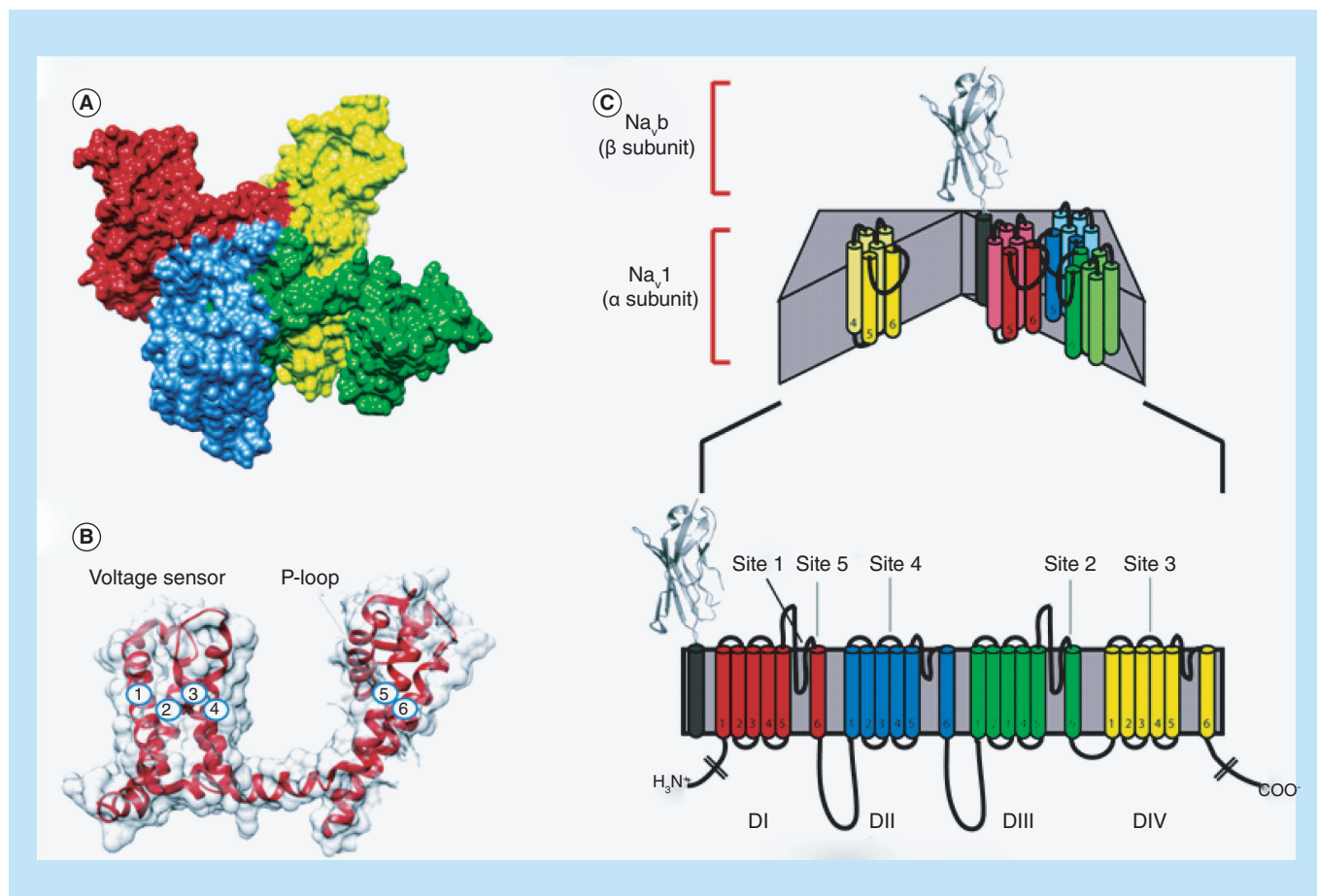


Figure 1. Voltage-gated sodium channels structure. (A) Crystal structure of the bacterial sodium channel Na_vAb (PDB code 4EKW). Structure illustrates the four homologous domains of the channel (DI–D4) arranged around the highly selective pore region through which Na⁺ permeates. (B) Individual domain comprising six membrane-spanning subunits (S1–S6) with the site of action (P-loop site 1) for μ -conotoxins discussed throughout this review [21]. (C) Cartoon of the VGSC α - and β -subunits. Selectivity filter is formed by the looped regions between S5 and S6 (i.e., P-loop). Approximate locations of neurotoxin-binding Sites 1–5 are shown on the α -subunit. Site 1, the location of μ -conotoxin binding, is emphasized. β -subunit crystal structure from Gilchrist *et al.* (PDB code 4MZZ) [26]. VGSC: Voltage-gated sodium channels.

Table 1. Sodium channel subtypes and their distribution.

Na _v 1-subtype [†]	Distribution	TTX sensitivity
Na _v 1.1	DRG, CNS, Heart	×
Na _v 1.2	DRG, CNS	×
Na _v 1.3 [‡]	DRG, CNS, PNS	×
Na _v 1.4	Muscle	×
Na _v 1.5	Heart	
Na _v 1.6 [‡]	DRG, CNS	×
Na _v 1.7	DRG, SCG	×
Na _v 1.8	DRG	
Na _v 1.9	DRG	

[†]To date, nine Na_v1-subtypes have been identified in the central/peripheral nervous systems or in muscle tissues (skeletal or cardiac). Many subtypes have been observed in the DRG with six of these subtypes being sensitive to block by the alkaloid neurotoxin TTX [20,27].

[‡]In addition to Na_v1.1 and 1.5 (as indicated above, Na_v1.3 and 1.6 have also been observed in cardiac tissue).

DRG: Dorsal root ganglia; PNS: Peripheral nervous system; SCG: Superior cervical ganglion neurons; TTX: Tetrodotoxin.

states, including nerve injury, spinal nerve ligation, postherpetic neuralgia and diabetic neuropathy [30–33]. Na_v1.7 is an essential and nonredundant requirement for nociception in humans [25]. Selective Na_v1.8 mRNA axonal transport and local upregulation may contribute to the hyperexcitability of peripheral nerves in some neuropathic pain states [34]. The Na_v1.9 subtype has also been suggested as a potential target for pain. However, this subtype is localized to the PNS and Na_v1.9 inhibitors may be more useful as treatments of inflammatory rather than neuropathic pain [28,35–36]. Taken together, these results provide support for the use of VGSC inhibitors that modulate neuronal excitability and could prove useful in the development of new analgesic compounds [22,37–40].

The alkaloid neurotoxins tetrodotoxin (TTX) and saxitoxin (STX) are potent inhibitors of VGSCs and were integral in defining neurotoxin binding site 1, a binding site deep inside the VGSC pore within the re-entrant P-loop region between S5 and S6 (Figure 1) [20,41]. However, TTX and STX have shown limited therapeutic potential due to their lack of selectivity among Na_v1 subtypes (TTX-sensitive subtypes include Na_v1.1–1.4, 1.6 and 1.7) [42–44]. Subtypes that are less sensitive to the effects of TTX are called ‘TTX resistant’ (Na_v1.5, 1.8 and 1.9). To mitigate potential adverse side effects arising from the lack of subtype specificity of TTX (e.g., cognitive effects, paralysis, ataxia), clinical investigations of TTX have been limited to focal (intramuscular) administration [37,45]. Several small molecule inhibitors of Na_v1-subtypes have also been described, but often lack target specificity leading to undesirable off-target effects (Figure 2). A potential advantage of peptide-based therapeutics is their intrinsic specificity for certain classes of molecular targets [27,46,47]. This specificity continues to be a

key driver of studies of *Conus* venoms that have led to characterization of the μ -conotoxins.1.

Numerous venom-derived neurotoxins elicit their biological effects through interaction at discrete sites within the α -subunit of the VGSC [48] (Figure 1C). Venom peptides have been shown to act at Site 1 (μ -conotoxins and nonpeptidic guanidinium toxins), Site 3 (scorpion α -toxins and anemone toxins), Site 4 (scorpion β -toxins, spider β -toxins and μ O-conotoxins) and Site 6 (δ -conotoxins), while Sites 2 and 5 are targeted predominantly by small organic neurotoxins such as the batrachotoxins and brevetoxins [49]. Peptide components of non-*Conus* origin have also been shown to block Na_v1, though the site of action of many of these toxins has yet to be fully defined. Among these are Tx1, hainantoxin-I and ProTx-II (which is of interest because of its subtype selective block of Na_v1.7) [39–40,50].

The μ -conotoxins are employed as paralytic tools by fish-hunting marine gastropods from the genus *Conus*. Over the nearly three decades since the first reports of μ -conotoxins isolated from the venom of

Key terms

Conotoxins: Neuroactive peptides isolated from the venoms of marine snails of the genus *Conus*, usually 10–30 amino acids in length and often cross-linked by one or more disulfide bridges.

Voltage-gated sodium channel: Membrane-spanning ion channel responsible for initiating and propagating action potentials in excitable tissues.

Sodium channel α -subunit (Na_v1): Na_v1-subtypes have four transmembrane spanning domains arranged around a central pore through which Na⁺ ions can permeate. The α -subunit is the minimum structure required for a functional voltage-gated sodium channel.

Conus geographus (μ -GIIIA/B/C), which preferentially blocked muscle subtypes, 17 distinct μ -conotoxins have been identified (Figure 3). More recently, μ -conotoxins with preference for neuronal subtypes were reported [51]. These peptides modulate the activity

of Na_v1 -subtypes by binding at the outer vestibule at Site 1 of the sodium channel pore, in many cases with submicromolar affinities [52,53]. This review summarizes the efforts to define the structural features of μ -conotoxins responsible for their potency and selectivity for Na_v1 -subtypes as a basis for the development of both novel pharmacological tools and potential therapeutics.

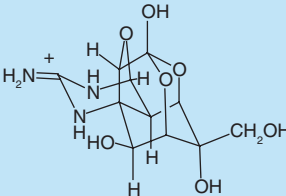
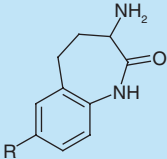
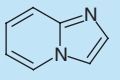
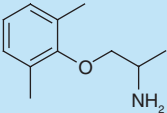
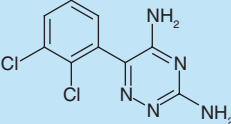
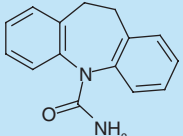
Compound	Molecular Target(s)
 4,9-anhydro-tetrodotoxin	$\text{Na}_v1.2$ – 1.8 Others: N/A
 1-benzazepin-2-one	$\text{Na}_v1.5$, 1.7 & 1.8 Others: Ca_v1 -channels
 Imidizopyridine	$\text{Na}_v1.7$ & 1.8 Others: GABA receptors
 Mexiletine [†]	$\text{Na}_v1.4$ Others: Ca_v1 -channels
 Lamotrigine [†]	$\text{Na}_v1.5$, 1.7 & 1.8 Others: NaChRs
 Carbamazepine [†]	$\text{Na}_v1.1$ – 1.8 Others: GABA receptors, hepatic enzymes, etc.

Figure 2. Examples of small molecule inhibitors of voltage-gated sodium channels.

[†]Indicates clinically used voltage-gated sodium channels.

Data taken from [27].

Muscle-subtype preferring μ -conotoxins

μ -Conotoxins from *Conus geographus*

The first μ -conotoxins to be isolated and characterized were μ -GIIIA and its congeners μ -GIIIB and μ -GIIIC, from the venom of *C. geographus* (Figure 4) [54]. Early work showed, for the first time, that μ -conotoxin GIIIA could discriminate between sodium channels isolated from muscle ($K_d = 25$ nM) and nerve ($K_d \sim 11,000$ nM) preparations [54,55]. This information was among the first to suggest that discrete VGSC isoforms existed within different excitatory tissue types. Recent work by Wilson *et al.* [53] established the selectivity profile for μ -GIIIA in *Xenopus* oocytes expressing rat or mouse Na_v1 -subtypes (Figure 5). Consistent with previous results, μ -GIIIA showed the highest potency for the skeletal muscle subtype $\text{Na}_v1.4$ (0.019 μM), followed by the neuronal subtypes $\text{Na}_v1.1$ (0.26 μM), $\text{Na}_v1.6$ (0.68 μM) and $\text{Na}_v1.2$ (17.8 μM) [53]. μ -GIIIA is a highly basic, 22 amino acid residue peptide that is stabilized by three disulfide bridges (Cys3–Cys15; Cys4–Cys20; Cys10–Cys21). Ala-replacement studies showed that the most critical residues for VGSC blockade are localized in the C-terminal half of the peptide (Arg13, Arg19, Hyp17 and Lys16) (Figure 6) [56]. The solution structure of the μ -GIIIA[R13A] mutant showed that these residues were located on the same face of the molecule, suggesting that this region of the peptide may interact directly with the channel [57]. The structure of μ -GIIIA also revealed the close proximity of the hydroxyl group of Hyp17 to the guanidino group of Arg13, which led to the hypothesis the μ -GIIIA interacted with Na_v1 subtypes in a similar manner to the guanidinium toxins at Site 1 [57]. Yanagawa *et al.* [58], showed that μ -GIIIA inhibited the VGSC binding of ^3H -Lys-TTX, and conversely, that ^3H -Pr-GIIIA prevented the binding of both TTX and STX, providing strong evidence that μ -GIIIA and the guanidinium toxins compete for the same binding site on muscle Na_v1 [55,58].

μ -Conotoxins from *Conus purpurascens*

More than a decade after the first report of μ -conotoxins from *C. geographus*, another 22-residue peptide sharing an identical Cys framework, μ -PIIIA, was identified from the venom of *C. purpurascens* (Figure 4) [60]. As

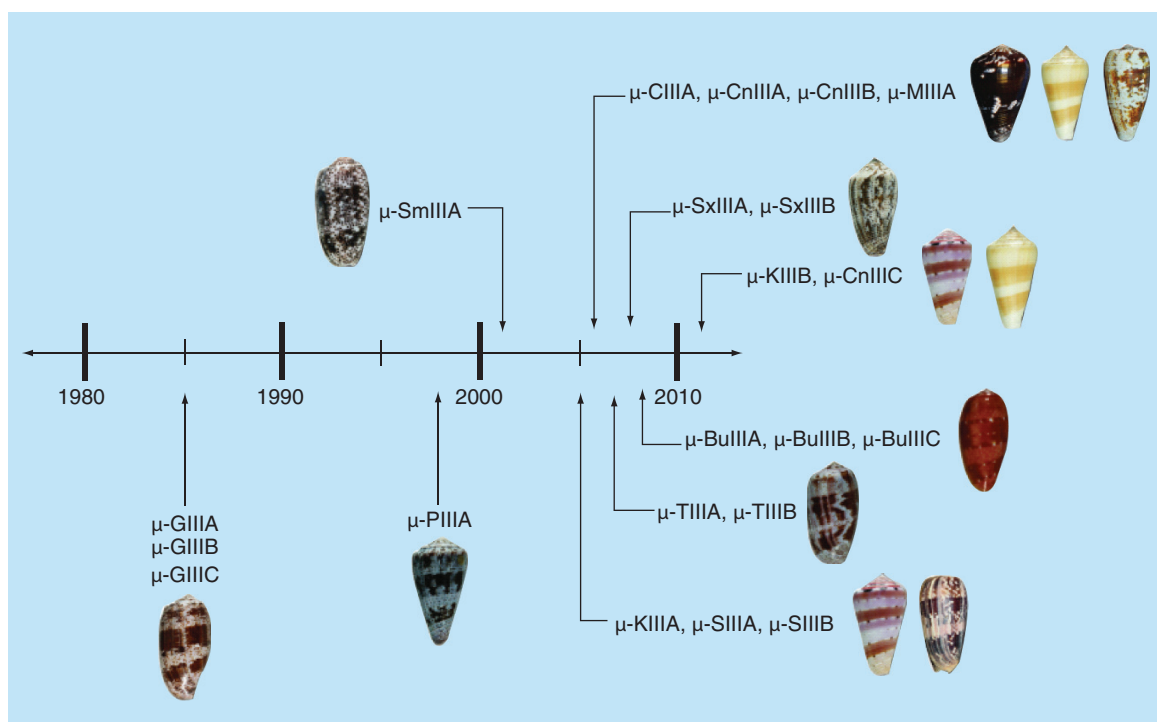


Figure 3. The μ -conotoxins as an emerging class of sodium channel blocking peptides. Timeline illustrates the relative discoveries and/or characterization of the members of this family. Data taken from [53].

with μ -GIIIA, this toxin showed a strong preference for muscle Na_v1 subtypes ($\text{IC}_{50} = 44 \text{ nM}$) over those from brain ($\text{IC}_{50} = 640 \text{ nM}$). In contrast to μ -GIIIA, μ -PIIIA exhibited nearly irreversible block of Na_v1 -subtypes [60]. The solution structure of μ -PIIIA confirmed the close proximity of the guanidino group of Arg14 to the hydroxyl group of Hyp18, providing further support for the proposed interactions between μ -GIIIA/PIIIA and Site 1 of the muscle VGSC subtype [61]. Like μ -GIIIA, μ -PIIIA exhibited the highest potency against $\text{Na}_v1.4$ ($0.036 \text{ }\mu\text{M}$), although affinities for other VGSC subtypes in the central (CNS) and peripheral (PNS) nervous systems were on average higher than those for μ -GIIIA (Figure 5) [53]. Because of the strong preference of μ -conotoxins μ -GIIIA/B/C and μ -PIIIA for muscle over neuronal subtypes, these peptides have also served as valuable tools for studying the VGSC isoform selectivity and function of skeletal muscle VGSCs [62].

μ -Conotoxins from *Conus stercusmuscarum*

μ -SmIIIA was predicted from the cDNA library from the venom of *C. stercusmuscarum* in 2002 [63]. μ -SmIIIA was shown to block Na^+ current in sympathetic neurons (TTX-resistant Na_v1 channels) with near irreversibility (for $0.5 \text{ }\mu\text{M}$ μ -SmIIIA, $k_{\text{obs}} = 0.24 \text{ min}^{-1}$) [63]. Notable differences between μ -SmIIIA and previously described μ -conotoxins included only modest

noncysteine sequence homology and the presence of Trp15 in the second intercysteine loop (Figure 4). The solution structure of μ -SmIIIA showed distinct differences from the μ -conotoxins of *C. geographus* both in its topology and the positioning of certain amino acid residues; it was hypothesized that these structural differences contributed to the block of TTX-resistant Na_v1 -subtypes by μ -SmIIIA [64]. This was supported by SmIIIA-PIIIA chimeras, which retained activity against amphibian TTX-resistant channels [64]. Block of TTX-resistant channels in amphibian preparations did not, however, translate to similar activities in mammalian channels [63]. Despite low nanomolar potency for $\text{Na}_v1.4$ (0.22 nM), μ -SmIIIA exhibited relatively poor selectivity among Na_v1 -subtypes in the CNS and PNS ($\text{Na}_v1.1$, 3.8 nM , $\text{Na}_v1.2$, 1.3 nM , $\text{Na}_v1.3$, 35 nM) (Figure 5). Moreover, μ -SmIIIA exhibited low micromolar block of the cardiac subtype $\text{Na}_v1.5$ [53], ruling it out as a viable candidate for therapeutic development.

μ -Conotoxins from *Conus striolatus*

The μ -conotoxins SxIIIA and SxIIIB, reported by Walewska *et al.* [65], also inhibited the skeletal muscle subtype preferentially ($\text{Na}_v1.4 = 0.007 \text{ }\mu\text{M}$; $\text{Na}_v1.2 = 1 \text{ }\mu\text{M}$) [53]. Among the conotoxins that preferentially target this subtype, there appears to be a pattern of hydroxyproline residues in the first and

	ER Signal sequence	Propeptide sequence	Mature toxin	Toxin name
m4 branch	MSKLGVLLTICLLFLPLTA	LPMDGDEPANRPVERMQDNISSEQYPLFEKR	RD <u>CC</u> TOOKK-CKD <u>R</u> OC <u>CKOQR</u> - <u>CCA</u>	μ -GIIIA
			RD <u>CC</u> TOORK-CKD <u>R</u> R <u>CKOMK</u> - <u>CCA</u>	μ -GIIIB
			RD <u>CC</u> TOOKK-CKD <u>R</u> R <u>CKOLK</u> - <u>CCA</u>	μ -GIIIC
			RHG <u>CC</u> KGOKG-CSS <u>R</u> E <u>CROQH</u> - <u>CC</u>	μ -TIIIA
			ZRL <u>CC</u> GFOKS-CRS <u>R</u> Q <u>CKOHR</u> - <u>CC</u>	μ -PIIIA
			R <u>CC</u> TGKKGS <u>CSGR</u> A <u>CKNLK</u> - <u>CCA</u>	μ -SxIIIA
			Z <u>KCC</u> TGKKGS <u>CSGR</u> A <u>CKNLR</u> - <u>CCA</u>	μ -SxIIIB
m5 branch	MSKLGVLLTICLLFLPLTA	LPMEDQPADQLEDQMDDISSEQYPSFVRR	Z <u>NCC</u> -NG--G <u>CS</u> <u>SK</u> W <u>CRD</u> HAR <u>CC</u>	μ -SIIIA
			Z <u>NCC</u> -NG--G <u>CS</u> <u>SK</u> W <u>CKG</u> HAR <u>CC</u>	μ -SIIIB
			<u>CC</u> -N----- <u>CS</u> <u>SK</u> W <u>CRD</u> H <u>SR</u> CC	μ -KIIIA
			NG <u>CC</u> -N----- <u>CS</u> <u>SK</u> W <u>CRD</u> H <u>SR</u> CC	μ -KIIIB
			Z <u>RCC</u> -NGRRG <u>CS</u> <u>S</u> W <u>CRD</u> H <u>SR</u> CC	μ -SmIIIA
			VT <u>DRC</u> CKNGKRG <u>G</u> - <u>R</u> W <u>CRD</u> H <u>SR</u> CC	μ -BuIIIA
			V <u>GER</u> CKNGKRG <u>G</u> - <u>R</u> W <u>CRD</u> H <u>SR</u> CC	μ -BuIIIB
			G <u>RCC</u> -EGPNG <u>CS</u> <u>S</u> W <u>CKD</u> HAR <u>CC</u>	μ -CIIIA
			G <u>RCC</u> -DVPNA <u>CS</u> <u>G</u> W <u>CRD</u> H <u>AQ</u> CC	μ -CnIIIA
			Z <u>GCC</u> -GEPNL <u>CFT</u> <u>R</u> W <u>CR</u> NNAR <u>CC</u> R <u>QQ</u>	μ -CnIIIB
			Z <u>GCC</u> -NGPKG <u>CS</u> <u>SK</u> W <u>CRD</u> HAR <u>CC</u>	μ -CnIIIC
			Z <u>GCC</u> -NVPNG <u>CS</u> <u>G</u> W <u>CRD</u> H <u>AQ</u> CC	μ -MIIIA

Figure 4. Summary of identified μ -conotoxins from m4 and m5 branches of the M-superfamily. ER signal and propeptide sequences for μ -GIIIA and μ -SIIIA are illustrated as examples. 'O' denotes hydroxyproline; 'Z' denotes pyroglutamic acid. Arg13 in μ -GIIIA, or the residue in the equivalent position, is underlined to illustrate the sequence differences among conotoxins that preferentially block muscle versus neuronal subtypes.

ER: Endoplasmic reticulum

Adapted with permission from [16,59].

third inter-cysteine loops that is absent in μ -SxIIIA/B (Figure 4). Similarly, among conotoxins that block neuronal subtypes there is a high degree of sequence homology within the third inter-cysteine loop. These peptides also possess a Trp residue at an equivalent position, which is absent in μ -SxIIIA/B (Figure 4). Intraperitoneal or subcutaneous injection of μ -SxIIIA resulted in paralysis in mice [65]. Furthermore, SxIIIA was found to block $\text{Na}_v1.4$, expressed in *Xenopus* oocytes, with low nanomolar potency ($\text{IC}_{50} = 7 \text{ nM}$) [65]. The selectivity profile for μ -SxIIIA was later established as: $\text{Na}_v1.4 \gg 1.1 > 1.6 > 1.2 \gg$ all other subtypes (Figure 5) [53]. Notably, μ -SxIIIA was used as a model peptide for NMR-based mapping of disulfide connectivity [65]. Cysteines I–III (with respect to the disulfide framework) of μ -SxIIIA were labeled with 100% $^{15}\text{N}/^{13}\text{C}$, while the remaining Cys-residues were labeled with a mixture of 70% ($^{14}\text{N}/^{12}\text{C}$):30% ($^{15}\text{N}/^{13}\text{C}$). This allowed for 3D triple-resonance NMR experiments to determine disulfide connectivity from Cys $\text{H}^\alpha/\text{H}^{\beta 2}/\text{H}^{\beta 3}$ NOESY cross peaks.

μ -Conotoxins from *Conus tulipa*

μ -TIIIA from *C. tulipa* potently inhibited both $\text{rNa}_v1.2$ and $\text{rNav}1.4$ expressed in *Xenopus* oocytes ($K_d = 45$ and 5 nM , respectively) [53,66] (Figure 5), but

showed little effect on isolated neurons from rat dorsal root ganglion (DRG). Alanine-replacement studies on μ -TIIIA showed that mutation of His2, Glu15 or Gln19 increased block of Na_v1 subtypes, whereas replacement of Lys6, Lys9, Arg17 and His20 reduced block (Figure 6). The μ -TIIIA[E15A] mutant not only improved block but also switched subtype preference in favor of the neuronal subtype [66]. It was suggested that the negative charge at this position created an unfavorable interaction with the binding site within the sodium channel [66]. More recent work has shown that addition of either a neutral residue (μ -TIIIA[E15A, 23A]) or basic residue (μ -TIIIA[E15A, 23K]) to the C-terminus decreased overall potency for all subtypes, but increased preference for $\text{Na}_v1.2$ [67]. Based on these findings, further positional scanning of Glu15 would be of interest to explore whether the selectivity profiles of μ -TIIIA could be shifted in favor of pain-relevant Na_v1 -subtypes.

Neuronal-subtype preferring μ -conotoxins

μ -Conotoxins from *Conus kinoshitai*

μ -KIIIA and μ -KIIIB are the shortest members of the μ -conotoxin family reported to date (Figure 4). In contrast to previously described μ -conotoxins, μ -KIIIA/B, preferentially blocked neuronal Na_v1 subtypes [51].

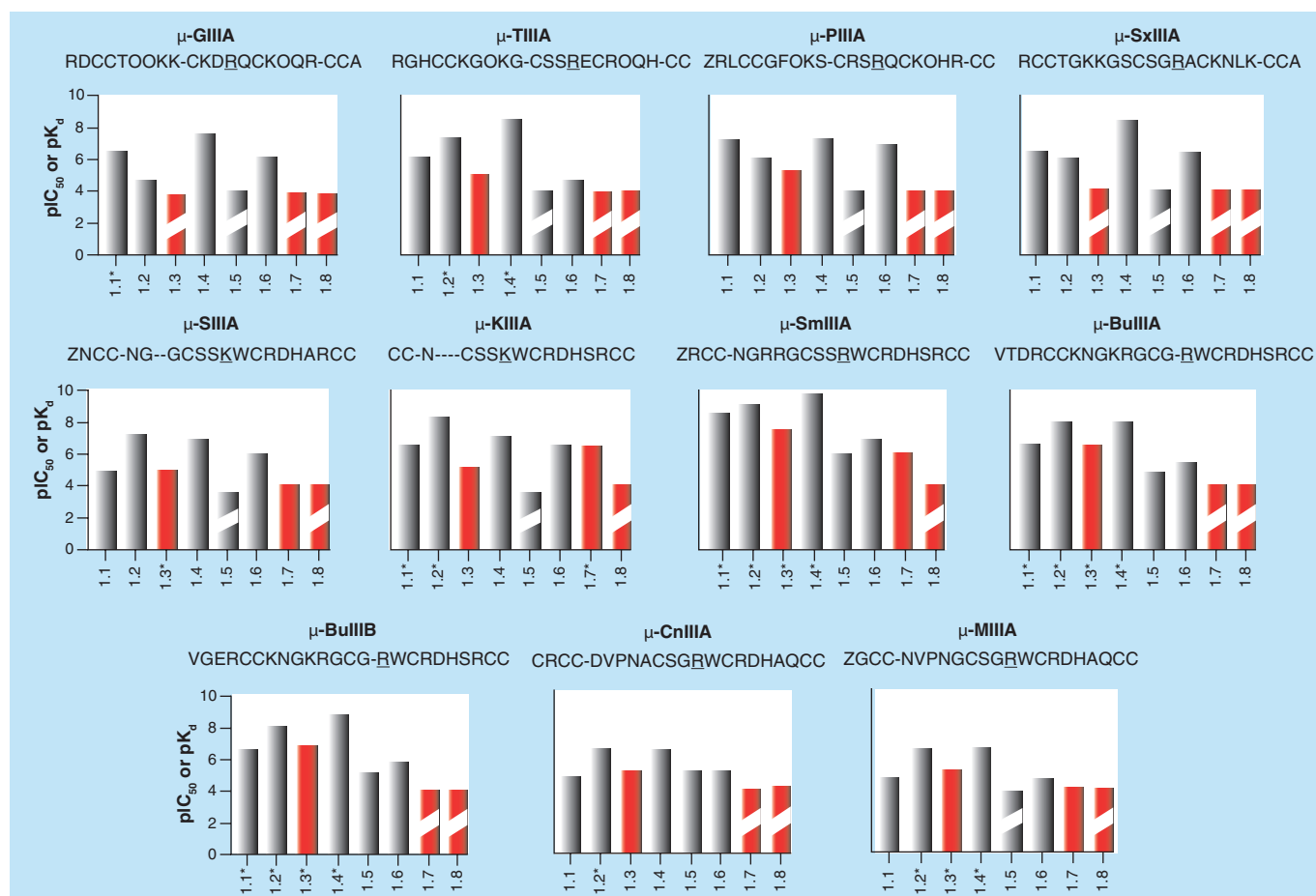


Figure 5. Selectivity profiles of μ -conotoxins against Na_v1 -subtypes. Data were obtained from reported IC_{50} values; *represents data obtained from pK_d values [53]. Pain-relevant subtypes are highlighted in red. Broken bars represent values greater than 100 μM . For color images please see online <http://www.future-science.com/doi/full/10.4155/FMC.14.107>

μ -KIIIA also showed significant differences in amino acid composition and intercysteine loop sizes compared with muscle subtype preferring μ -conotoxins (Figure 4). Another notable difference was the substitution of the typically conserved Arg residue in loop 2 with Lys. These toxins also have a Trp residue within the second intercysteine loop and more closely resembled μ -SmIIIA in the third loop. cDNA sequence data also identified a peptide with an extended N-terminus, μ -KIIIB [68]. The major folding isoforms for the short (μ -KIIIA) and extended (μ -KIIIB) peptides exhibited comparable activities when tested in *Xenopus* oocytes expressing $\text{Na}_v1.2$ [68,69]. As all available structure–activity relationship (SAR) data were obtained from the N-terminally truncated peptide, this review will focus on analogs of μ -KIIIA rather than μ -KIIIB. μ -KIIIA exhibited nearly 17-fold preference for neuronal over skeletal muscle subtypes (K_d $\text{rNa}_v1.2 = 0.003 \mu\text{M}$ and K_d $\text{rNa}_v1.4 = 0.05 \mu\text{M}$) [69], and Ala-walk studies showed that four residues within loops 2 and 3 contributed to its $\text{Na}_v1.2$ preference, namely, Trp8, Arg10, His12 and Arg14 [69]. Furthermore, block of the

muscle subtype was decreased by Ala replacement of Lys7, Trp8, Arg10, Asp11, His12 and Arg14 (Figure 6).

Arg13 in μ -GIIIA and Arg14 in μ -PIIIA were shown to be crucial for the inhibition of skeletal muscle Na_v1 -subtypes, with the conservative analog μ -GIIIA[R13K] showing 10-fold lower potency for skeletal muscle subtypes [70]. Intriguingly, the neuronal-preferring conotoxins such as μ -SIIIA or μ -KIIIA possess a lysine at the equivalent position [51], and SAR studies of μ -KIIIA showed that mutations at this position (Lys7) could influence $\text{Na}_v1.2$ subtype preference [51]. μ -KIIIA[K7A] retained similar activity to μ -KIIIA against $\text{rNa}_v1.2$, but showed reduced activity against $\text{rNa}_v1.4$, thereby increasing the selectivity window [69]. This was also shown in the block of $\text{Na}_v1.2$ by the μ -KIIIA[K7Nle] analog, which more closely mimicked the steric bulk of a lysine residue at position 7 (block = 83 vs 33%) [69]. McArthur *et al.* recently showed that Ala substitution of either Lys7 or Arg10 led to lower K_d values and decreased maximal block, but retained the wild-type selectivity profile ($\text{Na}_v1.2 > 1.4 > 1.7$), while replacement of either His12 or Arg14 decreased

potency and altered the Na_v1 selectivity profiles in favor of pain-relevant subtypes ($\mu\text{-KIIIA}[\text{H12A}] - \text{Na}_v1.2 > 1.7 > 1.4$ and $\mu\text{-KIIIA}[\text{R14A}] - \text{Na}_v1.7 > 1.2 > 1.4$) [71]. Taken together, these results demonstrated that Lys7 was important for both potency and efficacy of block by $\mu\text{-KIIIA}$.

Analogues of $\mu\text{-KIIIA}$ were also constructed that incorporated nonnatural *N*-substituted Gly monomers (e.g., *N*-methylglycine, *N*-butylglycine and *N*-octoylethylglycine) at position 7 to explore the effects on Na_v1 affinity (K_d or IC_{50}) and efficacy (% block) [72]. These analogues retained the ability to block $\text{Na}_v1.2$, although both the kinetics of block and affinities were affected. The *N*-methylglycine substituted peptide was the most potent of these analogues tested. Importantly, this peptide also exhibited the largest residual Na^+ current of the series demonstrating a correlation between the size of the R-group of the substituted monomer and efficacy [72].

Mutations at Trp8 led to increased discrimination between neuronal and muscle subtypes. Replacement by Ala or Leu decreased the maximal block of both $\text{Na}_v1.2$ and $\text{Na}_v1.4$ (50 and 19% decrease, respectively). These substitutions also affected the kinetics of block, where k_{obs} for $\text{Na}_v1.2$ was significantly increased and the rate of block of $\text{Na}_v1.4$ was essentially unchanged [69]. Van Der Haegen *et al.* replaced Trp8 with Arg, Gln or Glu to explore the electronic effects of varying charge at this position on Na_v1 inhibition [73]; in all instances, Na_v1 potency was decreased. More importantly, mutation of Trp8 resulted in increased selectivity for neuronal sodium channel subtypes through greater reduction in $\text{rNa}_v1.4$ potency. This work also showed that substitution of Trp8 with less hydrophobic amino acid residues, regardless of charge, increased the reversibility of blockade [73].

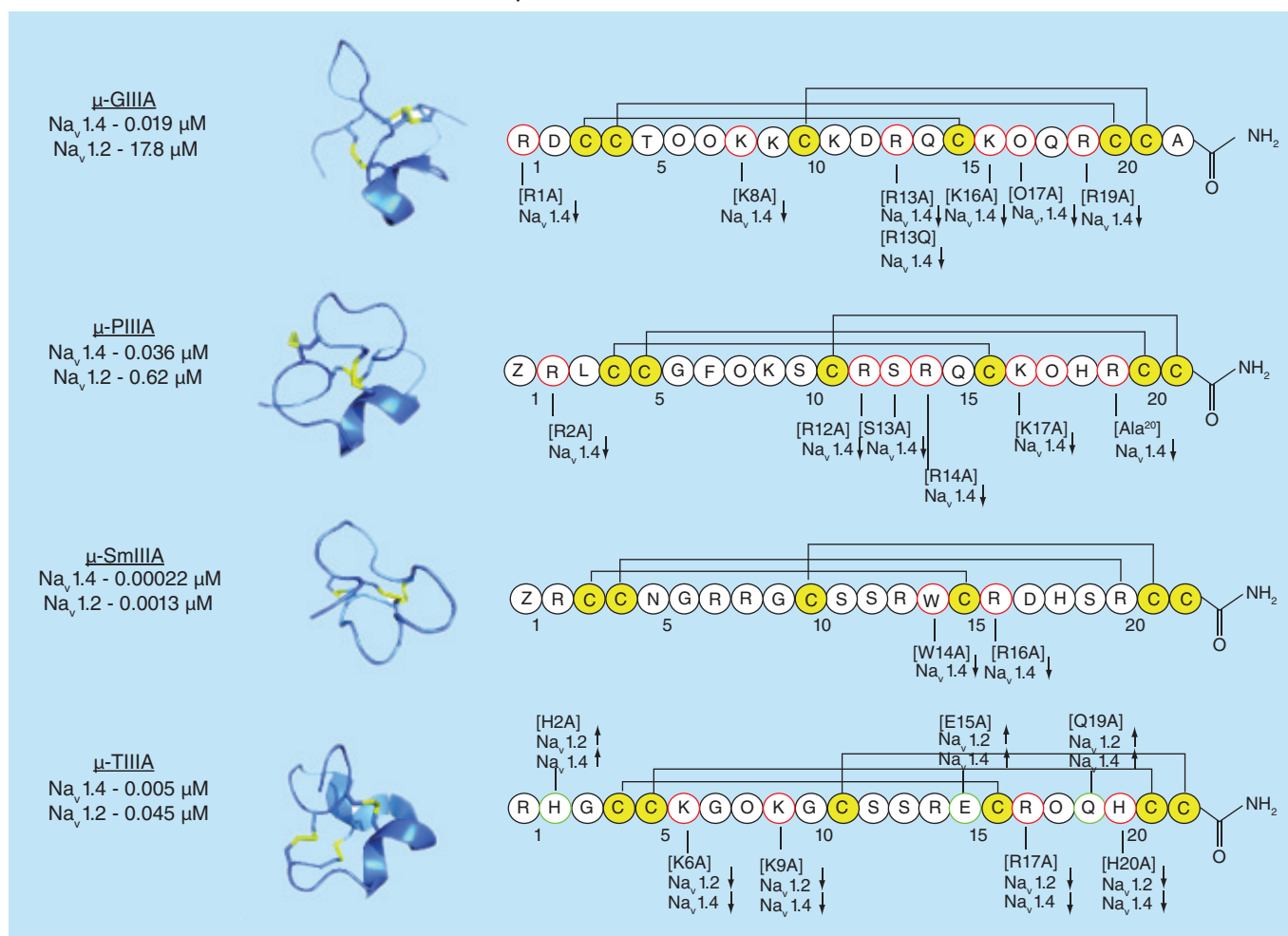


Figure 6. Structure–activity characterization of $\mu\text{-conotoxins}$. Potencies of characterized $\mu\text{-conotoxins}$ against skeletal ($\text{Na}_v1.4$) and neuronal ($\text{Na}_v1.2$) subtypes. Solution structures showing the folded peptide structures with disulfide connectivity. PDB ID# 1TCK ($\mu\text{-GIIIA}$), 1R9I ($\mu\text{-PIIIA}$), 1Q2J ($\mu\text{-SmIIIA}$), 2LXG ($\mu\text{-KIIIA}$) and 2LO9 ($\mu\text{-BullIB}$). BMRB Entry# 20024 ($\mu\text{-TIIIA}$) and 20023 ($\mu\text{-SIIIA}$). Results of individual amino acid replacements on Na_v1 -subtype blockade. (\uparrow) indicates mutations that improve potency against Na_v1 -subtypes, (\downarrow) denotes decreased potency and (\circ) represents no change in potency. (desZ1) indicates deletion of pyroglutamic acid in position 1 of $\mu\text{-SIIIA}$.

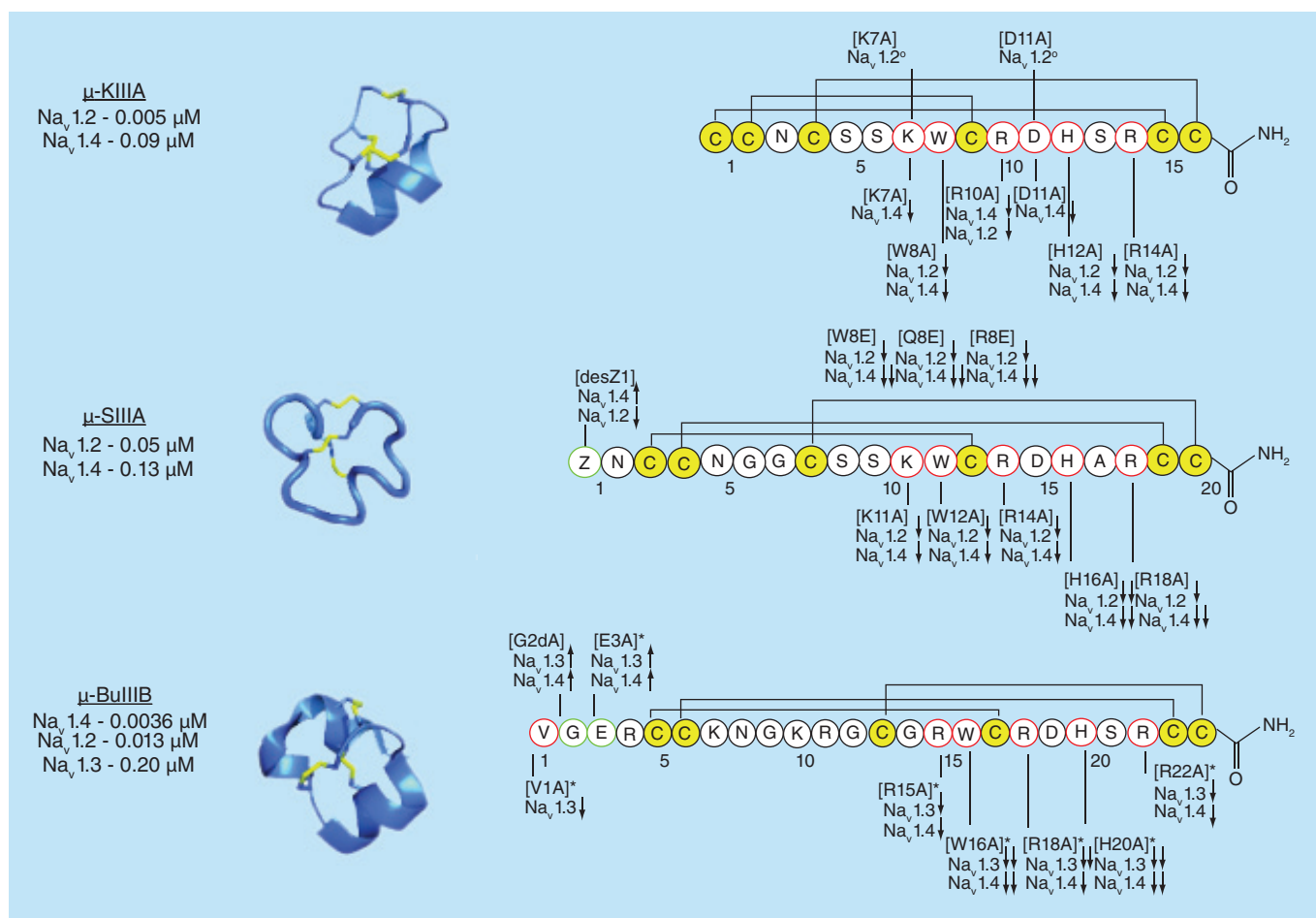


Figure 6. Structure–activity characterization of μ -conotoxins (cont.). Potencies of characterized μ -conotoxins against skeletal ($\text{Na}_v1.4$) and neuronal ($\text{Na}_v1.2$) subtypes. Solution structures showing the folded peptide structures with disulfide connectivity. PDB ID# 1TCK (μ -GIIIA), 1R9I (μ -PIIIA), 1Q2J (μ -SmIIIA), 2LXG (μ -KIIIA) and 2LO9 (μ -BullIB). BMRB Entry# 20024 (μ -TIIIA) and 20023 (μ -SIIIA). Results of individual amino acid replacements on Na_v1 -subtype blockade. (\uparrow) indicates mutations that improve potency against Na_v1 -subtypes, (\downarrow) denotes decreased potency and (*) represents no change in potency. (desZ1) indicates deletion of pyroglutamic acid in position 1 of μ -SIIIA.

Ala-substitution of basic residues (Lys7, Arg10, His12 and Arg14) influenced the affinity of and/or block by μ -KIIIA (Figure 6) [71]. Ala-substitution of His12 further improved the selectivity profile in favor of $\text{Na}_v1.2$, followed by $\text{Na}_v1.7$, and both were significantly preferred over $\text{Na}_v1.4$. A similar effect was observed in μ -KIIIA[R14A], with a complete shift in the selectivity profile ($\text{Na}_v1.7 > \text{Na}_v1.2 > \text{Na}_v1.4$). Alignment of the sequences of $\text{Na}_v1.2$, $\text{Na}_v1.4$ and $\text{Na}_v1.7$ subtypes showed that binding specificity was dependent upon interactions between Arg14 and Asp1241 of domain III of the outer ring of the P-loop. By mutating Arg14 to Ala, tight interactions with $\text{Na}_v1.2$ and $\text{Na}_v1.4$ were disrupted; it was hypothesized that the slow off-rates of μ -KIIIA ($k_{\text{off}} = 0.002 \text{ min}^{-1}$) were a consequence of these interactions [71]. Inspection of the h $\text{Na}_v1.7$ sequence revealed that the equivalent position within the P-loop of the channel contained Ile (Ile1410) rather than the Asp observed

in the neuronal and skeletal muscle subtypes. Using this information, future analogs may offer better discrimination between Na_v1 subtypes.

Disulfide-deficient KIIIA analogs were constructed based on the ‘canonical’ μ -conotoxin framework CysI–CysIV, CysII–CysV, CysIII–CysVI (Figure 4) [74]. Electrophysiology experiments revealed that the CysII–CysV and CysIII–CysVI disulfide pairs were most critical for Na_v1 -blockade [74]. The solution structures of these analogs showed that removal of the CysI–CysIV bridge resulted in greater N-terminal flexibility, but, did not disrupt the α -helical C-terminal region known to be important for biological activity [75]. Based on these findings, the [desC1]KIIIA[S3/4Aopn, C9A] analog was constructed, which lacked the CysI–CysIV bridge and replaced less-critical amino acid residues with an Aopn (5-amino-3-oxapentanoic acid) backbone spacer unit. This analog not only blocked $\text{Na}_v1.2$ with low nanomolar potency, but also exhibited

analgesic activity in a mouse model of inflammatory pain [74]. Recently, it has been shown that the disulfide connectivity for synthetic μ -KIIIA is different from that of previously described μ -conotoxins [68,76]. These results are discussed in greater detail below.

μ -Conotoxins from *Conus striatus*

μ -SIIIA and μ -SIIIB from the venom of *C. striatus* [51,77] differ from one another by only two amino acid residues within the third intercysteine loop (Arg14 and Asp15 in μ -SIIIA vs Lys14 and Gly15 in μ -SIIIB) (Figure 4). In *Xenopus* oocytes expressing Na_v1 -subtypes, μ -SIIIA displayed a threefold preference for $\text{Na}_v1.2$ over $\text{Na}_v1.4$ (0.05 vs 0.13 μM) [53]. Greater subtype discrimination was achieved through removal of the N-terminal pyroglutamate residue. For μ -SIIIA(2-20), affinity for $\text{Na}_v1.2$ was increased while that for $\text{Na}_v1.4$ was decreased, while the opposite was true for μ -SIIIB [77]. The importance of individual residues was assessed in μ -SIIIA(2-20) using an ^{125}I -TIIIA displacement assay against $\text{Na}_v1.2$ and $\text{Na}_v1.4$. Similar to μ -KIIIA, residues in the C-terminal helix were found to be most important for VGSC blockade. Alanine replacement of Lys11, Trp12, Arg14, His16 or Arg18 leads to the most pronounced effects on VGSC binding, with the majority of these mutations retaining preference for the neuronal subtype (Figure 6). Importantly, μ -SIIIA[H16A] exhibited a significant decrease in binding affinity for both neuronal and muscle subtypes, suggesting that this residue contributes to general Na_v1 binding.

Yao *et al.* undertook detailed structural analyses of μ -conotoxins that blocked neuronal VGSC subtypes (μ -SmIIIA, μ -SIIIA and μ -KIIIA) [78]. These peptides shared near sequence identity at the C-terminus but differed significantly from the C-termini of skeletal muscle preferring μ -conotoxins. In μ -SIIIA, residues 11–16 formed a well-defined helix, while residues 3–5 associated to form a 3_{10} -helix [78]. Dynamics measurements of μ -SIIIA made using ^{13}C NMR relaxation experiments showed that the N-terminus and Ser9 had larger magnitude motions on the subnanosecond timescale, while the C-terminus was more rigid. These data were interesting in light of functional data which suggested that the N-terminus was important for subtype selectivity, while the C-terminus contributed mainly to neuronal subtype interactions [78]. Schroeder *et al.* explored the structural and functional consequences of N-terminal modification of μ -SIIIA/B [67]. Replacement of the N-terminal pyroglutamate (Pyr1 or single letter code Z) with charged residues (i.e., μ -SIIIA[Z1R] and μ -SIIIB[Z1E]) either decreased (μ -SIIIA) or increased (μ -SIIIB) preference for $\text{Na}_v1.2$. Greater selectivity could also be obtained through extension of the N-terminus. The role of negatively-charged

residues at the N-terminus for $\text{Na}_v1.2$ subtype selectivity was further demonstrated by the μ -SIIIB analogs μ -SIIIB[E0, Z1R] and μ -SIIIB(22–0)[N2E], respectively. Extension of the C-terminus of μ -SIIIA[D15A], using charged amino acids, afforded greater selectivity for the neuronal subtype [67]; specifically, the μ -SIIIA analogs μ -SIIIA(2-21)[D15A, 21K] and μ -SIIIA(2-21)[D15A, 21D] showed improved discrimination between $\text{Na}_v1.2$ and $\text{Na}_v1.4$ [67].

The C-terminal regions of neuronal subtype preferring μ -conotoxins are highly homologous. However, the N-termini of these peptides have a decreasing number of residues in the first intercysteine loop across the series μ -SmIIIA > μ -SIIIA > μ -KIIIA. We previously investigated this region as a potential site for modification by flexible backbone spacer units such as 6-aminohexanoic acid (Ahx) and 3-oxapentanoic acid (PEG) with the goal of creating polymer-peptide hybrid analogs of μ -SIIIA with analgesic activity (e.g., polytides) [79]. At 25 μM , backbone spacer containing analogs of μ -SIIIA demonstrated approximately 80% block of TTX-sensitive sodium currents from mouse DRG neurons, compared with 65% block by wild-type μ -SIIIA. The μ -SIIIA polytide analogs produced not only increased block but also faster onset of action compared with the native peptide. These results provided further evidence that the μ -conotoxin scaffold could accommodate significant structural modifications and lent support to the concept of peptide engineering to enhance pharmacological properties. This work also demonstrated that μ -SIIIA analogs were potent analgesics in an *in vivo* pain model, with the most promising of the analogs (PEG-SIIIA) having higher potency of 0.05 mg/kg (μ -SIIIA = 0.9 mg/kg) following intraperitoneal administration [79].

μ -Conotoxins from *Conus consors*, *Conus catus* & *Conus magus*

In addition to a high degree of homology among the C-termini of μ -CnIIIA, μ -CnIIIB, μ -CIIIA and μ -MIIIA, these peptides also possess a characteristic Pro-Asn dipeptide in the first intercysteine loop (Figure 4) [80]. These peptides blocked sodium conductance of TTX-resistant Na_v1 in frog DRG neurons with varying potency and selectivity, with μ -CnIIIA (87% block – neuronal subtype selective) and μ -CIIIA (96% block – nonselective) being the most potent of this group. However, when tested in a mammalian system (mouse), μ -CnIIIA and μ -CIIIA blocked only weakly and lacked significant subtype selectivity [80]. μ -CnIIIA was nearly equipotent against neuronal and skeletal muscle subtypes (0.25 vs 0.27 μM). Likewise, μ -MIIIA showed poor discrimination between these two subtypes (0.45 vs 0.33 μM) (Figure 5) [53].

Recently, another μ -conotoxin from *C. consors* was reported by Favreau *et al.* [81]. This peptide was interesting in that the N-terminus of μ -CnIIIC was homologous to μ -TIIIA (loop 1), whereas the C-terminus resembled neuronal subtype-preferring conotoxins such as μ -KIIIA and μ -SIIIA in that μ -CnIIIC possesses a lysine in the equivalent position to Arg14 of μ -GIIIA (Figure 4). This peptide blocked $\text{Na}_v1.2$ ($\text{IC}_{50} = 1.3 \text{ nM}$) and $\text{Na}_v1.4$ (100% block at $1 \mu\text{M}$) with little or no effect on cardiac subtypes in HEK 293 cells. μ -CnIIIC also blocked the seemingly disparate nicotinic acetylcholine receptors (nAChR) $\alpha3\beta2$ subtype and inhibited global nerve action potentials from sciatic and olfactory nerves with slow reversibility [81]. The authors suggested that the effects of μ -conotoxins on nAChR targets responsible for the modulation of pain signals may be more widespread than originally thought, perhaps offering a potential new molecular target for these potent analgesic compounds [81].

μ -Conotoxins from *Conus bullatus*

Three μ -conotoxins (μ -BuIIIA, μ -BuIIIB and μ -BuIIIC) from the venom of *C. bullatus* blocked $\text{Na}_v1.4$ with near irreversibility [59]. These peptides had an extended N-terminus and a shorter second inter-cysteine loop compared with previously described μ -conotoxins (Figure 4). Wilson *et al.* determined the subtype-selectivity profiles for μ -BuIIIA and μ -BuIIIB and confirmed that $\text{Na}_v1.4$ was the preferred target, followed by $\text{Na}_v1.2$ and $\text{Na}_v1.3$ (Figure 5) [53].

Thus far, the μ -conotoxins in this review have been compared for their abilities to block either neuronal ($\text{Na}_v1.2$) or skeletal muscle ($\text{Na}_v1.4$) subtypes. However, μ -BuIIIB is also a potent inhibitor of $\text{Na}_v1.3$ (Figure 5) [53]. The exact pharmacological role of this subtype remains to be confirmed, but studies by Haines *et al.* demonstrated upregulation of $\text{Na}_v1.3$ following peripheral nerve axotomy, implicating this subtype as a potential target for the treatment of neuropathic pain [82,83]. Moreover, there are currently no selective probes of this channel subtype, making μ -BuIIIB an attractive lead compound to study $\text{Na}_v1.3$. Recent studies have focused on determination of interactions between μ -BuIIIB and $\text{Na}_v1.3$ [84,85]. The solution structure was determined by Kuang *et al.* [84] and it was hypothesized that the signature characteristics (an N-terminal extension and differences in inter-cysteine loop sizes) might contribute to the block of $\text{Na}_v1.3$ [84].

Ala-replacement of the N-terminal residues of μ -BuIIIB influenced its potency but not its selectivity (Figure 6). Substitution of either Gly2 or Glu3 resulted in significant improvements to $\text{Na}_v1.3$ potency. Importantly, substitution of Gly2 with D-Ala resulted

in a μ -BuIIIB analog with greater than 40-fold higher potency for $\text{Na}_v1.3$, presumably through stabilization of a type II β -turn at the N-terminus [84]. Interestingly, complete removal of the N-terminal extension still resulted in a fourfold improvement in the block of $\text{Na}_v1.3$ over wild-type μ -BuIIIB [84]. Despite the gains in potency, selectivity for $\text{Na}_v1.3$ was not generated. These observations suggested, however, that further SAR studies of μ -BuIIIB would be valuable in order to identify the key structural components involved in $\text{Na}_v1.3$ blockade.

Detailed SAR of μ -BuIIIB has been largely inhibited by synthetic inaccessibility owing to its propensity to form numerous folding isoforms during oxidative folding. A strategy was therefore devised that directed folding toward a single bridging pattern through incorporation of a diselenide bridge and disulfide bridge removal (Figure 7). The rationale for this strategy lies in two previous reports on μ -conotoxin KIIIA [72,74]. A disulfide-deficient, diselenide-containing scaffold was constructed in which Cys5 and Cys17 were replaced with selenocysteine and the Cys6–Cys23 pairing was removed by alanine substitution (i.e., ddSecBuIIIB) [85]. These studies provided valuable insight into which amino acids contributed to block of the $\text{Na}_v1.3$ subtype. Similar to the other μ -conotoxins, residues near the C-terminus of μ -BuIIIB were most important for Na_v1 block (Figure 6). In ddSecBuIIIB, the aromatic residues Trp16 and His20 were shown crucial for $\text{Na}_v1.3$ inhibition, with alanine-substituted analogs having K_d values of $>30 \mu\text{M}$ each, compared with $0.2 \mu\text{M}$ for wild-type μ -BuIIIB [85].

The highly basic character of μ -conotoxins is thought to contribute to their activity in the negatively charged pore of VGSCs. Early reports highlighted the critical role of a single basic residue near the C-terminus of μ -conotoxins (e.g., [μ -GIIIA[Arg13]]) for VGSC blockade [56,57]. Ala substitution of Arg15, Arg18 or Arg22 in ddSecBuIIIB resulted in K_d values of 1.84, 15.7 and $3.81 \mu\text{M}$, respectively [85]. Interestingly, the most ‘critical’ of these basic residues was not located at the position equivalent to Arg13 in μ -GIIIA. Instead, multiple basic residues were shown to be important for activity (Figure 6), consistent with models previously constructed by McArthur *et al.* using μ -PIIIA [71].

Key term

Selenocysteine: Often referred to as the 21st proteinogenic amino acid, selenocysteine is an isosteric replacement for cysteine. In selenocysteine, the sulfur-containing thiol of cysteine is replaced by a selenium-containing selenol.

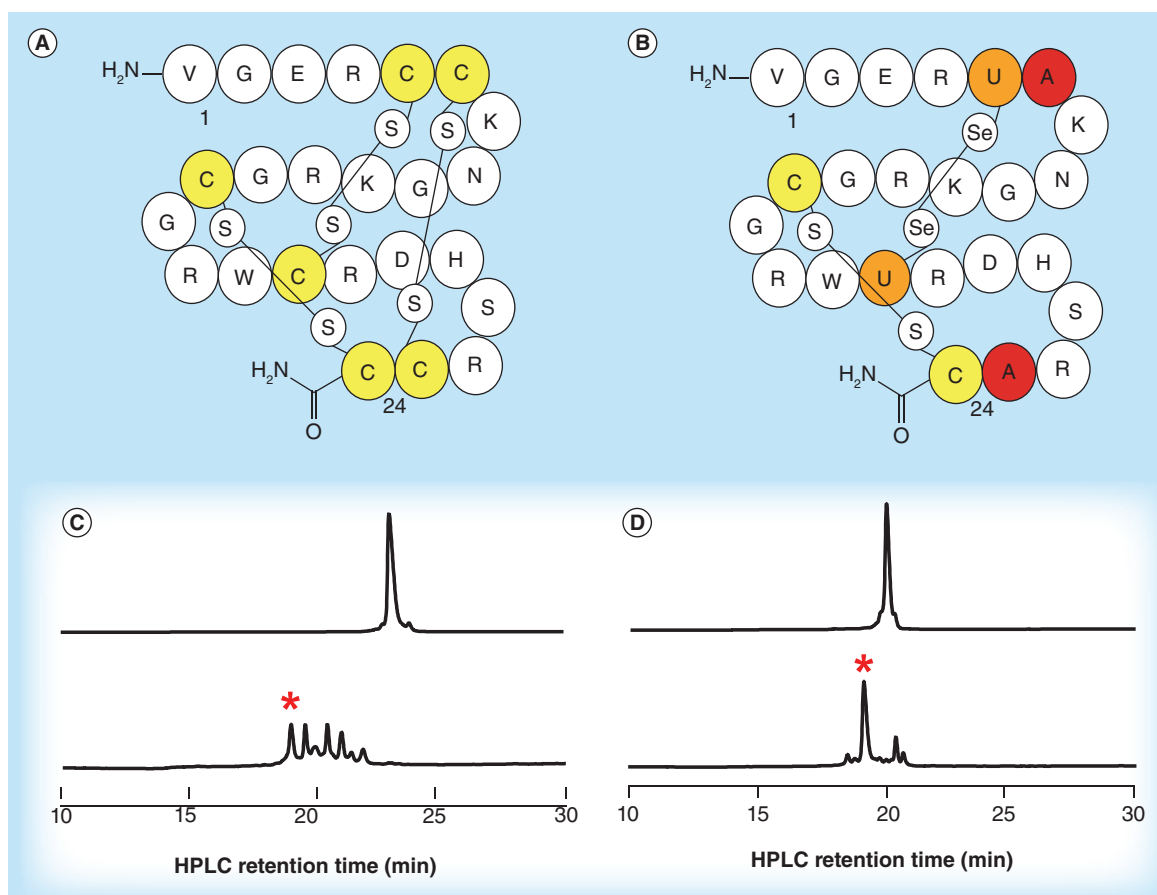


Figure 7. Description of the ddSec strategy used to facilitate structure–activity relationship studies of μ -BullIIB. (A) Cartoon depiction of μ -BullIIB showing disulfide connectivity between cysteine thiols. (B) Cartoon of ddSecBullIIB scaffold with disulfide depletion by removal of the Cys6–Cys23 bridge and diselenide bridge formation by selenocysteine replacement of Cys5 and Cys17. (Panels C and D) Upper and lower chromatograms show linear and folded elution patterns of μ -BullIIB (C) and ddSecBullIIB (D), respectively. *Indicates the properly folded isoform. Positional scanning of all noncysteine residues was subsequently performed using the ddSecBullIIB scaffold. Reproduced with permission from [85] © 2014 FEBS.

The ddSecBullIIB analog also served to identify residues for which Ala-substitution did not greatly affect biological activity (e.g., Val1, Gly2, Asn8, Gly14 and Ser21), suggesting these positions as possible sites for chemical modification to achieve enhanced pharmacological/physicochemical properties [85]. The most striking outcome of these studies was that the substitution of Glu3 increased $\text{Na}_v1.3$ potency ($K_d = 0.07 \mu\text{M}$). These findings were in agreement with the report by Kuang *et al.*, which suggested that the negative charge of Glu3 may result in unfavorable interactions with $\text{Na}_v1.3$ [84]. Current efforts are directed at modifying the above-mentioned positions, particularly position 3, with the goal of developing potent and selective inhibitors of $\text{Na}_v1.3$.

Disulfide connectivity in μ -conotoxins

Disulfide bridges serve to stabilize the global structure of conotoxins [86]. With three disulfide pairs, μ -conotoxins have the potential to form up to 15

distinct structural isomers. Some of these conformations will be naturally selected against because they are energetically disfavored, but ‘noncanonical’ isoforms do occur and may be observed in some abundance even upon reaching folding equilibrium. Following oxidation of the fully reduced peptide, the species found in highest abundance within the folding mixture has traditionally been assumed to be the native fold, although this has not been confirmed in most cases.

Until recently, the disulfide connectivity of all Na_v1 -targeting μ -conotoxins within the m4 and m5 branches of the M-superfamily (Figure 4) was assumed to be the same (CysI–CysIV; CysII–CysV; CysIII–CysVI). A recent report by Tietze *et al.* showed that three major folding isoforms, with differing disulfide connectivities, resulted from the direct oxidation of synthetic μ -PIIIA, namely, μ -PIIIA-1 (CysI–CysV; CysII–CysVI; CysIII–CysIV), μ -PIIIA-2

(CysI–CysIV; CysII–CysV; CysIII–CysVI) and μ -PIIIA-3 (CysI–CysII; CysIII–CysIV; CysV–CysVI) [87]. All three isoforms were shown to block $\text{Na}_v1.4$, albeit with different potencies: $\text{IC}_{50}\mu$ -PIIIA-1 = 46.7 nM, $\text{IC}_{50}\mu$ -PIIIA-2 = 103.2 nM and $\text{IC}_{50}\mu$ -PIIIA-3 = 203.7 nM [87]. These results showed that the ‘canonical’ disulfide bridging pattern for μ -PIIIA did not result in the most potent folding isoform [87]. Molecular dynamics simulations of each isoform in this study showed that the side-chain of Arg14 in μ -PIIIA-1 penetrated deeper into the binding pore, presumably contributing to the increased potency of this isomer [87].

Another study re-examined the ‘canonical’ μ -framework of μ -KIIIA [76]. Poppe *et al.* noted that, because through-bond scalar couplings between the two sulfur atoms are undetectable by NMR, interactions are typically inferred based on interproton distance constraints. To circumvent this problem, they developed a method known as the pattern of disulfides from local constraints (PADLOC) and suggested an alternative connectivity for the native fold of μ -KIIIA (CysI–CysV; CysII–CysIV; CysIII–CysVI) [76]. This was recently confirmed by Khoo *et al.*, who isolated the major folding oxidation products of synthetic μ -KIIIA and studied connectivity by collision-induced dissociation MS [68,88]. This confirmed the connectivity of the major folding isoform and determined the connectivity of the isomer in the next highest abundance as CysI–CysVI; CysII–CysIV; CysIII–CysV, neither of which matched the assumed connectivity for μ -conotoxins reported previously. Whether these connectivities are a consequence of the unique structural features of this peptide (μ -KIIIA has only a single residue between CysII and CysIII), or an indication of greater toxin diversity within the μ -conotoxin family remains to be determined. An intriguing possibility is that *Conus* produces multiple active folding isoforms to increase its toxin repertoire.

A recent study by Safavi-Hemami *et al.* [89] provided evidence for the presence of both the globular (CysI–CysIII; CysII–CysIV) and ribbon (CysI–CysIV; CysII–CysIII) forms of α -conotoxin ImI in the venoms of *Conus imperialis* [89]. Pharmacological studies have traditionally focused on the activities of the globular form, assuming this to be the native disulfide connectivity. However, the authors point out that in numerous cases (e.g., α -AuIB), it is actually the ribbon form that elicits the greatest biological effect [89,90]. Although these studies emphasized the presence of multiple folding isoforms of α -conotoxins, it is conceivable that multiple ‘noncanonical’ isomers of μ -conotoxins are also present in venom. In light of this, an in-depth re-examination

of μ -conotoxin connectivities would be beneficial, particularly for the remaining members of the m4 branch and for toxins belonging to the more recently described m5 branch.

Influence of $\text{Na}_v\beta$ subunit expression on μ -conotoxin activities

In vivo, VGSCs comprise both a pore-forming α -subunit (260 kDa) and one or more accessory sodium channel β -subunits (32–36 kDa) (Figure 1) [91]. To date, four β -subunit subtypes have been identified ($\text{Na}_v\beta1$ – $\text{Na}_v\beta4$). The odd-numbered subtypes ($\beta1$ and $\beta3$) associate with the α -subunit via noncovalent interactions whereas $\beta2$ and $\beta4$ subtypes are covalently linked to the α -subunit via disulfide bridges [92]. Despite these interactions, the α -subunit, which possesses the minimal essential features of a fully functioning VGSC, has traditionally been used to measure the effects of sodium channel agonists or antagonists in electrophysiology assays. However, co-expression of the β -subunit with the α -subunits influenced the steady-state activation of $\text{Na}_v1.8$ -subtypes expressed in *Xenopus* oocytes, suggesting a more significant role of the β -subunit in channel activation [91]. Furthermore, the β -subunits are of interest because expression levels are altered following spinal cord injury in multiple animal models [91].

Wilson *et al.* showed that co-expression of $\text{Na}_v1.8$ with any of the four β -subunits resulted in higher affinity block by $\mu\text{O-MrVIB}$, resulting from an increased k_{on} and modest decreases in k_{off} [93]. Most recently, Zhang *et al.* reported the importance of these accessory proteins with respect to the activities of a number of μ -conotoxins [94]. The binding kinetics of μ -conotoxins PIIIA, TIIIA, KIIIA and SmIIIA were examined by two-electrode voltage-clamp electrophysiology in *Xenopus* oocytes co-expressing Na_v1 with one of the four β -subunits. The key findings of this work were that co-expression of the $\beta1$ or $\beta3$ subunits in the presence of the Na_v1 α -subunit increased the on-rates (k_{on}) of μ -conotoxins, whereas k_{on} was dramatically

Key terms

Sodium channel β -subunit ($\text{Na}_v\beta$): Accessory proteins associated with the α -subunit by either noncovalent ($\text{Na}_v\beta1$ or $\beta3$) or covalent ($\text{Na}_v\beta2$ or $\beta4$) interaction. These subunits modulate channel gating, regulate VGSC trafficking/expression and promote cell adhesion/migration; $\text{Na}_v\beta$ -subtypes can also modulate biological activities of venom-derived toxins.

Two-electrode voltage-clamp electrophysiology:

A method that assesses the effects of ligands on heterologously expressed VGSCs, typically in *Xenopus* oocytes. Kinetics of block are measured by changes in ionic current resulting from Na^+ flow-through VGSCs.

decreased in the presence of either $\beta 2$ or $\beta 4$ with $\text{Na}_v 1$. Conversely, little or no effect was observed upon treatment of the same system with either of the alkaloid toxins TTX or STX [94]. These results highlight the importance of β -subunits in obtaining a complete and physiologically relevant assessment of engineered subtype-selective blockers based on μ -conotoxins.

Analgesic activities of μ -conotoxins

Discovery of so-called 'neuronal-preferring' μ -conotoxins encouraged exploration of these compounds in pain models. Three reports have documented the abilities of the neuronal subtype-preferring conotoxins μ -KIIIA and μ -SIIIA to suppress nociception in animal models [69,74,79]. In all instances, compounds were tested in the formalin-induced pain assay in mice following intraperitoneal administration. In this assay, μ -KIIIA was effective in suppressing paw-licking times during the Phase II nociceptive response (inflammatory pain) with a calculated ED_{50} of 0.1 mg/kg [69]. Similarly, μ -SIIIA and its analogs were shown to be analgesic in this model with an ED_{50} of 0.9 mg/kg. The analog in which noncritical residues were replaced with a PEG backbone spacer, possessed an ED_{50} of 0.05 mg/kg [79]. These results exemplified the relative ease by which peptidic scaffolds can be modified to engineer in enhanced pharmacological and physicochemical properties. Analgesic effects were also observed with the minimized peptide analog des[C1]KIIIA[S3/4Aopn, C9A], where intraperitoneal administration of 10 nmol resulted in a 54% decrease in the inflammatory pain response compared with the saline control [74]. Despite these encouraging results, further work is necessary to transform neuronal-subtype preferring μ -conotoxins into analgesic drug leads.

Future perspective

Accelerating the pace of μ -conotoxin discovery & development

A very small fraction (< 1%) of the total complement of neuroactive peptides in *Conus* venoms has been identified to date, let alone characterized [95]. The discovery of new conotoxins has traditionally relied on bioassay-directed fractionation of whole venoms, followed by sequencing of individual peptide components [96], and this approach has been responsible for the discovery of nearly all μ -conotoxins described to date. However, assay-driven identification of large numbers of unique toxin sequences is impractical because it is often labour intensive, time consuming and costly. New methodologies such as transcriptomics [12,96,97] and proteomics/peptidomics [98,99] are already accelerating the pace at which novel peptide sequences are discovered and characterized. Proteomic/peptidomic approaches can

be effective when coupled to other methods such as *de novo* sequencing. However, transcriptomics alone is not a viable option for the identification of new μ -conotoxins because of a higher propensity for base call errors (compared with traditional sequencing methods) and an inability to identify post-translationally modified residues, which are common in *Conus* toxins [100]. The most effective means for identifying new toxins from *Conus* venoms lies in the combination of the above-mentioned technologies with high-resolution MS [101,102]. In a recent article, Prashanth *et al.* suggested that the combination of transcriptomic and peptidomic methods, in conjunction with bioinformatics, could lead to the construction of large, searchable repositories for important sequence data [100]. Recently, such an approach was employed to identify new toxins and toxin families in the venoms of *C. consors* [11], *C. flavidus* [103] and *C. marmoreus* [102].

Future research on μ -conotoxin research will increasingly involve a combination of transcriptomic/proteomic approaches and high-throughput screening methods for the correlation of biological activities with new sequence information. Traditionally, determination of the biological activity of a newly identified conotoxin relied on patch-clamp or voltage-clamp electrophysiology assays, the major drawback of which is the inability to screen large numbers of peptide against multiple molecular targets. Calcium imaging studies employing Ca^{2+} -sensitive dyes to study the effects of conotoxins against their molecular targets [104,105] have proven to be highly amenable to implementation in high-throughput screening assays, as discussed in [100].

Another issue faced in the study and development of conotoxin-based drugs is one of production. Ideally, bacterial or yeast expression systems would help to solve this problem, but the abundance of post-translational modifications in these peptides has made these approaches particularly challenging [86,106]. Furthermore, the reducing environment of the bacterial cytoplasm commonly results in misfolded forms of the peptide or sequestration to inclusion bodies [107]. Peptides can be recovered from the insoluble fraction, but misfolded peptides must undergo reduction and *in vitro* oxidative refolding to obtain the final product [107]. Recent advances in recombinant methods have shown promise in addressing issues of misfolded conotoxin isoforms and have proven useful for sequences that draw from the naturally occurring 20 amino acid repertoire [107,108]. However, a major impediment to large-scale expression of conotoxins still remains, that being the inability of recombinant expression systems to 'decorate' the primary sequence with PTMs commonly found in conotoxins. Several enzymes responsible for such modifications have been identified in *Conus* and, in the future it may be fea-

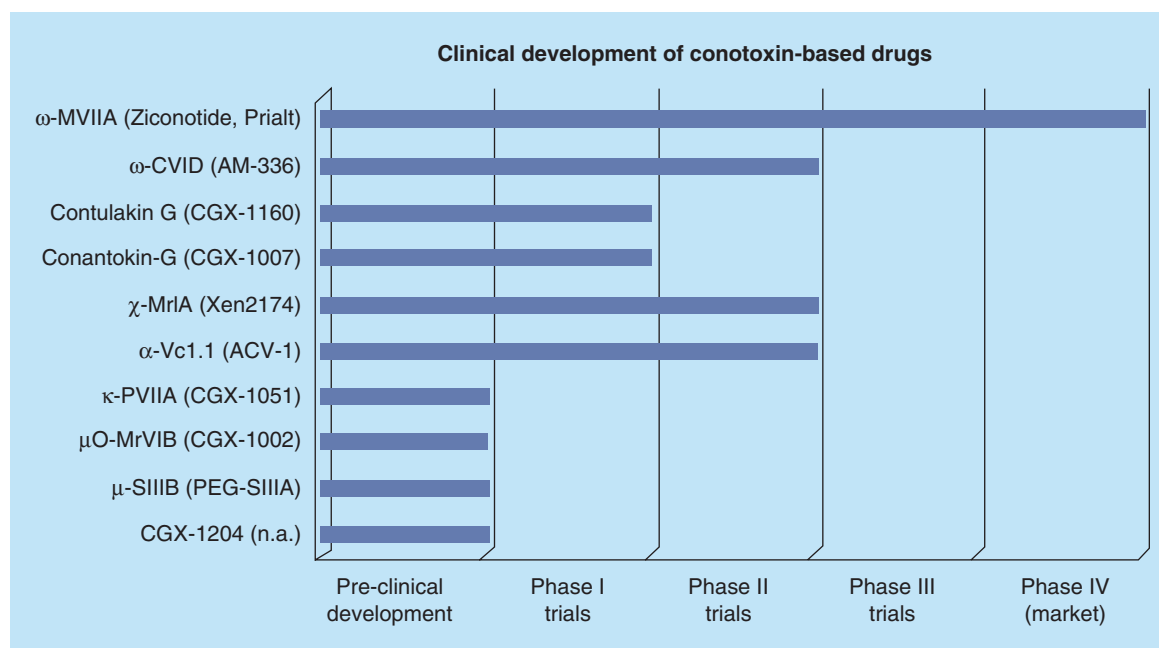


Figure 8. Conotoxins at various stages of preclinical and clinical development.

n.a.: Not available

Data taken from [9,132].

sible to modify recombinantly expressed peptide with such enzymes [109–111]. In the meantime, synthetic approaches such as solid-phase peptide synthesis remain the more practical approach to synthesis of conotoxins for structural or functional characterization.

Synthetic approaches for producing conotoxins have been largely dependent on solid-phase peptide synthesis using Fmoc or Boc chemistries. As new chemistries are developed, the pace at which new conotoxin sequences can be produced is expected to increase. A major issue in synthesizing conotoxins is ensuring proper cyclization patterns. Early efforts focused on stepwise oxidation of Cys thiols using trityl (Trt), acetamidomethyl (Acm) or other orthogonal protecting groups to direct folding to a major isoform [112]. The major drawback to this approach is the requirement for multiple purification steps, resulting in decreased yields of the fully folded product. Recently, proxies for disulfide bridges such as dicarba- [113,114], diselenide- [115–117] or thioether bridges [118] have been developed. A significant advantage of these methods is the independent formation of macrocycles either on-resin or following cleavage from solid support without additional purification steps.

An incomplete understanding of the interactions between μ -conotoxins and their molecular targets (i.e., VGSCs) has made the rational design of peptide analogs with improved pharmacological action challenging. Early studies of interactions between μ -conotoxins and Na_v1 -subtypes were almost entirely reliant on mutational studies [71,119].

However, computational studies and the emergence of bacterial sodium channel models are anticipated to increase the rate at which potent and selective blockers of VGSCs can be developed. Such studies can provide useful information about subtle interactions between the toxin and the channel that may lead to improved pharmacology. A recent example of how computational studies can aid in the design of potent peptide analogs can be found in a publication describing mutants of the *Stichodactyla helianthus* potassium channel-blocking toxin ShK, which were designed on the basis of modeling and docking studies and exhibited improved selectivity for $\text{K}_v1.3$ [120]. Unfortunately, in the absence of accurate models of human VGSCs, similar studies with μ -conotoxins have not been possible to date. The earliest modeling studies docked μ -GIIIA to a skeletal muscle VGSC model based upon the potassium channel and available mutational data [119]. These studies were valuable in defining the binding orientation of μ -GIIIA in the pore region of Domain II and they highlighted the importance of interactions between positively-charged μ -conotoxins and the negatively charged outer ring of the pore vestibule [119].

Recent crystal structures of bacterial VGSCs have provided another opportunity to discover important interactions between VGSCs and their ligands. In 2005, Pavlov *et al.* confirmed the critical role of the pore region for channel blockade using NaChBac, a prokaryotic VGSC [121]. The NaChBac model was useful from

the perspective of being a simplified VGSC structure that possessed multiple common features to eukaryotic VGSCs, but showed greater sequence similarity to calcium channels than sodium channels [121]. Recently, the crystal structures of a number of prokaryotic sodium channel orthologs have provided valuable insights into the structure and function of VGSCs [21,122]. These structures may eventually yield structural information to help in the design of μ -conotoxin analogs with improved VGSC potency and/or selectivity. Payandeh *et al.* reported the crystal structure of a bacterial sodium channel (Na_vAb) in its closed conformation in 2011 [21,123]. This structure helped explain the intrinsic selectivity of VGSCs for Na^+ ions and how these ions are translocated across the membrane. It also aided in the understanding and interpretation of previous SAR data since the pore regions of Na_vAb and the corresponding regions in vertebrate VGSCs share a significant degree of sequence homology [21]. Shortly after the first studies of Na_vAb , McCusker *et al.* reported the crystal structure of the pore domain of another prokaryotic VGSC, Na_vMs [122], which differed from Na_vAb in that it was in an open conformation. The open state of Na_vMs resembled the closed conformation of Na_vAb in that the selectivity filters appeared similar, but a major difference between the two structures was observed in the fenestrations within the transmembrane region. Na_vMs exhibits a much wider opening, suggesting that it may be able to accommodate large, hydrophobic pore-blocking drugs in the open state [122]. These models also differed in their putative mechanisms of

sodium conductance across the membrane. Although significant differences exist between prokaryotic and eukaryotic VGSC subtypes (i.e., lack of tetrameric symmetry, differences in amino acid composition and selectivity filter loop size), elucidation of bacterial sodium channel structures has served as a valuable starting point from which interactions of VGSC subtypes and their ligands (i.e., μ -conotoxins) can be understood [124]. Computational studies using these structures [124,125] are expected to result in more accurate depictions of channel–ligand interactions than those based on other ion channel families.

μ -conotoxins as pharmacological tools & drug leads for the treatment of pain

The μ -conotoxins are interesting not only from the perspective of identifying potent therapeutic leads, but also as scaffolds upon which novel functionalities may be presented. SAR studies on disulfide-rich peptides have identified single amino acids or short di- or tri-peptide segments between Cys-residues that can be removed or replaced without diminishing biological activity. Short peptide sequences have been ‘grafted’ into such regions of the ‘knottin’ peptides to generate powerful tumor imaging agents [126] or peptide analogs with additional therapeutic potential [127]. The μ -conotoxins are extremely hypervariable in these loop regions and, as such, are well suited for such studies. This hypervariability also makes these molecules ideal candidates for directed evolution experiments using scaffold-constrained random libraries in a manner described

Executive summary

Background

- Voltage-gated sodium channels (VGSCs) represent an attractive target for the treatment of neuropathic pain, epilepsy and a number of neurological disorders.
- More than 20 μ -conotoxins have been described to date, many with distinct selectivity profiles for VGSC subtypes in the CNS or PNS.

μ -Conotoxin inhibitors of VGSCs

- Early work identified μ -conotoxins that were selective for skeletal muscle subtypes and have been valuable in determining the structure and function of VGSCs.
- Neuronal subtype preferring μ -conotoxins have been important for discrimination of VGSC subtypes and for exploration as potential analgesics.
- Structure–activity relationship studies have identified critical residues in various μ -conotoxins as a basis for enhancing potency and/or selectivity.

Applications of μ -conotoxin inhibitors of VGSCs

- Muscle-preferring μ -conotoxins have been important for the study of VGSCs; these peptides may also be useful as myorelaxant drugs when administered focally.
- Neuronal subtype-preferring μ -conotoxins have shown analgesic activity and may be useful as treatments for pain, epilepsy or other neurological disorders.

Future perspectives

- The complexity of the more than 50,000 *Conus* venom peptides highlights the potential for discovery of numerous therapeutic peptides, including new μ -conotoxins.
- Differences in subtype-selectivity, in addition to the amenability of the μ -conotoxin scaffold to chemical modification, are expected to yield useful pharmacological probes in addition to potential drug leads.

in [128]. Another promising application of μ -conotoxins is bioconjugation with small molecule VGSC inhibitors for increased analgesic effect. Sata *et al.* have shown that neurosteroids such as allopregnanolone sulfate and endocannabinoids such as anandamide can inhibit pain-relevant Na_v1 -subtypes expressed in *Xenopus* oocytes [129,130]. Coupling of these molecules to μ -conotoxin scaffolds could conceivably generate peptide analogs with enhanced analgesic activity. Moreover, such peptides may display the target specificity that is often lacking in small molecule inhibitors.

The μ -conotoxins are clearly valuable pharmacological tools for identifying different Na_v1 -subtypes in neuronal membrane preparations [53]. The differences in selectivity profiles among this family have most recently allowed for examination of specific TTX-sensitive Na_v1 -subtypes in small and large DRG and superior cervical ganglion neurons [131]. It is anticipated that μ -conotoxins will continue to be used in these types of studies and that they will have prominent roles in probing the structure and function of VGSC subtypes in the future.

Several conotoxin-derived therapeutics are currently in various stages of preclinical or clinical evaluation (Figure 8). The development of μ -conotoxins has focused largely on identifying peptides that act as potent analgesics through inhibition of pain-relevant Na_v1 -subtypes in the periphery [71,85]. However, blockade of the muscle subtype $\text{Na}_v1.4$, long viewed as an undesirable characteristic of many μ -conotoxins, may in fact have clinical applications, as suggested by a recent report on μ -CnIIIC highlighting such inhibitors as potential myorelaxant drugs [81].

References

Papers of special note have been highlighted as:

• of interest; •• of considerable interest

- 1 Kaspar AA, Reichert JM. Future directions for peptide therapeutics development. *Drug Discov. Today* 18(171–178), 8078–9017 (2013).
- 2 Osborne R. Fresh from the biotech pipeline-2012. *Nat. Biotechnol.* 31(2), 100–103 (2013).
- 3 Tricoci P, Newby LK, Kandzari DE, Harrington RA. Present and evolving role of eptifibatid in the treatment of acute coronary syndromes. *Expert Rev. Cardiovasc. Ther.* 5(3), 401–412 (2007).
- 4 Warkentin TE, Koster A. Bivalirudin: a review. *Expert Opin. Pharmacother.* 6(8), 1349–1371 (2005).
- 5 Pope JE, Deer TR. Ziconotide: a clinical update and pharmacologic review. *Expert Opin. Pharmacother.* 14(7), 957–966 (2013).
- 6 Bhavsar S, Mudaliar S, Cherrington A. Evolution of exenatide as a diabetes therapeutic. *Curr. Diabetes Rev.* 9(2), 161–193 (2013).
- 7 King GF. Venoms as a platform for human drugs: translating toxins into therapeutics. *Expert Opin. Biol. Ther.* 11(11), 1469–1484 (2011).
- 8 Norton RS, Olivera BM. Conotoxins down under. *Toxicol.* 48(7), 780–798 (2006).
- 9 Han TS, Teichert RW, Olivera BM, Bulaj G. Conus venoms - a rich source of peptide-based therapeutics. *Curr. Pharm. Des.* 14(24), 2462–2479 (2008).
- 10 Vetter I, Lewis RJ. Therapeutic potential of cone snail venom peptides (conopeptides). *Curr. Top. Med. Chem.* 12(14), 1546–1552 (2012).
- 11 Violette A, Biass D, Dutertre S *et al.* Large-scale discovery of conopeptides and conoproteins in the injectable venom of a fish-hunting snail using a combined proteomic and transcriptomic approach. *J. Proteomics* 75(17), 5215–5225 (2012).
- 12 Hu H, Bandyopadhyay PK, Olivera BM, Yandell M. Elucidation of the molecular envenomation strategy of the cone snail *Conus geographus* through transcriptome sequencing of its venom duct. *BMC Genomics* 13, 1–12 (2012).

The intrinsic specificity of μ -conotoxins toward VGSCs, coupled with the fact that these peptides are amenable to chemical modification, makes these molecules an attractive alternative to currently used small molecule inhibitors of VGSCs. Modification of peptide scaffolds, either through amino acid substitution or by incorporation of nonnatural chemical motifs, has resulted in peptide analogs with improved pharmacological properties. These modifications have been underpinned by detailed structural and pharmacological studies. Furthermore, it has been estimated that fewer than 1% of all conotoxins have been pharmacologically characterized to date [133], which provides some perspective on the enormous potential of conotoxins, including the μ -conotoxins, as an emerging class of novel pharmaceutical tools.

Acknowledgements

The authors wish to thank D Yoshikami for numerous conversations integral to this work and BM Olivera for generous support and discussions.

Financial & competing interests disclosure

RS Norton acknowledges fellowship support from the NHMRC. This work was also supported by the National Institutes of General Medical Sciences, National Institutes of Health [Grant GM48677]. The authors have no other relevant affiliations or financial involvement with any organization or entity with a financial interest in or financial conflict with the subject matter or materials discussed in the manuscript apart from those disclosed.

No writing assistance was utilized in the production of this manuscript.

- 13 Olivera BM. Conus Snail Venom Peptides. In: *The Handbook of Biologically Active Peptides*. Kastin AJ (Ed.). Academic Press, Waltham, MA, USA, 381–388 (2006).
- 14 Carstens BB, Clark RJ, Daly NL, Harvey PJ, Kaas Q, Craik DJ. Engineering of conotoxins for the treatment of pain. *Curr. Pharm. Des.* 17(38), 4242–4253 (2011).
- 15 Puillandre N, Koua D, Favreau P, Olivera BM, Stöcklin R. Molecular phylogeny, classification and evolution of conopeptides. *J. Mol. Evol.* 74(56), 297–309 (2012).
- 16 Norton RS. μ -conotoxins as leads in the development of new analgesics. *Molecules* 15(4), 2825–2844 (2010).
- 17 Leipold E, Debie H, Zorn S *et al.* μ O-Conotoxins inhibit Na_v channels by interfering with their voltage sensors in domain-2. *Channels (Austin)* 1(4), 253–262 (2007).
- 18 Gajewiak J, Azam L, Imperial J *et al.* A disulfide tether stabilizes the block of sodium channels by the conotoxin $\mu\text{O}\xi$ -GVIIJ. *Proc. Natl Acad. Sci. USA* 111(7), 2758–2763 (2014).
- 19 Knapp O, McArthur JR, Adams DJ. Conotoxins targeting neuronal voltage-gated sodium channel subtypes: potential analgesics? *Toxins (Basel)* 4(11), 1236–1260 (2012).
- A detailed review of the structure and function of voltage-gated sodium channels.
- 20 Catterall WA. Voltage-gated sodium channels at 60: structure, function and pathophysiology. *J. Physiol.* 590(Pt 11), 2577–2589 (2012).
- First report of the crystal structure of a voltage-gated sodium channel.
- 21 Payandeh J, Scheuer T, Zheng N, Catterall WA. The crystal structure of a voltage-gated sodium channel. *Nature* 475(7356), 353–358 (2011).
- 22 Yu FH, Catterall WA. Overview of the voltage-gated sodium channel family. *Genome Biol.* 4(3), 207.201–207.207 (2003).
- 23 Waxman SG, Dib-Hajj S, Cummins TR, Black JA. Sodium channels and pain. *Proc. Natl Acad. Sci. USA* 96(14), 7635–7639 (1999).
- 24 Gilchrist J, Dutton S, Diaz-Bustamante M *et al.* $\text{Na}_v1.1$ modulation by a novel triazole compound attenuates epileptic seizures in rodents. *ACS Chem. Biol.* 9(5), 1204–1212 (2014).
- 25 Cox JJ, Reimann F, Nicholas AK *et al.* An SCN9A channelopathy causes congenital inability to experience pain. *Nature* 444(7121), 894–898 (2006).
- 26 Gilchrist J, Das S, Van Petegem F, Bosmans F. Crystallographic insights into sodium-channel modulation by the $\beta 4$ subunit. *Proc. Natl Acad. Sci. USA* 110(51), 5016–5024 (2013).
- 27 England S. Voltage-gated sodium channels: the search for subtype-selective analgesics. *Expert. Opin. Investig. Drugs* 17(12), 1849–1864 (2008).
- 28 Krafft DS, Bannon AW. Sodium channels and nociception: recent concepts and therapeutic opportunities. *Curr. Opin. Pharmacol.* 8(1), 50–56 (2008).
- 29 Priest BT. Future potential and status of selective sodium channel blockers for the treatment of pain. *Curr. Opin. Drug Discov. Devel.* 12(5), 682–692 (2009).
- 30 Waxman SG, Kocsis JD, Black JA. Type III sodium channel mRNA is expressed in embryonic but not adult spinal sensory neurons, and is reexpressed following axotomy. *J. Neurophysiol.* 72(1), 466–470 (1994).
- Describes the potential role of $\text{Na}_v1.3$ in neuropathic pain states.
- 31 Hains BC, Saab CY, Klein JP, Craner MJ, Waxman SG. Altered sodium channel expression in second-order spinal sensory neurons contributes to pain after peripheral nerve injury. *J. Neurosci.* 24(20), 4832–4839 (2004).
- 32 Hong S, Morrow TJ, Paulson PE, Isom LL, Wiley JW. Early painful diabetic neuropathy is associated with differential changes in tetrodotoxin-sensitive and -resistant sodium channels in dorsal root ganglion neurons in the rat. *J. Biol. Chem.* 279(28), 29341–29350 (2004).
- 33 Garry EM, Delaney A, Anderson HA *et al.* Varicella zoster virus induces neuropathic changes in rat dorsal root ganglia and behavioral reflex sensitization that is attenuated by gabapentin or sodium channel blocking drugs. *Pain* 118(12), 97–111 (2005).
- 34 Thakor DK, Lin A, Matsuka Y *et al.* Increased peripheral nerve excitability and local $\text{Na}_v1.8$ mRNA up-regulation in painful neuropathy. *Mol. Pain* 5(14) doi:10.1186/1744-8069-5-14 (2009).
- 35 Amaya F, Wang H, Costigan M *et al.* The voltage-gated sodium channel $\text{Na}_v1.9$ is an effector of peripheral inflammatory pain hypersensitivity. *J. Neurosci.* 26(50), 12852–12860 (2006).
- 36 Strickland IT, Martindale JC, Woodhams PL, Reeve AJ, Chessell IP, McQueen DS. Changes in the expression of $\text{Na}_v1.7$, $\text{Na}_v1.8$ and $\text{Na}_v1.9$ in a distinct population of dorsal root ganglia innervating the rat knee joint in a model of chronic inflammatory joint pain. *Eur. J. Pain* 12(5), 564–572 (2007).
- 37 Nieto FR, Cobos EJ, Tejada MÁ, Sánchez-Fernández C, González-Cano R, Cendán CM. Tetrodotoxin (TTX) as a therapeutic agent for pain. *Mar. Drugs* 10(2), 281–305 (2012).
- 38 Ekberg J, Jayamanne A, Vaughan CW *et al.* μO -conotoxin MrVIB selectively blocks $\text{Na}_v1.8$ sensory neuron specific sodium channels and chronic pain behavior without motor deficits. *Proc. Natl Acad. Sci. USA* 103(45), 17030–17035 (2006).
- 39 Schmalhofer WA, Calhoun J, Burrows R *et al.* Pro Tx-II, a selective inhibitor of $\text{Na}_v1.7$ sodium channels, blocks action potential propagation in nociceptors. *Mol. Pharmacol.* 74(5), 1476–1484 (2008).
- 40 Yang S, Xiao Y, Kang D *et al.* Discovery of a selective $\text{Na}_v1.7$ inhibitor from centipede venom with analgesic efficacy exceeding morphine in rodent pain models. *Proc. Natl Acad. Sci. USA* 110(43), 17534–17539 (2013).
- 41 Cestèle S, Catterall WA. Molecular mechanisms of neurotoxin act on voltage-gated sodium channels. *Biochimie* 82(9–10), 883–892 (2000).
- 42 Rosker C, Lohberger B, Hofer D, Steinecker B, Quasthoff S, Schreibmayer W. The TTX metabolite 4,9-anhydro-TTX is a highly specific blocker of the $\text{Na}_v1.6$ voltage-dependent sodium channel. *Am. J. Physiol. Cell Physiol.* 293(2), C783–C789 (2007).

- 43 Zhang MM, McArthur JR, Azam L *et al.* Synergistic and antagonistic interactions between tetrodotoxin and μ -conotoxin in blocking voltage-gated sodium channels. *Channels (Austin)* 3(1), 32–38 (2009).
- 44 Zhang MM, Gruszczynski P, Walewska A, Bulaj G, Olivera BM, Yoshikami D. Cooccupancy of the outer vestibule of voltage-gated sodium channels by μ -conotoxin KIIIA and saxitoxin or tetrodotoxin. *J. Neurophysiol.* 104(1), 88–97 (2010).
- 45 Hagen NA, Fisher KM, Lapointe B *et al.* An open-label, multi-dose efficacy and safety study of intramuscular tetrodotoxin in patients with severe cancer-related pain. *J. Pain Symptom Manage.* 34(2), 171–182 (2001).
- 46 Craik DJ, Fairlie DP, Liras S, Price D. The future of peptide-based drugs. *Chem. Biol. Drug Des.* 81(1), 136–147 (2013).
- 47 McCormack K, Santos S, Chapman ML. Voltage sensor interaction site for selective small molecule inhibitors of voltage-gated sodium channels. *Proc. Natl Acad. Sci. USA* 110(29), E2724–E2732 (2013).
- 48 Catterall WA, Cestèle S, Yarov-Yarovoy V, Yu FH, Konoki K, Scheuer T. Voltage-gated ion channels and gating modifier toxins. *Toxicon* 49(2), 124–141 (2007).
- 49 Stevens M, Peigneur S, Tytgat J. Neurotoxins and their binding areas on voltage-gated sodium channels. *Front. Pharmacol.* 2(71), 1–13 (2011).
- 50 Li D, Xiao Y, Hu W *et al.* Function and solution structure of hainantoxin-I, a novel insect sodium channel inhibitor from the Chinese bird spider *Selenocosmia hainana*. *FEBS Lett.* 555(3), 616–622 (2003).
- 51 Bulaj G, West PJ, Garrett JE *et al.* Novel conotoxins from *Conus striatus* and *Conus kinoshitai* selectively block TTX-resistant sodium channels. *Biochemistry* 44(19), 7259–7265 (2005).
- 52 French RJ, Terlau H. Sodium channel toxins - receptor targeting and therapeutic potential. *Curr. Med. Chem.* 11(23), 3053–3064 (2004).
- **Pharmacological characterization of various μ -conotoxins against $\text{Na}_v1.1$ – $\text{Na}_v1.8$. This work established the selectivity profiles for a number of sodium channel blocking conotoxins.**
- 53 Wilson MJ, Yoshikami D, Azam L *et al.* μ -Conotoxins that differentially block sodium channels $\text{Na}_v1.1$ through 1.8 identify those responsible for action potentials in sciatic nerve. *Proc. Natl Acad. Sci. USA* 108(25), 10302–10307 (2011).
- 54 Cruz LJ, Gray WR, Olivera BM *et al.* *Conus geographus* toxins that discriminate between neuronal and muscle sodium channels. *J. Biol. Chem.* 260(16), 9280–9288 (1985).
- 55 Moczydlowski E, Olivera BM, Gray WR, Strichartz GR. Discrimination of muscle and neuronal Na-channel subtypes by binding competition between [^3H]saxitoxin and μ -conotoxins. *Proc. Natl Acad. Sci. USA* 83(14), 5321–5325 (1986).
- 56 Sato K, Ishida Y, Wakamatsu K *et al.* Active site of μ -conotoxin GIIIA, a peptide blocker of muscle sodium channels. *J. Biol. Chem.* 266(26), 16989–16991 (1991).
- 57 Wakamatsu K, Kohda D, Hatanaka H *et al.* Structure-activity relationships of μ -conotoxin GIIIA: structure determination of active and inactive sodium channel blocker peptides by NMR and simulated annealing calculations. *Biochemistry* 31(50), 12577–12584 (1992).
- **Established the discrete location for μ -conotoxin binding as neurotoxin binding site 1 in the pore region of the α -subunit.**
- 58 Yanagawa Y, Abe T, Satake M. μ -Conotoxins share a common binding site with tetrodotoxin/saxitoxin on eel electroplax Na channels. *N. Neurosci.* 7(5), 1498–1505 (1987).
- 59 Holford M, Zhang MM, Gowd KH *et al.* Pruning nature: biodiversity-derived discovery of novel sodium channel blocking conotoxins from *Conus bullatus*. *Toxicon* 53(1), 90–98 (2009).
- 60 Shon KJ, Olivera BM, Watkins M *et al.* μ -Conotoxin PIIIA, a new peptide for discriminating among tetrodotoxin-sensitive Na channel subtypes. *J. Neurosci.* 18(12), 4473–4481 (1998).
- 61 Nielsen KJ, Watson M, Adams DJ *et al.* Solution structure of μ -conotoxin PIIIA, a preferential inhibitor of persistent tetrodotoxin-sensitive sodium channels. *J. Biol. Chem.* 277(30), 27247–27255 (2002).
- 62 Li RA, Tomaselli GF. Using the deadly μ -conotoxins as probes of voltage-gated sodium channels. *Toxicon* 44(2), 117–122 (2004).
- 63 West PJ, Bulaj G, Garrett JE, Olivera BM, Yoshikami D. μ -Conotoxin SmIIIA, a potent inhibitor of tetrodotoxin-resistant sodium channels in amphibian sympathetic and sensory neurons. *Biochemistry* 41(51), 15388–15393 (2002).
- 64 Keizer DW, West PJ, Lee EF *et al.* Structural basis for tetrodotoxin-resistant sodium channel binding by μ -conotoxin SmIIIA. *J. Biol. Chem.* 278(47), 46805–46813 (2003).
- 65 Walewska A, Skalicky JJ, Davis DR *et al.* NMR-based mapping of disulfide bridges in cysteine-rich peptides: application to the μ -conotoxin SxIIIA. *J. Am. Chem. Soc.* 130(43), 14280–14286 (2008).
- 66 Lewis RJ, Schroeder CI, Ekberg J *et al.* Isolation and structure-activity of μ -conotoxin TIIIA, a potent inhibitor of tetrodotoxin-sensitive voltage-gated sodium channels. *Mol. Pharmacol.* 71(3), 676–685 (2007).
- 67 Schroeder CI, Adams D, Thomas L, Alewood PF, Lewis RJ. N- and C-terminal extensions of μ -conotoxins increase potency and selectivity for neuronal sodium channels. *Biopolymers* 98(2), 161–165 (2012).
- 68 Khoo KK, Gupta K, Green BR *et al.* Distinct disulfide isomers of μ -conotoxins KIIIA and KIIIB block voltage-gated sodium channels. *Biochemistry* 51(49), 9826–9835 (2012).
- 69 Zhang MM, Green BR, Catlin P *et al.* Structure/function characterization of μ -conotoxin KIIIA, an analgesic, nearly irreversible blocker of mammalian neuronal sodium channels. *J. Biol. Chem.* 282(42), 30699–30706 (2007).
- 70 Nakamura M, Niwa Y, Ishida Y *et al.* Modification of Arg-13 of μ -conotoxin GIIIA with piperidinyl-Arg analogs and their relation to the inhibition of sodium channels. *FEBS Lett.* 503(1), 107–110 (2001).

- 71 McArthur JR, Singh G, McMaster D, Winkfein R, Tieleman DP, French RJ. Interactions of key charged residues contributing to selective block of neuronal sodium channels by μ -conotoxin KIIIA. *Mol. Pharmacol.* 80(4), 573–584 (2011).
- 72 Walewska A, Han TS, Zhang MM, Yoshikami D, Bulaj G, Rolka K. Expanding chemical diversity of conotoxins: peptoid-peptide chimeras of the sodium channel blocker μ -KIIIA and its selenopeptide analogues. *Eur. J. Med. Chem.* 65, 144–150 (2013).
- 73 Van Der Haegen A, Peigneur S, Tytgat J. Importance of position 8 in μ -conotoxin KIIIA for voltage-gated sodium channel selectivity. *FEBS J.* 278(18), 3408–3418 (2011).
- 74 Han TS, Zhang MM, Walewska A *et al.* Structurally minimized μ -conotoxin analogues as sodium channel blockers: implications for designing conopeptide-based therapeutics. *ChemMedChem* 4(3), 406–414 (2009).
- 75 Khoo KK, Feng ZP, Smith BJ *et al.* Structure of the analgesic μ -conotoxin KIIIA and effects on the structure and function of disulfide deletion. *Biochemistry* 48(6), 1210–1219 (2009).
- **Showed that μ -conotoxins, specifically μ -KIIIA, could preferentially adopt disulfide frameworks that differed from the canonical μ -conotoxin connectivity.**
- 76 Poppe L, Hui JO, Ligutti J, Murray JK, Schnier PD. PADLOC: a powerful tool to assign disulfide bond connectivities in peptides and proteins by NMR spectroscopy. *Anal. Chem.* 84(1), 262–266 (2012).
- 77 Schroeder CI, Ekberg J, Nielsen KJ *et al.* Neuronally μ -conotoxins from *Conus striatus* utilize an alpha-helical motif to target mammalian sodium channels. *J. Biol. Chem.* 283(31), 21621–21628 (2008).
- 78 Yao S, Zhang MM, Yoshikami D *et al.* Structure, dynamics, and selectivity of the sodium channel blocker μ -conotoxin SIIIA. *Biochemistry* 47, 10940–10949 (2008).
- **Demonstrated the amenability of the μ -conotoxin scaffold for chemical modification. It also showed the analgesic activity of μ -SIIIA and its analogs following intraperitoneal (ip) administration.**
- 79 Green BR, Catlin P, Zhang MM *et al.* Conotoxins containing nonnatural backbone spacers: cladistic-based design, chemical synthesis, and improved analgesic activity. *Chem. Biol.* 14(4), 399–407 (2007).
- 80 Zhang MM, Fiedler B, Green BR *et al.* Structural and functional diversities among μ -conotoxins targeting TTX-resistant sodium channels. *Biochemistry* 45(11), 3723–3732 (2006).
- 81 Favreau P, Benoit E, Hocking HG *et al.* A novel μ -conopeptide CnIIIC, exerts potent and preferential inhibition of $\text{Na}_v1.2/1.4$ channels and blocks neuronal nicotinic acetylcholine receptors. *Br. J. Pharmacol.* 166(5), 1654–1668 (2012).
- 82 Hains BC, Klein JP, Saab CY, Craner MJ, Black JA, Waxman SG. Upregulation of sodium channel $\text{Na}_v1.3$ and functional involvement in neuronal hyperexcitability with central neuropathic pain after spinal cord injury. *J. Neurosci.* 23(26), 8881–8892 (2003).
- 83 Lindia JA, Köhler MG, Martin WJ, Abbadie C. Relationship between sodium channel $\text{Na}_v1.3$ expression and neuropathic pain behavior in rats. *Pain* 117(1–2), 145–153 (2005).
- 84 Kuang Z, Zhang MM, Gupta K *et al.* Mammalian neuronal sodium channel blocker μ -conotoxin BuIIIB has a structured N-terminus that influences potency. *ACS Chem. Biol.* 8, 1344–1351 (2013).
- 85 Green BR, Zhang MM, Chhabra S *et al.* Interactions of disulfide-deficient selenocysteine analogs of μ -BuIIIB with the voltage-gated sodium channel $\text{Na}_v1.3$. *FEBS J.* 281(13), 2885–2898 (2014).
- 86 Bulaj G, Olivera BM. Folding of conotoxins: formation of the native disulfide bridges during chemical synthesis and biosynthesis of *Conus* peptides. *Antioxid. Redox. Signal.* 10(1), 141–155 (2008).
- 87 Tietze AA, Tietze D, Ohlenschläger O *et al.* Structurally diverse μ -conotoxin PIIIA isomers block sodium channel $\text{Na}_v1.4$. *Angew. Chem. Int. Ed. Engl.* 51(17), 4058–4061 (2012).
- 88 Bhattacharyya M, Gupta K, Gowd KH, Balaram P. Rapid mass spectrometric determination of disulfide connectivity in peptides and proteins. *Mol. Biosyst.* 9(6), 1340–1350 (2013).
- 89 Safavi-Hemami H, Gorasia DG, Steiner AM *et al.* Modulation of conotoxin structure and function is achieved through a multienzyme complex in the venom glands of cone snails. *J. Biol. Chem.* 287(41), 34288–34303 (2012).
- 90 Dutton JL, Bansal PS, Hogg RC, Adams DJ, Alewood PF, Craik DJ. A new level of conotoxin diversity, a non-native disulfide bond connectivity in α -conotoxin AuIB reduces structural definition but increases biological activity. *J. Biol. Chem.* 277(50), 48849–48857 (2002).
- 91 Vijayaragavan K, Powell AJ, Kinghorn IJ, Chahine M. Role of auxiliary $\beta1$ -, $\beta2$ -, and $\beta3$ -subunits and their interaction with $\text{Na}_v1.8$ voltage-gated sodium channel. *Biochem. Biophys. Res. Commun.* 319(2), 531–540 (2004).
- 92 Chahine M, O’Leary ME. Regulatory role of voltage-gated Na channel β subunits in sensory neurons. *Front. Pharmacol.* 2(70), 1–8 (2011).
- 93 Wilson MJ, Zhang MM, Azam L, Olivera BM, Bulaj G, Yoshikami D. $\text{Na}_v\beta$ subunits modulate the inhibition of $\text{Na}_v1.8$ by the analgesic gating modifier μ O-conotoxin MrVIB. *J. Pharmacol. Exp. Ther.* 338(2), 687–693 (2011).
- **Showed the influence of the β -subunit on voltage-gated sodium channels (VGSC) blockade by μ -conotoxins.**
- 94 Zhang MM, Wilson MJ, Azam L *et al.* Co-expression of $\text{Na}_v\beta$ subunits alters the kinetics of inhibition of voltage-gated sodium channels by pore-blocking μ -conotoxins. *Br. J. Pharmacol.* 168(7), 1597–1610 (2013).
- 95 Lewis RJ, Dutertre S, Vetter I, Christie MJ. *Conus* venom pharmacology. *Pharmacol. Rev.* 64(2), 259–298 (2012).
- 96 Robinson SD, Safavi-Hemami H, McIntosh LD, Purcell AW, Norton RS, Papenfuss AT. Diversity of conotoxin gene superfamilies in the venomous snail, *Conus victoriae*. *PLoS One* 9(2), e87648 (2014).
- 97 Hu H, Bandyopadhyay PK, Olivera BM, Yandell M. Characterization of the *Conus bullatus* genome and its venomduct transcriptome. *BMC Genomics* 12(60), 11–5 (2011).

- 98 Ueberheide B, Fenyő D, Alewood PF, Chait BT. Rapid sensitive analysis of cyseine rich peptide venom components. *Proc. Natl Acad. Sci. USA* 106(17), 6910–6915 (2009).
- 99 Bhatia S, Kil YJ, Ueberheide B *et al.* Constrained *de novo* sequencing of conotoxins. *J. Proteome Res.* 11(8), 4191–4200 (2012).
- 100 Prashanth JR, Lewis RJ, Dutertre S. Towards an integrated approach for accelerated conopeptide discovery. *Toxicon* 60, 470–477 (2012).
- 101 Terrat Y, Biass D, Dutertre S *et al.* High-resolution picture of a venom gland transcriptome: case study with the marine snail *Conus consors*. *Toxicon* 59(1), 34–46 (2012).
- 102 Dutertre S, Jin AH, Kaas Q, Jones A, Alewood PF, Lewis RJ. Deep venomics reveals the mechanism for expanded peptide diversity in cone snail venom. *Mol. Cell Proteomics* 12(2), 312–329 (2013).
- 103 Lu A, Yang L, Xu S, Wang C. Various conotoxin diversifications revealed by a venom study of *Conus flavidus*. *Mol. Cell Proteomics* 13(1), 105–118 (2014).
- 104 Teichert RW, Raghuraman S, Memon T *et al.* Characterization of two neuronal subclasses through constellation pharmacology. *Proc. Natl Acad. Sci. USA* 109(31), 12578–12763 (2012).
- 105 Imperial JS, Cabang AB, Song J *et al.* A family of excitatory peptide toxins from venomous crassispine snails: using constellation pharmacology to assess bioactivity. *Toxicon* 89, 45–54 (2014).
- 106 Craig AG, Bandyopadhyay PK, Olivera BM. Post-translationally modified neuropeptides from *Conus* venoms. *Eur. J. Biochem.* 264(2), 271–275 (1999).
- 107 Klint JK, Senff S, Saez NJ *et al.* Production of recombinant disulfide-rich venom peptides for structural and functional analysis via expression in the periplasm of *E. coli*. *PLoS One* 8(5), e63865 (2013).
- 108 Nguyen VD, Hatahet F, Salo KEH, Enlund E, Zhang C, Ruddock LW. Pre-expression of a sulfhydryl oxidase significantly increases the yields of eukaryotic disulfide bond containing proteins expressed in the cytoplasm of *E. coli*. *Microb. Cell Fact.* 10, 1–13 (2011).
- 109 Stanley TB, Stafford DW, Olivera BM, Bandyopadhyay PK. Identification of a vitamin K-dependent carboxylase in the venom duct of a *Conus* snail. *FEBS Lett.* 407(1), 85–88 (1997).
- 110 Bandyopadhyay PK, Garrett JE, Shetty RP, Keate T, Walker CS, Olivera BM. γ -Glutamyl carboxylation: an extracellular posttranslational modification that antedates the divergence of molluscs, arthropods, and chordates. *Proc. Natl Acad. Sci. USA* 99(3), 1264–1269 (2002).
- 111 Ul-Hasan S, Burgess DM, Gajewiak J *et al.* Characterization of the peptidylglycine α -amidating monooxygenase (PAM) from the venom ducts of neogastropods, *Conus bullatus* and *Conus geographus*. *Toxicon* 74, 215–224 (2013).
- 112 Hargittai B, Barany G. Controlled syntheses of natural and disulfide-mispaired regioisomers of α -conotoxin S1. *J. Pept. Res.* 54(6), 468–479 (1999).
- 113 Macrauld CA, Illesinghe J, Leirop BJV *et al.* Structure and activity of (2,8)-dicarba-(3,12)-cystino α -ImI, an α -conotoxin containing a nonreducible cystine analogue. *J. Med. Chem.* 52, 755–762 (2009).
- 114 Van Leirop BJ, Robinson SD, Kompella SN *et al.* Dicarba α -conotoxin Vc1.1 analogues with differential selectivity for nicotinic acetylcholine and GABA_B receptors. *ACS Chem. Biol.* 8(8), 1815–1821 (2013).
- 115 Walewska A, Zhang MM, Skalicky JJ, Yoshikami D, Olivera BM, Bulaj G. Integrated oxidative folding of cysteine/selenocysteine containing peptides: improving chemical synthesis of conotoxins. *Angew. Chem. Int. Ed. Engl.* 48(12), 2221–2224 (2009).
- 116 Armishaw CJ, Daly NL, Nevin ST, Adams DJ, Craik DJ, Alewood PF. α -selenoconotoxins, a new class of potent α_7 neuronal nicotinic receptor antagonists. *J. Biol. Chem.* 281(20), 14136–14143 (2006).
- 117 Steiner AM, Woycechowsky KJ, Olivera BM, Bulaj G. Reagentless oxidative folding of disulfide-rich peptides catalyzed by an intramolecular diselenide. *Angew. Chem. Int. Ed. Engl.* 51(23), 5580–5584 (2012).
- 118 De Araujo AD, Mobli M, King GF, Alewood PF. Cyclization of peptides by using selenolanthionine bridges. *Angew. Chem. Int. Ed. Engl.* 51(41), 10298–10302 (2012).
- 119 Choudhary G, Aliste MP, Tieleman DP, French RJ, Dudley SCJ. Docking of μ -conotoxin GIIIA in the sodium channel outer vestibule. *Channels (Austin)* 1(5), 344–352 (2007).
- 120 Rashid MH, Heinzlmann G, Hug R *et al.* A potent and selective peptide blocker of the K_v1.3 channel: prediction from free-energy simulations and experimental confirmation. *PLoS One* 8(11), e78712 (2013).
- 121 Pavlov E, Bladen C, Winkfein R, Diao C, Dhaliwal P, French RJ. The pore, not cytoplasmic domains, underlies inactivation in a prokaryotic sodium channel. *Biophys. J.* 89, 232–242 (2005).
- 122 McCusker EC, Bagn eris C, Naylor CE *et al.* Structure of a bacterial voltage-gated sodium channel pore reveals mechanisms of opening and closing. *Nat. Commun.* 3, 1102 (2012).
- **Crystal structures of Na_vAb in two potentially inactivated states, providing insight into VGSC gating.**
- 123 Payandeh J, El-Din TMG, Scheuer T, Zheng N, Catterall WA. Crystal structure of a voltage-gated sodium channel in two potentially inactivated states. *Nature* 486, 135–140 (2012).
- 124 Rashid MH, Mahdavi S, Kuyucak S. Computational studies of marine toxins targeting ion channels. *Mar. Drugs* 11(3), 848–869 (2013).
- 125 Chen R, Chung SH. Binding modes of μ -conotoxin to the bacterial sodium channel (Na_vAb). *Biophys. J.* 102(3), 483–488 (2012).
- 126 Moore SJ, Leung CL, Norton HK, Cochran JR. Engineering agatoxin, a cystine-knot peptide from spider venom, as a molecular probe for *in vivo* tumor imaging. *PLoS One* 8(4), e60498 (2013).
- 127 Vita C, Roumestand C, Toma F, M enez A. Scorpion toxins as natural scaffolds for protein engineering. *Proc. Natl Acad. Sci. USA* 92(14), 6404–6408 (1995).

- 128 Kolmar H. Alternative binding proteins: biological activity and therapeutic potential of cysteine-knot miniproteins. *FEBS J.* 275(11), 2684–2690 (2008).
- 129 Horishita T, Yanagihara N, Ueno S *et al.* Neurosteroids allopregnanolone sulfate and pregnanolone sulfate have diverse effect on the α subunit of the neuronal voltage-gated sodium channels Na_v1.2, Na_v1.6, Na_v1.7, and Na_v1.8 expressed in *Xenopus* oocytes. *Anesthesiology* 121(3), 620–631 (2014).
- 130 Okura D, Horishita T, Ueno S *et al.* The endocannabinoid anandamide inhibits voltage-gated sodium channels Na_v1.2, Na_v1.6, Na_v1.7, and Na_v1.8 in *Xenopus* oocytes. *Anesth. Analg.* 118(3), 554–562 (2014).
- 131 Zhang MM, Wilson MJ, Gajewiak J *et al.* Pharmacological fractionation of tetrodotoxin-sensitive sodium currents in rat dorsal root ganglion neurons by μ -conotoxins. *Br. J. Pharmacol.* 169(1), 102–114 (2013).
- 132 Essack M, Bajic VB, Archer JA. Conotoxins that confer therapeutic possibilities. *Mar. Drugs* 10(6), 1244–1265 (2012).
- 133 Lewis RJ. Conotoxins: molecular and therapeutic targets. *Prog. Mol. Subcell. Biol.* 46, 45–65 (2009).

Chapter 4

Correlation of Activity with Disulfide-bridging Pattern in μ -Conotoxin BuIII B

The previous chapter described the structure-activity relationship studies of μ -conotoxins to identify the critical features of these peptides that contribute to their potent block of VGSCs. Many of these studies focused on the outcome of individual amino acid substitutions for activity, this chapter explores the importance of disulfide bridging patterns for the activity of the μ -conotoxin BuIII B.

This chapter consists of the following manuscript in preparation:

Green, B. R.; Leung, E. W. W.; Yoshikami, D.; Olivera, B. M.; Balaram, P.; Norton, R. S.
Correlation of activity with disulfide-bridging pattern in μ -conotoxin BuIII B. (*In Preparation*).

4.1 Declaration for Thesis Chapter 4

4.1.1 Declaration by candidate

In the case of Chapter 4, the nature and extent of my contribution to the work was the following:

Nature of contribution	Contribution (%)
Jointly conceived the study and wrote the manuscript. Designed and executed experiments, and analysed experimental data.	65%

The following co-authors contributed to the work. If co-authors are students at Monash University, the extent of their contribution in percentage terms must be stated:

Name	Nature of contribution	Contribution (%)
Eleanor W. W. Leung	Assisted with recombinant expression.	
Doju Yoshikami	Contributed reagents/materials/analysis tools.	
Baldomero M. Olivera	Contributed reagents/materials/analysis tools	
Padmanabhan Balaram	Performed collision-induced dissociation experiments to determine disulfide connectivity.	
Raymond S. Norton	Assisted with manuscript preparation and intellectual input. Corresponding author	

The undersigned hereby certify that the above declaration correctly reflects the nature and extent of the candidate's and co-authors' contributions to this work*.

**Candidate's
signature**



Date

22.01.16

**Main
supervisor's
signature**



Date

22.01.16

Correlation of activity with disulfide-bridging pattern in μ -conotoxin BuIIIb

Brad R. Green^{1,2}, Eleanor W. W. Leung¹, Sunita Prakash³, M. Vijayasathy³, Doju Yoshikami²,
Baldomero M. Olivera², Padmanabhan Balaram³, and Raymond S. Norton¹

¹*Monash Institute of Pharmaceutical Sciences (MIPS) Parkville, Victoria 3052, Australia*

²*University of Utah: Department of Biology, Salt Lake City, Utah, 84112, USA*

³*Indian Institute of Sciences, Molecular Biophysics Unit, Bangalore, Karnataka, 560 012, India*

To whom correspondence should be addressed:

R. S. Norton, Monash Institute of Pharmaceutical Sciences, 381 Royal Parade, Parkville, Vic. 3052,
Australia. 

KEYWORDS: conotoxin, Collision-Induced Dissociation Mass Spectrometry, disulfide,
electrophysiology, sodium channel

4.2 Abstract

μ -Conotoxin BuIIIb is a sub-micromolar inhibitor of voltage-gated sodium channels (VGSCs). It has attracted interest for its ability to potently block the sodium channel subtype Nav1.3, which is of interest for its possible role in neuropathic pain. Recent structure-activity relationship studies identified important amino acid residues for VGSC blockade. Beyond the roles of individual amino acids for VGSC blockade, the roles of different disulfide bridging patterns are also of interest. For any three disulfide bridge-containing peptide, up to 15 distinct bridging patterns are possible, and even under steady-state equilibration, μ -BuIIIb oxidizes into numerous folding isoforms. To test the effects of different folding patterns on Nav1.3 block, we expressed the free acid variant of μ -BuIIIb (rBuIIIb[^]) in *Rosetta gami* (DE3) *Escherichia coli* cells and tested the five major folding isoforms against Nav1.3. Importantly, the first peak in the folding mixture (Isoform 1) of rBuIIIb[^] showed no statistical difference in potency for Nav1.3 compared to the synthetic, amidated peptide (0.20 ± 0.09 versus 0.14 ± 0.12 μ M). Our results showed that five of the seven folding isoforms inhibited Na⁺ current, although to varying degrees. The disulfide connectivity of two of the five isoforms tested (e.g. rBuIIIb[^] Isoforms 4 and 5) was established by CID-MS/MS. rBuIIIb[^] Isoform 5 exhibited an unusual connectivity in that it possessed a vicinal disulfide bridge between Cys5-Cys6.

4.3 Introduction

μ -conotoxin BuIIIb (μ -BuIIIb) is a 24-residue peptide isolated from the venom of the fish-hunting marine snail *Conus bullatus* (Figure 1, Panel A) (103). This peptide, like all other members of the μ -conotoxin class, potently blocks voltage-gated sodium channels (VGSCs) through direct occlusion of the Na⁺ conductance pore by binding to neurotoxin binding Site 1 of the α -subunit (Nav1) (104). μ -BuIIIb shares a high degree of sequence homology in the C-terminal residues with the other μ -conotoxins that preferentially inhibit the neuronal VGSC subtype (Nav1.2), but differs significantly from these by an extended N-terminus and an elongated first inter-cysteine loop (Figure 1, Panels A – B) (105,106). Perhaps more interesting, is the ability of this peptide to potently inhibit Nav1.3 (107), which has been implicated in the initiation and propagation of action potentials associated with painful neuropathies (108-110). This role has, however, been disputed (111,112), and the exact role of Nav1.3 in neuropathic pain is still not well understood. Identification and development of potent inhibitors of this subtype would not only be useful to clarify the role of Nav1.3, but might also serve as potential drug leads for neuropathic pain. One issue that continues to impede the development of peptide-based therapeutics has been the efficient

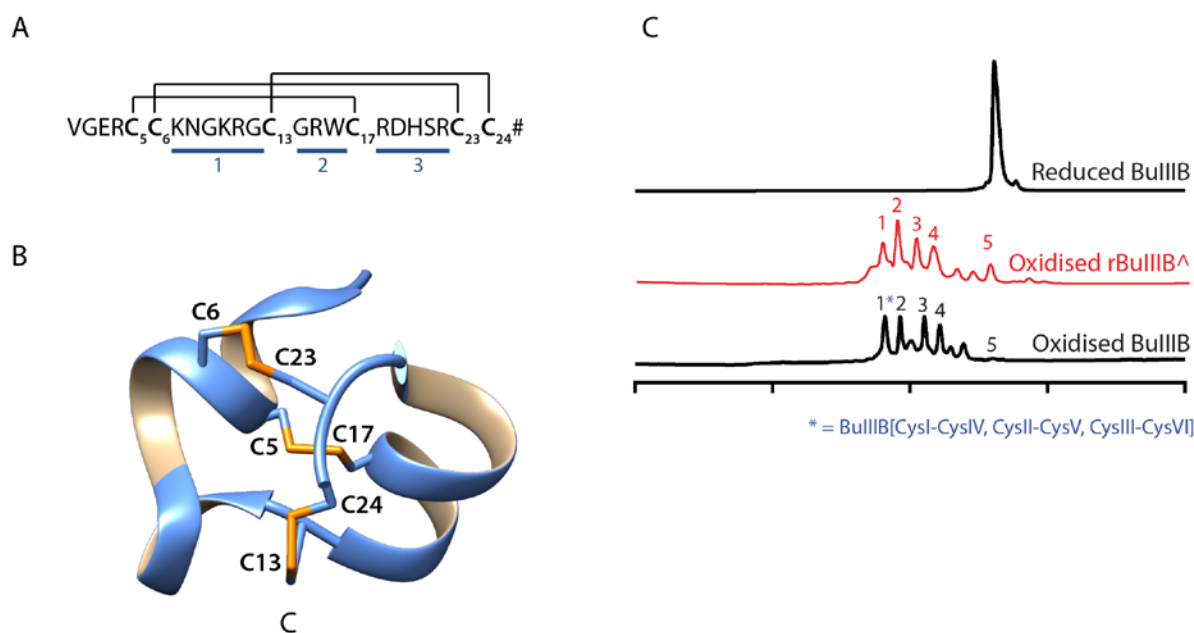


Figure 4.1. The structure of μ -conotoxin BuIII B. (A) Amino acid sequence and disulfide connectivity of the ‘native’ fold. Underlined regions denote inter-cysteine loops 1 – 3. (B) NMR structure of μ -BuIII B (PDB ID 2LO9) by Kuang (105). Disulfide connectivity of the ‘native’ isoform was determined by CID-MS/MS and this peptide exhibited the canonical μ -conotoxin framework (CysI-CysIV; CysII-CysV; CysIII-CysVI). Disulfide bridges are coloured orange. (C) Representative reversed-phase HPLC chromatograms of the oxidative folding of synthetic μ -BuIII B and recombinantly expressed rBuIII B[^]. The peak highlighted by an asterisk (*) represents the [Cys5-Cys17; Cys6-Cys23; Cys13-Cys24] connectivity. Oxidative folding of the synthetic peptide was conducted in a buffered solution (pH 7.5) containing a mixture of 1 mM oxidised and 1 mM reduced glutathione, 1 mM EDTA and 1 M NaCl for 4 h at room temperature.

production of these compounds for detailed structure-activity relationship (SAR) studies. SAR studies have typically focused on identifying important amino acid residues and determining interactions of these residues with their respective molecular targets (113-115). Another important structural feature of *Conus*-derived peptides is the disulfide connectivity. The ‘native’ connectivity for μ -conotoxins has traditionally been described as CysI-CysIV;CysII-CysV;CysIII-CysVI, with respect to the cysteine framework (116). However, recent reports have called into question the existence of a single ‘canonical’ disulfide connectivity (80,117), and as the number of described μ -conotoxins increases, so too has the diversity of disulfide-bridging patterns within this class. Different disulfide connectivities in μ -PIIIA were previously shown to affect the block of VGSCs to varying degrees (118). Tietze and co-workers showed that the non-canonical pattern of CysI-CysV;CysII-CysVI;CysIII-CysIV exhibited a four-fold increase in potency against Nav1.4 (46.7 nM versus 203.7 nM) (118). Moreover, the disulfide connectivity of the major product of μ -conotoxin KIIIA was examined by NMR (80) and by PADLOC disulfide bond determination (117)

and was found to have an entirely different connectivity CysI-CysV/CysII-CysIV/CysIII-CysIV. Oxidative folding of the majority of μ -conotoxins yields one or two major folding products which can be readily tested in pharmacological assays (i.e. electrophysiology). However, under optimised conditions, *in vitro* oxidation of synthetic μ -BuIIIb resulted in numerous folding species, even at steady-state equilibration (106).

Given the propensity of μ -BuIIIb to oxidize to multiple folding isoforms (Figure 1, Panel C), recombinant methods were explored in an attempt to produce large quantities of the native peptide (Figure 2). Recombinant methodologies are well established as a means for the efficient large-scale production of several peptide-based therapeutics (119-121). Production of μ -conotoxins has been limited predominantly to chemical synthetic methods, largely due to the frequency of multiple post-translational modifications in these peptides (e.g. glycosylation, hydroxylation, N-terminal cyclisation of Glu or Gln, C-terminal amidation and others). Aside from C-terminal amidation, μ -BuIIIb lacks the post-translational modifications common to other members of this class. As such, the carboxylated form of μ -BuIIIb (rBuIIIb⁺; where ⁺ implies the C-terminal free carboxylate) was selected as a good model to 1) employ a method for recombinant expression to produce fully-oxidised μ -conotoxin and 2) produce sufficient quantities of the major folding isoforms of μ -BuIIIb to study the effects of different disulfide-bridging frameworks on biological activity against Nav1.3 (Figure 1, Panel C).

4.4 Materials and Methods

4.4.1 Construction of the expression plasmid Trx-BuIIIb

The BuIIIb gene was codon optimised and synthesised by Genescript (Piscataway, NJ). The gene was digested with KpnI and NcoI and cloned into pET32a to form the pET32-BuIIIb fusion expression plasmid. This construct, which was ampicillin resistant, possessed a thioredoxin tag, an N-terminal hexahistidine affinity tag and an enterokinase cleavage site (DDDDK) (Figure 2, Panel A).

4.4.2 Fusion protein expression and purification

The pET32-BuIIIb fusion expression plasmid was transformed into competent Rosetta-gami (DE3) *Escherichia coli* cells (Novagen) by heat shock at 42 °C for 45 s. Transformed cells were plated on LB agar plates supplemented with 0.1 mg/mL ampicillin and 0.03 mg/mL chloramphenicol and were incubated for 24 h at 37 °C. Three to four colonies were selected and 3 mL seed cultures were prepared in LB media containing 0.1 mg/mL ampicillin and 0.03 mg/mL chloramphenicol and

were grown for 3h, or until OD₆₀₀ exceeded 0.3, at 37 °C under steady mixing on an orbital shaker. Half of this material (1 mL) was concentrated by centrifugation and the cell pellet was lysed overnight at -20 °C with 60 µL BugBuster Master Mix (EMD Millipore). The remaining culture was induced with 1 mM Isopropyl β-D-1-thiogalactopyranoside (IPTG) in LB media containing 0.1 mg/mL ampicillin and 0.03 mg/mL chloramphenicol. Induction was allowed to proceed overnight at room temperature on a rotary mixer. Four 1L cultures were inoculated with the induced cells and mixed vigorously for 4 h at 37 °C, or until OD₆₀₀ reached 0.6. Bacterial cultures were centrifuged at 7000 rpm for 10 min at 10 °C and cells were lysed with 4 mL/g Bug Buster mix containing 1 Complete ULTRA EDTA-free tablet (Roche Diagnostics). Lysis proceeded for 3 h at 4 °C under gentle mixing. Lysis mixture was filtered twice through a 0.8 µm syringe filter and the solution was purified by hydrophobic interaction chromatography (HIC). Briefly, 3 mL of Fast Flow chelating Sepharose (GE Healthcare Life Sciences) was washed with two bed volumes of milliQ H₂O. Following washing, the resin was charged with five bed volumes 100 mM NiSO₄. The column was then equilibrated with five bed volumes 20 mM Tris, pH 8.0, containing 500 mM NaCl and 10 mM imidazole. The filtered lysate was passed over the column twice and the resin was washed repeatedly (approximately 200 mL total volume) with 20 mM Tris, pH 8.0 containing 500 mM NaCl and 10 mM imidazole. The purified protein was then eluted off the column using 25 mL of a solution containing 20 mM Tris, pH 8.0 containing 100 mM NaCl and 50 mM imidazole. Column flow-through was analysed by SDS-Page (12% SDS-Page gel, 240 V, 23 min).

4.4.3 Purification of rBuIIIB[^] from fusion protein

Fusion protein-containing fractions were pooled, buffer exchanged and concentrated to 10 mL by repeated washing and centrifugation through an Amicon Ultra-15 centrifugal filter unit (EMD Millipore). Sample was diluted up to 30 mL with 20 mM Tris, pH 7.4 containing 50 mM NaCl and 5µL (5 units) enterokinase was added to cleave rBuIIIB[^] from the thioredoxin tag. Cleavage was allowed to proceed under gentle mixing at room temperature for 24 h. Following enterokinase cleavage, the rBuIIIB folding mixture was further purified by reversed-phase HPLC over a gradient of 5 – 35% Solvent B₉₀ (90% acetonitrile, 0.1% TFA) in 35 min. Individual folding isoforms were then purified by analytical RP-HPLC purification over a linear gradient of 5 - 35% B₉₀ (90% acetonitrile, 10% H₂O and 0.1% trifluoroacetic acid) in 35 min. Identities of individual peaks were confirmed by MALDI-TOF mass spectrometry.

4.4.4 Screening of rBuIIIIB^Δ folding isoforms against rNav1.3

Two-electrode voltage-clamp electrophysiology. All analogues were screened against rat Nav1.3 exogenously expressed in *Xenopus laevis* oocytes. The Nav1.3 clones (NM_013119) were obtained from Alan Goldin (University of California, Irvine). Oocytes were injected with 30-50 nL Nav1.3 cRNA in RNase-free water and were incubated overnight at 16 °C in ND96 (96 nM NaCl, 2 mM KCl, 1.8 mM CaCl₂, and 5 mM HEPES, pH 7.5), supplemented with antibiotics (100 units/mL penicillin, 0.1 mg/mL streptomycin, 0.1 mg/mL amikacin and 0.2 mg/mL septr). Voltage-clamping was performed on a Warner OC-725C amplifier (Warner Instruments) using 3 M KCl-filled microelectrodes (resistance < 0.5 MΩ) (114). Oocytes expressing rNav1.3 were placed in a 4 mm diameter chamber (30 μL well volume) filled with ND96 and were clamped to -80 mV holding potential. Voltage-gated sodium currents (I_{Na}) were induced in 20 s intervals with a 50 ms depolarizing pulse to -10 mV. Each of the major isoforms was prepared by dissolving the lyophilised peptide in ND96 to 10X the desired final concentration. After collecting a number of control pulses to ensure equilibration of the system, toxins were applied under static bath conditions in 3 μL volumes (1:10 dilution of sample in the chamber). Static bath conditions were necessary given the limited quantities of each analogue. Immediately following application, peptides were mixed in the chamber by gentle aspiration of the bath solution. All experiments were performed at room temperature.

Analysis of oocyte data. Time-course data were fitted to a single-exponential function using in-house developed LabVIEW software. An assumption was made to describe peptide interaction with the channel as a simple bimolecular reaction with the kinetics following the equation: $k_{\text{obs}} = k_{\text{on}}[\text{peptide}] + k_{\text{off}}$. The time-course of peak I_{Na} was plotted before application, during toxin exposure and following toxin washout. On-rate constants (k_{on}) were determined by fitting of the onset of block at a given concentration to a single-exponential function to yield the observed rate constant (k_{obs}). On-rates were derived from the slope of a linear regression plot where k_{obs} was plotted against [peptide] for ≥ 3 oocytes at ≥ 3 different peptide concentrations (122). Since all analogues tested were very slowly reversible (i.e. < 50% recovery after 20 min washout or $k_{\text{off}} < 0.035 \text{ min}^{-1}$), off-rates were estimated from the level of recovery after 20 min washout, following a single-exponential time-course for ≥ 9 oocytes. To avoid discrepancies in data resulting from baseline drift, times longer than this were not used. Electrophysiology data are presented as the mean ± SD and statistical significance was determined using the two-tailed unpaired *t* test in GraphPad Prism.

4.4.5 Determination of disulfide connectivity for rBuIIIB^Δ isoforms

Mass Spectrometry. Collision-Induced Dissociation Tandem Mass Spectrometry (CID-MS/MS) was employed to determine disulfide connectivities of the rBuIIIB^Δ folding isoforms. Isoforms 1-5 were subjected to trypsin digestion for 15 min at room temperature. Briefly, 10 nmol of each isoform was digested with a solution containing 29 ng/μL trypsin and 100 mM NH₄HCO₃. Liquid chromatography-mass spectrometry (LC-MS) of the digestion mixture was performed by coupling the Bruker Q-ToF ion trap mass spectrometer with an Agilent 1100 RP-HPLC equipped with an analytical C18 column (Agilent 4.6 x 150 mm). Samples were eluted from the column using a mixture of H₂O/acetonitrile and 0.1% formic acid as the solvent system with a flow rate of 0.2 mL/min. The MS experiments were performed by selecting the precursor ion, followed by fragmentation through collision with He(g). The fragmentation amplitude (V_{p-p}) was maintained between 1 and 3 and spectra were averaged over four scans.

4.5 Results

Recombinant Expression of Carboxylated μ-BuIIIB. Rosetta-gami (DE3) *E. coli* cells containing the recombinant plasmid pET32-BuIIIB were induced in the log phase by addition of IPTG. Following IPTG induction, the whole cell lysate was analysed by SDS-PAGE and a clear band was observed near 17.5 kDa (Figure 2, Panel B). Optimization of IPTG induction conditions showed that maximal protein expression could be attained by overnight induction at 25 °C and that the expressed protein could be found in the soluble fraction. Large-scale induction was carried out by adding IPTG to a final concentration of 1 mM and incubating for 16 h at 25 °C.

Purification and Identification of Trx-BuIIIB. The thioredoxin fusion protein was purified from the crude extract by Fast Protein Liquid Chromatography (FPLC) using a Ni-NTA affinity column. The fusion protein was eluted from the column using a buffer containing 20 mM Tris, pH 8.0, containing 100 mM NaCl and 50 mM imidazole. The purified fusion protein was analysed by SDS-PAGE and exhibited an electrophoretic mobility near the anticipated molecular weight of 17.5 kDa. Approximately 80 mg of the purified fusion protein was recovered from 1 L of bacterial culture. The free-acid form of BuIIIB (e.g. rBuIIIB^Δ) was liberated from the thioredoxin-His fusion protein by 72 h exposure to enterokinase at 25 °C (Figure 2, Panel C). Analytical RP-HPLC of the cleaved material showed numerous peaks, presumably all isoforms of the folded peptide. The initial folding mixture was purified by semi-preparative RP-HPLC and individual peaks were more rigorously purified by analytical RP-HPLC (Figure 3, Panel A). It was observed that all major HPLC peaks (Isoforms 1 – 5) yielded an identical mass (MH^{+1} Monoisotopic mass = 2763.13 Da) (Figure 3,

Panel B). This value was consistent with a fully-folded peptide containing three disulfide bridges. The folding profile for rBuIIIb^Δ differed slightly from that of the amidated peptide (Figure 1, Panel C). However, these results were not without precedent as Kang and co-workers previously showed that removal of the C-terminal amide group had some effect on the folding and distribution of oxidised products in the α -conotoxin ImI (123).

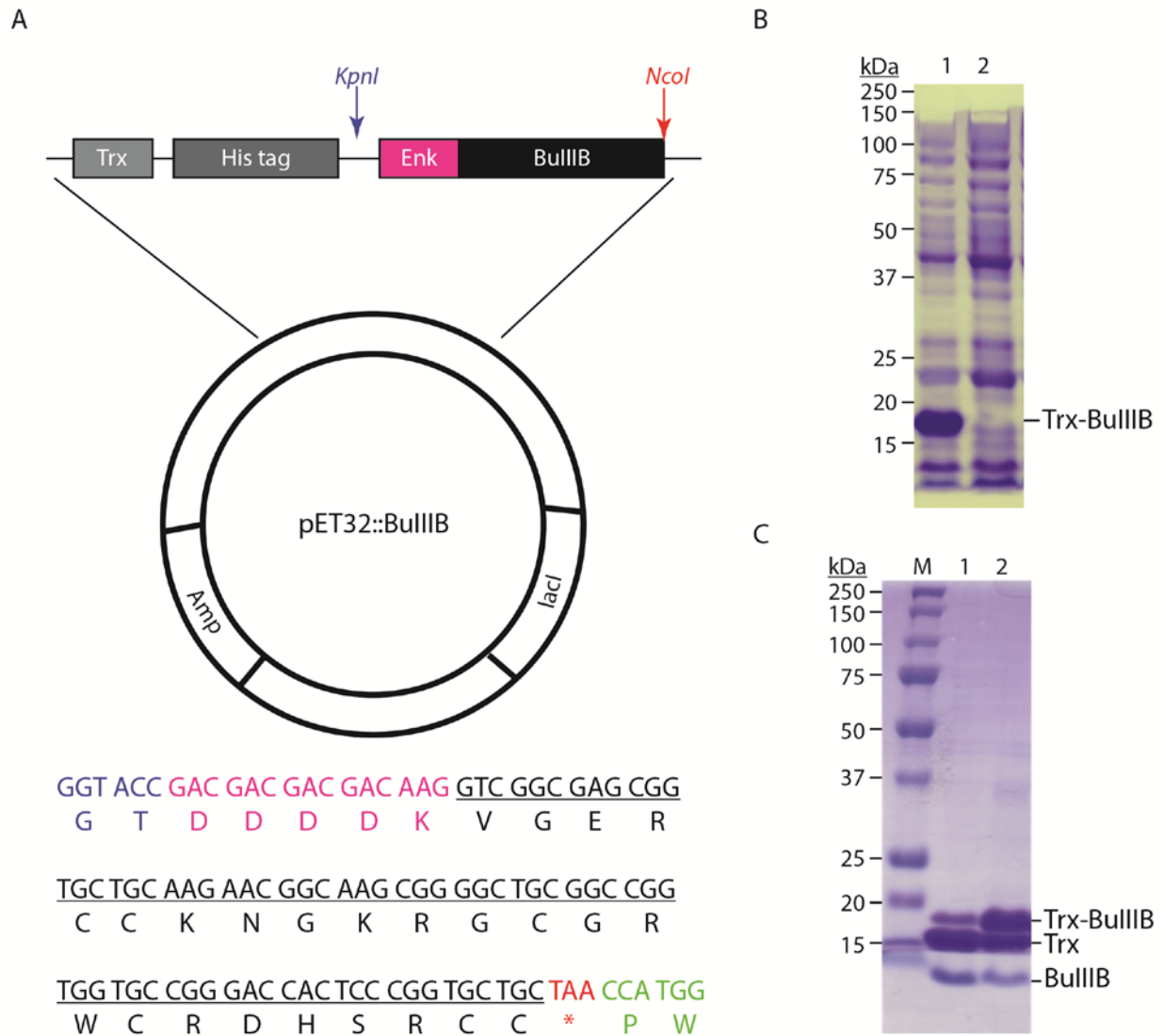


Figure 4.2. Recombinant expression of the free acid form of μ -BullIB. (A) His-tagged BullIB was inserted into the pET32 vector containing ampicillin resistance. The insert was removed using *KpnI* and *NcoI*. (B) 12% SDS-PAGE gel showing successful induction of the construct following 16 h induction with IPTG at 25 °C. Lane 1 shows the induced sample, Lane 2 is the uninduced sample (C) The enterokinase cut site that was engineered into the construct facilitated release of the folded rBullIB^Δ after 24 h exposure to enterokinase. Lane 1 is the sample after 24 h and Lane 2 is the sample after 12 h cleavage.

Nav1.3 Inhibition by rBuIIIIB^Δ Isoforms. The ability of the major folding isoforms in the folding mixture to block Nav1.3 was assessed electrophysiologically as described in Materials & Methods. Previous studies of the synthetic, C-terminally amidated form of the peptide showed that μ -BuIIIIB blocked Nav1.3 with a $K_d = 0.2 \pm 0.086 \mu\text{M}$ (107). Five of the major folding isoforms within the rBuIIIIB^Δ folding mixture were tested and all exhibited some degree of activity (Table 1). As expected, the most hydrophilic peak within the folding mixture (Isoform 1), was the most active component with a $K_d = 0.1448 \pm 0.1237 \mu\text{M}$ (Figure 3, Panel C). When compared to Isoform 1 of the synthetic peptide, this value was not statistically different (p-value = 0.2880). Other isoforms in the folding mixture showed a noticeable decrease in activity against Nav1.3 (Table 1). Off-rates (k_{off}) for each of the isoforms were essentially the same across all isoforms. The largest differences were seen in on-rates (k_{on}), where the more hydrophobic isoforms (as defined by RP-HPLC retention times) exhibited slower on-rates; this was the case for Isoforms 4 and 5 which were observed to block the channel, but with on-rates that were too slow to accurately measure during the experimental time frame (Table 1 and Figure 3, Panel D).

Table 4.1. Kinetics of block of rNav1.3 by rBuIIIIB^Δ isoforms^a

Peptide/Isoform	MW [M+H] ⁺		k_{on} ($\mu\text{M} \times \text{min}$) ⁻¹	k_{off} ^c (min) ⁻¹	K_d ^d (μM)
	(Calculated/Expected)	% Area ^b			
μ -BuIIIIB Isoform 1 ^e	2761.20/2761.19	16%	0.085 ± 0.01	0.017 ± 0.007	0.20 ± 0.086
rBuIIIIB ^Δ Isoform 1	2763.20/2763.13	10%	0.035 ± 0.004	0.005 ± 0.004	0.14 ± 0.124
rBuIIIIB ^Δ Isoform 2	2763.20/2763.13	13%	0.011 ± 0.001	0.005 ± 0.004	0.43 ± 0.328
rBuIIIIB ^Δ Isoform 3	2763.20/2763.13	12%	0.006 ± 0.001	0.005 ± 0.003	0.83 ± 0.517
rBuIIIIB ^Δ Isoform 4 ^e	2763.20/2763.14	11%	n.a.	n.a.	$> 10 \mu\text{M}^e$
rBuIIIIB ^Δ Isoform 5 ^e	2763.20/2763.14	4%	n.a.	n.a.	$> 10 \mu\text{M}^e$

^aValues (mean \pm standard deviation; $n \geq 3$ oocytes) were obtained by two-electrode voltage clamp electrophysiology of *Xenopus* oocytes expressing rat Nav1.3 channels as described in Materials and Methods. ^b% Area calculated as the peak area for each isoform relative to the total mixture as determined from integration of the RP-HPLC chromatogram ^cOff-rates (k_{off}) were generally very slow (i.e. $< 50\%$ recovery after 20 min washout or $k_{\text{off}} < 0.035 \text{ min}^{-1}$) and were estimated from the level of recovery after 20 min washout for ≥ 9 oocytes assuming a single-exponential time-course. ^dFrom $k_{\text{off}}/k_{\text{on}}$. ^eValues for μ -BuIIIIB Isoform 1 as determined previously. ^fBlock of Nav1.3 was observed, however values for k_{on} were too slow to accurately measure over the experimental time frame, even at [peptide] $\geq 10 \mu\text{M}$.

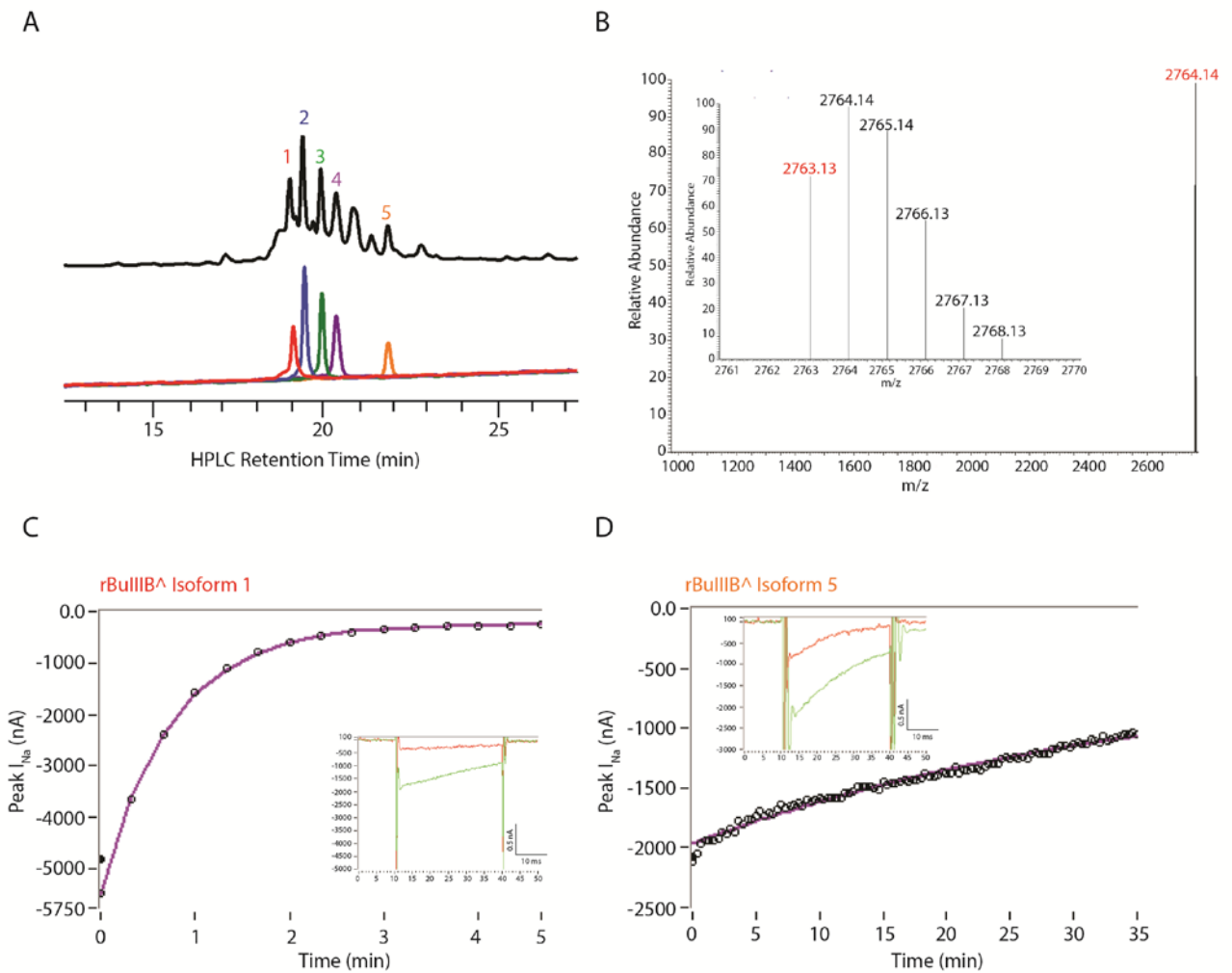


Figure 4.3. Characterization of rBuIIIB^Δ folding isoforms. (A) Reversed-phase HPLC of the recombinant BuIIIB folding mixture. The major peaks (Isoforms 1-5) were re-purified by analytical HPLC for structural and functional characterization. Additional peaks were present between the peaks corresponding to Isoforms 4 and 5. However, sufficient quantities of these isoforms were unattainable due to impurity caused by smaller contaminant peaks. (B) MALDI-TOF mass spectra of rBuIIIB^Δ Isoform 1. All isoforms described in this work possessed the same mass, corresponding to the fully-oxidised peptide with three disulfide bridges. The isotopic distribution of Isoform 1 is also included (inset). (C-D) Two electrode voltage-clamp electrophysiology traces of 33 μM rBuIIIB Isoform 1 and 33 μM Isoform 5 showing the differences in on-rates for rBuIIIB^Δ folding isoforms. Inset: Current traces obtained before (green) and during (red) exposure to peptide. All major isoforms were capable of blocking Nav1.3 and were slowly reversible. On-rates (k_{on}) differed across the isoforms 1- 5. The on-rates of rBuIIIB^Δ for the more hydrophobic isoforms were very slow and did not reach saturation during the experimental timeframe. All peptides in the folding mixture were capable of Nav1.3 block (See Table 1). Only the most active (Isoform 1) and least active (Isoform 5) isoforms are shown here.

Mass Spectrometric Determination of Disulfide Connectivities. Oxidation of μ-BuIIIB could, in principle, yield up to 15 distinct folding isoforms (Supplementary Figure S1). The connectivity of two of the five major isoforms was determined by CID-MS/MS, a technique that was previously shown to be successful for the *de novo* determination of disulfide connectivity for the major folding

isoforms of μ -KIIIA (80) and the synthetic, amidated form of μ -BuIIIB (105). CID-MS/MS is reliant on the interpretation of direct MS fragmentation data, under ion trap mass spectrometric conditions, of peptides that have either all disulfide bridges intact or have been proteolytically ‘nicked’ using trypsin. The structures of individual ions were then determined using *DisConnect* software (81). Analyses were performed on all major isoforms within the folding mixture with successful disulfide connectivity being established for the two least potent folding species (Isoforms 4 and 5) (Figure 4 – 5).

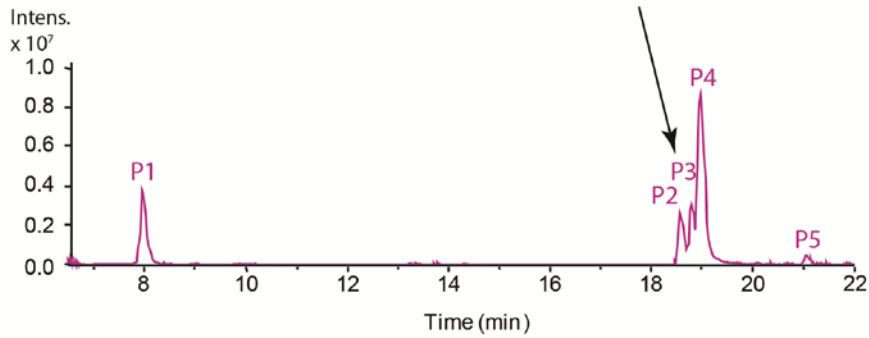
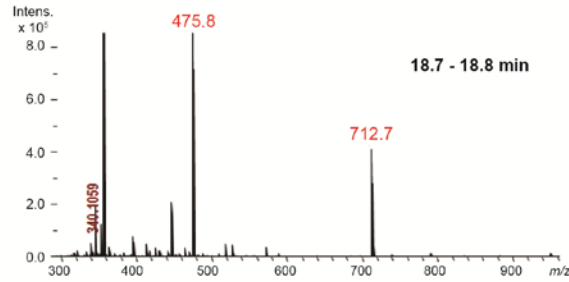
In theory, tryptic digestion of possible μ -BuIIIB isoforms should generate two distinct groups (Figure S1). The first group would consist of eight folding isoforms in which all six cysteine residues were still disulfide bonded following proteolysis. The $[M+H]^+ 1424.4$ m/z and/or multiply charged ions of $[M+2H]^{+2} 713.2$, $[M+3H]^{+3} 475.8$ and $[M+4H]^{+4} 357.1$ m/z would be diagnostic of this group. The second group would consist of seven isoforms that did not display the ions listed above but could be identified by specific fragments detected in the proteolysis mixture. MS/MS fragmentation of the $[M+H]^+ 1425.4$ m/z ion, or its multiply charged states, would yield fragments containing a single S-S linkage facilitating assignment of disulfide connectivity (Figure S1).

rBuIIIB^ Isoforms 1-3. Isoforms 1, 2 and 3 shared too many common disulfide-bonded fragment ions in MS/MS spectra to confidently assign disulfide connectivity (Supplemental Figures S2 - S4). However, one might speculate that, given the position in the folding mixture (i.e. the first major elution product by RP-HPLC), and essentially equivalent activity against Nav1.3 ($K_d = 0.14$ μ M versus 0.20 μ M for μ -BuIIIB), that the connectivity for *rBuIIIB^ Isoform 1* might be the same as that for the synthetic, amidated form reported by Kuang et al. (Cys5-Cys16; Cys6-Cys23; Cys13-Cys24) (105).

rBuIIIB^ Isoform 4. Tryptic digestion of Isoform 4 yielded five distinct peaks in the total ion chromatograph (Figure 4, Panel A). In Peak 3 of the total ion chromatograph, ions of 475.8 and 712.7 m/z were observed. These ions were consistent with the doubly ($[M+2H]^{+2}$) and triply ($[M+3H]^{+3}$) charged ion ($[M+H]^+ = 1425.4$ m/z), characteristic of Group 2 disulfide connectivity (Figure 4, Figure S1). MS/MS fragmentation of the $[M+2H]^{+2}$ ion yielded two ions (846.2 and 780.2 m/z , respectively) that corresponded unique m/z assignments (Figure 4, Panel B). Likewise, fragmentation of the triply charged ion produced several diagnostic ions (e.g. 383.0, 537.2, 613.1 and 814.3 m/z) that indicated that the Cys5Cys6 peptide fragment must be attached to the Cys23Cys24 peptide fragment (Figure 4, Panel B and Figure S7). Taken together, this information allowed us to establish the connectivity of Isoform 4 as Cys5-Cys24; Cys6-Cys17; Cys13-Cys23 (CysI-CysV; CysII-CysIV; CysIII-CysVI).

rBuIIIB[^] Isoform 5. Tryptic digestion of isoform 5 produced five distinct peaks in the total ion chromatogram (Figure 5). Peak 2 contained ions of $[M+H]^+ 650.3$ and $[M+H]^+ 806.4$ m/z which corresponded to the tryptic peptide fragments CCKNGK, and CCKNGKR, respectively. This was consistent with vicinal disulfide bridge formation between Cys5 and Cys6 in this isoform, leaving three possible disulfide connectivities for the remaining four cysteine residues. Peak 4 of the total ion chromatogram had ions of $[M+H]^+ 1074.4$, $[M+2H]^{+2} 537.7$ and $[M+3H]^{+3} 358.8$ m/z which corresponded to the tryptic peptide fragment GCGRWCRCC, eliminating the possibility of a bead connectivity for the remaining two disulfides of isoform 5. Upon MS/MS fragmentation of the tryptic peptide fragment GCGRWCRCC, two diagnostic ions were generated. $[M+H]^+ 510.2$ and $[M+H]^+ 1074.4$ m/z were consistent with a disulfide connectivity of isoform 5 as Cys5-Cys6; Cys13-Cys24; Cys17-Cys23 (CysI-CysII;CysIII-CysV;CysIV-CysVI).

A



B

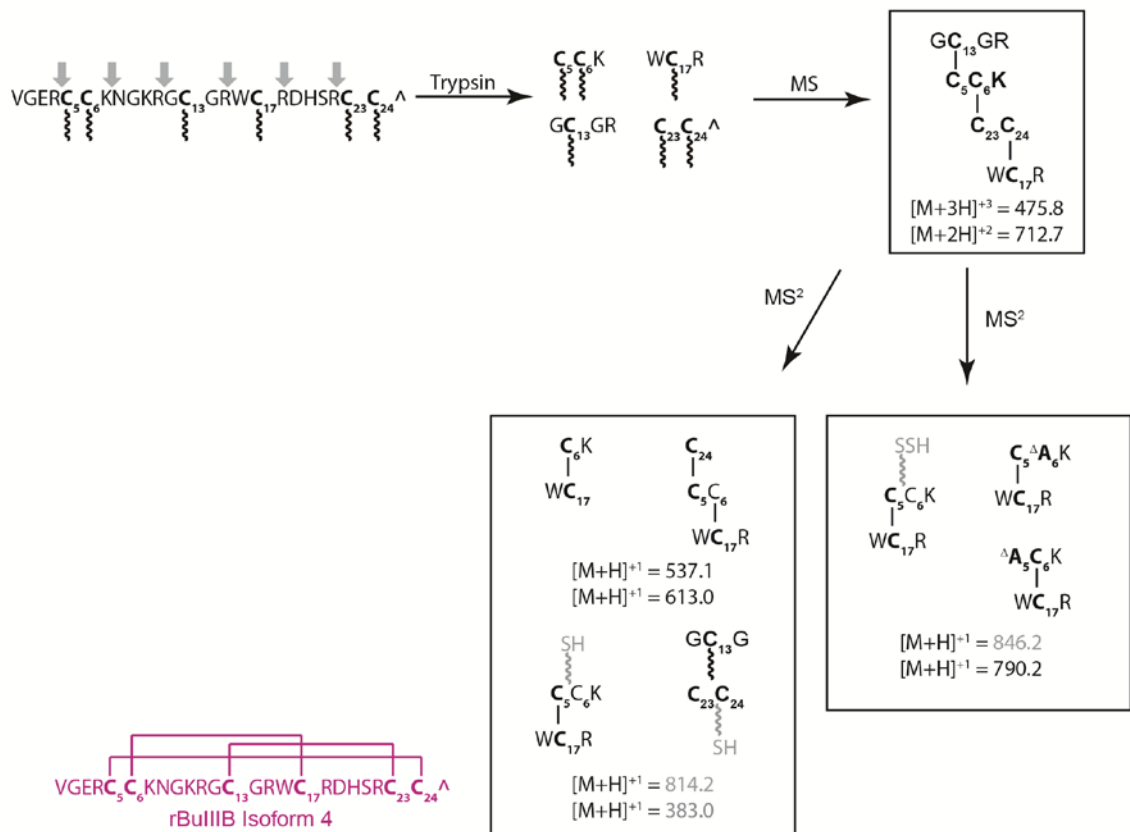


Figure 4.4. Experimentally determined disulfide connectivity of rBuIIIB[^] Isoform 4. (A) Five peaks (P1 - P5) were observed in the total ion chromatograph following tryptic digestion of rBuIIIB[^] Isoform 4. Ions of 475.8 and 712.7 Da were observed for Peak 3, corresponding to the doubly and triply charged ions of the diagnostic isoform containing all three disulfide bridges intact (Figure S1). (B) Ions [M+2H]⁺² 475.8 and [M+3H]⁺³ were fragmented by MS/MS and several diagnostic peptide fragment ions were observed. Based on these ions, the connectivity for Isoform 4 was established as [Cys5-Cys24; Cys6-Cys17; Cys13-Cys23]. Indeterminate connectivity is indicated by wavy lines. Gray text indicates fragmented S-S bonds.

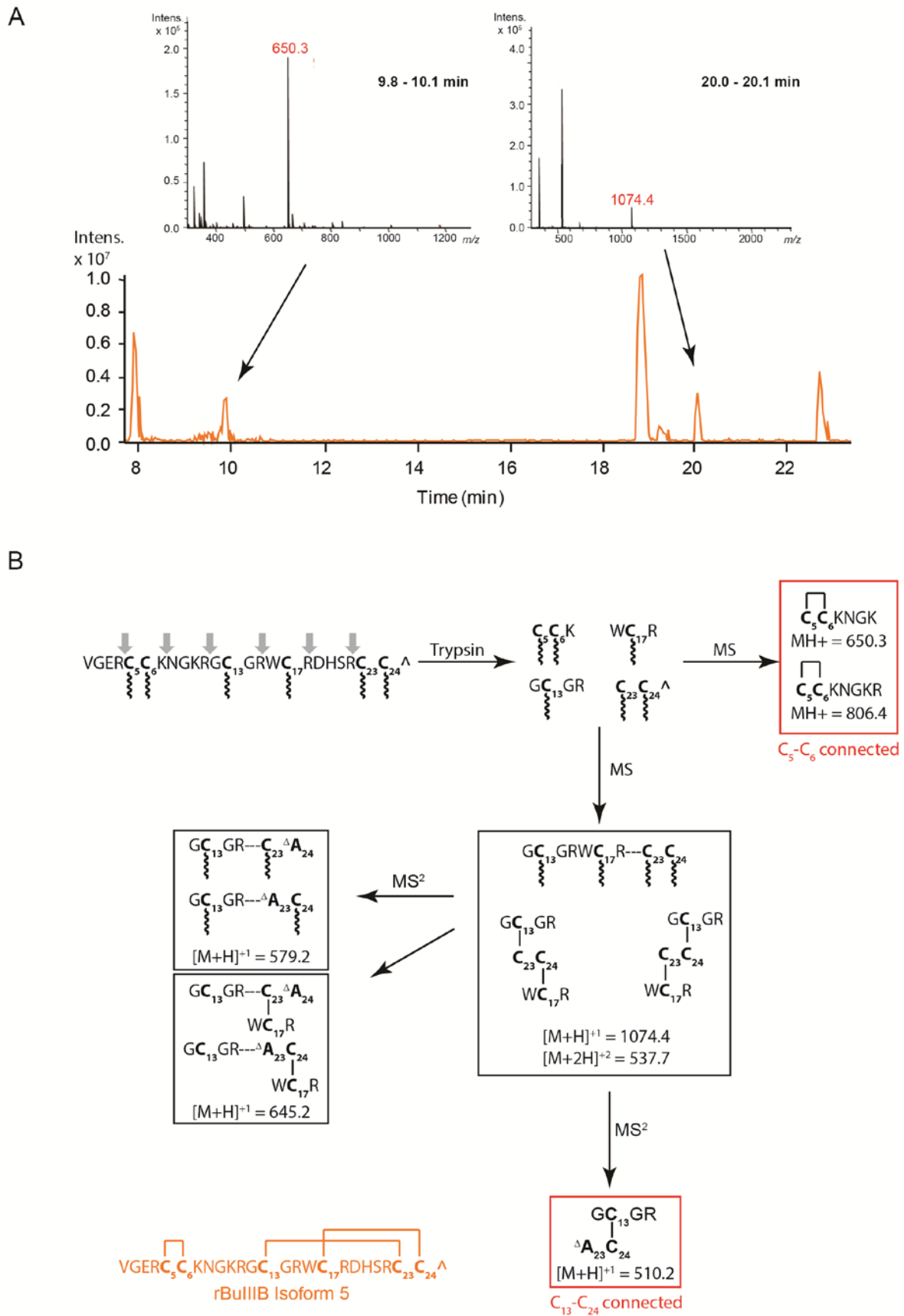


Figure 4.5. Experimentally determined disulfide connectivity of rBuIIIB^Δ isoform 5. (A) Seven peaks (P1 – P7) were observed in the total ion chromatograph following tryptic digestion of rBuIIIB^Δ Isoform 5. Peak 2 diagnostic ions of $[M+H]^+$ 650.3 and $[M+H]^+$ 806.4 m/z that corresponded to the tryptic peptide

fragments CCKNGK, and CCKNGKR, respectively. This information pointed towards a disulfide bridge between vicinal cysteines Cys5 and Cys6. The connectivity of the remaining two bridges was established by MS/MS fragmentation of the $[M+H]^+ = 1074.4$ and $[M+2H]^{+2}$ ions of Peak 5 in the total ion chromatograph. Together, this information established the connectivity of Isoform 5 as [Cys5-Cys6; Cys13-Cys24; Cys17-Cys23].

4.6 Discussion

The individual peptide components that comprise *Conus* venoms often contain a remarkably high number of post-translational modifications (33). These modifications increase the chemical diversity of the *Conus* toxin repertoire and play important roles in stabilization, and sometimes activity of these compounds. To date, at least 16 distinct PTMs have been identified in conotoxins isolated directly from *Conus* venoms (www.conoserver.org), including hydroxylation, carboxylation, bromination, epimerization, cyclization, sulfation, and O-glycosylation (33,124). The most common PTM in conotoxins, however, is the disulfide bridge with most conotoxins containing between two and four disulfide bridges (47). The μ -conotoxins fall within this group, and are characterised by six cysteine residues that form three disulfide bridges between them.

The disulfide connectivity pattern has been shown previously to influence μ -conotoxin activity against their voltage-gated sodium channel targets (80,118). It has been generally assumed that the earliest eluting (i.e. most hydrophilic) major oxidation product within the folding mixture was the most active peak and therefore corresponded to the 'native' fold expected to be observed in the venom. However, recent evidence suggests that peptides containing 'non-native' disulfide bridging frameworks could be observed directly in the venom and that these isoforms may also exhibit activity against their respective targets (49). Dutton and co-workers demonstrated that an alternative bridging pattern in α -conotoxin AuIB improved activity by nearly 10-fold compared to the globular form of the peptide (125). We set out to answer the question of whether non-canonical disulfide bridging patterns within the complex folding mixture of oxidised μ -BuIIIIB might possess equivalent, or even superior, activity against VGSC subtypes. μ -BuIIIIB was chosen as a model system because, in contrast to other members of this toxin family that fold efficiently into a single major isoform (126), this peptide yields numerous isoforms, in roughly equal amounts, following *in vitro* oxidation. In this report, we explored the consequences of non-canonical disulfide bridging patterns in oxidised μ -BuIIIIB for Nav1.3 blockade. The primary target for μ -BuIIIIB is, in fact, the skeletal muscle VGSC subtype (e.g. Nav1.4). However, μ -BuIIIIB was previously shown to also block Nav1.3 with sub-micromolar potency (80), making it the most potent peptide inhibitor of this subtype described to date. Due to the purported role of Nav1.3 in pain associated with spinal cord injury (107), we explored the potential of different folding isoforms of rBuIIIIB[^] to block this

subtype. For consistency with the previous results (80), peptides were tested against the α -subunit (e.g. Nav1.3) alone as this structure has been shown to be the minimal requisite structure to carry out the processes of a fully functional channel (9). It is important to note that, *in vivo*, functional VGSCs are comprised of not only the α -subunit, but also one or more associated β -subunits (Nav β) (12). As these ‘accessory’ proteins have been previously shown to affect the kinetics of block by μ -conotoxins, future studies will look at the effects of non-canonical disulfide bridging patterns in the context of β -subunit co-expression with pain-relevant Nav1-subtypes. To obtain larger quantities of each of the isoforms in the folding mixture, we employed an *E. coli* expression system to produce the recombinant free-acid form of μ -BuIIIb (i.e. rBuIIIb[^]). This approach has been shown effective for the production of other disulfide-rich toxins, including ShK (127).

The major advantages of recombinant methods over chemical syntheses include low cost, scalability and the elimination of potentially hazardous coupling reagents (128). However, the largest impediment to the widespread use of recombinant expression as a means of producing conotoxins in large quantities is the relatively limited capacity to incorporate several of the PTMs common in conotoxins. While μ -BuIIIb does possess multiple disulfide bridges, in addition to C-terminal amidation, it is believed to lack many of the other PTMs that are characteristic of this toxin class. Comparison of the ‘native’ isoforms for the synthetic, amidated (μ -BuIIIb) against the recombinant, free-acid (rBuIIIb[^]) forms of the peptide showed no statistical difference in Nav1.3 inhibition, suggesting that observable differences in activity could be attributed to variations in disulfide connectivity. As mentioned, the isoform exhibiting the canonical disulfide connectivity (Isoform 1) was capable of potent block of Nav1.3. Of note, the remaining isoforms in the mixture were also capable of inhibiting this subtype, although to a lesser degree. Our results were consistent with the findings of Tietze et al. that alternative isoforms of μ -PIIIa could also block Nav1.4 (118). Furthermore, structural studies demonstrated that less compact isoforms of μ -PIIIa exhibited less potent block (118). We employed CID-MS/MS to determine the disulfide connectivity in the major isoforms for rBuIIIb[^] and were successful in establishing the connectivity for Isoforms 4 and 5. Our data (electrophysiology and RP-HPLC analyses) suggested that the connectivity of Isoform 1 was that of the ‘native’ peptide, but this could not be unambiguously confirmed by MS/MS experiments given the similarities between Isoform 1, 2 and 3 with respect to ion fragmentation. Our current hypothesis is that Isoform 1 exhibits the ‘canonical’ μ -conotoxin bridging pattern, but additional studies will be required to confirm this.

Isoforms 4 and 5 were significantly less potent than the other isoforms in rBuIIIb[^]. This decrease in activity may be a consequence of disulfide bridging patterns that result in less well-ordered

structures for these isoforms, similar to what was observed with μ -PIIIA isoforms (118). Based on RP-HPLC retention times for Isoforms 4 and 5, we expect these peptides to be less compact than Isoform 1. In future studies, isotopically-labeled rBuIIIB^Δ could be produced using the recombinant expression methods described here. Such studies would be instrumental in determining the relative ‘compactness’ of Isoforms 4 and 5 compared to the peptide containing the ‘canonical’ fold.

CID-MS/MS experiments allowed us to identify the disulfide connectivities of two of the less-active isoforms of rBuIIIB^Δ. To the best of our knowledge, this is the first experimental evidence of the [CI-CV; CII-CIV; CIII-CV] and [CI-CII; C3-CVI; CIV-CV] isoforms resulting from oxidation of the linear peptide. The established connectivity for Isoform 5 (e.g. the vicinal disulfide pairing between Cys5-Cys6 and Cys17-Cys23), would lend support to a less-structured isoform. It is regrettable that, given the similarities in the spectra for Isoforms 1 - 3, we were unable to unambiguously assign connectivity for the remaining three isoforms. Efforts are currently underway to improve the MS/MS experiments which would be useful in differentiating between these three isoforms.

The methods associated with CID-MS/MS are relatively straightforward. Challenges in assigning connectivity typically arise during the analysis and interpretation of MS² or MS³ fragmentation data. Nonetheless, CID-MS/MS is an attractive alternative to the traditional approach (79), where peptides undergo selective reduction/alkylation experiments followed by amino acid sequencing experiments. CID-MS/MS eliminates the requirement for large amounts of starting material to compensate for loss during repeated purification steps.

We have shown here that frameworks such as those with disulfide bridges between vicinal cysteines, that would be anticipated to be less well structured, maintain the ability to modulate the activities of peptides against their respective molecular targets. Additional experiments are still needed to establish the disulfide connectivities of Isoforms 1 – 3. As mentioned, Isoform 1 is anticipated to possess the ‘canonical’ μ -connectivity, but this must be confirmed experimentally. Furthermore, the vicinal disulfide bridge in Isoform 5 is unusual and warrants further structural and functional characterization.

4.7 Acknowledgements

The authors would like to thank Grzegorz Bulaj and Samuel Robinson for review of the manuscript and for numerous helpful discussions pertinent to this work. We also thank William Low for MALDI-TOF analysis of the μ -BuIIIB isoforms, Alan Goldin for the rNav1.3 clones and Layla Azam for preparation of the rNav1.3 cRNA. This work was supported by National Institutes of

Health Grants GM 048677, GM 099939 and GM 103362. R.S.N. acknowledges fellowship support from the Australian National Health and Medical Research Council.

4.8 Supporting information

Correlation of activity with disulfide-bridging pattern in μ -conotoxin BuIIIb

Brad R. Green^{1,2}, Eleanor W. W. Leung¹, Sunita Prakash³, M. Vijayasathy³, Doju Yoshikami²,
Baldomero M. Olivera², Padmanabhan Balaram³, and Raymond S. Norton¹

¹*Monash Institute of Pharmaceutical Sciences (MIPS) Parkville, Victoria 3052, Australia*

²*University of Utah: Department of Biology, Salt Lake City, Utah, 84112, USA*

³*Indian Institute of Sciences, Molecular Biophysics Unit, Bangalore, Karnataka, 560 012, India*

To whom correspondence should be addressed:

R. S. Norton, Monash Institute of Pharmaceutical Sciences, 381 Royal Parade, Parkville, Vic. 3052,
Australia. 

Figure S4.1. Possible disulfide-bridging patterns for three disulfide-bridge containing μ -conotoxins and expected diagnostic ions resulting from tryptic digestion of rBuIIIb⁺.

Figure S4.2. Analysis of rBuIIIb⁺ Isoform 1 by MS

Figure S4.3. Analysis of rBuIIIb⁺ Isoform 2 by MS

Figure S4.4. Analysis of rBuIIIb⁺ Isoform 3 by MS

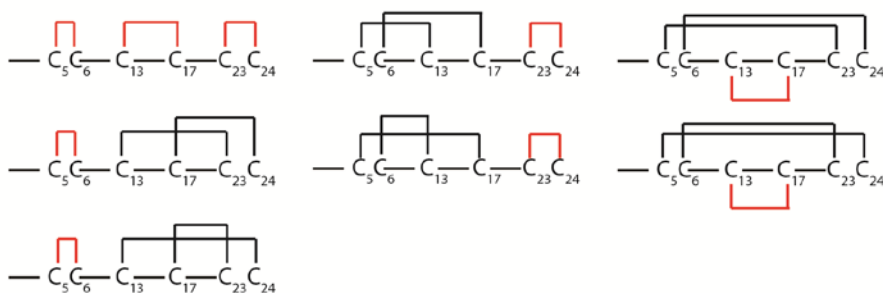
Figure S4.5. Analysis of rBuIIIb⁺ Isoform 4 by MS

Figure S6. Analysis of rBuIIIb⁺ Isoform 5 by MS

Figure S4.7. MS/MS fragmentation of diagnostic ions from of the total ion chromatograph of rBuIIIb⁺ Isoform 4 Peak 3.

VGER|C₅C₆K|INGLKRI|GC₁₃GRI|WC₁₇R|DHSR|C₂₃C₂₄

Group I:



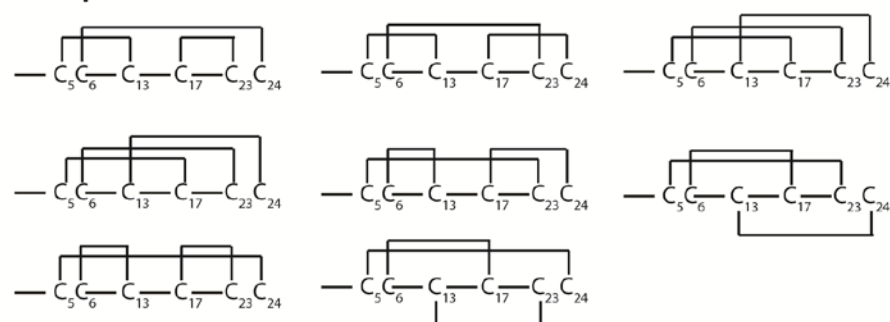
Diagnostic Ions

|GC₁₃GRI|WC₁₇R|
 [M+H]⁺ = 834.3
 [M+H]⁺ = 852.3

|C₅C₆K|
 [M+H]⁺ = 350.1

|C₂₃C₂₄R|
 [M+H]⁺ = 222.0

Group II:



Diagnostic Ions

|GC₁₃GRI|
 |C₅C₆K|
 |C₂₃C₂₄R|
 |WC₁₇R|
 [M+H]⁺ = 1425.4

Figure S4.1. Possible disulfide-bridging patterns for three disulfide-bridge containing μ -conotoxins and expected diagnostic ions resulting from tryptic digestion of rBuIIIIB^Δ.

rBuIIIB^Δ Isoform 1

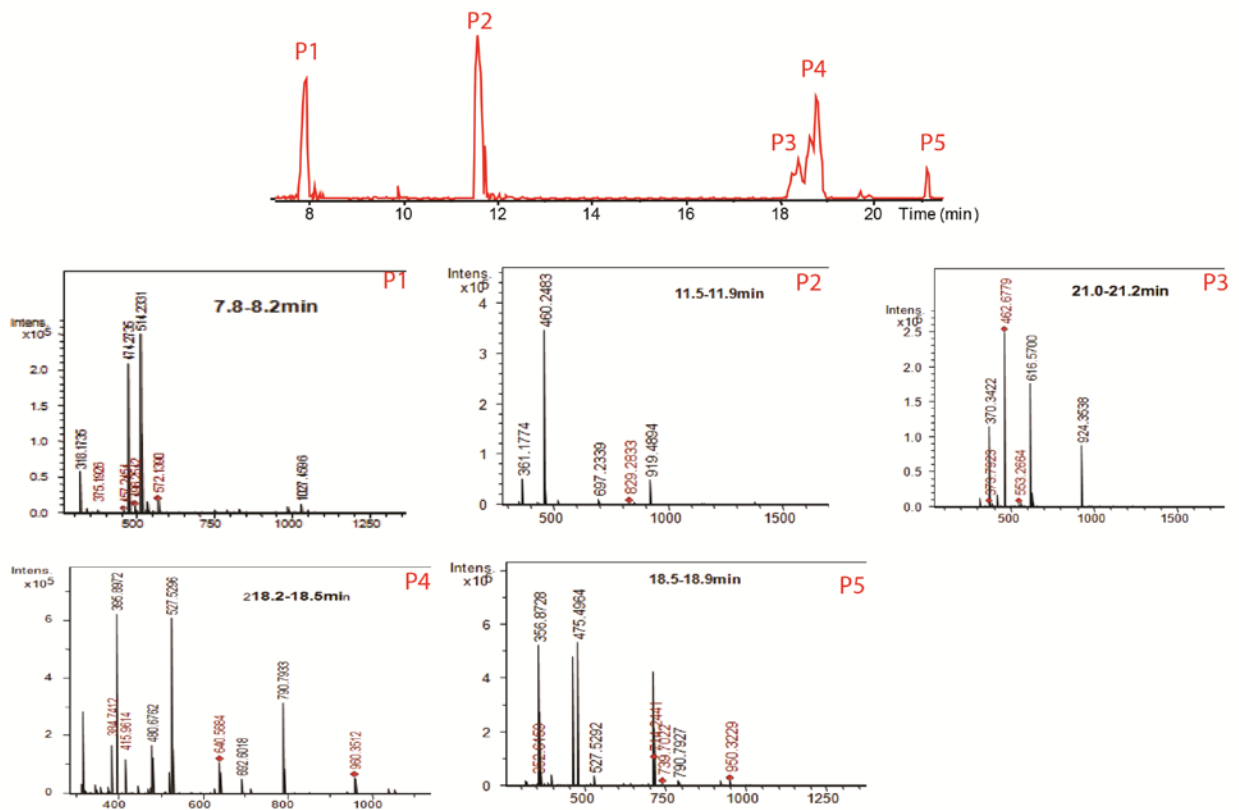


Figure S4.2. Analysis of rBuIIIB^Δ Isoform 1 by MS (Top) Total ion chromatograph of the tryptic cleavage products of rBuIIIB^Δ Isoform 1. (Bottom) MS spectra of each of the tryptic cleavage products.

rBuIIIB^Δ Isoform 2

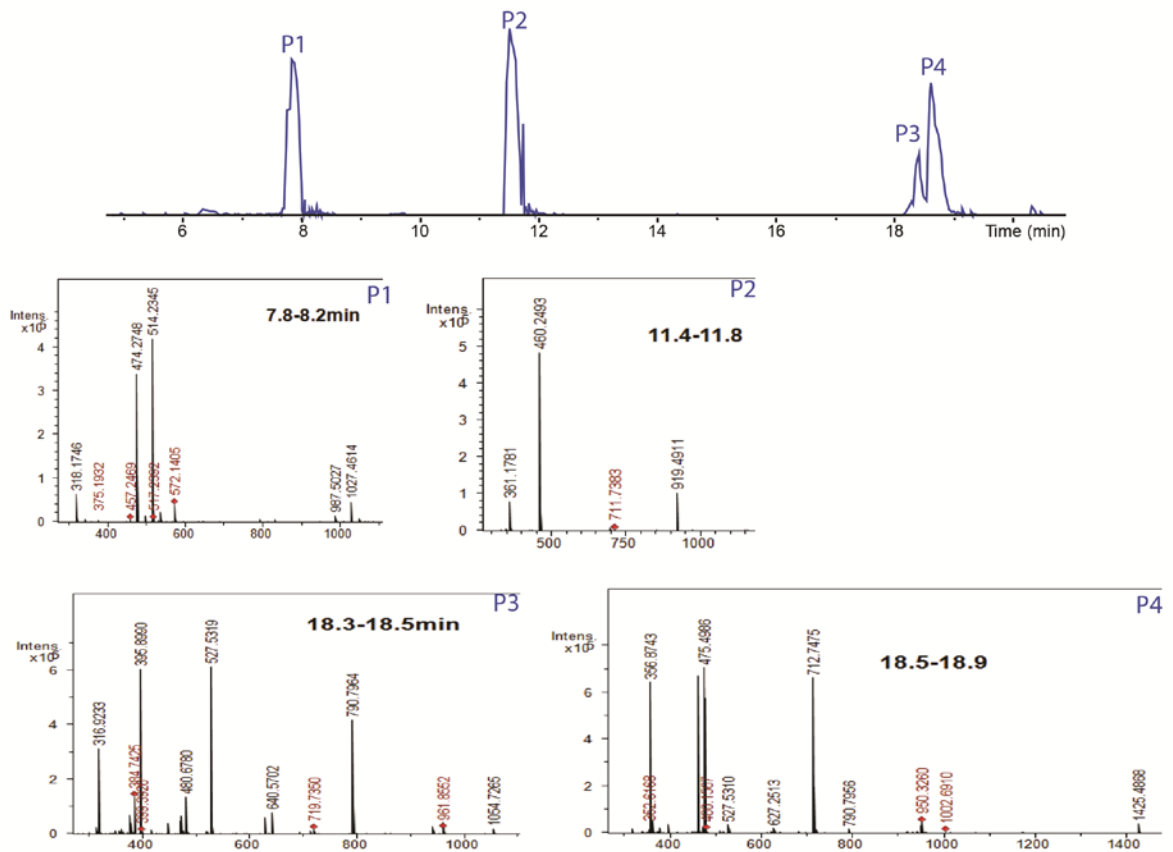


Figure S4.3. Analysis of rBuIIIB^Δ Isoform 2 by MS (Top) Total ion chromatograph of the tryptic cleavage products of rBuIIIB^Δ Isoform 2. (Bottom) MS spectra of each of the tryptic cleavage products.

rBullIB^Δ Isoform 3

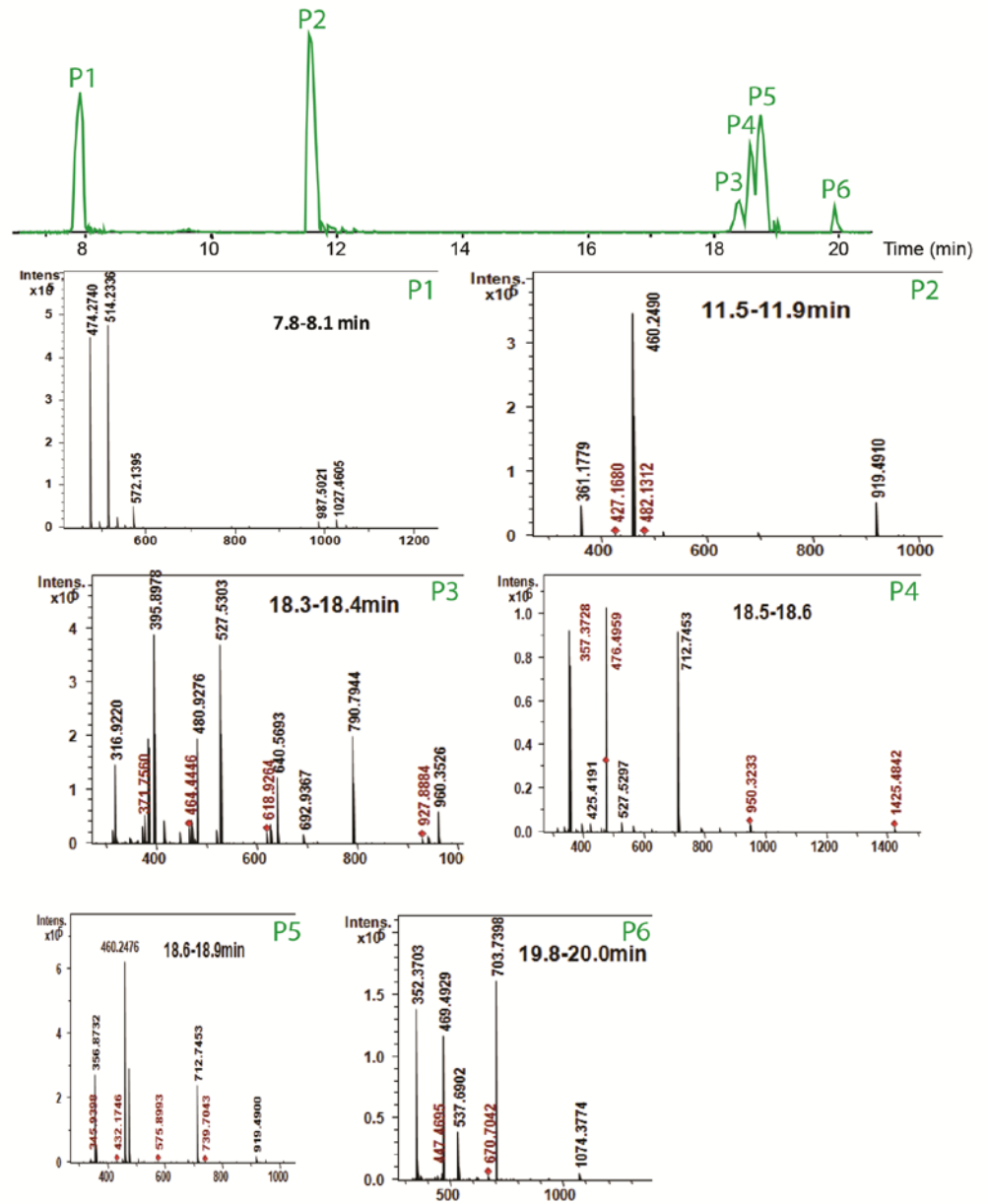


Figure S4.4. Analysis of rBullIB^Δ Isoform 3 by MS (Top) Total ion chromatogram of the tryptic cleavage products of rBullIB^Δ Isoform 3. (Bottom) MS spectra of each of the tryptic cleavage products.

rBuIIIB^Δ Isoform 4

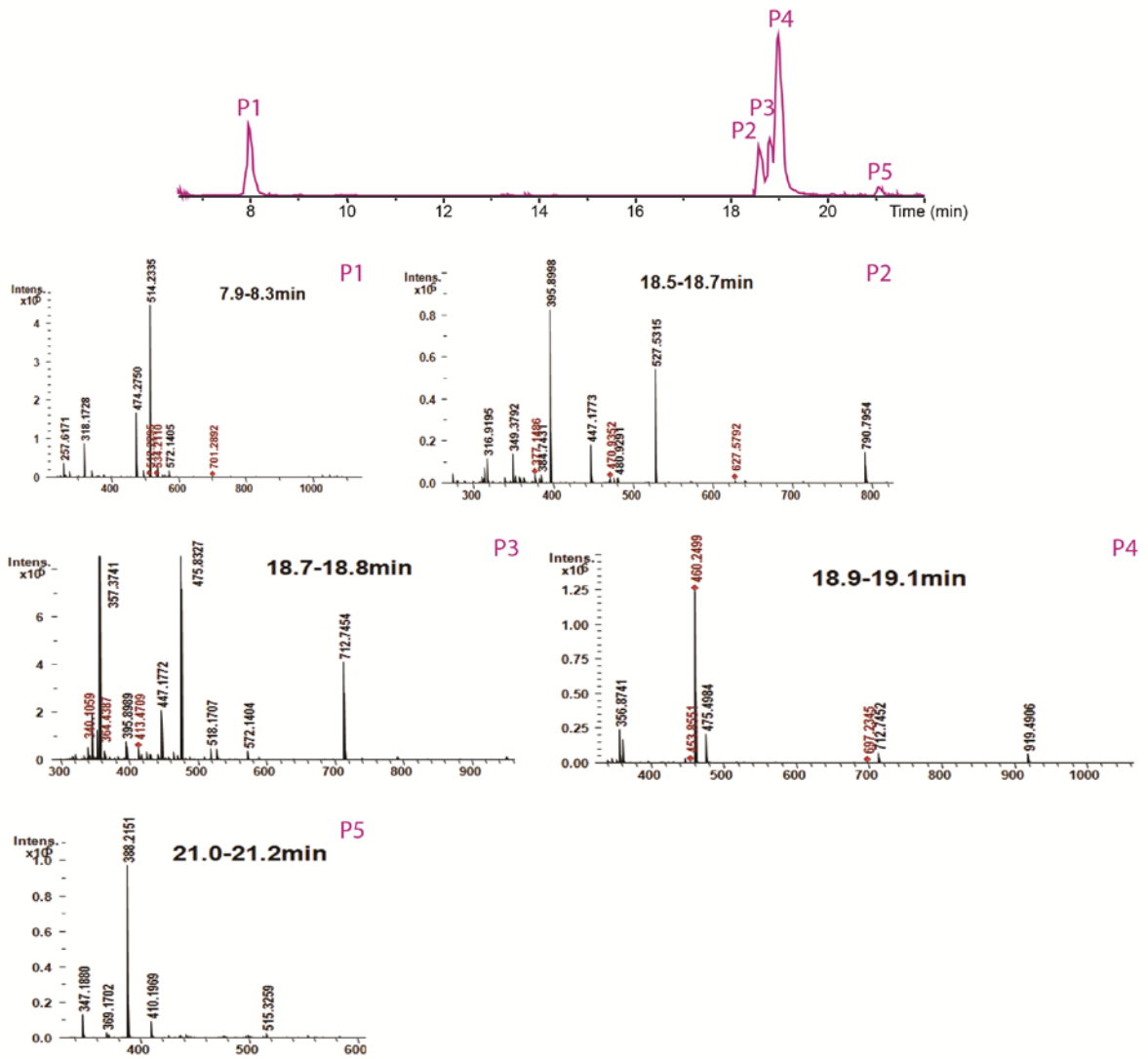


Figure S4.5. Analysis of rBuIIIB^Δ Isoform 4 by MS (Top) Total ion chromatograph of the tryptic cleavage products of rBuIIIB^Δ Isoform 4. (Bottom) MS spectra of each of the tryptic cleavage products.

rBuIIIB^Δ Isoform 5

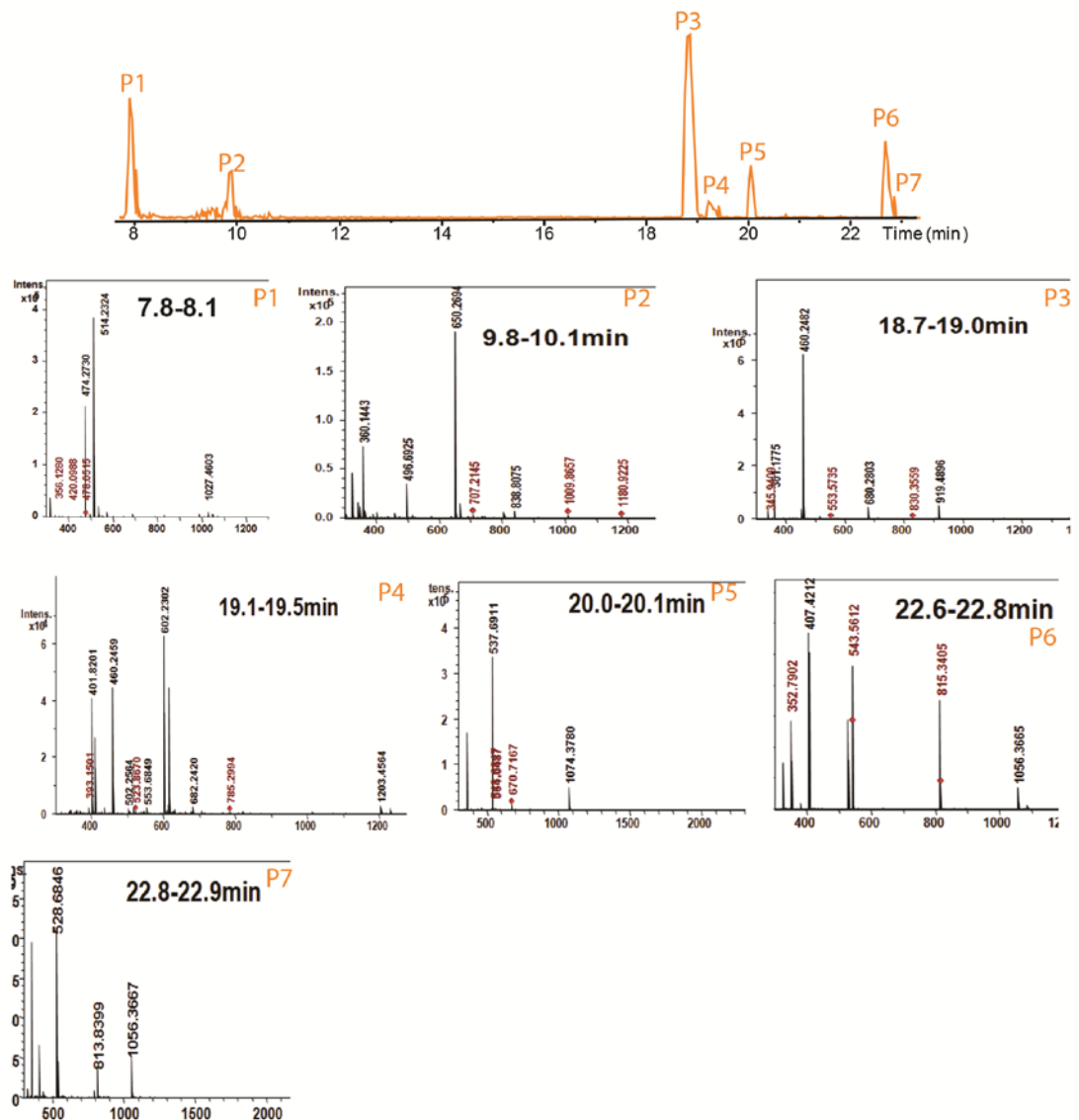


Figure S4.6. Analysis of rBuIIIB^Δ Isoform 5 by MS (Top) Total ion chromatograph of the tryptic cleavage products of rBuIIIB^Δ Isoform 5. (Bottom) MS spectra of each of the tryptic cleavage products.

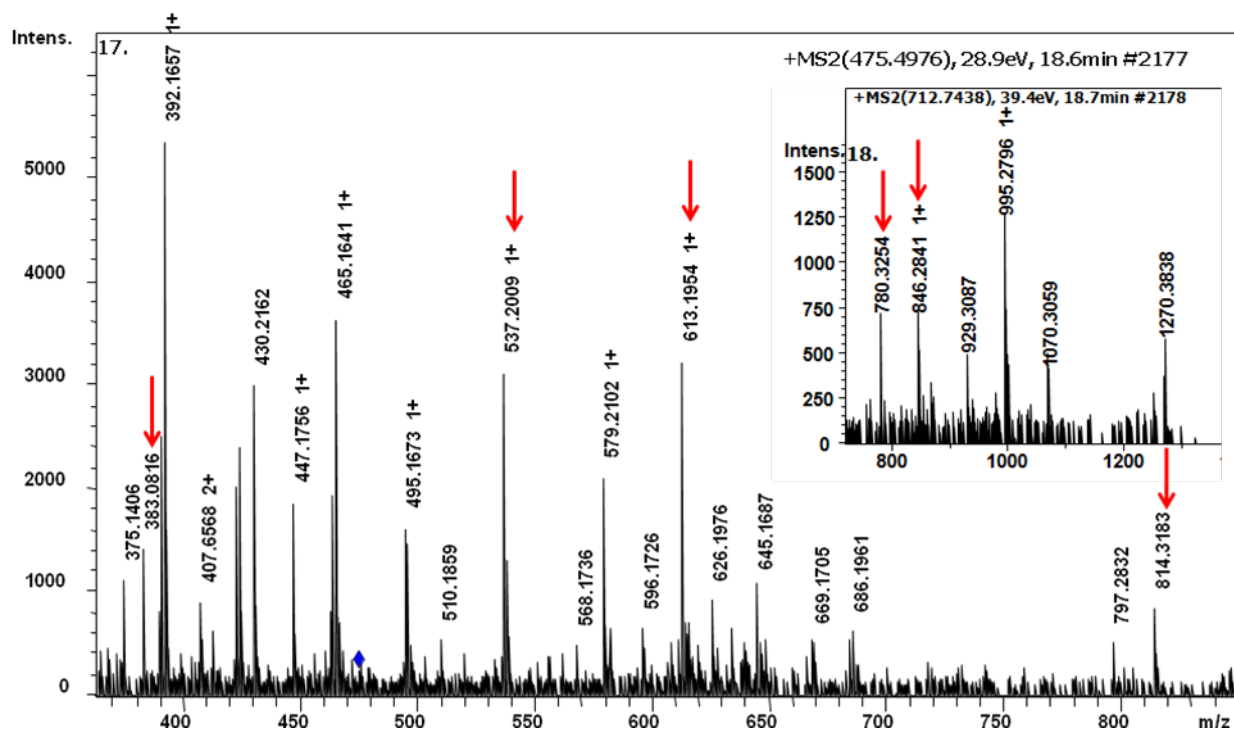


Figure S4.7. MS/MS fragmentation of diagnostic ions from of the total ion chromatograph of rBuIIIb[^] Isoform 4 Peak 3. Fragmentation was performed on the double-charged $[M+2H]^{+2}$ and triple-charged $[M+3H]^{+3}$ ions of 475.8 and 712.7 (inset) m/z , respectively. Unique fragment ions that were instrumental in establishing the connectivity of Isoform 4 are indicated by red arrows.

Chapter 5

Interactions of Disulfide-deficient Selenocysteine Analogues of μ -Conotoxin BuIIIb with the α -subunit of the Voltage-gated Sodium Channel Subtype Nav1.3

Once the disulfide connectivity for the most active isoform had been established, an efficiently folding analogue of μ -BuIIIb was constructed that facilitated comprehensive SAR studies of non-cysteine residues. These studies served to identify important amino acid residues for block of VGSCs.

This chapter consists of the published manuscript:

Green, B. R.; Zhang, M. M.; Chhabra, S.; Robinson, S. D.; Wilson, M. J.; Redding, A.; Olivera, B. M.; Yoshikami, D.; Bulaj, G.; Norton, R. S. Interactions of disulfide-deficient selenocysteine analogues of μ -conotoxin BuIIIb with the α -subunit of the voltage-gated sodium channel subtype 1.3. *FEBS J.* 2014, 281(13): 2885-2898.

5.1 Declaration for Thesis Chapter 5

5.1.1 Declaration by candidate

In the case of Chapter 5, the nature and extent of my contribution to the work was the following:

Nature of contribution	Contribution (%)
Jointly conceived the study and wrote the paper. Designed and executed experiments, and analysed experimental data.	70%

The following co-authors contributed to the work. If co-authors are students at Monash University, the extent of their contribution in percentage terms must be stated:

Name	Nature of contribution	Contribution (%)
Min-Min Zhang	Assisted with electrophysiology experiments	
Sandeep Chhabra	Assisted with NMR experiments.	
Samuel D. Robinson	Assisted with NMR experiments.	
Michael J. Wilson	Assisted with electrophysiology experiments	
Addison Redding	HPLC purification and folding of analogues.	
Baldomero M. Olivera	Contributed reagents/materials/analysis tools.	
Doju Yoshikami	Contributed reagents/materials/analysis tools.	
Grzegorz Bulaj	Contributed reagents/materials/analysis tools.	
Raymond S. Norton	Assisted with manuscript preparation and intellectual input. Corresponding author	

The undersigned hereby certify that the above declaration correctly reflects the nature and extent of the candidate's and co-authors' contributions to this work*.

Candidate's
signature 

Date
22.01.16

Main
supervisor's
signature 

Date
22.01.16

Interactions of disulfide-deficient selenocysteine analogs of μ -conotoxin BullIB with the α -subunit of the voltage-gated sodium channel subtype 1.3

Brad R. Green^{1,2}, Min-Min Zhang³, Sandeep Chhabra¹, Samuel D. Robinson¹, Michael J. Wilson³, Addison Redding³, Baldomero M. Olivera³, Doju Yoshikami³, Grzegorz Bulaj^{2,3} and Raymond S. Norton¹

¹ Medicinal Chemistry, Monash Institute of Pharmaceutical Sciences, Monash University, Parkville, Vic., Australia

² Department of Medicinal Chemistry, College of Pharmacy, University of Utah, Salt Lake City, UT, USA

³ Department of Biology, University of Utah, Salt Lake City, UT, USA

Keywords

conotoxin; disulfide; neuropathic pain; selenocysteine; voltage-gated sodium channel

Correspondence

R. S. Norton, Monash Institute of Pharmaceutical Sciences, 381 Royal Parade, Parkville, Vic. 3052, Australia

Fax: +61 3 9903 9582

Tel: +61 3 9903 9167

E-mail: ray.norton@monash.edu

G. Bulaj, Department of Medicinal Chemistry, College of Pharmacy, University of Utah, Salt Lake City, UT, USA

Fax: +1 801 581 7087

Tel: +1 801 581 4371

E-mail: grzegorz.bulaj@hsc.utah.edu

(Received 10 March 2014, revised 18 April 2014, accepted 5 May 2014)

doi:10.1111/febs.12835

Inhibitors of the α -subunit of the voltage-gated sodium channel subtype 1.3 ($\text{Na}_V1.3$) are of interest as pharmacological tools for the study of neuropathic pain associated with spinal cord injury and have potential therapeutic applications. The recently described μ -conotoxin BullIB (μ -BullIB) from *Conus bullatus* was shown to block $\text{Na}_V1.3$ with submicromolar potency ($K_d = 0.2 \mu\text{M}$), making it one of the most potent peptidic inhibitors of this subtype described to date. However, oxidative folding of μ -BullIB results in numerous folding isoforms, making it difficult to obtain sufficient quantities of the active form of the peptide for detailed structure–activity studies. In the present study, we report the synthesis and characterization of μ -BullIB analogs incorporating a disulfide-deficient, diselenide-containing scaffold designed to simplify synthesis and facilitate structure–activity studies directed at identifying amino acid residues involved in $\text{Na}_V1.3$ blockade. Our results indicate that, similar to other μ -conotoxins, the C-terminal residues (Trp16, Arg18 and His20) are most crucial for Na_V1 blockade. At the N-terminus, replacement of Glu3 by Ala resulted in an analog with an increased potency for $\text{Na}_V1.3$ ($K_d = 0.07 \mu\text{M}$), implicating this position as a potential site for modification for increased potency and/or selectivity. Further examination of this position showed that increased negative charge, through γ -carboxyglutamate replacement, decreased potency ($K_d = 0.33 \mu\text{M}$), whereas replacement with positively-charged 2,4-diaminobutyric acid increased potency ($K_d = 0.036 \mu\text{M}$). These results provide a foundation for the design and synthesis of μ -BullIB-based analogs with increased potency against $\text{Na}_V1.3$.

Introduction

The μ -conotoxins are a family of venom-derived peptides that block the α -subunit of the voltage-gated sodium channels (Na_V1), several of which are implicated in various pain pathways. These peptides act by

binding at neurotoxin receptor site 1 on the outer vestibule of the Na^+ conductance pore [1]. The μ -conotoxins are characterized by a six-cysteine framework ($\text{C}_I\text{C}_{II}(\text{X}_n)\text{C}_{III}(\text{X}_n)\text{C}_{IV}(\text{X}_n)\text{C}_V\text{C}_{VI}$) cross-linked

Abbreviations

1D, one-dimensional; 2D, 2-dimensional; ACN, acetonitrile; ddSecBullIB, disulfide-deficient selenocysteine-containing BullIB; DTNP, 2,2'-dithiobis(5-nitropyridine); Na_V1 , the α -subunit of the voltage-gated sodium channel subtype 1, cloned from rat; SAR, structure–activity relationship; TFA, trifluoroacetic acid; μ -BullIB, μ -conotoxin BullIB.

by three disulfide bridges. The earliest reports identified μ -conotoxins, specifically μ -GIIIA and μ -PIIIA, that were selective for the skeletal muscle subtype ($\text{Na}_V1.4$) [2,3]. More recent studies have focused on μ -conotoxins such as μ -KIIIA and μ -SIIIA, which preferentially block neuronal subtypes ($\text{Na}_V1.2$) over skeletal ($\text{Na}_V1.4$) and cardiac ($\text{Na}_V1.5$) muscle subtypes. These peptides have attracted considerable interest because of their potent analgesic activity in animal models of pain [4], although nonselective blockade of other Na_V1 subtypes has hindered their development as therapeutics. In an attempt to engineer in subtype selectivity, structure–activity relationship (SAR) studies were conducted to determine critical amino acid residues and subsequently identify potential sites for chemical modification. To date, detailed SAR studies have been carried out on a limited number of these peptides, including μ -GIIIA, μ -PIIIA, μ -KIIIA and μ -SIIIA [3–7].

Recently, several new μ -conotoxins were identified in the venom of *Comus bullatus* [8]. μ -conotoxin BuIIIB (μ -BuIIIB) exhibited significant differences from previously described μ -conotoxins, particularly with respect to the primary sequence at the N-terminus (Fig. 1A). Initial studies revealed that μ -BuIIIB almost completely blocked the sodium current in the $\text{Na}_V1.4$ (skeletal muscle) subtype, with near irreversibility [8]. More recently, Wilson *et al.* [9] showed that μ -BuIIIB also blocked the $\text{Na}_V1.3$ subtype with relatively high potency ($K_d = 0.2 \mu\text{M}$), whereas μ -KIIIA and μ -SIIIA exhibited only modest blockade of this subtype ($\text{IC}_{50} = 8$ and $11 \mu\text{M}$, respectively). The importance of $\text{Na}_V1.3$ with respect to neuropathic pain lies in its increased expression after axotomy, where the expression of other subtypes such as $\text{Na}_V1.8$ and $\text{Na}_V1.9$ is decreased [10,11]. To further examine the role of $\text{Na}_V1.3$ in neuropathic pain, potent and selective inhibitors of this channel are needed. However, such ligands are currently unavailable.

In the present study, we describe the development of a disulfide-deficient, diselenide-bridge containing analog of μ -conotoxin BuIIIB (disulfide-deficient selenocysteine-containing BuIIIB; ddSecBuIIIB) as the basis for an alanine scan to identify residues that contribute to blockade of $\text{Na}_V1.3$ (Fig. 1B). The advantages of this approach over a more traditional Ala-scan using the peptide containing three disulfide bridges are a simplification of the oxidative folding pathway and unambiguous assignment of the disulfide connectivity. μ -BuIIIB was chosen as a model system for the present study because of the particular challenges faced by oxidative folding of this peptide. By reducing the number of potential folding intermediates through diselenide

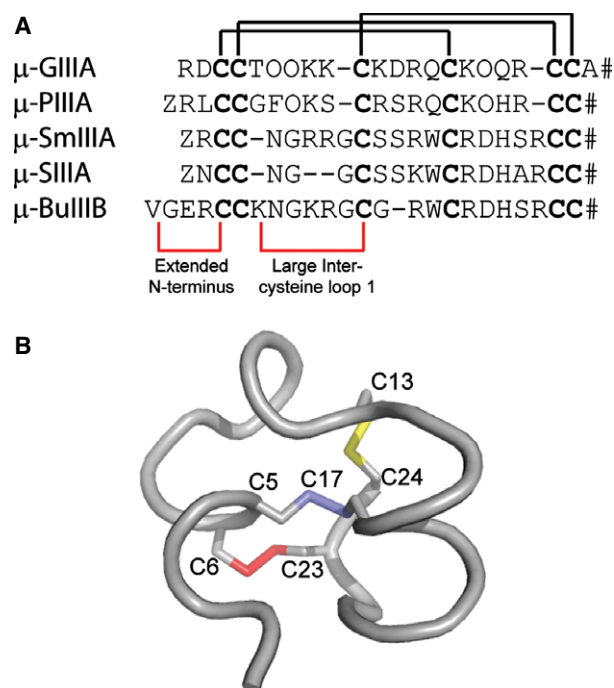


Fig. 1. (A) Sequence alignment of μ -BuIIIB with other μ -conotoxins. These toxins are characterized by a shared disulfide-framework and the ability to block voltage-gated sodium channel subtypes. μ -BuIIIB is distinguished from other members of this class by an extended N-terminus, in addition to increased length of inter-cysteine loop 1. (B) Description of the ddSecBuIIIB scaffold. Solution structure of μ -BuIIIB, with disulfide connectivity, is shown (Protein Data Bank code: [2LO9](#)) (19). Diselenide replacement of the Cys5-Cys17 bridge (blue) facilitated cyclization between these two residues independent of disulfide bridge formation. Removal of the Cys6-Cys23 bridge (red), by replacement with Ala, reduced the number of possible folding species to three for each ddBuIIIB analog shown. The BuIIIB[C5U,C17U,C6A,C23A] analog (i.e. ddSecBuIIIB) was selected as a framework to carry out Ala-replacement studies based on the ‘native-like’ blockade of $\text{Na}_V1.3$ ($K_d = 0.2 \mu\text{M}$). The ddSecBuIIIB scaffold was employed to assess the importance of each noncysteine residue within the primary sequence against $\text{Na}_V1.3$ and $\text{Na}_V1.4$.

replacement of the Cys5-Cys17 pairing, and by elimination of the Cys6-Cys23 disulfide bridge, we created a peptide scaffold in which the individual contributions of noncysteine amino acid residues could be studied. Disulfide deletion and diselenide-bridge incorporation have previously been used, either individually or in combination, to facilitate oxidative folding studies of other conotoxins such as μ -SIIIA, μ -KIIIA and ω -GVIA [12–14], although these strategies have yet to be employed to facilitate SAR studies of disulfide-rich conotoxins. This approach could also be employed to rapidly determine amino acid residues critical for biological activity in other cysteine-rich peptides.

Results

Chemical synthesis

The synthesis, purification and oxidative folding steps are often the greatest impediments to SAR studies of disulfide-rich conotoxins. Oxidation of such conotoxins can result in multiple folding isoforms, yielding limited quantities of the properly folded peptide for pharmacological characterization. Furthermore, determination of the disulfide connectivities of the active isoform can be labor intensive and often requires sophisticated analysis methods, such as selective reduction-alkylation, direct MS fragmentation or NMR methods [15,16]. Before embarking on SAR studies of μ -BuIIIB, we first determined the contributions of individual disulfide bridges in μ -BuIIIB to $\text{Na}_v1.3$ inhibition.

An initial series of disulfide-deficient analogs was constructed where we systematically replaced the pair of cysteines in each disulfide with a pair of alanines (Table 1). Removal of the Cys5-Cys17 bridge led to a slight increase in k_{on} (0.17 versus $0.085 \mu\text{M}^{-1}\cdot\text{min}^{-1}$) and a much greater increase in k_{off} compared to the unmodified peptide (2.6 versus 0.07min^{-1}). These values translated to a significant decrease in potency for BuIIIB[C5A,C17A] ($K_d = 15.7$ versus $0.2 \mu\text{M}$), indicating that this bridge is important for $\text{Na}_v1.3$ inhibition. The Cys5-Cys17 bridge was therefore selected for replacement by a redox-favored diselenide bridge. Removal of either the Cys6-Cys23 or Cys13-Cys24 bridges yielded similar results, with k_{on} values of 0.23 and $0.34 \mu\text{M}^{-1}\cdot\text{min}^{-1}$, respectively. The k_{off} values were also similar, and closer to that of the unmodified peptide (0.059 and 0.038min^{-1} , respectively). These values translated to potencies in blocking $\text{Na}_v1.3$ equal to or greater than that of wild-type μ -BuIIIB (K_d of 0.26 and $0.11 \mu\text{M}$ for BuIIIB[C6A,C23A] and BuIIIB[C13A,C24A], respectively) (Table 1). The solution structure of μ -BuIIIB shows that the N-terminal helix is anchored to the core of the molecule by the Cys5-

Cys17 and Cys6-Cys23 disulfide bridges [16]. Removal of either the Cys6-Cys23 or Cys13-Cys24 bridges would be expected to have structural consequences, although it appears that those changes do not significantly affect the peptide's activity against $\text{Na}_v1.3$.

Using the information obtained from disulfide-deficient BuIIIB analogs, two additional analogs, BuIIIB [C5U,C17U,C6A,C23A] and BuIIIB[C5U,C17U,C13A,C24A], were constructed to identify the optimal disulfide-deficient, selenoconotoxin scaffold as a basis for SAR studies. Slight differences in biological activity were observed between the disulfide-deficient analogs and the ddSecBuIIIB scaffolds. BuIIIB[C5U,C17U,C6A,C23A] exhibited a faster k_{on} and k_{off} than BuIIIB [C5U,C17U,C13A,C24A], resulting in a scaffold that exhibited 'native-like' potency for $\text{Na}_v1.3$ ($K_d = 0.2 \mu\text{M}$) (Table 1).

Oxidative folding

Crude peptide was removed from the solid support resin using modified reagent K cleavage mixture containing 2,2'-dithiobis(5-nitropyridine) (DTNP) as described previously [17,18]. Briefly, the cleavage mixture was supplemented with 1.3 equivalents DTNP to remove the *p*-methoxybenzyl protecting group from selenocysteine, resulting in a selenocysteine–2-thio-5-nitropyridine adduct. This adduct was then removed by treatment for 2 h with 50 mM dithiothreitol, leading to spontaneous formation of the diselenide bridge between residues 5 and 17 (Sec5-Sec17) [19]. Deprotection and cyclization steps were performed directly on the crude mixture to minimize losses from additional purification steps. As such, quantitative yields of deprotection were not determined. However, analysis of the crude, Se-Se containing BuIIIB[C5U,C17U,C6A,C23A] analog revealed a single major product comprising 22% of the total mixture based on analytical HPLC peak area. The diselenide-containing peptides were then purified in parallel by C_{18} solid-phase

Table 1. Structural and pharmacological characterization of ddBuIIIB and ddSecBuIIIB scaffolds. Analogs were screened against r- $\text{Na}_v1.3$. U, selenocysteine. ΔK_d , ratio of each analog to wild-type μ -BuIIIB.

Peptide	M_r (calculated/observed)	Correct isomer	k_{on} ($\mu\text{M}\cdot\text{min}^{-1}$)	k_{off} (min^{-1})	K_d (μM)	ΔK_d
μ -BuIIIB	2761.20/2761.19 ^a	16%	0.085 ± 0.01	0.017 ± 0.007	0.20 ± 0.02	
BuIIIB[C5A,C17A]	2700.25/2700.24 ^a	32%	0.16 ± 0.06	2.6 ± 0.86	15.7 ± 2.6	79
BuIIIB[C6A,C23A]	2700.25/2700.24 ^a	37%	0.23 ± 0.02	0.059 ± 0.004	0.26 ± 0.03	1.3
BuIIIB[C13A,C24A]	2700.25/2700.80 ^a	35%	0.34 ± 0.03	0.038 ± 0.003	0.11 ± 0.013	0.55
BuIIIB[C5U,C17U,C6A,C23A]	2796.13/2796.13 ^b	51%	0.12 ± 0.01	0.026 ± 0.004	0.2 ± 0.04	
BuIIIB[C5U,C17U,C13A,C24A]	2796.13/2796.14 ^b	43%	0.19 ± 0.02	0.08 ± 0.005	0.42 ± 0.05	2.1

^a Masses determined by MALDI-TOF.

^b Masses determined by ESI-MS.

extraction. Finally, formation of either the Cys13-Cys24 or Cys6-Cys23 bridge was achieved using the solid support oxidant CLEAR-Ox[®] (Peptides International, Louisville, KY, USA). For each of the ddSec-BullIB analogs, a well-separated major peak corresponding to the fully folded peptide was observed (Fig. 2). Oxidative folding resulted in greater accumulation of the desired products, as determined by peak area using analytical HPLC, for both BullIB[C5U, C17U, C6A, C23A] (51%) and BullIB[C5U, C17U, C13A, C24A] (43%) compared to 16% for the unmodified μ -BullIB (Fig. 2B,E and Table 1).

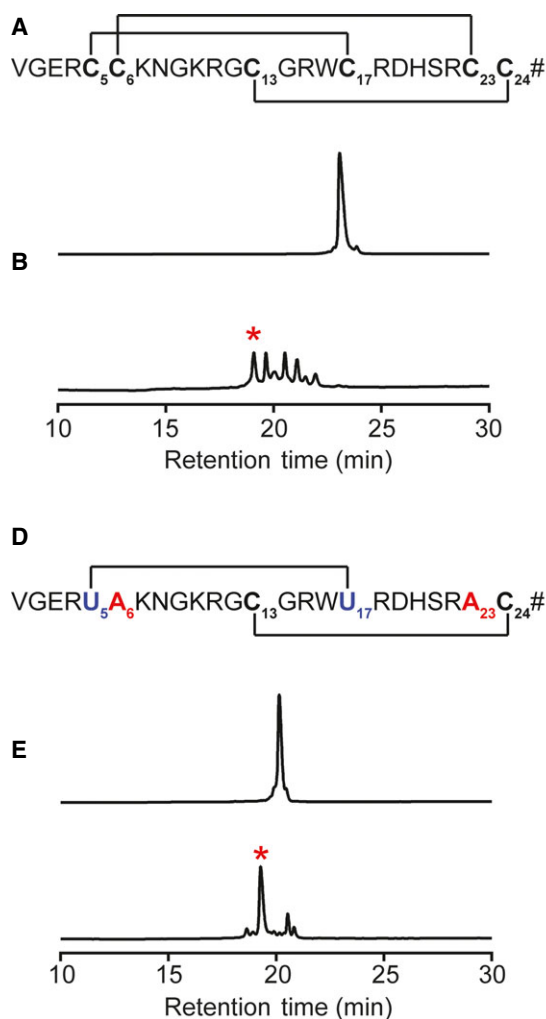
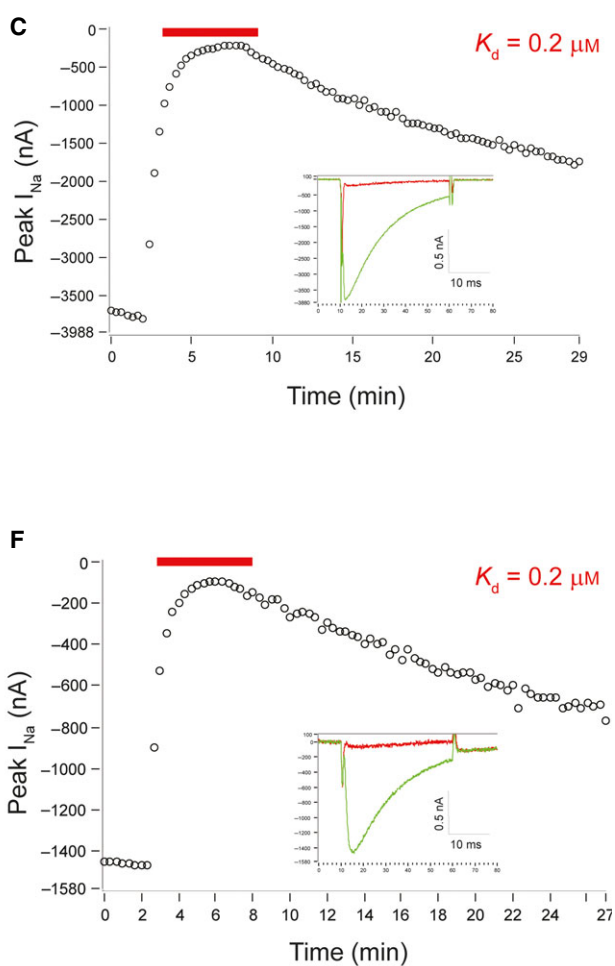


Fig. 2. Comparison of wild-type μ -BullIB with ddSecBullIB. (A) Sequence of the unmodified peptide showing experimentally-determined disulfide connectivity. (B) HPLC folding profiles of linear peptide (top) and folding mixture (bottom); asterisks indicate peaks tested for functional activity. (C) Representative time course of the blockade of rNav_v1.3 by 10 μ M peptide (bar indicates when peptide was present). Inset shows current traces obtained before (green) and during (red) exposure of the peptide. (D) Sequence of the ddSecBullIB scaffold showing the positions of the selenocysteine (U) and alanine replacements. (E) HPLC profile of linear peptide (top) and folding mixture (bottom); asterisks indicate peak tested for functional activity. The sample profile illustrates the efficiency of the folding pathway. (F) Representative time course of the blockade of Nav_v1.3 (for comparison of kinetic constants, see Table 1). Inset: current traces obtained before (green) and during (red) exposure to peptide.

¹H NMR of ddSecBullIB

The conformation of BullIB[C5U, C17U, C6A, C23A] was compared with that of the native peptide using NMR spectroscopy. After optimization of the pH and temperature (Fig. 3), one-dimensional (1D) and two-dimensional (2D) ¹H NMR spectra were acquired at pH 3.0 and 35 °C, ¹H chemical shifts were determined by standard sequential assignment (Tables S1 and S2; BMRB ID #19923) and plots of deviations from random coil chemical shifts [20] for ddSecBullIB and μ -BullIB were constructed. The 1D ¹H spectrum for



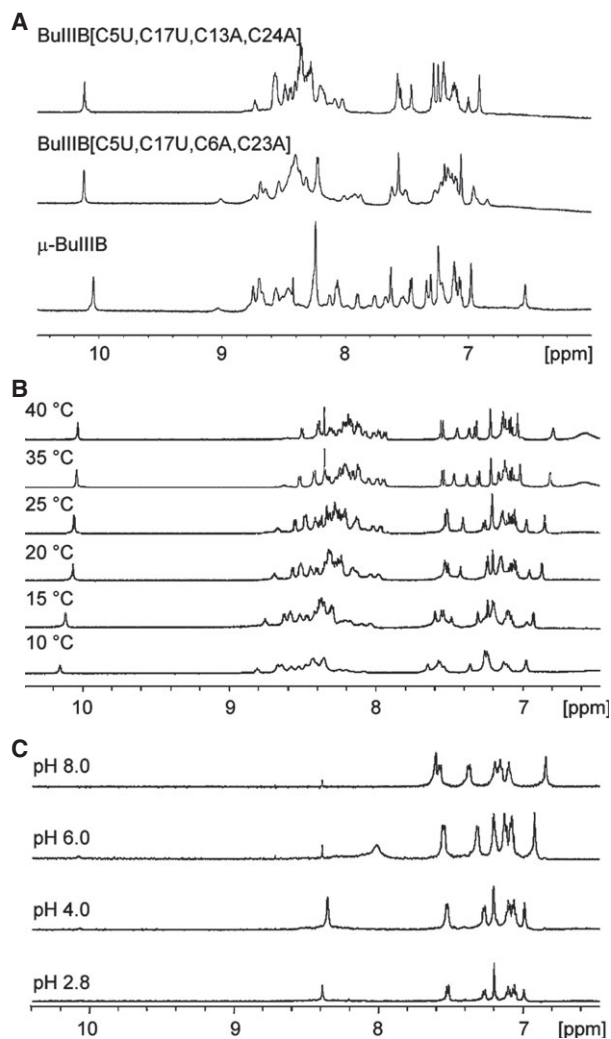


Fig. 3. Optimization of NMR conditions for ddSecBuIIIIB. (A) 1D ^1H NMR spectra of BuIIIIB[C5U,C17U,C13A,C24A] and BuIIIIB[C5U,C17U,C6A,C23A] versus μ -BuIIIIB. Peptide samples were 160 μM in 10 mM phosphate buffer containing 5% $^2\text{H}_2\text{O}$ (pH 5.5). The water signal was suppressed by excitation sculpting. Spectra were recorded at 22 $^\circ\text{C}$ over 128 scans at 600 MHz at a spectral width of 11 p.p.m. The amide/aromatic region has been shown to illustrate the decreased spectral dispersion of the disulfide-deficient, diselenide bridge-containing analogs compared to the wild-type μ -BuIIIIB. (B) 1D ^1H NMR spectra of BuIIIIB[C5U,C17U,C6A,C23A] (ddSecBuIIIIB) at different temperatures in 5% $^2\text{H}_2\text{O}$. The sample pH was 4.8 and spectra were acquired using a Bruker 600 MHz spectrometer using 128 scans at a spectral width of 12 p.p.m. (C) pH titration of ddSecBuIIIIB. 1D ^1H NMR spectra were collected in 100% $^2\text{H}_2\text{O}$, the pH was adjusted to with NaO^2H and spectra were acquired at 25 $^\circ\text{C}$. Spectra were collected using 32 scans at a spectral width of 16 p.p.m. The amide/aromatic region is shown.

ddSecBuIIIIB was less well dispersed than that of μ -BuIIIIB (Fig. 4A). H^α chemical shift deviations from random coil (Fig. 4) suggested that the N-terminus of

ddSecBuIIIIB was largely unstructured, with some degree of helicity near the C-terminus between residues Gly14 and His20. H^α chemical shifts were generally similar to μ -BuIIIIB, whereas the H^N shifts showed greater differences compared to the native peptide (Fig. 4B). The solution structure of native μ -BuIIIIB contains helices at both the N- and C-termini [16] and it is clear that the C-terminal helix is partially preserved in ddSecBuIIIIB but the N-terminal region is less structured. These results are of interest because it was reported previously that functionally important residues in μ -KIIIA reside in the C-terminal helical region of that peptide [21].

Structure–activity studies on ddSecBuIIIIB

Although NMR suggested conformational differences between ddSecBuIIIIB and μ -BuIIIIB, structure–activity studies were carried out to identify amino acid residues in ddSecBuIIIIB that contributed to $\text{Na}_\text{V}1.3$ blockade. These studies identified a number of residues, particularly near the C-terminus, that were important for $\text{Na}_\text{V}1.3$ potency (Table 2). Specifically, Ala-replacement of Trp16 or His 20 resulted in slow on-rate kinetics, which prevented steady-state binding from being achieved within the experimental time window at peptide concentrations near the expected K_d or IC_{50} . These analogs had an estimated 150-fold lower potency compared to μ -BuIIIIB or ddSecBuIIIIB ($K_\text{d} > 30 \mu\text{M}$). Ala-replacement of Arg15, Arg18 or Arg22 also led to deleterious effects on $\text{Na}_\text{V}1.3$ blockade ($K_\text{d} = 1.84, 15.7$ and $3.81 \mu\text{M}$, respectively) (Fig. 5 and Table 2). These results were interesting because earlier studies identified a crucial role for basic residues at the equivalent position to Arg15 in μ -BuIIIIB [5]. Although mutations at this position decreased potency, it is clear that the other positively-charged residues in this region play more pronounced roles in $\text{Na}_\text{V}1.3$ inhibition. These results were consistent with those reported by McArthur *et al.* [22], which showed three basic residues (Arg12, Arg14 and Lys17) near the C-terminus of μ -PIIIA contributing to the blockade of $\text{Na}_\text{V}1.2$ despite sharing a high degree of sequence homology with $\text{Na}_\text{V}1.4$ -selective μ -GIIIA. Our results highlight the importance of basic residues at the C-terminus of ddSecBuIIIIB for blockade of $\text{Na}_\text{V}1.3$ (Fig. 5 and Table 2).

Replacement of Val1, Asn8, Gly9, Gly12, Gly14 or Ser21 with Ala had little effect on $\text{Na}_\text{V}1.3$ potency (Table 2). These positions in the sequence are therefore potential sites of modification for peptide engineering to improve the physicochemical and/or pharmacological properties of μ -BuIIIIB. Similar

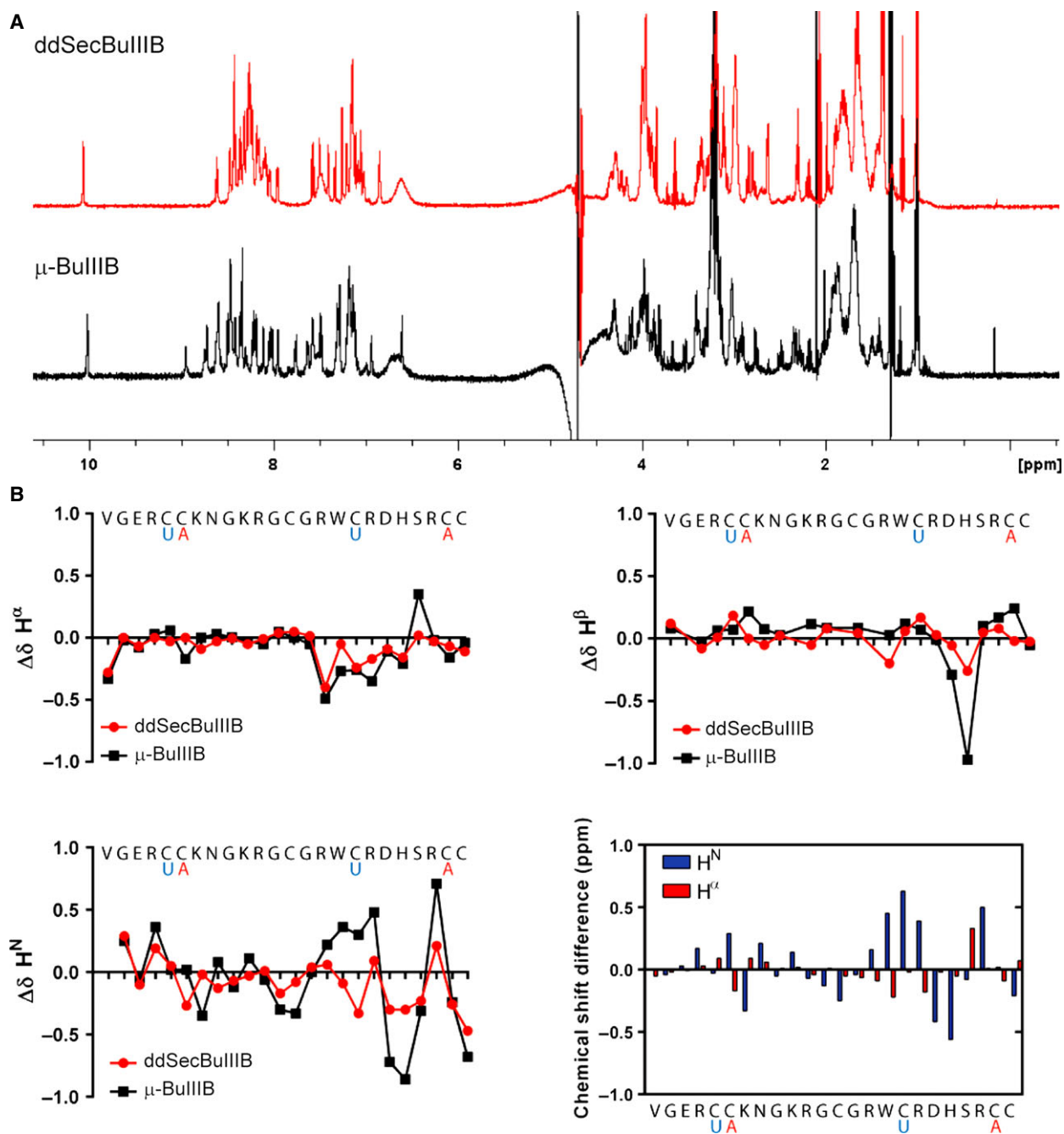


Fig. 4. Structural comparisons of μ -BullIB and ddSecBullIB. (A) 1D ^1H NMR spectra of ddSecBullIB scaffold (red) and wild-type μ -BullIB (black) at 35 °C, pH 3.0 and 600 MHz. (B) Deviation from random coil shifts of the H^α , H^β and H^N resonances of μ -BullIB (black) and ddSecBullIB (red) at 35 °C and pH 3.0 [20]. Random coil shift values for oxidized Cys were used to estimate chemical shift deviation from random coil for selenocysteines. H^N and H^α chemical shift differences between ddSecBullIB and μ -BullIB are also plotted.

approaches were applied previously, resulting in potent and/or selective analogs of the μ -conotoxins KIIIA and SIIIA [3,23]. In the context of the ddSecBullIB scaffold, mutations made to the basic residues in loop 1 (Lys7, Lys10 and Arg11) led to moderate effects on $\text{Na}_\text{V}1.3$ inhibition (K_d = 0.71, 1.02 and 1.12 μM ,

respectively) and little or no effect on $\text{Na}_\text{V}1.4$ inhibition (Fig. 5).

The most striking outcome of these studies was the improved potency obtained through substitution of Glu3 with Ala. This replacement actually improved $\text{Na}_\text{V}1.3$ potency by nearly three-fold (K_d = 0.07 μM)

Table 2. Summary of the ability of μ -BullIIB and Ala-scan analogs of ddSecBullIIB to block rNav_v1.3 and rNav_v1.4 expressed in *X. laevis* oocytes, as determined by two-electrode voltage-clamp measurements.

Analog	Nav _v 1.3			Nav _v 1.4		
	k_{on} ($\mu\text{M}\cdot\text{min}^{-1}$)	k_{off} (min^{-1})	K_{d} (μM)	k_{on} ($\mu\text{M}\cdot\text{min}^{-1}$)	k_{off} (min^{-1})	K_{d} (μM)
μ -BullIIB	0.085 ± 0.01	0.017 ± 0.007	0.2 ± 0.086	4.20 ± 0.760	0.015 ± 0.005	0.004 ± 0.001
ddSecBullIIB	0.13 ± 0.07	0.026 ± 0.002	0.2 ± 0.02	7.15 ± 0.036	0.009 ± 0.002	0.001 ± 0.000
[V1A] ^a	0.17 ± 0.015	0.038 ± 0.001	0.22 ± 0.02	0.940 ± 0.011	0.026 ± 0.002	0.027 ± 0.002
[G2A] ^a	0.087 ± 0.013	0.042 ± 0.003	0.48 ± 0.08	1.64 ± 0.258	0.054 ± 0.007	0.033 ± 0.007
[E3A] ^a	0.29 ± 0.047	0.02 ± 0.001	0.07 ± 0.012	41.6 ± 2.973	0.030 ± 0.002	0.001 ± 0.000
[R4A] ^a	0.026 ± 0.005	0.028 ± 0.003	1.1 ± 0.23	0.78 ± 0.081	0.022 ± 0.001	0.028 ± 0.003
[K7A] ^a	0.07 ± 0.005	0.05 ± 0.005	0.71 ± 0.088	1.73 ± 0.187	0.010 ± 0.001	0.006 ± 0.001
[N8A] ^a	0.062 ± 0.007	0.016 ± 0.001	0.26 ± 0.032	1.45 ± 0.220	0.005 ± 0.000	0.003 ± 0.001
[G9A] ^a	0.068 ± 0.013	0.027 ± 0.001	0.4 ± 0.08	1.03 ± 0.100	0.012 ± 0.001	0.012 ± 0.001
[K10A] ^a	0.050 ± 0.004	0.051 ± 0.004	1.02 ± 0.11	2.05 ± 0.276	0.008 ± 0.001	0.004 ± 0.001
[R11A] ^a	0.033 ± 0.002	0.037 ± 0.005	1.12 ± 0.15	1.11 ± 0.190	0.010 ± 0.000	0.009 ± 0.002
[G12A] ^a	0.098 ± 0.019	0.033 ± 0.004	0.34 ± 0.08	5.12 ± 0.068	0.008 ± 0.001	0.002 ± 0.000
[G14A] ^a	0.190 ± 0.002	0.070 ± 0.006	0.230 ± 0.107	5.53 ± 0.262	0.014 ± 0.001	0.003 ± 0.000
[R15A] ^a	0.060 ± 0.008	0.240 ± 0.012	1.84 ± 0.385	0.410 ± 0.035	0.105 ± 0.005	0.260 ± 0.026
[W16A] ^a	NA	1.69 ± 0.180	> 30	NA	1.68 ± 0.123	2.07 ± 0.284
[R18A] ^a	0.06 ± 0.008	0.78 ± 0.075	15.7 ± 0.296	1.26 ± 0.124	0.147 ± 0.008	0.13 ± 0.009
[D19A] ^a	0.22 ± 0.012	0.73 ± 0.073	0.54 ± 0.027	22.5 ± 3.005	0.144 ± 0.009	0.009 ± 0.001
[H20A] ^a	NA	1.01 ± 0.119	> 30	0.03 ± 0.004	0.219 ± 0.023	10.3 ± 2.448
[S21A] ^a	0.09 ± 0.003	0.02 ± 0.003	0.37 ± 0.059	3.41 ± 0.078	0.018 ± 0.002	0.005 ± 0.001
[R22A] ^a	0.06 ± 0.002	0.24 ± 0.012	3.81 ± 0.194	NA	0.174 ± 0.007	0.28 ± 0.005

Rate constants were calculated from at least three independent experiments using PRISM software (GraphPad Software Inc., San Diego, CA, USA). $K_{\text{d}} = k_{\text{off}}/k_{\text{on}}$. NA, K_{d} value was not available as a result of slow kinetics, which precluded steady state from being achieved at concentrations tested within the experimental time frame. Kinetic data for μ -BullIIB are from Wilson *et al.* [9].

^a Analogs possessing the ddSecBullIIB scaffold (BullIIB[C5U,C17U,C6A,C23A]).

(Fig. 5 and Table 2). To further investigate the effects of amino acid replacement of the acidic residue, a positional scan of Glu3 was conducted.

Positional scanning Glu3

Removal of the negatively-charged residue at position 3 led to increased potency against Nav_v1.3. This was consistent with findings by Ekberg *et al.* [24], who showed that the charge state of μ -conotoxins was important for interaction with the negatively-charged voltage-gated sodium channel pore region. To further explore the effects of charge at this position, analogs were constructed where Glu3 was replaced with either γ -carboxyglutamate (Gla; -2 charge) or L-2,4-diaminobutyric acid (Dab; $+1$ charge) (Fig. 6). Increasing the negative charge at position 3 reduced Nav_v1.3 potency by more than 1.5-fold ($K_{\text{d}} = 0.33 \mu\text{M}$), whereas reversal of the negative charge increased Nav_v1.3 potency ($K_{\text{d}} = 0.038 \mu\text{M}$) beyond that of the (neutral) Ala substitution (Fig. 6).

The steric effects of basic residues at this position were also examined (Fig. 7). A series of positively-charged analogs was synthesized and tested that

replaced Glu3 with L-Dap, Orn, Lys, Arg or His. All analogs containing basic residues at position 3 exhibited improved Nav_v1.3 potency. These studies revealed an optimal size for the side chain at this position, with groups smaller (e.g. Dap) or larger (e.g. ornithine, lysine, arginine and histidine) than Dab resulting in decreased potency compared to BullIIB[C5U,C17U,C6A,C23A,E3Dab] (Fig. 7). Similar to what was seen in experiments using Nav_v1.3, the [E3Dab] mutant showed increased potency against Nav_v1.4, with $k_{\text{on}} = 32.1 \mu\text{M}\cdot\text{min}^{-1}$, $k_{\text{off}} = 0.017 \pm 0.001 \text{ min}^{-1}$ and $K_{\text{d}} = 0.0005 \pm 0.0001 \mu\text{M}$ (data not shown). The SAR data suggested that any changes in Nav_v1.3 potency were closely mirrored by changes in potency against Nav_v1.4. As such, the other analogs were assayed against Nav_v1.3 only because the focus of the present study was on potency against Nav_v1.3 rather than subtype selectivity.

Discussion

We have created an analog of the μ -conotoxin BullIIB, ddSecBullIIB, which folds efficiently during oxidative folding to a single major product with well-defined

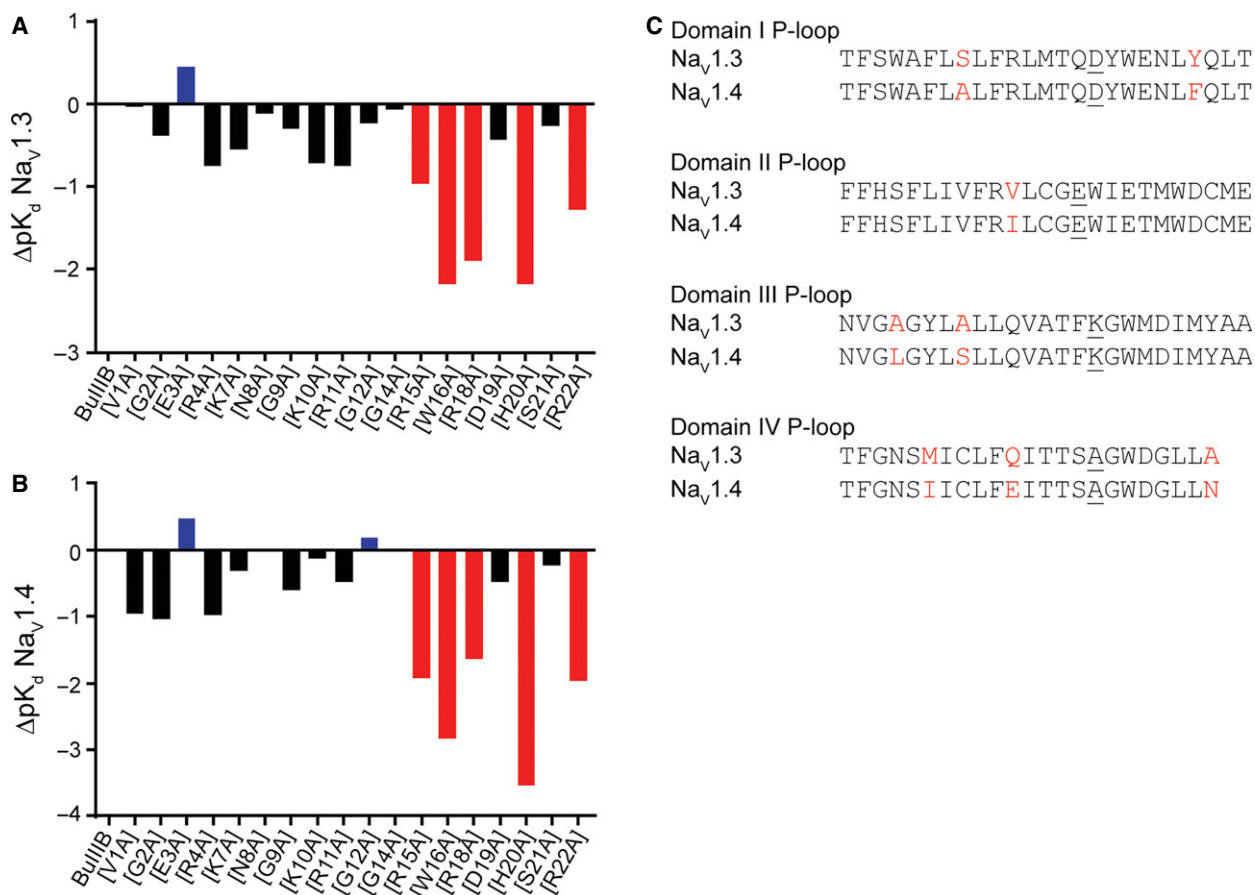


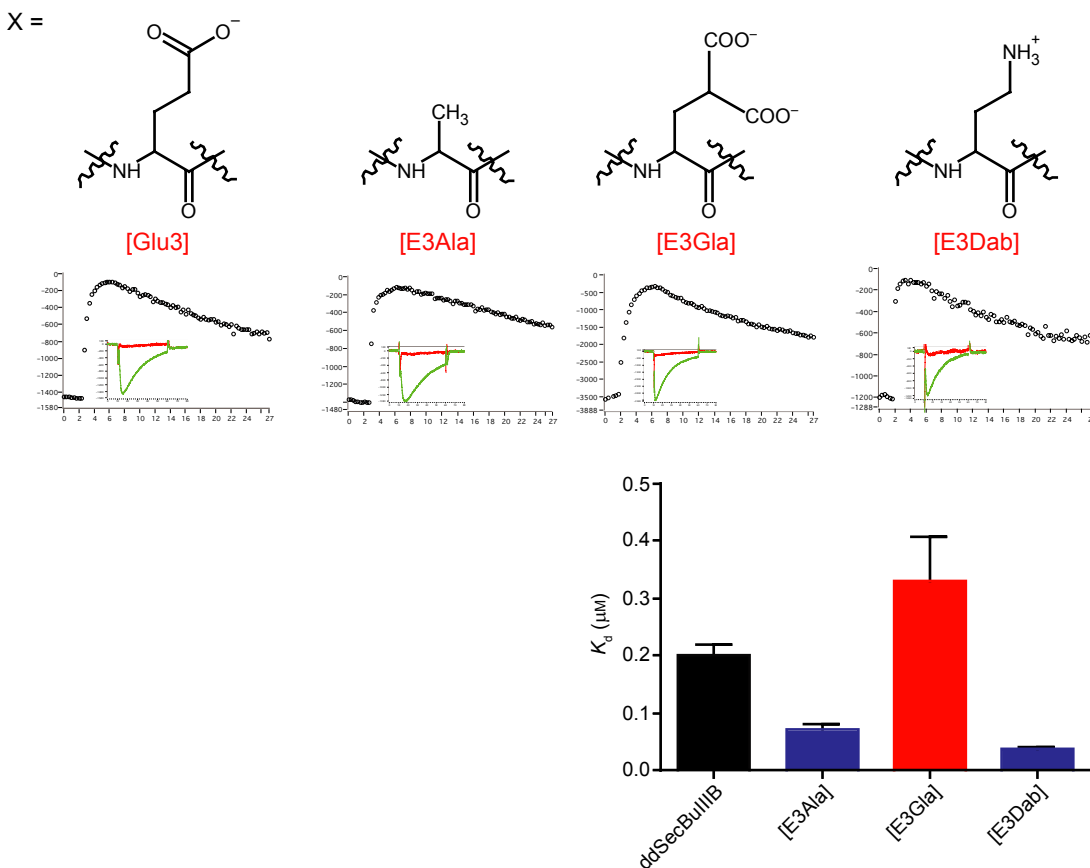
Fig. 5. Effects of Ala-substitution of noncysteine residues in the ddSecBullIB scaffold. Bar graphs compare the potencies (ΔpK_d s) of ddSecBullIB Ala-walk analogs with that of wild-type μ -BullIB ($\Delta pK_d = 0$) against Na_v1.3 (A) and Na_v1.4 (B). Substitutions that increased potency are shown in blue, those that dramatically decreased potency are shown in red, and those that produced mild to moderate effects are shown in black. (C) Sequence alignment of the P-loop regions of Na_v1.3 and Na_v1.4, which is the site of interaction of all μ -conotoxins, including μ -BullIB. Amino acid differences between subtypes in this region are indicated in red; residues comprising the selectivity filter (D, E, K and A) are underlined.

disulfide/diselenide connectivity. This stands in marked contrast to the native peptide, where, under optimized glutathione-assisted folding conditions, the biologically-active isoform comprised only 16% of the total folding mixture (Fig. 2 and Table 1).

¹H NMR spectra of the ddSecBullIB scaffold showed reduced amide peak dispersion compared to μ -BullIB. The differences in structure presumably resulted from greater flexibility of the molecule caused by removal of the Cys6-Cys23 disulfide bridge. It is intriguing, therefore, that this analog retained native-like potency for Na_v1.3. These results are not without precedent because Tietze *et al.* [25] showed that less-structured forms of the conotoxin μ -PIIIA also exhibited activity against the muscle subtype Na_v1.4, albeit with lower potency. Closer examination of chemical shift plots (Fig. 4) shows that ddSecBullIB retains some degree of α -helical content near the C-terminus,

which is known to be important for Na_v1-subtype blockade. In light of the conformational differences between the two peptides in solution, we suggest that the ddSecBullIB scaffold should be considered as a new blocker of this channel rather than simply as a proxy for native μ -BullIB. This analog therefore represents a useful new pharmacological tool for studies of Na_v1 channels, one that, importantly, refolds very efficiently to a well-defined product.

Structure–activity studies using ddSecBullIB identified the critical roles of aromatic and basic residues near the C-terminus of ddSecBullIB (Fig. 5). These results were largely consistent with previous SAR studies of other μ -conotoxins, presumably as a result of the high degree of homology amongst the neuronal-subtype preferring μ -conotoxins at the C-terminus. This region is considered to contribute to general voltage-gated sodium channel target specificity, whereas

A VGXRUA**K**NGKRGCGRWURDHS**RAC**

B

Analog	Nav1.3			
	k_{on} ($\mu\text{M}\cdot\text{min}^{-1}$)	k_{off} (min^{-1})	K_d (μM)	ΔK_d
BullIIB[C5U,C17U,C6A,C23A]	0.130 ± 0.007	0.026 ± 0.002	0.200 ± 0.020	–
BullIIB[C5U,C17U,C6A,C23A,E3Ala]	0.290 ± 0.047	0.020 ± 0.001	0.070 ± 0.012	0.35
BullIIB[C5U,C17U,C6A,C23A,E3Gla]	0.095 ± 0.013	0.031 ± 0.006	0.330 ± 0.077	1.6
BullIIB[C5U,C17U,C6A,C23A,E3Dab]	1.06 ± 0.054	0.040 ± 0.003	0.038 ± 0.003	0.19

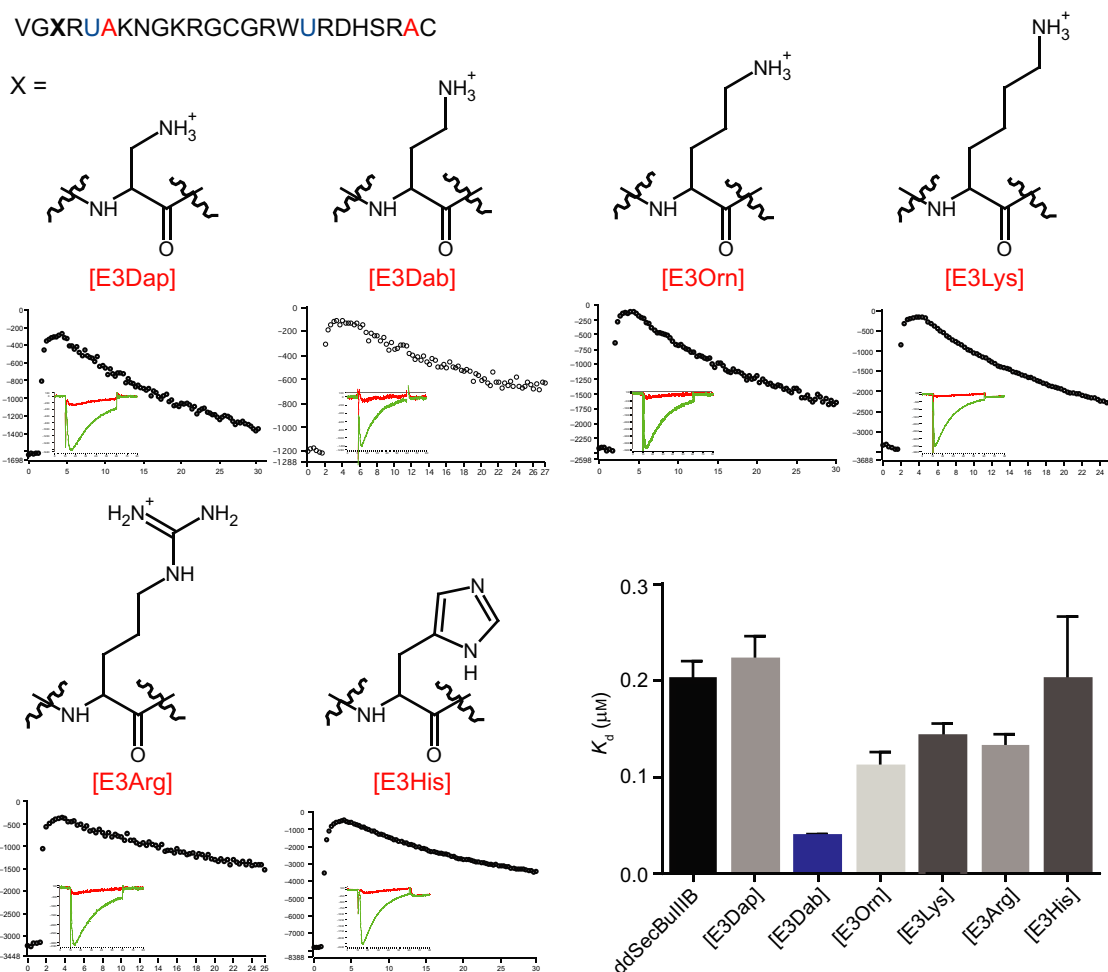
Fig. 6. Exploration of charge effects at position 3 using the ddSecBullIIB scaffold. (A) Representative electrophysiology traces of ddSecBullIIB analogs that reveal the consequences of different charges at position 3. (B) Table of kinetics of the blockade of Nav1.3 by ddSecBullIIB analogs. Each value represents the mean of at least three different peptide concentrations tested in triplicate. BullIIB[C5U, C17U, C6A, C23A, E3Dab] was almost three-fold more potent than μ -BullIIB in blocking Nav1.3. Current traces obtained before (green) and during (red) exposure of the peptide.

structural diversity at the N-termini is considered to aid in discrimination amongst voltage-gated sodium channel subtypes [26]. μ -BullIIB differs from previously described μ -conotoxins in having a short, helical extension of the N-terminus. The ddSecBullIIB [V1A] and [G2A] analogs exhibited native-like potency for Nav1.3 ($K_d = 0.2$ and $0.48 \mu\text{M}$, respectively). This differs slightly from the results for N-terminally

substituted analogs of μ -BullIIB described by Kuang *et al.* [16], which showed a modest decrease in potency against Nav1.3 upon Ala-replacement of Val1 ($K_d = 0.71 \pm 0.3 \mu\text{M}$) [16]. The differences between Nav1.3 potencies for ddSecBullIIB and μ -BullIIB likely arise from greater flexibility in the N-terminus resulting from removal of the stabilizing effects of the Cys6-Cys23 bridge. In further support of this, previous

A VGXRUA^KAKNGKRGCGRWURDHSRAC

X =



B

Analog	Na _v 1.3			
	k_{on} ($\mu\text{M}\cdot\text{min}$) ⁻¹	k_{off} (min) ⁻¹	K_d (μM)	ΔK_d
BullIB[C5U,C17U,C6A,C23A]	0.130 ± 0.007	0.026 ± 0.002	0.200 ± 0.020	—
BullIB[C5U,C17U,C6A,C23A,E3Dap]	0.230 ± 0.025	0.051 ± 0.002	0.220 ± 0.026	1.1
BullIB[C5U,C17U,C6A,C23A,E3Dab]	1.06 ± 0.054	0.040 ± 0.003	0.038 ± 0.003	0.19
BullIB[C5U,C17U,C6A,C23A,E3Omn]	0.410 ± 0.035	0.047 ± 0.005	0.110 ± 0.016	0.55
BullIB[C5U,C17U,C6A,C23A,E3Lys]	0.500 ± 0.038	0.070 ± 0.007	0.140 ± 0.015	0.65
BullIB[C5U,C17U,C6A,C23A,E3Arg]	0.400 ± 0.045	0.051 ± 0.002	0.130 ± 0.015	0.65
BullIB[C5U,C17U,C6A,C23A,EHis]	0.250 ± 0.044	0.050 ± 0.014	0.200 ± 0.066	1

Fig. 7. Exploration of steric effects at position 3 in the ddSecBullIB scaffold. (A) Representative electrophysiology traces of ddSecBullIB analogs that reveal the consequences of increased steric bulk of residue side-chains at position 3. (B) Table of kinetics of the blockade of Na_v1.3 by ddSecBullIB analogs. Each value represents the mean of at least three experiments tested in triplicate. Analogs with increased or decreased steric bulk, relative to that of BullIB[C5U,C17U,C6A,C23A,E3Dab], had greater potency than μ -BullIB in blocking Na_v1.3, although not to the extent that BullIB[C5U,C17U,C6A,C23A,E3Dab] did. Current traces obtained before (green) and during (red) exposure of the peptide.

NMR studies showed that the conformation of the N-terminus of μ -BuIIIB could be further constrained through replacement of Gly2 with D-Ala, resulting in increased $\text{Na}_V1.3$ potency above that of wild-type μ -BuIIIB [16]. Similar improvement to $\text{Na}_V1.3$ blockade was not, however, seen with the [G2DA] replacement on the ddSecBuIIIB background, where the results more closely reflected those of unmodified ddSec-BuIIIB (data not shown).

In addition to the N-terminal extension, another distinguishing feature of μ -BuIIIB, as well as other μ -conotoxins from *C. bullatus* described to date (μ -Bu-III A and μ -Bu-III C), is an extended inter-cysteine loop between the second and third Cys ranging between five and eight residues (Fig. 1 and Table 3). This loop includes a characteristic Lys10-Arg11 dipeptide that is not observed in the other neuronal Na_V1 -preferring μ -conotoxins. μ -SmIII A also possesses a basic dipeptide at the equivalent position (Arg7-Arg8) and exhibits potent blockade of $\text{Na}_V1.3$, which may make loop 1 of interest for designing subtype-preferring peptide analogs [9]. Additionally, there appear to be differences in both the contributions and distribution of residues that confer mild to moderate effects on Na_V1 inhibition within this region. Where previous studies of μ -conotoxins showed little to no effect of Ala-substitution of residues near the N-terminus, μ -BuIIIB appears more sensitive to modification in this region. This is illustrated by an increased number of residues for which a three- to five-fold decrease in Na_V1 potency was observed after Ala-replacement (Table 3).

The structural basis for μ -conotoxin blockade of Na_V1 channels has been investigated extensively, and models of these interactions have been constructed [22,27,28]. Because of the large amount of available SAR data, efforts have focused primarily on interactions between μ -conotoxin GIII A and $\text{Na}_V1.4$. The selectivity of μ -conotoxins for $\text{Na}_V1.3$ or other Na_V1 subtypes is most likely caused by interactions with the

turret region (Fig. 5C), for which there are no similar sequences in databases, making modeling a challenging task (S. Kuyucak, personal communication).

Crystal structures of bacterial sodium channels have been reported recently [29,30]. Unfortunately, the lack of tetrameric symmetry, coupled with differences in amino acid composition and selectivity filter loop size of the bacterial channels, have limited their use as proxies for mammalian Na_V1 subtypes. Until accurate models of the mammalian channel are developed, μ -conotoxin analogs such as those described in the present study will prove useful as molecular tools for testing and refining models of $\text{Na}_V1.3$.

The ddSec-strategy has proven valuable for facilitating the rapid identification of amino acid residues critical for $\text{Na}_V1.3$ blockade, as well as those amenable to modification for potential improved pharmacological activity. It is also likely that the strategy employed in the present study will be more broadly applicable to other disulfide-rich peptides for which inefficient oxidative folding precludes detailed SAR studies.

Experimental procedures

Ethics statement

The use of animals in this study followed protocols approved by the University of Utah's Animal Care and Use Committee that conform to the National Institutes of Health Guide for the Care and Use of Laboratory Animals.

Peptide synthesis

All analogs were synthesized at a 30- μmol scale using an Apex 396 automated peptide synthesizer (AAPPTec, Louisville, KY, USA) employing standard Fmoc-protocols. Peptides were constructed using pre-loaded Fmoc-Cys(Trt) Rink Amide MBHA resin (Peptides International, Louisville, KY,

Table 3. Contributions of individual amino acids to activity in μ -conotoxins possessing three disulfide bridges.

Peptide	Na_V1 -subtype	Reference
μ -TIIIA	$\text{Na}_V1.2$	Khoo <i>et al.</i> [21]
μ -KIIIA	$\text{Na}_V1.2$	Ekberg <i>et al.</i> [24]
μ -SIIIA	$\text{Na}_V1.2$	McArthur <i>et al.</i> [22]
μ -BuIIIB	$\text{Na}_V1.3$	Present study
μ -BuIIIB	$\text{Na}_V1.4$	Present study
μ -PIIIA	$\text{Na}_V1.4$	Xue <i>et al.</i> [27]

The relative importance of residues near the N-terminus of μ -BuIIIB is highlighted; other μ -conotoxins appeared to be insensitive to changes in this region. Z, pyroglutamic acid; O, hydroxyproline. All peptides are amidated at the C-terminus. Residues are categorized by the effect of neutral amino acid replacement at each position (red, significant reduction in Na_V1 potency; pink, moderate reduction in Na_V1 potency; green, increased Na_V1 potency).

USA) (substitution = $0.32 \text{ meq}\cdot\text{g}^{-1}$). Fmoc-removal was accomplished with 20 min of deprotection using 20% (v/v) piperidine in dimethylformamide. Standard amino acids were purchased from AAPPTec and used without further purification. Fmoc-L-Sec(pMeOBzl)-OH was purchased from Chem-Impex International, Inc. (Wood Dale, IL, USA). Amino acid coupling was accomplished using one equivalent of 0.22 M benzotriazol-1-yl-oxytriethylphosphonium hexafluorophosphate and two equivalents 2 M diisopropylethyl amine in *N*-methyl-2-pyrrolidone. Standard amino acids were coupled for 60 min in 10-fold excess and Fmoc-selenocysteine was coupled for 90 min in three-fold excess. Upon completion of peptide synthesis, crude peptides were cleaved from solid-support resin by 5 h of treatment with enriched reagent K [trifluoroacetic acid (TFA)/thioanisole/phenol/ $n\text{H}_2\text{O}$ (90 : 2.5 : 7.5 : 2.5, v/v/v/v)] containing 1.3 equivalents of DTNP. DTNP was added to the mixture to facilitate removal of Mob-protecting groups from selenocysteine side-chains. Crude peptides were removed from resin by vacuum filtration and were precipitated overnight at -20°C in chilled methyl-tert butyl ether. Precipitate was washed repeatedly with chilled methyl-tert butyl ether. 5-thionitropyridyl derivatives were removed from Sec side chains, with concomitant diselenide-bridge formation by 2 h of treatment with 50 mM dithiothreitol, 0.1 M Tris-HCl and 1 mM EDTA (pH 7.5) at room temperature.

RP-HPLC purification and oxidative folding

Crude peptide analogs containing the pre-formed diselenide bridge were purified, in parallel, by solid phase extraction using a Supelco Visiprep vacuum manifold (Supelco, Bellefonte, PA, USA). Briefly, 3-mL Supelco Discovery DSC-18 solid phase extraction columns were conditioned with five column volumes of solvent B₉₀ [90% (v/v) acetonitrile (ACN); 10% (v/v) H₂O; 0.1% (v/v) TFA] followed by equilibration with five column volumes of solvent A [0.1% (v/v) TFA; $n\text{H}_2\text{O}$]. A gradient of increasing organic solvent concentration was applied to each column ranging from 5 to 35% solvent B₉₀, and flow-through was checked for purity by analytical RP-HPLC equipped with a C₁₈ column (catalog number 218TP54; Vydac, Hesperia, CA, USA) over a linear gradient ranging from 10 to 50% solvent B₉₀ with 10 min of pre-equilibration at the initial conditions. Clean fractions were pooled and final yields were calculated by UV absorbance at 280 nm.

Formation of the Cys13-Cys24 disulfide bridge was performed in parallel using a 48 M equivalent excess (one equivalent = $2.768 \mu\text{g resin}\cdot\text{nmol peptide}^{-1}\cdot\text{number of disulfides oxidized}^{-1}$) of the solid-support oxidant CLEAR-Ox[®] (Peptides International, Inc., Louisville, KY, USA). Resin was prepared by first swelling in 500 μL of dichloromethane for 30 min at room temperature. Excess dichloromethane was removed by vacuum filtration and the resin was washed once with 500 μL of each of: dimethylformamide, MeOH,

50% (v/v) ACN in H₂O and 0.05 M Tris-HCl; 75% (v/v) ACN (pH 8.7). Peptide was dissolved in 0.05 M Tris-HCl; 75% (v/v) ACN (pH 8.7) to a final concentration of 3 mM and added directly to CLEAR-Ox[®] resin. Oxidation was allowed to proceed for 2 h at room temperature, after which folding was quenched by 100-fold dilution with solvent A. Folded analogs were purified by preparative RP-HPLC over a linear gradient ranging from 10 to 50% solvent B₉₀ over 40 min with a 10-min pre-equilibration at the initial conditions. The folded peptide analogs were quantified by UV absorbance ($\lambda = 280 \text{ nm}$). Molecular masses of the folded disulfide-depleted, diselenide-containing peptides were confirmed by ESI-MS (Table 1).

Two-electrode voltage clamp electrophysiology

Xenopus laevis oocytes were injected either with $2.5 \text{ ng}\cdot\mu\text{L}^{-1}$ Na_v1.3 or $94 \text{ ng}\cdot\mu\text{L}^{-1}$ Na_v1.4 cRNA. Although μ -conopeptide activity can be sensitive to co-expression of Na_v β -subunits [31], neither Na_v1 was co-expressed with any Na_v β -subunits so that the results could be compared directly with those obtained previously [9]. Two-electrode voltage clamping was performed using microelectrodes containing 3 M KCl ($< 0.5 \text{ m}\Omega$). Sodium currents were acquired using a holding potential of -80 mV and stepping to 0 mV for 50 ms every 20 s. Peptides were applied to oocytes under static bath conditions. Off-rates (k_{off}) were calculated from single exponential fits of the time course of recovery from block after washout. On-rates (k_{on}) were calculated by linear regression of the slopes of plots of k_{obs} versus peptide concentration. Dissociation constants (K_d) were determined from the ratio of $k_{\text{off}}/k_{\text{on}}$. Experiments were all conducted in triplicate ($n = 3$ oocytes) for each data point at room temperature.

NMR spectroscopy

Peptide samples were dried by lyophilization and dissolved to a final concentration of 500 μM (ddSecBuIIIIB) or 80 μM (μ -BuIIIIB) in 95% (v/v) H₂O, 5% (v/v) ²H₂O, and the pH was adjusted to 3.0. All spectra were acquired on a Bruker 600 MHz NMR spectrometer (Bruker Instruments, Inc., Bellerica, MA, USA). For 1D ¹H NMR the water signal was suppressed using excitation sculpting [32,33]. Experimental conditions were established through a series of temperature dependence and pH titration experiments, which showed better dispersion at elevated temperature and acidic pH (Fig. 3). Chemical shifts were referenced to water. 2D ¹H NMR spectra were acquired with a mixing time of 200 ms (NOESY) and spin-lock times of 30 and 70 ms (TOCSY). Data were processed with NMR PIPE (<http://spin.niddk.nih.gov/NMRPipe/>) and ¹H chemical shifts were determined by standard sequential assignment of the NOESY and TOCSY spectra in CCPNMR ANALYSIS [34].

Acknowledgements

This project was supported by the National Institutes of Health Grant GM 48677. We thank Dr Joanna Gajewiak for critically reviewing the manuscript and for numerous discussions integral to the success of this work. RSN acknowledges fellowship support from the National Health and Medical Research Council of Australia.

Author Contribution

BRG, GB and RSN designed experiments. BRG performed the peptide synthesis and NMR analyses. MMZ and MJW performed the electrophysiology assays and DJ assisted with their analysis. SC and SDR assisted with acquisition and analysis of NMR spectra. AR assisted in the preparation of disulfide-deficient analogs. BMO, GB and RSN conceived the study and BRG and RSN wrote the paper with input from all authors.

References

- Cestèle S & Catterall WA (2000) Molecular mechanisms of neurotoxin action on voltage-gated sodium channels. *Biochimie* **82**, 883–892.
- Cruz LJ, Gray WR, Olivera BM, Zeikus RD, Kerr L, Yoshikami D & Moczydlowski E (1985) *Conus geographus* toxins that discriminate between neuronal and muscle sodium channels. *J Biol Chem* **260**, 9280–9288.
- Shon K-J, Olivera BM, Watkins M, Jacobsen RB, Gray WR, Floresca CZ, Cruz LJ, Hillyard DR, Brink A, Terlau H *et al.* (1998) μ -Conotoxin PIIIA, a new peptide for discriminating among tetrodotoxin-sensitive Na channel subtypes. *J Neurosci* **18**, 4473–4481.
- Zhang M-M, Green BR, Catlin P, Fiedler B, Azam L, Chadwick A, Terlau H, McArthur JR, French RJ, Gulyas J *et al.* (2007) Structure/function characterization of μ -conotoxin KIIIA, an analgesic, nearly irreversible blocker of mammalian neuronal sodium channels. *J Biol Chem* **282**, 30699–30706.
- Wakamatsu K, Kohda D, Hatanaka H, Lancelin JM, Ishida Y, Oya M, Nakamura H, Inagaki F & Sato K (1992) Structure–activity relationships of μ -conotoxin GIIIA: structure determination of active and inactive sodium channel blocker peptides by NMR and simulated annealing calculations. *Biochemistry* **31**, 12577–12584.
- Schroeder CI, Ekberg J, Nielsen KJ, Adams D, Loughnan ML, Thomas L, Adams DJ, Alewood PF & Lewis RJ (2008) Neuronally selective μ -conotoxins from *Conus striatus* utilize an α -helical motif to target mammalian sodium channels. *J Biol Chem* **283**, 21621–21628.
- Norton RS (2010) μ -conotoxins as leads in the development of new analgesics. *Molecules* **15**, 2825–2844.
- Holford M, Zhang M-M, Gowd KH, Azam L, Green BR, Watkins M, Ownby J-P, Yoshikami D, Bulaj G & Olivera BM (2009) Pruning nature: biodiversity-derived discovery of novel sodium channel blocking conotoxins from *Conus bullatus*. *Toxicon* **53**, 90–98.
- Wilson MJ, Yoshikami D, Azam L, Gajewiak J, Olivera BM, Bulaj G & Zhang M-M (2011) μ -Conotoxins that differentially block sodium channels Na_v1.1 through 1.8 identify those responsible for action potentials in sciatic nerve. *Proc Natl Acad Sci USA* **108**, 10302–10307.
- Hains BC, Klein JP, Saab CY, Craner MJ, Black JA & Waxman SG (2003) Upregulation of sodium channel Na_v1.3 and functional involvement in neuronal hyperexcitability associated with central neuropathic pain after spinal cord injury. *J Neurosci* **23**, 8881–8892.
- Hains BC, Saab CY, Klein JP, Craner MJ & Waxman SG (2004) Altered sodium channel expression in second-order spinal sensory neurons contributes to pain after peripheral nerve injury. *J Neurosci* **24**, 4832–4839.
- Walewska A, Zhang M-M, Skalicky JJ, Yoshikami D, Olivera BM & Bulaj G (2009) Integrated oxidative folding of cysteine/selenocysteine containing peptides: improving chemical synthesis of conotoxins. *Angew Chem Int Ed* **48**, 2221–2224.
- Han TS, Zhang M-M, Gowd KH, Walewska A, Yoshikami D, Olivera BM & Bulaj G (2010) Disulfide-depleted selenoconopeptides: a minimalist strategy to oxidative folding of cysteine-rich peptides. *ACS Med Chem Lett* **1**, 140–144.
- Gowd KH, Blais KD, Elmsie KS, Steiner AM, Olivera BM & Bulaj G (2012) Dissecting a role of evolutionary-conserved but noncritical disulfide bridges in cysteine-rich peptides using ω -conotoxin GVIA and its selenocysteine analogs. *Biopolymers* **98**, 212–223.
- Khoo KK, Gupta K, Green BR, Zhang M-M, Watkins M, Olivera BM, Balaram P, Yoshikami D, Bulaj G & Norton RS (2012) Distinct disulfide isomers of ω -conotoxins KIIIA and KIIIB block voltage-gated sodium channels. *Biochemistry* **51**, 9826–9835.
- Kuang Z, Zhang M-M, Gajewiak J, Gulyas J, Rivier JE, Olivera B, Yoshikami D & Norton RS (2013) Mammalian neuronal sodium channel blocker ω -conotoxin BuIIIB has a structured N-terminal extension that influences potency. *ACS Chem Biol* **8**, 1344–1351.
- Harris KM, Flemer SJ & Hondal RJ (2007) Studies on deprotection of cysteine and selenocysteine side-chain protecting groups. *J Pept Sci* **13**, 81–93.

- 18 Steiner AM & Bulaj G (2010) Optimization of oxidative folding methods for cysteine-rich peptides: a study of conotoxins containing three disulfide bridges. *J Pept Sci* **17**, 1–7.
- 19 Hondal RJ, Marino SM & Gladyshev VN (2013) Selenocysteine in thiol/disulfide-like exchange reactions. *Antioxid Redox Signal* **18**, 1675–1689.
- 20 Wishart DS, Bigam CG, Holme A, Hodges RS & Sykes BD (1995) ^1H , ^{13}C and ^{15}N random coil NMR chemical shifts of the common amino acids. I Investigations of the nearest-neighbor effects. *J Biomol NMR* **5**, 67–81.
- 21 Khoo KK, Wilson MJ, Smith BJ, Zhang M-M, Gulyas J, Yoshikami D, Rivier J, Bulaj G & Norton RS (2011) Lactam-stabilized helical analogues of the analgesic ω -conotoxin KIIIA. *J Med Chem* **54**, 7558–7566.
- 22 McArthur JR, Ostroumov V, Al-Sabi A, McMaster D & French RJ (2011) Multiple, distributed interactions of μ -conotoxin PIIIA associated with broad targeting among voltage-gated sodium channels. *Biochemistry* **50**, 116–124.
- 23 Han TS, Zhang M-M, Walewska A, Gruszczynski P, Robertson CR, Cheatham TE 3rd, Yoshikami D, Olivera BM & Bulaj G (2009) Structurally minimized μ -conotoxin analogues as sodium channel blockers: implications for designing conopeptide-based therapeutics. *ChemMedChem* **4**, 406–414.
- 24 Ekberg J, Craik DJ & Adams DJ (2008) Conotoxin modulation of voltage-gated sodium channels. *Int J Biochem Cell Biol* **40**, 2363–2368.
- 25 Tietze AA, Tietze D, Ohlenschläger O, Leipold E, Ullrich F, Kühl T, Mischo A, Buntkowsky G, Görlach M, Heinemann SH *et al.* (2012) Structurally-diverse ω -conotoxin PIIIA isomers block sodium channel $\text{Na}_V1.4$. *Angew Chem Int Ed* **51**, 4058–4061.
- 26 Yao S, Zhang M-M, Yoshikami D, Azam L, Olivera BM, Bulaj G & Norton RS (2008) Structure, dynamics and selectivity of the sodium channel blocker ω -conotoxin SIIIA. *Biochemistry* **47**, 10940–10949.
- 27 Xue T, Ennis IL, Sato K, French RJ & Li RA (2003) Novel interactions identified between μ -conotoxin and the Na^+ channel domain I P-loop: implications for toxin-pore binding geometry. *Biophys J* **85**, 2299–2310.
- 28 Choudhary G, Aliste MP, Tieleman DP, French RJ & Dudley SCJ (2007) Docking of μ -conotoxin GIIIA in the sodium channel outer vestibule. *Channels (Austin)* **1**, 344–352.
- 29 Payandeh J, Scheuer T, Zheng N & Catterall WA (2011) The crystal structure of a voltage-gated sodium channel. *Nature* **475**, 353–358.
- 30 McCusker EC, Bagn ris C, Naylor CE, Cole AR, D’Avanzo N, Nichols CG & Wallace BA (2012) Structure of a bacterial voltage-gated sodium channel pore reveals mechanisms of opening and closing. *Nat Commun* **3**, 1102.
- 31 Zhang M-M, Wilson MJ, Azam L, Gajewiak J, Rivier JE, Bulaj G, Olivera BM & Yoshikami D (2013) Co-expression of $\text{Na}_V\beta$ subunits alters the kinetics of inhibition of voltage-gated sodium channels by pore-blocking ω -conotoxins. *Br J Pharmacol* **168**, 1597–1610.
- 32 Hwang T-L & Shaka AJ (1996) Water suppression that works. Excitation sculpting using arbitrary waveforms and pulsed field gradients. *J Magn Reson* **112A**, 275–279.
- 33 Callihan D, West J, Kumar S, Schweitzer BI & Logan TM (1996) Simple, distortion-free homonuclear spectra of peptides and nucleic acids in water using excitation sculpting. *J Magn Reson* **112B**, 82–85.
- 34 Wim F, Vranken WB, Stevens TJ, Fogh RH, Pajon A, Llinas M, Ulrich EL, Markley JL, Ionides J & Laue ED (2005) The CCPN data model for NMR spectroscopy: development of a software pipeline. *Proteins* **59**, 687–696.

Supporting information

Additional supporting information may be found in the online version of this article at the publisher’s web site:

Table S1. Chemical shifts for wild-type μ -BuIIIB at 35 °C (pH 3.0).

Table S2. Chemical shifts for BuIIIB[C5U,C17U,C6A,C23A] at 35 °C (pH 3.0).

Supplemental Data

Interactions of Disulfide-deficient Selenocysteine Analogs of μ -Conotoxin BuIIIb with the Voltage-Gated Sodium Channel Na_v1.3

Brad R. Green,^{1,2} Min-Min Zhang,³ Sandeep Chhabra,¹ Samuel D. Robinson,¹ Michael J. Wilson,³ Addison Redding,³ Baldomero M. Olivera,³ Doju Yoshikami,³ Grzegorz Bulaj,^{2,3,‡} and Raymond S. Norton^{1,‡}

¹ Medicinal Chemistry, Monash Institute of Pharmaceutical Sciences, Monash University, 381 Royal Parade, Parkville 3052, Australia; ² Department of Medicinal Chemistry, College of Pharmacy, University of Utah, Salt Lake City, Utah 84108, USA; ³ Department of Biology, University of Utah, Salt Lake City, Utah 84112, USA

*Running Title: *Structure-Activity Studies of μ -BuIIIb Analogs*

‡ To whom correspondence should be addressed: Raymond S. Norton, Monash Institute of Pharmaceutical Sciences, 381 Royal Parade, Parkville, VIC 3052, Australia, [REDACTED] or Grzegorz Bulaj, Dept. of Medicinal Chemistry, College of Pharmacy, University of Utah, Salt Lake City, UT, USA, [REDACTED]

Table of Contents:

Table S1: Chemical shifts for wild-type μ -BuIIIb at 35 °C, pH 3.0

Table S2: Chemical shifts for BuIIIb[C5U,C17U,C6A,C23A] at 35 °C, pH 3.0 (BMRB ID #19923)

Table S1. Chemical shifts (ppm) for wild-type μ -BuIII B at 35 °C, pH 3.0. Data for μ -BuIII B were previously reported by Kuang et al (19) at 600 MHz at 5 °C and pH 5.5.

Residue	H ^N	H ^{α}	H ^{β}	Others
Val1		3.79	2.16	H ^{γ} 0.99
Gly2	8.58	3.91, 3.97		
Arg4	8.59	4.37	1.85, 1.90	H ^{γ} 1.66; H ^{δ} 3.16; H ^{ϵ} 7.13
Cys5	8.45	4.77	3.24, 3.14	
Cys6	8.45	4.54	3.51, 3.16	
Lys7	7.94	4.32	1.87	H ^{γ} 1.40; H ^{δ} 1.77, 1.68; H ^{ϵ} 3.00; H ^{ζ} 7.50
Asn8	8.48	4.77	2.90, 2.74	H ^{δ} 7.56, 6.92
Gly9	8.21	3.84, 4.09		
Lys10	8.40	4.29	1.91	H ^{γ} 1.48; H ^{δ} 1.82, 1.70; H ^{ϵ} 3.01; H ^{ζ} 7.50
Arg11	8.17	4.29	1.93, 1.86	H ^{γ} 1.69, 1.72; H ^{δ} 3.23; H ^{ϵ} 7.18
Gly12	8.03	4.10, 3.92		
Cys13	8.10	4.71	3.29, 3.12	
Gly14	8.33	3.85, 3.97		
Arg15	8.45	3.85	1.89	H ^{γ} 1.65; H ^{δ} 3.23; H ^{ϵ} 7.31
Trp16	8.61	4.39	3.40	H ^{δ} 7.27, 1.68; H ^{ϵ} 10.01, 7.47; H ^{ζ} 7.16, 7.12
Cys17	8.73	4.45	3.12, 3.26	
Arg18	8.71	3.99	1.85, 1.75	H ^{γ} 1.57; H ^{δ} 3.17, 3.23; H ^{ϵ} 7.17
Asp19	7.62	4.53	2.32, 2.47	
His20	7.56	4.52	2.89, 1.62	H ^{δ} 6.59; H ^{ϵ} 8.33
Ser21	8.00	4.82	4.01, 3.95	
Arg22	8.94	4.42	1.98	H ^{γ} 1.80, 1.68; H ^{δ} 3.21; H ^{ϵ} 7.16
Cys23	8.19	4.55	3.36	
Cys24	7.75	4.67	2.96, 3.18	

Table S2. Chemical shifts (ppm) for BuIII[B(C5U,C17U,C6A,C23A)] at 35 °C, pH 3.0. Spectra were collected under these conditions based on results from temperature and pH titration experiments, which indicated that better resolution/dispersion of peaks was achieved at elevated temperature and lower pH.

Residue	H ^N	H ^α	H ^β	Others
Val1		3.84	2.20	H ^γ 1.01
Gly2	8.62	3.96		
Glu3	8.32	4.28	1.89, 1.97	H ^γ 2.31
Arg4	8.42	4.34	1.82	H ^γ 1.61; H ^δ 3.12; H ^ε 7.08
Sec5	8.48	4.68	3.37, 3.24	
Ala6	8.23	4.35	1.39	
Lys7	8.27	4.23	1.82	H ^γ 1.43; H ^δ 1.67; H ^ε 2.98; H ^ζ 7.48
Asn8	8.27	4.71	2.79, 2.84	H ^δ 6.85, 7.50
Gly9	8.26	3.93, 3.98		
Lys10	8.26	4.27	1.82	H ^γ 1.43; H ^δ 1.66; H ^ε 2.99; H ^ζ 7.48
Arg11	8.24	4.33	1.89	H ^γ 1.65; H ^δ 3.20; H ^ε 7.15
Gly12	8.16	4.00		
Cys13	8.35	4.76	3.24, 3.09	
Gly14	8.37	4.00, 3.95		
Arg15	8.29	3.94	1.57, 1.65	H ^γ 1.29; H ^δ 3.00; H ^ε 7.02
Trp16	8.16	4.61	3.28, 3.40	H ^δ 7.25; H ^ε 10.07, 7.57; H ^ζ 7.11, 7.33; H ^η 7.16
Sec17	8.10	4.47	3.35, 3.23	
Arg18	8.32	4.17	1.84	H ^γ 1.66, 1.84; H ^δ 3.19; H ^ε 7.15
Asp19	8.04	4.55	2.63	
His20	8.12	4.57	3.24, 2.69	H ^δ 7.05; H ^ε 8.42
Ser21	8.08	4.49	3.97, 3.89	
Arg22	8.44	4.31	1.89	H ^γ 1.64; H ^δ 3.19; H ^ε 7.15
Ala23	8.18	4.28	1.37	
Cys24	7.96	4.60	2.99, 3.20	

Chapter 6

Structural Basis for the Inhibition of Voltage-gated Sodium Channels by Conotoxin $\mu\text{O}\delta\text{-GVIIJ}$

Cone snail venoms are complex mixtures of bioactive peptides and several classes of conotoxins have been identified that modulate VGSC activity. Chapter 6 focuses on the structure-activity relationship studies of a recently discovered conotoxin that binds at a site close to, but distinct, from the μ -conotoxin binding site on the VGSC. These studies identified the critical structural features of $\mu\text{O}\delta\text{-GVIIJ}$ for blocking VGSCs.

This chapter consists of the submitted manuscript:

Green, B. R.; Gajewiak, J.; Chhabra, S.; Skalicky, J. J.; Zhang, M. M.; Rivier, J. E.; Bulaj, G.; Olivera, B. M.; Yoshikami, D.; Norton, R. S. Structural basis for the inhibition of voltage-gated sodium channels by conotoxin $\mu\text{O}\delta\text{-GVIIJ}$. *J. Biol. Chem.* (Submitted).

6.1 Declaration for Thesis Chapter 6

6.1.1 Declaration by candidate

In the case of Chapter 6, the nature and extent of my contribution to the work was the following:

Nature of contribution	Contribution (%)
Jointly designed and executed experiments, analysis of results and manuscript preparation.	70%

The following co-authors contributed to the work. If co-authors are students at Monash University, the extent of their contribution in percentage terms must be stated:

Name	Nature of contribution	Contribution (%)
Joanna Gajewiak	Assisted with synthesis of selected analogues	
Sandeep Chhabra	Assisted with NMR experiments.	
Jack J. Skalicky	Assisted with NMR experiments	
Min-Min Zhang	Assisted with electrophysiology experiments	
Jean E. Rivier	Contributed reagents/materials for studies	
Grzegorz Bulaj	Contributed reagents/materials/analysis tools.	
Baldomero M. Olivera	Contributed reagents/materials/analysis tools.	
Doju Yoshikami	Contributed reagents/materials/analysis tools.	
Raymond S. Norton	Assisted with manuscript preparation and intellectual input. Corresponding author	

The undersigned hereby certify that the above declaration correctly reflects the nature and extent of the candidate's and co-authors' contributions to this work*.

Candidate's
signature 

Date
22.01.16

Main
supervisor's
signature 

Date
22.01.16

**Structural basis for the inhibition of voltage-gated sodium channels by
conotoxin μ O ξ -GVIIJ**

Brad R. Green^{1,2}, Joanna Gajewiak^{2*}, Sandeep Chhabra^{1*}, Jack J. Skalicky³, Min-Min Zhang², Jean E. Rivier⁴, Grzegorz Bulaj⁵, Baldomero M. Olivera², Doju Yoshikami² and Raymond S. Norton¹

¹*Medicinal Chemistry, Monash Institute of Pharmaceutical Sciences, Monash University, Parkville, Victoria 3052, Australia*

²*Department of Biology, University of Utah, Salt Lake City, Utah 84112, USA*

³*Department of Biochemistry, University of Utah, Salt Lake City, Utah 84108, USA*

⁴*The Clayton Foundation Laboratories for Peptide Biology, The Salk Institute, La Jolla, California 92037, USA*

⁵*Department of Medicinal Chemistry, College of Pharmacy, University of Utah, Salt Lake City, Utah 84108, USA*

**Contributed equally to this work*

To whom correspondence should be addressed:

R. S. Norton, Monash Institute of Pharmaceutical Sciences, 381 Royal Parade, Parkville, Vic. 3052, Australia. [REDACTED]

D. Yoshikami, Department of Biology, University of Utah, 257 South 1400 East, Salt Lake City, UT, 84112, U.S.A. [REDACTED]

KEYWORDS: conotoxin; NMR; peptide synthesis; peptide structure; electrophysiology; SAR; sodium channel

6.2 Abstract

Cone snail toxins are well-known blockers of voltage-gated sodium channels, a property that is of broad interest in biology and therapeutically in treating neuropathic pain and neurological disorders. While most conotoxin channel blockers function by direct binding to a channel and disrupting its normal ion movement, conotoxin μ O ξ -GVIIJ channel blocking is unique, using both favorable binding interactions with the channel and a direct tether via an intermolecular disulfide bond. Disulfide exchange is possible since conotoxin μ O ξ -GVIIJ contains an S-cysteinylated Cys-24 residue that is capable of exchanging with a free cysteine thiol on the channel surface. Here, we present the solution structure of an analogue of μ O ξ -GVIIJ (GVIIJ[C24S]) and the results of structure-activity (SAR) studies with synthetic μ O ξ -GVIIJ variants. GVIIJ[C24S] adopts an inhibitor cystine knot structure, with two antiparallel β -strands stabilized by three disulfide bridges. The loop region linking the β -strands (loop 2) presents residue 24 in a configuration where it could bind to the proposed free cysteine of the channel (Cys-910, rat Nav1.2 numbering; at site 8). The SAR study shows that three residues (Lys-12, Arg-14 and Tyr-16) located in loop 4, and spatially close to residue 24, were also important for functional activity. We propose that the interaction of μ O ξ -GVIIJ with the channel depends on not only disulfide tethering via Cys-24 to a free cysteine at site 8 on the channel, but also the participation of key residues of μ O ξ -GVIIJ on a distinct surface of the peptide.

6.3 Introduction

Marine snails of the genus *Conus* employ a complex venom cocktail to subdue prey and as an effective means of defending against predation. The active venoms contain an array of peptides that bind to and modulate the properties of ion channels, G-protein-coupled receptors (GPCRs), and neurotransmitter receptors (129). Several peptides modulate the activities of voltage-gated sodium channels (VGSCs), which are implicated in numerous neurological disorders as well as neuropathic pain. Four classes of conopeptides have been shown to affect VGSC activity. Peptides belonging to the ι - and δ -families promote activation and inhibit inactivation, respectively, while the μ - and μ O-conotoxins inhibit VGSCs by either blocking the Na⁺ conductance pore or preventing channel activation, respectively (130,131). Recently, the founding member of a fifth class of VGSC inhibitors was identified, which blocks the channel through interaction with a previously-unidentified neurotoxin binding site, site 8 (Fig. 6.1A) (93).

$\mu\text{O}\xi\text{-GVIIJ}$ is a 35-residue peptide isolated from the venom of the piscivorous snail *Conus geographus* (Fig. 6.1B). *In vitro* folding of linear $\mu\text{O}\xi\text{-GVIIJ}$ with thiol-reactive oxidants (i.e. glutathione, L-cystine or cystamine) resulted in adducts where Cys-24 was disulfide-bonded with glutathione, cysteine or cysteamine, respectively (abbr. $\text{GVIIJ}_{\text{SSG}}$, $\text{GVIIJ}_{\text{SSC}}$, and $\text{GVIIJ}_{\text{SSEA}}$, respectively, see Fig. 6.1C for structures). Of these, the $\text{GVIIJ}_{\text{SSC}}$ variant most closely resembled the native peptide, which also has a Cys disulfide bonded to its Cys-24 residue. For largely historical reasons, the glutathione adduct ($\text{GVIIJ}_{\text{SSG}}$) was tested by two-electrode voltage-clamp electrophysiology against rat Nav1.1 – 1.8 expressed in *X. laevis* oocytes, and it was found to

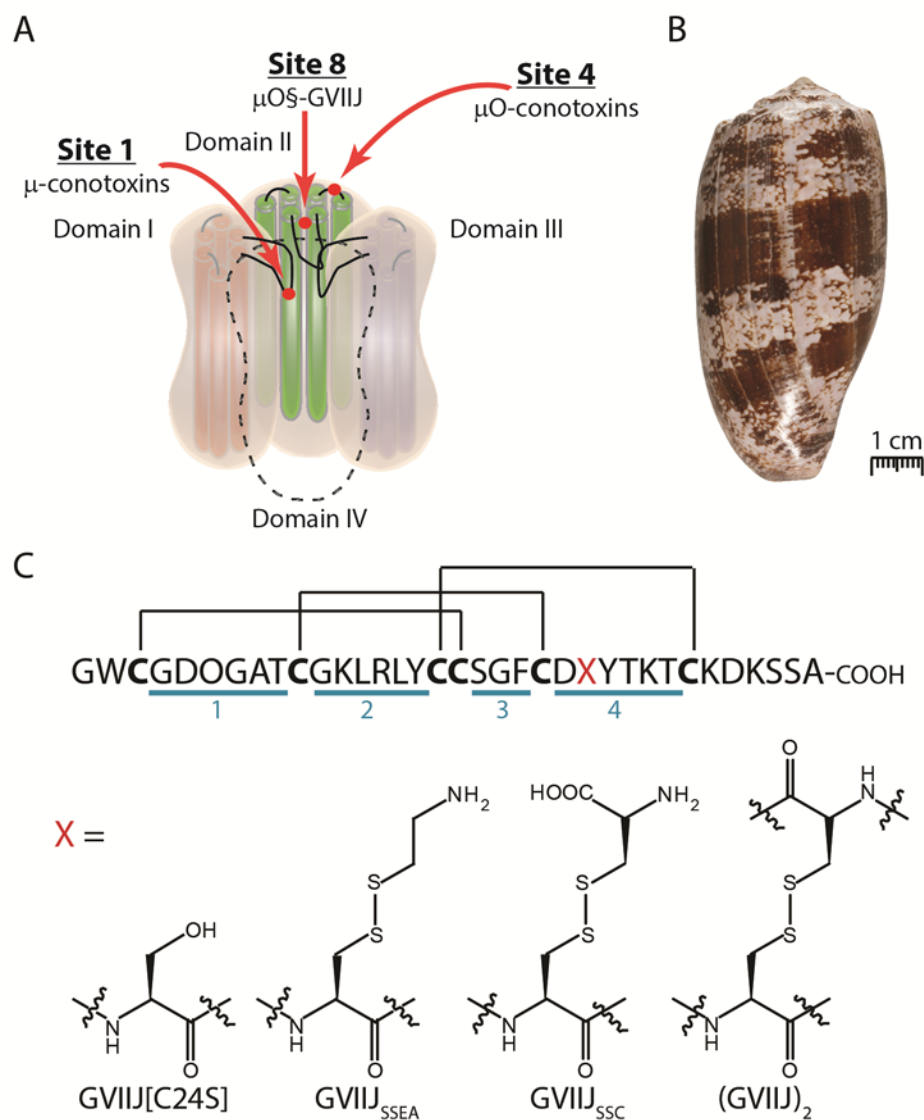


Figure 6.1. Binding site of $\mu\text{O}\xi\text{-GVIIJ}$ on the channel and its peptide sequence. (A) Binding sites of VGSC-inhibiting conotoxins. Pore-blocking $\mu\text{-conotoxins}$ bind deep within the Na^+ conductance pore, and compete with tetrodotoxin for neurotoxin binding site 1. Site 1 is located near the bottom of the reentrant loops in all four domains (DI-DIV), but only one site of interaction is shown in this figure. In contrast, $\mu\text{O-conotoxins}$ MrVIA/B bind to the voltage sensor of domain II (DII) at neurotoxin binding site 4 (131), while $\mu\text{O}\xi\text{-GVIIJ}$, whose mechanism of block remains to be determined, binds to the loop in the pore module of domain II

(DII) at site 8 (93). (B) Photograph of the shell of the fish-hunting cone snail *Conus geographus*. (C) Primary sequence of $\mu\text{O}\xi\text{-GVIII}$, displaying the previously determined disulfide framework (93). Intercysteine loops 1 – 4 are underlined. X represents modifications at position 24 used in the structural and pharmacological studies described in this report; their structures are shown at the bottom.

block all tested Nav1 isoforms with a K_d or $IC_{50} < 0.4 \mu\text{M}$ except Nav1.5, which was blocked with an IC_{50} of $207 \mu\text{M}$, and Nav1.8, which was not blocked at all ($IC_{50} > 1 \text{ mM}$). When screened against the neuronal VGSC subtype Nav1.2, the three analogues possessed nearly identical off-rates (k_{off} s) but different on-rates (k_{on} s) (93). An explanation consistent with these results is that the glutathione, cysteine, or cystamine moiety disulfide bonded to Cys-24 of the peptide acts as a leaving group when, by disulfide exchange, Cys-24 forms a disulfide bridge with a free cysteine on the α -subunit (specifically Cys-910, in the case of rNav1.2 (93)). This explanation was supported by the results of experiments that tested four additional adducts with different groups disulfide bonded to Cys-24 against both rat Nav1.2 and mouse Nav1.6, where it was observed that for a given Nav1-isoform the adducts had widely varying k_{on} s but the same k_{off} (132).

Here we have determined the solution structure of $\mu\text{O}\xi\text{-GVIII}$ using an analogue of this peptide, GVIII[C24S], which would not undergo dimerization (132) during NMR studies. The solution structure of GVIII[C24S] closely resembled that of the inhibitor cystine knot (ICK) class of peptides in that it possessed two short β -strands and was cross-linked by three disulfide bridges in the ‘core’ of the molecule (66,133,134). The ICK motif is found in peptides from numerous phyla and is of particular interest for pharmaceutical development owing to its inherent stability and amenability to chemical modification for enhanced pharmacological effect (134). Importantly, this structure identified the location and position of residue 24 in a loop linking the two β -strands, where it would be available to interact with the channel.

To complement these structural studies, we performed detailed structure-activity relationship (SAR) studies to identify amino acid residues critical for inhibition of rat Nav1.2 (rNav1.2), a VGSC isoform found in the central nervous system. SAR studies were performed on rNav1.2 exogenously expressed in *Xenopus laevis* oocytes using mutants of a potent analogue of $\mu\text{O}\xi\text{-GVIII}$, GVIII_{SSEA}, in which Cys-24 was modified by cysteamine (Fig. 6.1C). These studies identified three functionally important residues, Lys-12, Arg-14 and Tyr-16, located on a face of the peptide adjacent to the loop with residue 24. Thus, these results suggest a ‘functionally bipartite’ mechanism of interaction by $\mu\text{O}\xi\text{-GVIII}$, where a disulfide bridge ‘tethers’ the peptide to a channel cysteine at site 8, while residues on a different surface of the peptide are also important for interaction with the channel.

To demonstrate that site 8 was physically distinct from site 1, where tetrodotoxin (TTX), saxitoxin (STX) and μ -conotoxins bind and plug the Na⁺-conducting pore (Fig. 6.1A), we previously employed a 'leaky' μ -conotoxin, μ -KIIIA[K7A] (135,136), and showed that pre-equilibrating rNav1.2 with this peptide did not interfere with the block by μ O ξ -GVIIJ_{SSG} (93). However, as noted (93), μ -KIIIA[K7A] has 16 amino-acid residues, so these results did not exclude the possibility that a larger μ -conotoxin, such as μ -GIIIA (with 22 residues), might intrude into μ O ξ -GVIIJ's binding space. We examined this possibility in the present study with a point mutant of μ -PIIIA (which, like μ -GIIIA, has 22 residues and blocks rNav1.4 with high affinity); namely, μ -PIIIA[R14Q]. We chose this mutant because others have shown that it binds to rNav1.4 reasonably well with a significant residual current (rI_{Na} or 'leak') (137). We show here that pre-equilibrating rNav1.4 with near-saturating levels of μ -PIIIA[R14Q] did not interfere with the block by μ O ξ -GVIIJ_{SSG}. In contrast, the rate of block by a dimer of μ O ξ -GVIIJ, (μ O ξ -GVIIJ)₂, whose monomers were disulfide bonded to each other via the thiols of their Cys-24 residues (132), was decreased by the presence of μ -PIIIA[R14Q]. These results lead us to conclude that sites 1 and 8 are distinct although not very far apart.

Table 6.1. Characterization of $\mu\text{O}\xi$ -GVIII analogues by HPLC retention time, purity and molecular mass.

Peptide	HPLC RT (min)	Purity (%)	[MH] ⁺ Predicted (Da)	[MH] ⁺ Observed (Da)
GVIII _{SSEA}	18.5	>97	3812.52	3812.18
GVIII _{SSC}	18.3	99	3856.51	3856.60
GVIII[C24S]	18.4	>96	3721.57	3721.52
[W2A] _{SSEA}	21.8	93	3697.48	3697.76
[D5K] _{SSEA}	17.9	99	3825.59	3825.22
[O6A] _{SSEA}	17.3	92	3770.51	3770.28
[T9A] _{SSEA}	17.5	99	3782.51	3782.43
[K12D] _{SSEA}	19.9	99	3799.45	3799.36
[L13A] _{SSEA}	14.2	99	3770.48	3770.41
[R14D] _{SSEA}	19.2	98	3771.45	3771.28
[L15A] _{SSEA}	15.1	99	3770.48	3770.70
[Y16A] _{SSEA}	16.8	94	3720.50	3720.82
[S19A] _{SSEA}	18.1	93	3796.53	3796.28
[F21A] _{SSC}	17.7	99	3780.67	3780.58
[D23Gla] _{SSEA}	18.6	89	3870.53	3871.50
[D23N] _{SSEA}	18.3	93	3811.54	3811.65
[Y25A] _{SSEA}	17.2	99	3720.50	3720.63
[Y25R] _{SSEA}	17.4	99	3805.56	3805.27
[Y25D] _{SSEA}	17.4	99	3764.49	3764.90
[T26A] _{SSC}	17.4	80	3826.51	3825.90
[K27D] _{SSEA}	18.5	99	3799.45	3798.90
[K27G] _{SSEA}	18.2	98	3741.45	3741.36
[K27F] _{SSEA}	18.1	96	3831.50	3831.26
[T28A] _{SSC}	17.6	85	3826.50	3826.06
[K30A] _{SSEA}	17.8	99	3755.46	3755.14
[D31K] _{SSEA}	18.2	99	3825.59	3825.43
[K32D] _{SSEA}	19.2	97	3799.45	3799.07

GVIII_{SSEA} and GVIII_{SSC} are analogues where Cys-24 is disulfide bonded with cysteamine (2-aminoethanethiol) or cysteine, respectively. Retention time (RT) was assessed by RP-HPLC with respect to the start of the HPLC run using an analytical C18 column and an elution gradient ranging from 15% to 45% of solvent B in 30 min at different stages of the project. All “poorly” folding analogues of GVIII were characterized either by HPLC peak broadening or by tailing of the peak.

6.4 Experimental procedures

6.4.1. Peptide synthesis, oxidative folding and purification

Native Peptide. The native $\mu\text{O}\xi$ -GVIII has three posttranslational modifications: bromination of Trp-2, hydroxylation of Pro-6 and S-cysteinylation of Cys-24. All $\mu\text{O}\xi$ -GVIII analogues synthesized for SAR and NMR studies lacked bromination of Trp-2 since it was shown previously that both the brominated and non-brominated forms of the peptide exhibited comparable functional activity (93) and the cost of the synthesis of the non-brominated peptide was significantly lower.

Structure-activity studies of $\mu\text{O}\xi\text{-GVIII}$ were carried out on either the $\text{GVIII}_{\text{SSEA}}$ or $\text{GVIII}_{\text{SSC}}$ backgrounds and analogues were designed and synthesized that substituted non-cysteine residues with alanine (i.e. Trp-2, Thr-9, Leu-13, Leu-15, Tyr-16, Ser-19, Phe-21, Tyr-25, Thr-26 and Thr-28) or replaced acidic/basic residues with those of the opposite charge (i.e. Asp-5, Lys-12, Arg-14, Asp-23, Lys-27, Lys-30 and Lys-32) (Table 6.1).

Solid-phase peptide synthesis. Analogues of $\mu\text{O}\xi\text{-GVIII}$ were synthesized on a 50- μmol scale with an AAPPTec Apex 396 synthesizer (AAPPTec, LLC, Louisville, KY) using standard solid-phase Fmoc (9-fluorenylmethyloxycarbonyl) protocols. Fmoc-protected amino acids, including the pseudoproline dipeptide (Fmoc-Tyr(tBu)-Thr($\psi^{\text{Me,Me}}$ pro)-OH), were purchased from AAPPTec. $N\text{-}\alpha\text{-Fmoc-O-t-butyl-L-trans-4-hydroxyproline}$ (Hyp) was purchased from EMD Millipore (Darmstadt, Germany), and Fmoc- γ -carboxy-L-Glu(OtBu)₂-OH (Gla or γ) was obtained from Advanced ChemTech (Louisville, KY). Peptides were assembled on pre-loaded Fmoc-L-Ala-Wang resin (substitution, 0.38 mmol·g⁻¹; Peptides International Inc., Louisville, KY). Side-chain protection for amino acids was: Arg, 2,2,4,6,7-pentamethyldihydrobenzofuran-5-sulfonyl (Pbf); Asp, Gla and Glu, *O-tert-butyl* (OtBu); Lys and Trp, *tert*-butyloxycarbonyl (Boc); Hyp, Ser, Thr and Tyr, *tert*-butyl (tBu); and Asn and Cys, trytl (Trt). Coupling of each amino acid was achieved using 1 equivalent of 0.4 M benzotriazol-1-yl-oxytripyrrolidinophosphonium hexafluorophosphate (PyBOP) and 2 equivalents of 2 M *N,N*-diisopropylethyl amine (DIPEA) in *N*-methyl-2-pyrrolidone (NMP). Amino acids were used in ten-fold excess (60 min coupling), with the exception of Hyp and the pseudoproline dipeptide Tyr-Thr, which were used in five-fold excess (90 min coupling). Double-coupling was performed on residues following Cys-residues in the $\mu\text{O}\xi\text{-GVIII}$ sequence. Fmoc-protecting groups were removed by 20 min treatment with 20% (v/v) piperidine in dimethylformamide (DMF).

Peptide cleavage, purification and folding. Peptides were cleaved from the resin by treatment with Reagent K (TFA/H₂O/phenol/thioanisole/1,2-ethanedithiol; 82.5/5/5/5/2.5 by volume) for 3 h at room temperature. The crude peptide was separated from resin by vacuum-filtration. The cleavage product was precipitated in cold methyl-*tert*-butyl ether, centrifuged and washed again with the ether. Crude peptide was purified by reversed-phase HPLC (RP-HPLC) using a Vydac C18 semi-preparative column (218TP510, 250 mm x 10 mm, 5 μm particle size) eluted with a linear gradient ranging from 15% to 45% solvent B (90% acetonitrile in 0.1% trifluoroacetic acid (TFA)) in 30 min. Oxidative folding of the linear peptide was performed in a buffered solution containing 20 μM peptide, 0.1 M Tris-HCl (pH 7.5) and 1 mM EDTA. Oxidizing reagents used included a 1:1 mM

mixture of reduced:oxidized glutathione (GVIIJ[C24S]), 1 or 2 mM cystamine dihydrochloride (GVIIJ_{SSEA}) or 2 mL of an L-cystine-containing solution (6 mg/mL) in 5% v/v acetonitrile and 0.1% TFA (GVIIJ_{SSC}), as described previously (93,132). Oxidative folding was carried out overnight at room temperature. The oxidation reaction was quenched by acidification with formic acid (final concentration 8% (v/v)). Folded analogues were purified by semi-preparative RP-HPLC. Purities for analogues used in NMR studies were greater than 95%, whereas those used in electrophysiological assays ranged from 80 – 99%. The identities of the oxidized peptides were confirmed by MALDI-TOF mass spectrometry, except GVIIJ[D23γ]_{SSEA}, for which electrospray mass spectrometry was employed.

Other toxins. Syntheses of μ-GIIIA, and μ-PIIIA[R14Q] were performed essentially as previously described (138,139). The synthesis of (μOξ-GVIIJ)₂ (a dimer in which Cys-24 of one monomer was disulfide bonded to its counterpart on the other monomer) was described recently (132).

6.4.2. Nuclear magnetic resonance (NMR) spectroscopy

NMR spectra were acquired using either a Varian Inova 600 or Bruker DRX-600 spectrometer. Lyophilized samples were dissolved to final concentrations of 1.4 mM (GVIIJ[C24S]) or 0.68 mM (GVIIJ_{SSEA}) in a mixture of 90% H₂O/10% ²H₂O at pH 3.2. Spectra were collected, and chemical shift assignments for backbone and side-chain proton resonances were obtained from 2D [¹H,¹H] total-correlation spectroscopy (TOCSY; spin lock time, 30 and 70 ms) and [¹H,¹H]-nuclear Overhauser effect spectroscopy (NOESY; mixing time, 150 ms) acquired at 298 K. For GVIIJ[C24S], ¹⁵N chemical shifts were obtained from a 2D [¹⁵N,¹H] HSQC spectrum, and ¹³C chemical shifts were obtained using both 2D [¹³C,¹H] HSQC and HMBC spectra. To obtain amide temperature coefficients, a series of 1D ¹H spectra and 2D TOCSY (spin-lock time, 70 ms) experiments were acquired at 288, 293, and 298 K. Amide (¹H→²H) exchange rates were measured by dissolving lyophilized GVIIJ[C24S] in ²H₂O at pH 3.2 (0.71 mM final concentration) and then recording a time-course of one-dimensional spectra, followed by acquisition of a 70 ms TOCSY spectrum at 298 K. Spectra were processed using TOPSPIN (version 3.2) and were analyzed in CcpNmr-Analysis (version 2.1.5). Spectra were referenced either directly or indirectly to the DSS methyl signal at 0.0 ppm. Chemical shifts were deposited into the BioMagResBank Data Bank (140,141) with accession numbers 26674 and 26675 for GVIIJ[C24S] and GVIIJ_{SSEA}, respectively.

6.4.3. Structural constraints and calculations

Distance constraints for structural calculations were generated from assigned cross-peaks in NOESY spectra (150 ms mixing time) acquired at 298 K, pH 3.2. Dihedral angle constraints (ϕ and ψ) were generated from TALOS-N predictions (92) and from $^3J_{\text{HN-H}\alpha}$ coupling constants according to the following criteria: $^3J_{\text{HN-H}\alpha} > 8$ Hz, $\phi = -120 \pm 40^\circ$; $^3J_{\text{HN-H}\alpha} < 6$ Hz, $\phi = -60 \pm 40^\circ$. Disulfide bond constraints were added according to the previous experimentally determined connectivity illustrated in Fig. 6.1C (93). Deuterium exchange rates and temperature coefficients were used to identify H-bonded backbone amides; where H-bond acceptors could be identified from initial rounds of structural calculation (present and consistent in $\geq 80\%$ of structures) and were included in subsequent structural calculations. Initial structure calculations were optimized for a low target function using the noeassign macro in CYANA 3.0 (94). Structures generated by CYANA were then used to resolve the assignment of any remaining ambiguous inter-residue NOEs. Following optimization, the final set of constraints was entered into CNS version 1.3 (95), and an ensemble of 100 structures was generated. Of these, the 20 lowest energy structures without violations were selected to represent the solution structure of GVIIJ[C24S]. Validation of the final calculated structures was accomplished using PROCHECK-NMR (96). Secondary structure prediction was performed using DSSP (97) and PROMOTIF (98) based on the closest-to-average structure of GVIIJ[C24S]. Classification of β -turns was based on the criteria reported in (99). Structures were analyzed using MOLMOL (100), and structural representations were constructed using UCSF Chimera (<http://www.cgl.ucsf.edu/chimera>).

6.4.4. Structure-activity studies on GVIIJ_{SSEA} and GVIIJ_{SSC} with rNav1.2 and competition experiments of μ - versus $\mu\text{O}\S$ -conotoxins with rNav1.4.

Two-electrode voltage-clamp electrophysiology. All $\mu\text{O}\S$ -GVIIJ analogues were screened against rat Nav1.2 exogenously expressed in *Xenopus laevis* oocytes. Oocytes were also used to express rat Nav1.4 in experiments to assess competition between μ -PIIIA[R14Q] and $\mu\text{O}\S$ -GVIIJ_{SSG} or $\mu\text{O}\S$ -GVIIJ dimer and, in positive control tests, between μ -PIIIA[R14Q] and μ -GIIIA. The Nav1.2 (NM_012647) and Nav1.4 (NM_013178) clones were obtained from Alan Goldin (University of California, Irvine). Oocytes were injected with 30-50 nL of Nav1.2 or Nav1.4 cRNA (1.5 or 0.6 ng, respectively) in RNase-free water and incubated overnight at 16 °C in ND96 (96 nM NaCl, 2 mM KCl, 1.8 mM CaCl₂, and 5 mM HEPES, pH 7.5), supplemented with antibiotics (100 units/ml penicillin, 0.1 mg/ml streptomycin). Voltage-clamping was performed with a Warner OC-725C amplifier (Warner Instruments) using 3 M KCl-filled microelectrodes (resistance < 0.5 M Ω) (142).

An oocyte was placed in a 4 mm diameter well (30 μ L volume) filled with ND96 and clamped at a holding potential of -80 mV. Voltage-gated sodium currents (I_{Na}) were induced at 20 s intervals with a 50 ms depolarizing pulse to -10 mV. The peptides to be tested were dissolved in ND96 at 10X the desired final concentration (0.1 – 333 μ M) and applied in 3 μ L volumes to the static bath containing the voltage-clamped oocyte. A static bath was used to conserve the limited quantities of analogues. Immediately following peptide application, the solution in the well was gently mixed through repeated pipetting of the bath solution. All experiments were performed at room temperature. Washout of peptide was performed by perfusing the chamber initially at a rate of 1 ml/min for 1 min followed by 0.2 ml/min for 19 min. Use of *X. laevis* frogs, which provided oocytes for this study, followed protocols approved by the University of Utah Institutional Animal Care and Use Committee, which conform to the National Institutes of Health Guide for the Care and Use of Laboratory Animals.

Analysis of electrophysiological data. The time-course of peak I_{Na} was plotted before and during toxin exposure as well as following toxin washout. The observed rate constants (k_{obs}) were determined by fitting of the onset of block to a single-exponential function for ≥ 3 oocytes at each of three different peptide concentrations. Since all μ O δ -GVIII analogues tested were very slowly reversible (i.e. < 50% recovery after 20 min washout or $k_{off} < 0.035 \text{ min}^{-1}$), off rates (k_{off}) were estimated from the level of recovery after 20 min washout for ≥ 9 oocytes assuming a single-exponential time-course (107). To minimize effects of baseline drift, times longer than 20 min were not used. Values of k_{obs} were plotted against [peptide], and k_{on} values were obtained from the slope of the linear regression line assuming the equation, $k_{obs} = k_{on}[\text{peptide}] + k_{off}$ (122). Electrophysiology data are presented as the mean \pm SD, unless specified otherwise, and statistical significance was determined using the two-tailed unpaired *t* test in GraphPad Prism or Excel. Percentage block of the peak sodium current (I_{Na}) by conotoxins or their analogues was calculated as defined in (107) by the following equation: % block (Peak I_{Na}) = [(average ≥ 3 traces at steady state)/(average ≥ 3 baseline traces)] $\times 100$.

6.5 Results

Peptide Synthesis and Analysis. GVIII[C24S] and GVIII_{SSEA}, which were used for NMR studies, were synthesized as described in *Experimental Procedures*. All peptide analogues used in SAR studies were synthesized following folding and purification protocols described for GVIII_{SSEA}. These syntheses generated, on average, between 500 and 900 nmol of purified linear peptide per

100 mg resin cleaved. Oxidative folding of most of the linear analogues produced a single major product comprising between 40% - 60% of the total folding mixture. Exceptions were the [O6A], [D23N] and [D23 γ] analogues, for which the major product comprised only 9, 17 and 28% of the mixture, respectively. Folding of the [F21A], [T26A] and [T28A] analogues in the presence of cystamine dihydrochloride did not lead to a single major product as monitored by RP-HPLC. However, oxidation of these analogues in the presence of L-cystine showed modest improvement in producing a major folding product. The [S19A] analogue exhibited poor folding properties independent of the oxidant used, with the major peak being just 8% of the total mixture. Broadening and “tailing” of the purified HPLC peaks characterized all “poorly” folding analogues, resulting in final purities of 80-93%.

NMR Spectroscopy. Good-quality ^1H NMR spectra were obtained for GVIIJ[C24S] and GVIIJ_{SSEA} at pH 3.2. Comparison of NOESY spectra of GVIIJ[C24S] at pH 3.2 with spectra at pH 7.4 showed that several key long-range NOEs involving pairs of non-exchangeable protons (e.g. Lys-30 H^β - Asp-23 H^β ; Cys-29 H^β - Hyp-6 H^α ; Ala-8 H^β - Cys-29 H^α ; Thr-9 H^α - Thr-28 $\text{H}^{\gamma 2}$; Gly-7 H^α - Thr-28 H^α) were present at both pH values, implying that the structure determined at pH 3.2 was representative of that at physiological pH. Sequential assignments were derived from 2D TOCSY and NOESY spectra. The temperature dependence of amide proton chemical shifts is shown in Fig. 6.2A. Deviations from random coil values (143,144) for backbone H^{N} and H^α chemical shifts of GVIIJ[C24S] and GVIIJ_{SSEA} are plotted in Fig. 6.3. The near identity of these plots confirms adoption of similar backbone structures for these two analogues. Both structures have chemical shifts close to random coil values at the N- and C-termini. Small differences between the two peptides were observed for the residues of loop 2 (Gly-11 – Tyr-16) and loop 4 (Asp-23 - Thr-28).

Solution structures. Structures were generated in CYANA and then refined in CNS (95) using a total of 401 NOE-derived distance constraints, 39 dihedral, 9 $\chi 1$ angle constraints (from $^3J_{\text{HN-H}\alpha}$ J -coupling measurements and TALOS-N predictions) and 5 hydrogen-bond restraints (from amide temperature coefficients and ^2H exchange experiments). A summary of experimental constraints and structural statistics for GVIIJ[C24S] is provided in Table 6.2.

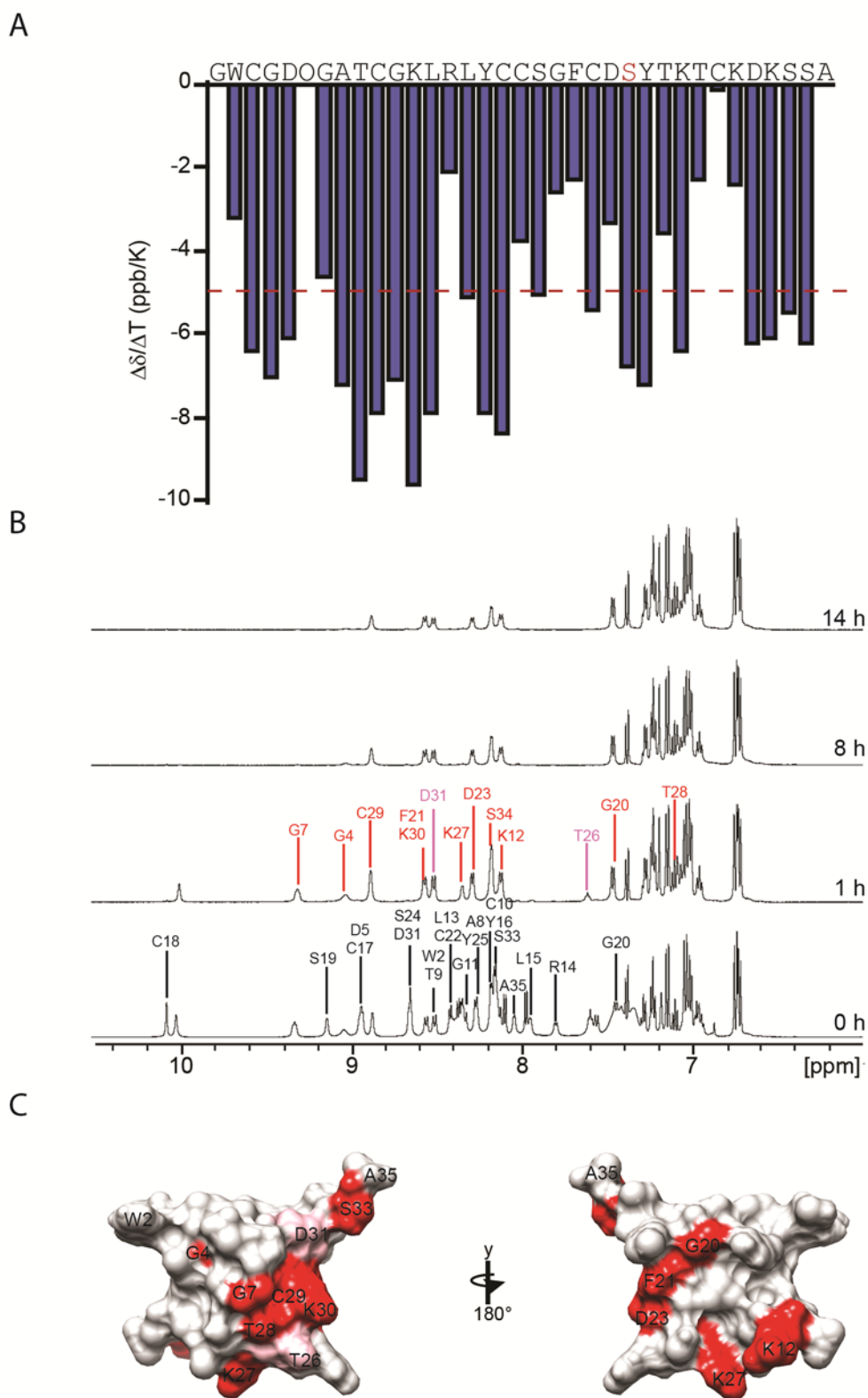


Figure 6.2. Characterization of GVIIJ[C24S] by NMR spectroscopy. (A) Temperature dependence experiments identified several residues that exhibited amide proton chemical shifts of magnitude < 4 ppb/K, including: Trp-2, Arg-14, Cys-18, Gly-20, Phe-21, Asp-23, Thr-26, Thr-28, Cys-29 and Lys-30. These shifts suggest partial protection of the residues from solvent. (B) Amide exchange experiments demonstrated that Cys-10, Lys-12, Arg-14, Leu-15, Cys-29, Phe-21, Lys-30 and Ser-33 exchanged slowly in 100% $^2\text{H}_2\text{O}$ at 25 $^\circ\text{C}$. These amide protons were either inaccessible to solvent through their location in the folded peptide or

were protected from exchange by interactions such as hydrogen bonds. Amide and aromatic regions of 1D ^1H -NMR spectra in 100% $^2\text{H}_2\text{O}$ at 25 °C between 0 and 14 h are shown. Data were acquired using a Bruker DRX-600 spectrometer. Rapidly exchanging amide protons (0 – 1 h) are listed in black, medium exchange (1 – 8 h) in pink and slowly exchanging (> 8 h) amide protons are in red. (C) Locations of rapidly exchanging amide protons mapped onto the structure of GVIIJ[C24S] (see below). Fast (white), medium (pink) and slow (red) exchanging amide protons are shown on the closest-to-average structure of GVIIJ[C24S]. Structure is rotated by 180 ° in the anticlockwise direction to show labile protons on the opposite face of the peptide.

Table 6.2: Structural statistics for GVIIJ[C24S]	
Variable	Value
Total no. of distance restraints	401
intraresidue ($i = j$)	144
short/sequential ($ i - j = 1$)	116
medium-range ($1 < i - j < 5$)	39
long-range ($ i - j > 5$)	102
hydrogen bond	5
Total no. of dihedral restraints	39
Energies (kcal·mol ⁻¹)*	
E_{NOE}	12.16 ± 3.60
E_{DIH}	0.43 ± 0.167
RMSD from experimental data	
NOEs (Å)	0.035 ± 0.005
dihedrals (deg)	0.379 ± 0.071
Deviations from ideal geometry [†]	
angles (deg)	0.475 ± 0.015
bonds (Å)	0.007 ± 0.000
impropers (deg)	0.477 ± 0.009
Atomic RMSD [‡]	
backbone heavy atoms	0.762 (2-32)
all heavy atoms	1.549 (2-32)
Ramachandran plot [§]	
most favored (%)	91.0 (2-32)
allowed (%)	8.8 (2-32)
additionally allowed (%)	0.0 (2-32)
disallowed (%)	0.2 (2-32)

*The values for E_{NOE} were calculated from a square-well potential with force constants of 150 kcal·mol⁻¹·Å². †The values for bonds, angles and impropers show the deviations from ideal values as defined by the CNS force field. ‡Average RMSD to the mean calculated in MOLMOL. §Reported by PROCHECK-NMR. (2-32) indicates the range over which RMSD values and Ramachandran plots were determined.

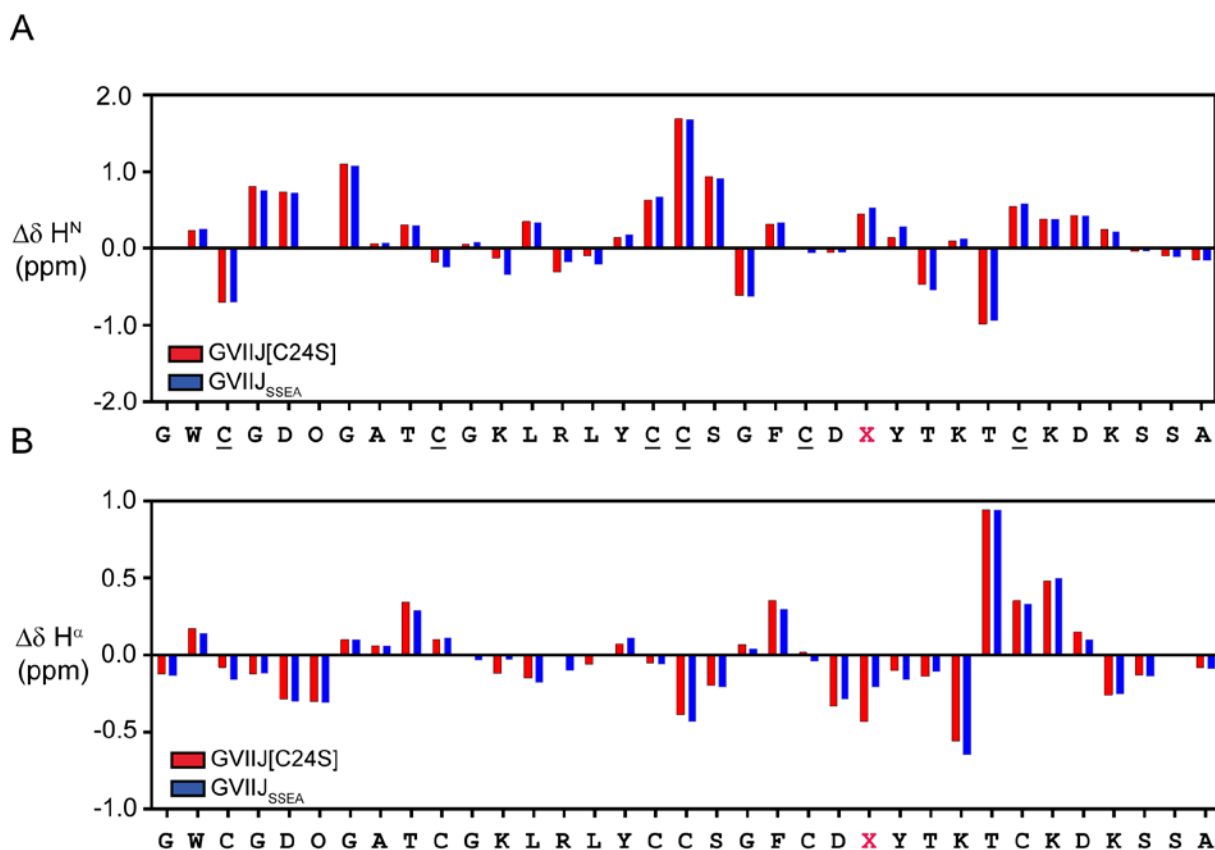


Figure 6.3. Deviation of backbone amide (H^N) and C^α proton (H^α) chemical shifts from random coil values at 25 °C (144). (A) H^N chemical shift deviations for GVIIJ[C24S] (red) and GVIIJ_{SSEA} (blue). (B) H^α chemical shift deviations for GVIIJ[C24S] (red) and GVIIJ_{SSEA} (blue). O is hydroxyproline. X is either serine (GVIIJ[C24S]) or *S*-((2-aminoethyl)thio)cysteine (GVIIJ_{SSEA}).

GVIIJ[C24S] is structurally well-defined, with a mean global RMSD of 0.76 Å (over the backbone heavy atoms N, CA, C of residues 2-32) (Table 6.2, Fig. 6.4A). The structure is characterized by two short antiparallel β -strands encompassing Cys-22 – Asp-23 (β_1) and Thr-28 – Cys-29 (β_2), linked by a distorted Type I β -turn (99) spanning residues Asp-23 (*i*) – Thr-26 (*i*+3) (backbone heavy atom RMSD of 0.07 Å) (Fig. 6.4B). The β -strands, together with the β -turn, form a 4:4 β -hairpin (145), near the tip of which is the side chain of residue 24. These secondary structure features were supported by weak or absent sequential H^N - H^N NOEs and stronger H^N - H^α sequential NOEs, as well as a number of $^3J_{H^N H^\alpha}$ coupling constants ≥ 8 Hz (Fig. 6.5A-B). Hydrogen bonds were observed between Asp-23 H^N – Thr-28 O, Thr-28 H^N – Asp-23 O and Lys-30 H^N – Phe-21 O (20 of 20 structures), as well as between Lys-27 H^N - Ser-24 O (7 of 20 structures) and Thr-26 H^N - Asp-23 O (14 of 20 structures). Within this region, backbone amides of Phe-21, Asp-23, Ser-24, Thr-26, Lys-27, Thr-28 and Cys-29 were slowly exchanging (Fig. 6.4A, Fig. 6.2B-C) and many

(e.g. Phe-21, Asp-23, Thr-26, Thr-28 and Cys-29) exhibited temperature coefficients of magnitude < 4 ppb/K (Fig. 6.2A).

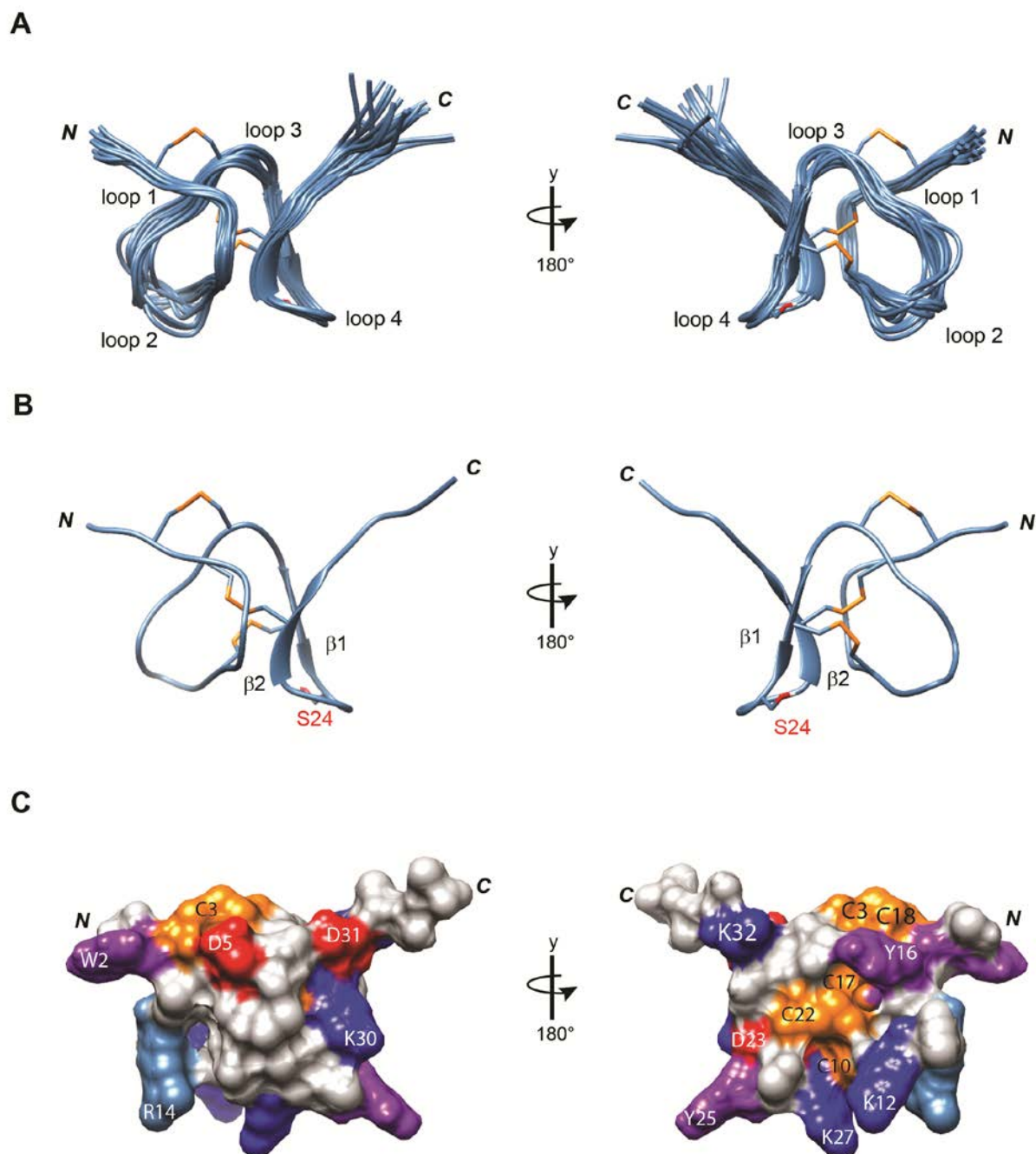


Figure 6.4. Structure of the $\mu\text{O}\xi$ -GVIIJ analogue GVIIJ[C24S]. (A) Family of 20 final structures for GVIIJ[C24S], superimposed on backbone heavy atoms of residues 2-32. Disulfide bonds are shown in orange according to the previously established connectivity: Cys-3 - Cys-18; Cys-10 - Cys-22; Cys-17 - Cys-29. (B) Ribbon representation of the closest-to-average structure with calculated β -sheets at residues 22-23 (β 1) and 28-29 (β 2). Position of Ser-24 (in loop 4) is indicated. In the panel on the left, residues 8 - 10 are located in the looped region adjacent to the β 2-strand of GVIIJ[C24S]. (C) Surface representation of GVIIJ[C24S], with basic residues colored light and dark blue (Arg and Lys, respectively); acidic residues (Asp) colored red; Cys residues colored orange; aromatic residues (Trp and Tyr) colored purple; and all others shown in white. Depictions rotated by 180° about the y-axis are also shown.

Within loop 1 (Gly-4 – Thr-9), adjacent to the β 2-strand, is a small segment of the peptide that exhibits modest levels of extended structure (Fig. 6.4B). Indeed, hydrogen bonds were observed between Cys-29 H^N and Ala-8 O (14 of 20 structures) and Cys-10 H^N – Lys-27 O (20 of 20 structures). In ICK peptides that display intercysteine loop lengths similar to those of μ O ξ -GVIII, this region of extended structure is often present, sometimes as a third β -strand (66,133). However, in GVIII[C24S], this region was too short to be designated as such by DSSP or PROMOTIF secondary structure prediction programs.

Other secondary structure features include a Type IV β -turn encompassing Cys-10 – Leu-13 within intercysteine loop 2 (Gly-11 – Tyr-16) (Fig. 6.4C). This loop was less well-defined than the remainder of the peptide, with angular order parameters for ϕ and $\psi < 0.8$ and RMSD of 1.2 Å over the backbone heavy atoms N, CA, C of residues Gly-11 – Tyr-16 (Fig. 6.5D-F). Several rapidly exchanging backbone amide protons were identified in this region by H/D exchange experiments (Fig. 6.5A, Fig. 6.2B-C), indicating that this loop was solvent exposed. Backbone angular order parameters for residues at the N- and C-termini were also ≤ 0.8 (Fig. 6.5D-F).

Oxidative folding of μ O ξ -GVIII analogues. Residue 24, which in the native peptide presents the ‘extra’ cysteine responsible for tethering to the channel, is located within the β -turn of loop 4 (Fig. 6A). Asp-23, at the start of the turn, was critical for folding of the GVIII_{SEA} analogues, with substitution by either lysine or alanine resulting in inefficient formation of a major folding product (Fig. 6.6B). A major product was observed in the [D23N] and [D23 γ] analogues, albeit in lower overall yields compared to efficiently folding analogues. This restoration in folding was presumably due to interactions between O γ in the side chain of Asp-23 and the backbone H^N of Tyr-25 ($i + 2$) and H^N of Thr-26 ($i + 3$) (99). Hydrogen bonds between the side chain of Asp-23 and the H^N of Tyr-25 were observed in half the structures and between Asp-23 and Thr-26 in about 25% of structures. Replacement of Tyr-25 by Asp made the peptide more prone to dimerization, decreasing the yield for the desired product by about 10%. In many Type I β -turns, Asp is one of three preferred residues for electrostatic interactions with the backbone H^N of residue 25 (99); it may be that this substitution further exposed Cys-24, where it could conceivably undergo dimerization. Restoration of the folding yield was observed for the Arg-25 ($i + 2$) mutation, which may have resulted from stabilization of loop 4 through a weak interaction between N ^{ϵ} of Arg-25 and the main chain oxygen of Asp-23.

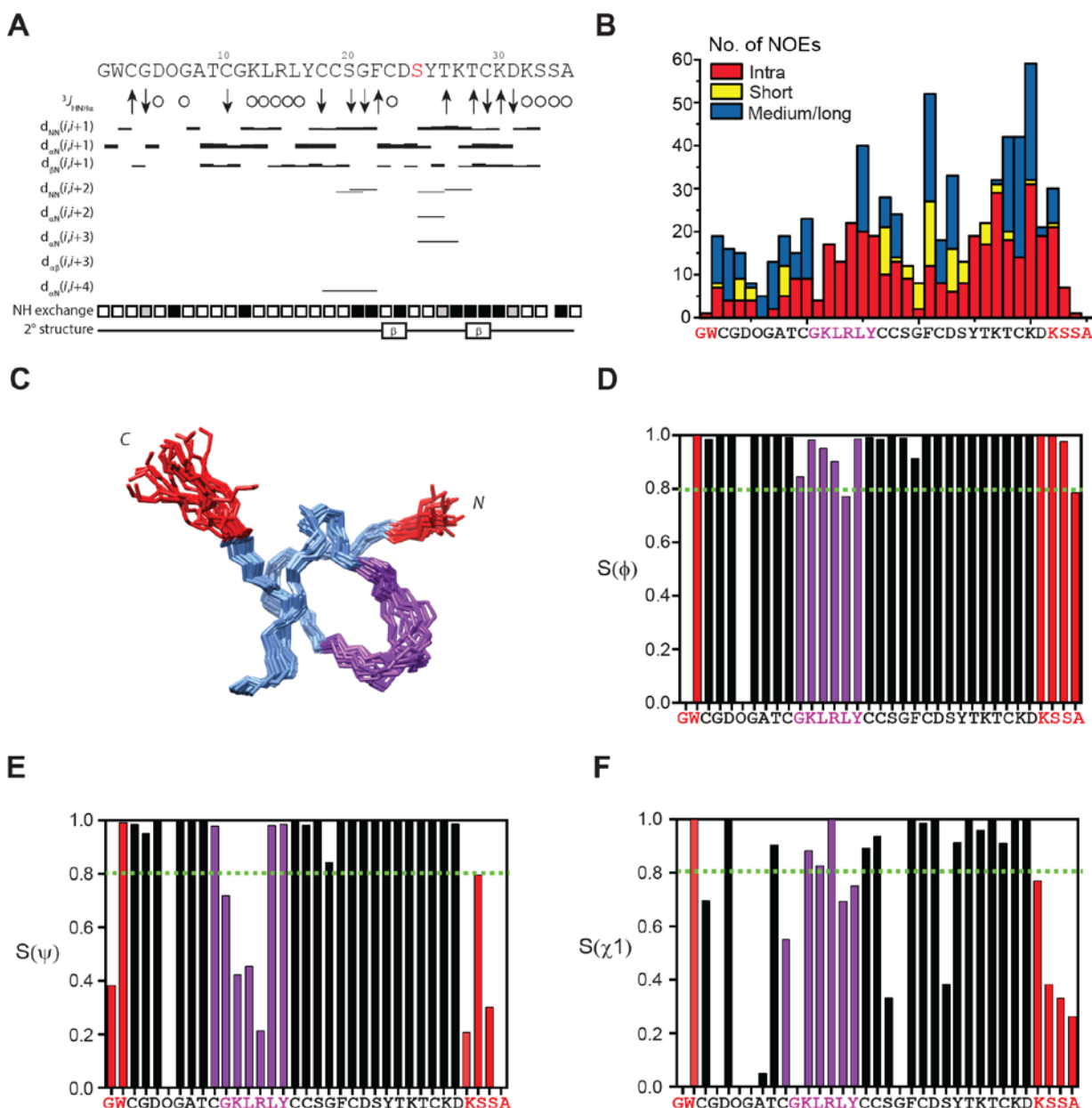


Figure 6.5. Characterization of the final 20 structures of GVIIJ[C24S]. (A) Sequential and medium-range NOE connectivities for GVIIJ[C24S] (298 K, pH 3.2) according to CYANA structure calculation. Intensities of d_{NN} , $d_{\alpha\text{N}}$ and $d_{\beta\text{N}}$ are proportional to the height of the bars. Measurable $^3J_{\text{HNH}\alpha}$ are noted as follows: $^3J_{\text{HNH}\alpha} < 6$ Hz (\downarrow), $^3J_{\text{HNH}\alpha}$ 6–8 Hz (○) and $^3J_{\text{HNH}\alpha} > 8$ Hz (\uparrow). Amide proton exchange rates for residues 1 – 35 are designated as follows: open box, fast exchange rate (0–1 h); gray box, medium exchange rate (1–8 h); black box, slow exchange rate (>8 h). Regions containing elements of secondary structure (β -strands between Cys-22 – Asp-23 and Thr-28 – Cys-29) are indicated. (B) CYANA output showing the number of long range ($i-j \geq 6$), short range ($2 \leq i-j \leq 5$) and intra-residue NOE restraints used in the calculation of the final structure. (C) Minimal backbone structure of the ensemble of 20 structures of GVIIJ[C24S] showing disordered N- and C-termini (red) and the dynamic loop 2 region (Cys-11 – Tyr-16) of the peptide (purple). (D–F) Angular order parameters (S) for backbone (ϕ , ψ) and sidechain (χ_1) dihedral angles.

Several residues in close proximity to this β -turn also appeared to be important for stabilization of loop 4 (Asp-23 – Thr-28). In all 20 structures, the side chain of Lys-30 points back into the loop

where it could participate in electrostatic interactions with either Asp-23 or Thr-26. In the closest-to-average structure of GVIIJ[C24S], the Hⁿ of Lys-30 and the side chain oxygen atoms of Asp-23 or Thr-26 were separated by just 3.4 and 4.4 Å, respectively (Fig. 6.6A). The importance of such interactions was illustrated by the inability of the [K30D] analogue to produce a single, major folding product. Replacement of Lys-30 with an acidic residue such as aspartate presumably had a destabilizing effect on loop 4 (Asp-23 – Thr-28), but substitution with a small, uncharged residue in the [K30A] analogue restored efficient folding. Other residues found to be important for the folding of μO§-GVIIJ included Thr-26 and Thr-28. Neither [T26A] nor [T28A] yielded a single major product following cystamine oxidation. Again, based on the calculated distances between the side chains in the closest-to-average structure, this was probably caused by removal of stabilizing interactions between the side chains of these residues and Hⁿ of Lys-30. The use of a different oxidant (i.e. L-cystine) resulted in formation of a major product in each case, albeit in significantly lower yields compared to other analogues used in this study (Fig.6. 6B).

Structure-activity relationship studies of the block of Nav1.2 by μO§-GVIIJ analogues. The ability of peptides to block Nav1.2 expressed in *Xenopus* oocytes was assessed electrophysiologically as described in Experimental Procedures. We used rNav1.2 as the target channel to maintain consistency with the previous studies of μO§-GVIIJ analogues (93,132). The GVIIJ[C24S] analogue, which was used in NMR studies, blocked Nav1.2 rapidly and reversibly (Fig. 6.7A). The rapidity precluded accurate determination of k_{on} and k_{off} values. The IC₅₀ for GVIIJ[C24S] was 4.8 μM (with 95% CI of 3.7 – 6.2 μM) (Fig. 6.7B).

All SAR studies were performed with analogues of GVIIJ_{SSEA}, which itself is slightly more potent than GVIIJ_{SSC}, against Nav1.2 (K_d = 2.3 versus 3.4 nM) (132). An initial series of analogues was designed and synthesized to investigate the importance of the residues of loop 4 (Asp-23 – Thr-28) in the immediate vicinity of Cys-24. Amino acid substitutions in loop 4 appeared to have significant effects on the structural stability of the peptide, as evidenced by the inability of some of the variants to form a single, major folding product (Fig. 6.6B). However, most of these substitutions had little effect on the peptide's ability to block rNav1.2 (Fig. 6.6C). The on-rate constants varied considerably

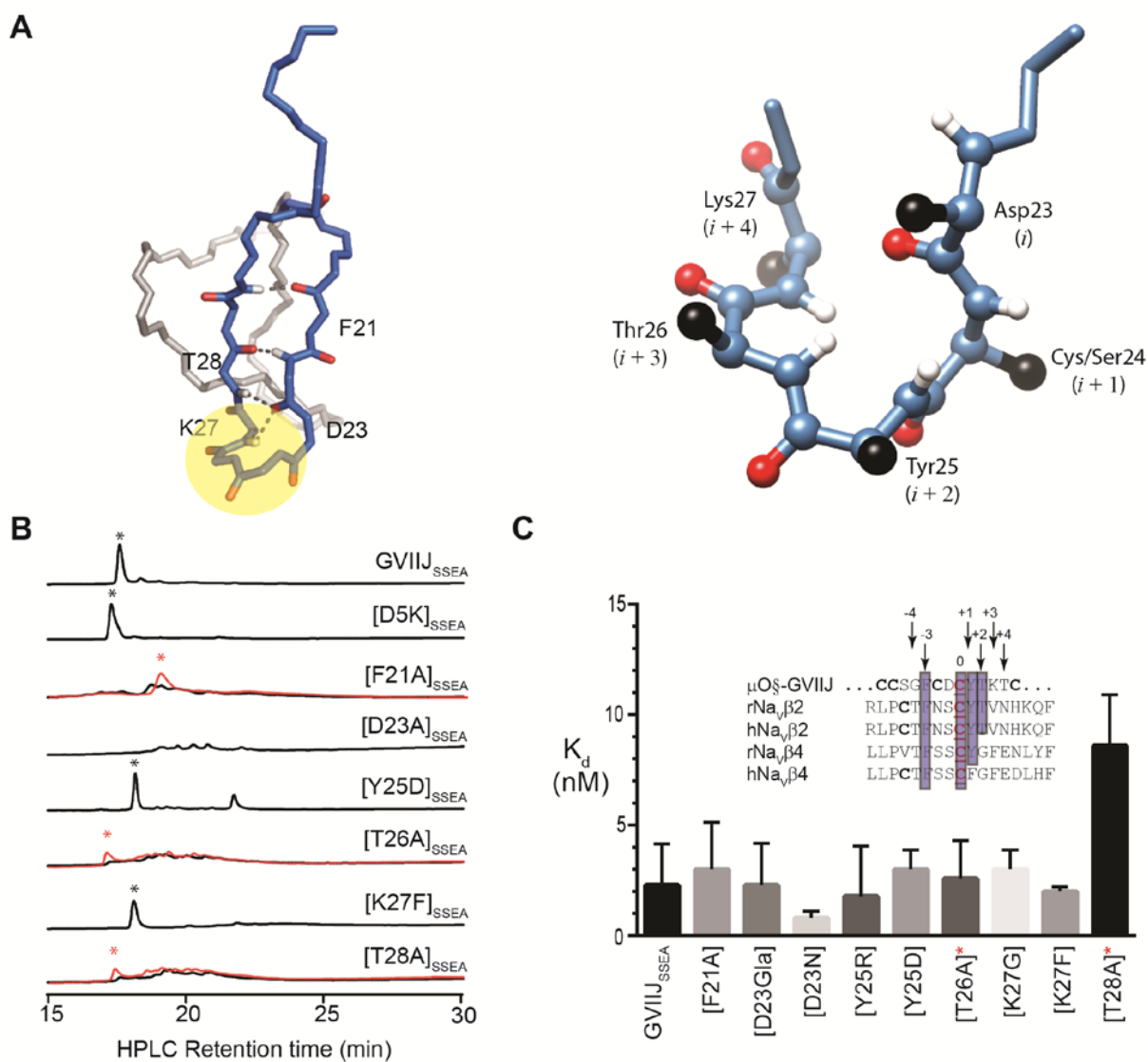


Figure 6.6. Structure-activity relationship studies of residues in the Cys-24-containing loop 4. (A) The closest-to-average backbone structure of GVIIJ[C24S] is stabilized by numerous H-bonds between backbone atoms as well as by side-chain to backbone interactions between the residues in this loop (Phe-21 – Thr-28). A Type I β -turn between two antiparallel β -strands is stabilized by interactions between residues in this turn (Asp-23 – Thr-26). (B) HPLC-elution profiles of GVIIJ_{SSEA} analogues following folding. Conventional folding of Ala-replacement mutants of Phe-21, Asp-23, Thr-26 and Thr-28 did not yield a single, major folding species (black trace); however, folding in the presence of L-cystine (red trace) resulted in a major product (red asterisk), although with significantly lower yields compared to other mutants (black asterisks). The [D5K] analogue was included to show that charge reversal did not affect accumulation of a major product when the substitution was made to residues spatially distinct from loop 4. (C) Comparison of Nav1.2 blockade by GVIIJ_{SSEA} mutants in the Cys-24 containing loop. Data are from Table 6.3. Analogues constructed on the GVIIJ_{SSC} background are denoted by a red asterisk. Nearly all analogues were functionally equipotent with the unmodified peptide, suggesting that residues in this region are important for stability, but not activity. One exception to this was the [T28A] analogue, which exhibited a K_d value of 8.60 ± 2.30 nM, significantly lower (P -value = 0.0212) than that of unmodified peptide. Selection of some amino acid replacements in this loop was based on modest sequence homology between loop 4 of μ O ϕ -GVIIJ and rat or human Nav β 2 and β 4-subunits, whose partial homologous sequences are shown in the inset.

across all analogues, whereas recovery from block (reflected in k_{off}) was very slow and showed little variation (Table 6.3). The largest k_{on} s were observed in mutants of Thr-9 ([T9A]), Asp-23 ([D23N]) and Lys-30 ([K30A]), with values in the range of 4 to 5 $\mu\text{M}^{-1}\cdot\text{min}^{-1}$. Conversely, the analogues with the smallest k_{on} s were located in loop 2 (Gly-11 – Tyr-16), namely Lys-12 ([K12D]), Arg-14 ([R14D]) and Tyr-16 ([Y16A]) ($k_{on} = 0.01, 0.03$ and $0.06 \mu\text{M}^{-1}\cdot\text{min}^{-1}$, respectively). The lower k_{on} values observed with these analogues, in turn, resulted in increased K_d values ranging from about 50 to 280-fold higher than GVIIJ_{SSEA} (Fig. 6.7C-F, Table 6.3).

Block by μ -GIIIA, $\mu\text{O}\xi$ -GVIIJ_{SSG}, or $(\mu\text{O}\xi$ -GVIIJ)₂ of naïve rNav1.4 versus rNav1.4 pre-equilibrated with μ -PIIIA[R14Q]. μ -PIIIA[R14Q] blocked Nav1.4 with an IC_{50} of 0.25 μM (95% CI of 0.19 – 0.33 μM) (Fig. 6.8A). At saturating concentrations, μ -PIIIA[R14Q] blocked incompletely and left a residual current (rI_{Na}) of $27 \pm 3.5 \%$ (Fig. 6.8A). As a positive control for competition between μ -PIIIA[R14Q] and another site 1 antagonist, we used μ -GIIIA, the first μ -conotoxin used to help define site 1 (138,146). μ -GIIIA (10 μM) rapidly blocked the I_{Na} of rNav1.4 (Fig. 6.8B inset). However, when rNav1.4 was pre-equilibrated with 33 μM μ -PIIIA[R14Q], the block of the resulting rI_{Na} by μ -GIIIA was significantly slower (Fig. 6.8B, Table 6.4) as would be expected if the two μ -conotoxins competed for the same site on the channel. In contrast, the rate of block by 3.3 μM $\mu\text{O}\xi$ -GVIIJ_{SSG} was unaffected by the presence of 33 μM μ -PIIIA[R14Q] (Fig. 6.8C, Table 6.4), which indicates that the two peptides (μ - and $\mu\text{O}\xi$ -conotoxins) do not compete for the same site to block the channel. On the other hand, the rate of block by 10 μM $(\mu\text{O}\xi$ -GVIIJ)₂ (i.e., the $\mu\text{O}\xi$ -GVIIJ dimer) was slightly, but significantly, decreased by the presence of μ -PIIIA[R14Q] (Fig. 6.8D, Table 6.4).

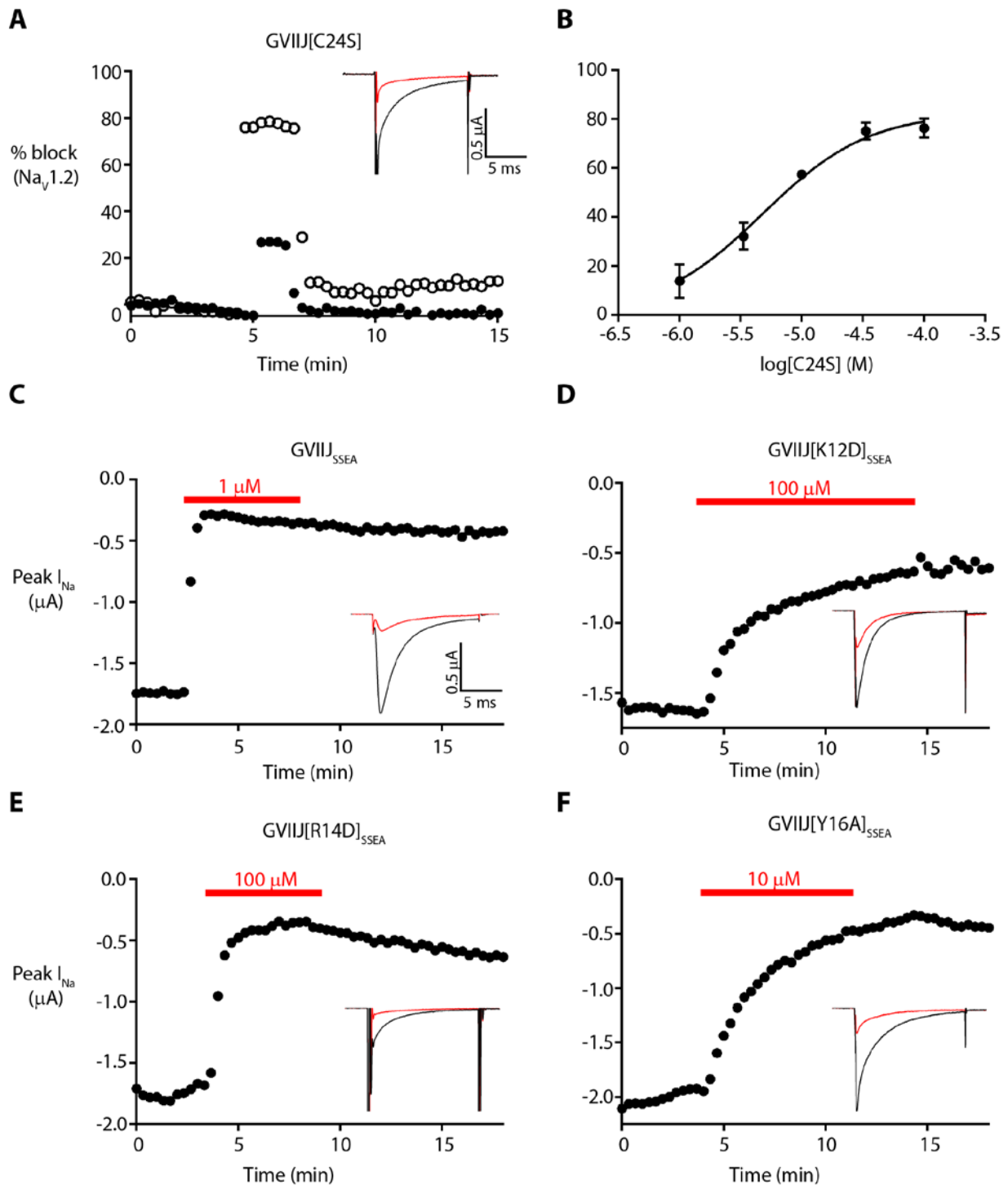


Figure 6.7. Nav1.2 block by $\mu\text{O}\delta$ -GVIIJ analogues. (A) Comparison of Nav1.2 blockade by 3.3 μM (filled circles) and 33 μM (open circles) GVIIJ[C24S]. Block was rapidly reversible at all concentrations tested. Responses did not completely return to baseline following washout of high concentrations of peptide; studies are underway to better understand this phenomenon. Inset shows the current traces before (black) and after (red) application of 33 μM GVIIJ[C24S]. (B) Concentration-response curve for GVIIJ[C24S]. Data points are mean \pm SE ($n \geq 3$ oocytes). Solid line is the best-fit curve to the equation % Peak I_{Na} blocked = $Y_{\text{max}}/(1 + (\text{IC}_{50}/[\text{Peptide}]))$, where Y_{max} , the extrapolated level of block at saturating peptide concentrations, was 82.8% (with 95% CI of 77.5 – 88.10), and the IC_{50} was 4.8 μM (with 95% CI of 3.7 – 6.2 μM); "CI" indicates confidence interval. (C) GVIIJ_{SSEA} (1 μM) rapidly blocked ~70% of the sodium current. In contrast to the [C24S] analogue, this analogue_{SSEA} exhibited nearly irreversible block of Nav1.2 following washout, which is

attributed to ‘tethering’ to site 8 of the channel (93,132). (D-F) Substitution of critical amino acids Lys-12, Arg-14 and Tyr-16 resulted in analogues with lower k_{obs} for the inhibition of Nav1.2 (see also Table 6.3). Insets depict the ability of each analogue to block sodium currents (I_{Na}) in an *X. laevis* oocyte expressing rNav1.2 that was voltage clamped at -80mV and I_{Na} evoked by a voltage step to -10 mV applied every 20 s. The major plot shows the time course of block (the red bar represents when oocyte was exposed to the peptide). Insets in each panel show the current traces before (black) and during (red) exposure to the indicated peptides.

6.6 Discussion

The structural and functional studies of $\mu\text{O}\xi$ -GVIIJ described here have revealed several important features of the peptide that contribute to its functional activity. The solution structure of GVIIJ[C24S] is a classical ICK motif (66,133), exhibiting two antiparallel β -strands cross-linked by three disulfide bridges that formed a knot-like structure in which the Cys-17 - Cys-29 disulfide crossed the macrocycle formed by the remaining two disulfide bridges and the interconnecting backbone. ICK peptides are abundant in nature, with many being observed in toxin or toxin-like peptides (Fig. 6.9), and are of significant interest as therapeutic scaffolds because of their relative ease of synthesis, stability and amenability to sequence mutations (134). Important in the structure of GVIIJ[C24S] was the presentation of residue 24, within the β -turn of loop 4 (Asp-23 – Thr-26), such that it could readily interact with the channel. It was shown recently that the cysteine residue at this position is a key determinant of the off-rate of the peptide (93,132). Our results lend support to this as all peptide analogues investigated here exhibited k_{off} values that were close to that of unmodified GVIIJ_{SSEA} (Table 6.3). Presumably this is because, once bound to the channel, the energetics of dissociation are resilient to changes in individual amino acid side chains. These results suggested that the structural features that had the greatest influence on the biological activity of $\mu\text{O}\xi$ -GVIIJ are those that affect k_{on} .

The solution structure of $\mu\text{O}\xi$ -GVIIJ was solved using an analogue in which Cys-24 was replaced with serine in order to avoid the risk of dimerization during the course of NMR studies. The block by GVIIJ[C24S] was rapidly reversible, in contrast to that of GVIIJ_{SSC} or GVIIJ_{SSEA}, which blocked nearly irreversibly. The differences in kinetics between GVIIJ[C24S] and GVIIJ_{SSC} or GVIIJ_{SSEA} can be attributed to the inability of

GVIIJ[C24S] to tether to its binding site on the channel. Given the low nanomolar potency of GVIIJ_{SSEA} for Nav1.2, this analogue was used as the basis for SAR studies to assess the importance of individual non-cysteine residues. Deviations from random coil chemical shift plots were nearly identical for GVIIJ[C24S] and GVIIJ_{SSEA} (Fig. 6.3), which validated their use for structural and functional studies, respectively.

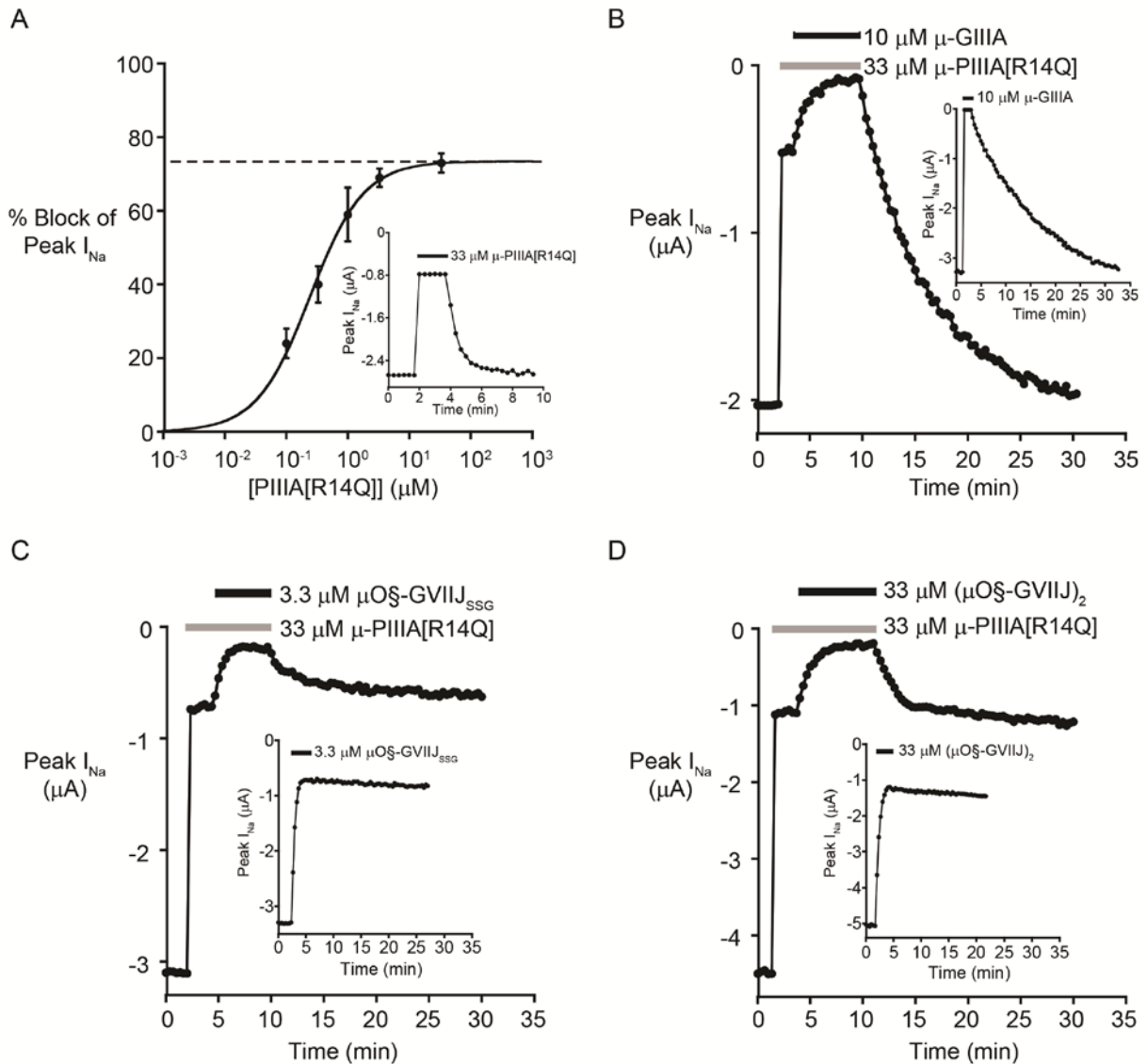


Figure 6.8. Block of $\text{Nav}_{1.4}$ by $\mu\text{-PIIIA[R14Q]}$, $\mu\text{-GIIIA}$, $\mu\text{O}\S\text{-GVIIJ}$ or $(\mu\text{O}\S\text{-GVIIJ})_2$, alone or in binary combinations. Peak I_{Na} of voltage-clamped oocytes expressing rat $\text{Nav}_{1.4}$ were monitored as described in Materials and Methods. Bars in representative time courses of block indicate when peptides were present in the (static) bath. Values are mean \pm SD or 95% confidence intervals ($n \geq 5$ oocytes). (A) Concentration-response curve of $\mu\text{-PIIIA[R14Q]}$; solid line is best fit curve to the binding equation provided in Fig. 6.7; $\text{IC}_{50} = 0.25 \mu\text{M}$ (95% CI of $0.19 - 0.33 \mu\text{M}$) and percentage block at saturating [peptide] was $73 \pm 3.5\%$ (dashed line) (i.e., residual current, rI_{Na} , was 27%). Inset, representative time course of block of I_{Na} by $33 \mu\text{M} \mu\text{-PIIIA[R14Q]}$ and recovery following peptide washout; average value of k_{off} was $1.2 \pm 0.32 \text{ min}^{-1}$. (B) As in inset of a A except that after the block by $\mu\text{-PIIIA[R14Q]}$ had reached steady state, the bath was supplemented with $\mu\text{-GIIIA}$ ($10 \mu\text{M}$ final concentration) to observe its block of rI_{Na} , then both peptides were washed out. Inset, time course of block by $10 \mu\text{M} \mu\text{-GIIIA}$ alone. Note, $\mu\text{-GIIIA}$ blocked the rI_{Na} much more slowly than the control I_{Na} illustrated in the inset, which indicates that $\mu\text{-PIIIA[R14Q]}$ and $\mu\text{-GIIIA}$ competed for the same site to block the channel. (C) As in B, except the bath was supplemented with $\mu\text{O}\S\text{-GVIIJ}_{\text{SSG}}$ ($3.3 \mu\text{M}$ final concentration) to observe its block of rI_{Na} . Inset, time course of block by $3.3 \mu\text{M} \mu\text{O}\S\text{-GVIIJ}_{\text{SSG}}$ alone. Note, $\mu\text{O}\S\text{-GVIIJ}_{\text{SSG}}$ blocked rI_{Na} essentially as fast as it did control I_{Na} illustrated in the inset, which indicates that $\mu\text{-PIIIA[R14Q]}$ and $\mu\text{O}\S\text{-GVIIJ}$ did not compete with each other to block the channel. (D) As in B, except the bath was supplemented with $33 \mu\text{M} (\mu\text{O}\S\text{-GVIIJ})_2$ to observe its block of rI_{Na} . Inset, time course of block by $33 \mu\text{M} (\mu\text{O}\S\text{-GVIIJ})_2$ alone. Although not evident by visual inspection, $(\mu\text{O}\S\text{-GVIIJ})_2$ blocked rI_{Na} slightly more slowly than it did control I_{Na} (see Table 6.4 for average k_{obs} values).

Table 6.3. Kinetics of block of rNaV1.2 by $\mu\text{O}\delta$ -GVIIJ analogues

Peptide	k_{on}^* ($\mu\text{M}\cdot\text{min}^{-1}$)	k_{off}^\dagger (min^{-1})	K_{d}^\ddagger (nM)
GVIIJ _{SSEA} [¶]	2.10 ± 0.19	0.0049 ± 0.0039	2.30 ± 1.87
GVIIJ _{SSC} [§]	1.66 ± 0.05	0.0057 ± 0.0022	3.40 ± 1.30
[W2A] _{SSEA}	0.25 ± 0.01	0.0058 ± 0.0030	23.2 ± 13.2
[D5K] _{SSEA}	2.51 ± 0.54	0.0070 ± 0.0045	2.90 ± 2.10
[O6A] _{SSEA}	2.23 ± 0.17	0.0076 ± 0.0020	3.40 ± 0.90
[T9A] _{SSEA}	4.74 ± 0.56	0.0056 ± 0.0032	1.20 ± 0.70
[K12D] _{SSEA}	0.01 ± 0.00	0.0081 ± 0.0056	644 ± 455
[L13A] _{SSEA}	0.50 ± 0.06	0.0067 ± 0.0021	13.4 ± 4.50
[R14D] _{SSEA}	0.03 ± 0.00	0.0099 ± 0.0065	307 ± 204
[L15A] _{SSEA}	1.98 ± 0.32	0.0055 ± 0.0035	2.80 ± 1.82
[Y16A] _{SSEA}	0.06 ± 0.01	0.0071 ± 0.0063	122 ± 108
[S19A] _{SSEA}	0.58 ± 0.07	0.0069 ± 0.0030	12.1 ± 5.40
[F21A] _{SSC}	2.02 ± 0.15	0.0061 ± 0.0043	3.00 ± 2.14
[D23Gla] _{SSEA}	2.10 ± 0.19	0.0049 ± 0.0039	2.30 ± 1.90
[D23N] _{SSEA}	5.09 ± 0.65	0.0040 ± 0.0015	0.80 ± 0.31
[Y25A] _{SSEA}	0.68 ± 0.08	0.0056 ± 0.0038	8.30 ± 5.70
[Y25R] _{SSEA}	2.26 ± 0.20	0.0041 ± 0.0051	1.80 ± 2.26
[Y25D] _{SSEA}	1.34 ± 0.14	0.0040 ± 0.0011	3.00 ± 0.88
[T26A] _{SSC}	1.36 ± 0.21	0.0036 ± 0.0022	2.60 ± 1.70
[K27D] _{SSEA}	0.19 ± 0.05	0.0059 ± 0.0031	30.6 ± 18.1
[K27G] _{SSEA}	2.10 ± 0.30	0.0064 ± 0.0016	3.00 ± 0.88
[K27F] _{SSEA}	2.41 ± 0.08	0.0049 ± 0.0005	2.00 ± 0.22
[T28A] _{SSC}	1.92 ± 0.36	0.0166 ± 0.0032	8.60 ± 2.30
[K30A] _{SSEA}	3.71 ± 0.26	0.0114 ± 0.0085	3.10 ± 2.30
[D31K] _{SSEA}	2.80 ± 0.58	0.0061 ± 0.0031	2.20 ± 1.20
[K32D] _{SSEA}	0.77 ± 0.07	0.0075 ± 0.0026	9.70 ± 3.40

Values represent mean ± SD (n ≥ 3 oocytes for each of the ≥ 3 different concentrations of each analogue). *On-rate constants were determined from the onsets of block at varying peptide concentrations (see *Experimental Procedures*). †Off-rate constants were determined from toxin-washout curves (see *Experimental Procedures*). ‡ K_{d} is the ratio, $k_{\text{off}}/k_{\text{on}}$. GVIIJ_{SSEA} and GVIIJ_{SSC} are analogues where Cys-24 is disulfide bonded with cysteamine (2-aminoethanethiol) or cysteine, respectively. ¶From Zhang et al (132). §From Gajewiak et al (129).

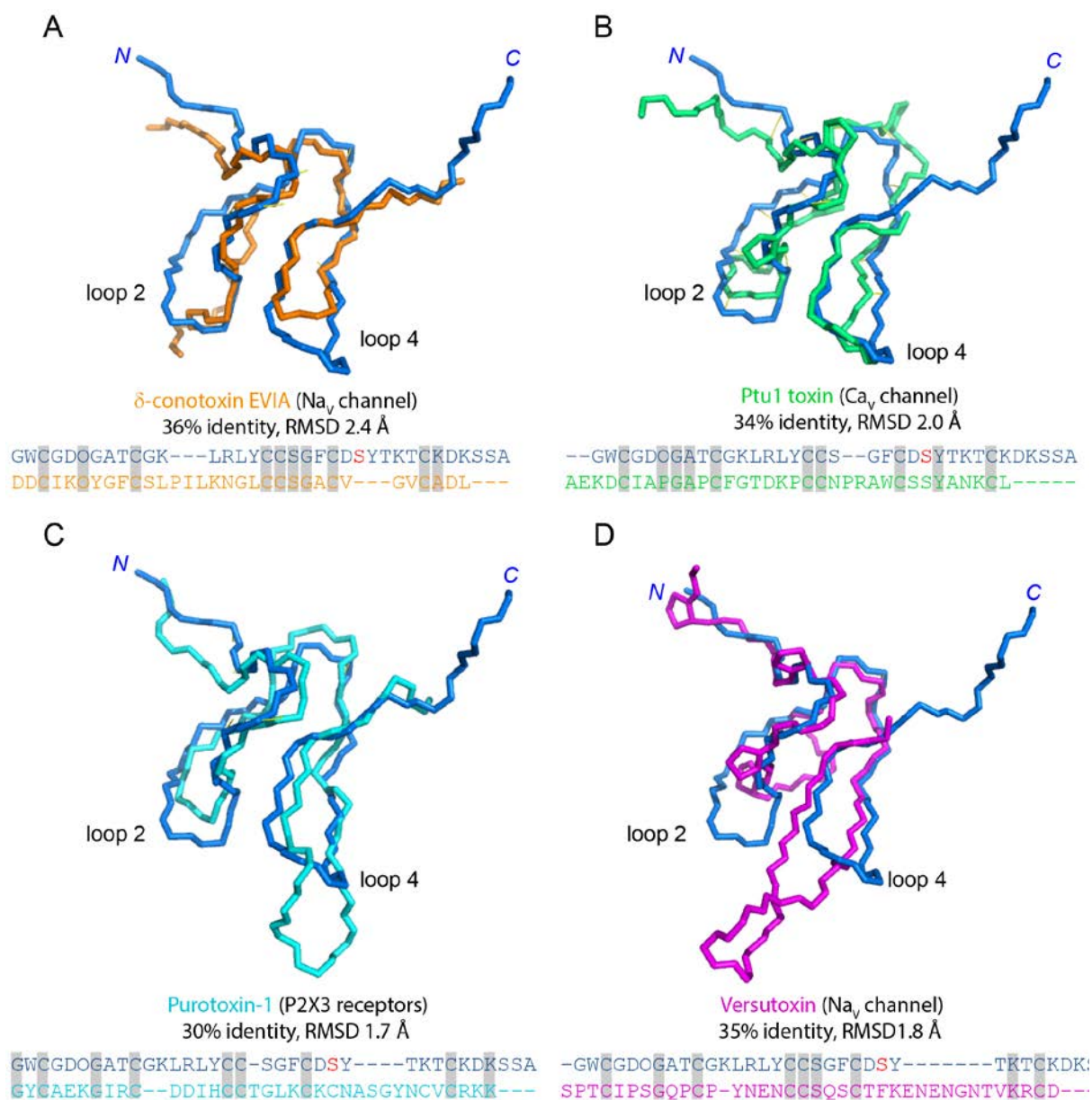


Figure 6.9. Structural comparison of the GVIIJ[C24S] backbone with those of other ICK motif-containing peptides. The backbone of the closest-to-average structure of GVIIJ[C24S] (blue) was aligned with the backbones of (A) δ -conotoxin EVIA from *Conus ermenius* (PDB ID code 1G1P), (B) Ptu1 toxin from the assassin beetle (PDB ID code 1I26), (C) purotoxin-1 from the burrowing wolf spider (PDB ID code 2KGU) and (D) vesutoxin from the Australian Blue Mountain funnel web spider (PDB ID code 1AHX). Structural alignments were made using DaliLite version 3 (147). The ion channel modulating toxins shown in this figure were selected based on the following criteria: sequence homology $\geq 30\%$, similar size (30-36 amino acid residues) and a Z-score ≥ 2.0 .

SAR studies focused initially on mutations of residues in loop 4 (Asp-23 – Thr-28) in the vicinity of Cys-24. Alignment of this loop with the free cysteine-containing loops of $\text{Nav}\beta 2$ (Phe-23 – Thr-28) or $\beta 4$ (Phe-55 – Gly-60) revealed modest levels of sequence homology (Fig. 6.6C) (148,149). This is of interest in light of previous work which showed that co-expression of $\text{Nav}1$ -subtypes with

Nav β 2 or β 4 inhibited the ability of μ O δ -GVIIJ analogues to block (93), suggesting that μ O δ -GVIIJ and the β -subunits may interact at the same site on the ectodomain of the α -subunit. Numerous residues in this region of the peptide had significant effects on the ability of the analogue to fold into a major product, implying that interactions among residues within the β -turn of this loop (Asp-23 – Thr-26) were important for stabilization of the peptide, even though they had much less bearing on the peptide's functional activity. Thus, little difference was observed between K_d values of loop 4 mutants and that of GVIIJ_{SSEA} (Table 6.3).

Our SAR results nonetheless identified a number of functionally important residues in GVIIJ_{SSEA}, most of which are located in the structurally less well-defined loop 2 (Gly-11 – Tyr-16). The [K12D], [R14D] and [Y16A] analogues in this loop exhibited on-rate constants that were significantly lower than that of the unmodified peptide, giving rise to higher K_d values. There is a dearth of medium- and long-range NOEs in this region, and the ϕ - and ψ - angular order parameters for residues in this region fall below 0.8 (Fig. 6.5). This loop may adopt a more rigid structure upon interaction with the channel, but further studies will be required to confirm this.

As described in the Introduction, the lack of overlap of sites 1 and 8 was observed initially with μ -KIIIA[K7A] and rNav1.2 (93). We had shown previously that μ -KIIIA and its analogues block rNav1.2 and compete for, and can even co-occupy, site 1 with the guanidinium alkaloids TTX, STX and STX congeners (63,135,136). In the present experiments, we employed μ -PIIIA[R14Q] and rNav1.4. The site 1 blocker μ -PIIIA[R14Q] was first characterized by French's laboratory (137) who performed single-channel measurements in planar lipid bilayers to show that this peptide, like μ -GIIIA[R13Q], blocked rNav1.4 with a significant residual current, but unlike μ -GIIIA[R13Q], which has ~100-fold lower affinity than its parent μ -GIIIA (150), μ -PIIIA[R14Q]'s affinity was only ~10-fold lower than its wild-type counterpart (Arg-13 of μ -GIIIA and Arg-14 of μ -PIIIA are homologous residues). Thus, we chose to use μ -PIIIA[R14Q] for our studies here to further explore the distinction between site 1 and site 8. In oocytes expressing rNav1.4, μ -PIIIA[R14Q] blocked with an IC_{50} only seven-fold higher than that of native μ -PIIIA (0.25 *versus* 0.036 μ M, Fig. 6.8A and ref. (107), respectively). At saturating concentrations, μ -PIIIA[R14Q] blocked with an rI_{Na} of 27% (Fig. 6.8A) whereas the native peptide, μ -PIIIA, blocked with essentially no rI_{Na} (107). μ -GIIIA blocked μ -PIIIA[R14Q]'s rI_{Na} with a k_{obs} much smaller than that of control I_{Na} (Fig. 6.8B, Table 6.4), consistent with the two peptides competing for the same site (site 1) on the channel. In contrast, the k_{obs} of the block by μ O δ -GVIIJ_{SSG} was not affected by the presence of μ -PIIIA[R14Q] (Fig. 6.8C, Table 6.4), indicating that μ -PIIIA[R14Q] did not interfere with the block by μ O δ -GVIIJ_{SSG} and therefore that sites 1 and 8 are distinct. These results are consistent with those of

earlier competition experiments performed with μ -KIIIA[K7A] and rNav1.2 (93). Finally, the k_{obs} of the dimer of μ O \S -GVIIJ_{SSG} was slightly, but significantly, decreased by the presence of μ -PIIIA[R14Q] (Fig. 6.8D, Table 6.4), suggesting that sites 1 and 8 are close to each other.

Previously we tested seven μ O \S -GVIIJ_{SSR} derivatives (where SR was a different R-group disulfide bonded to Cys-24, including Cys-24 of another μ O \S -GVIIJ monomer to form the (μ O \S -GVIIJ)₂ dimer). They all blocked rNav1.2 with the same k_{off} and mNav1.6 with a k_{off} 17-fold larger than for rNav1.2 (5). These results led us to propose that for all seven peptides, the same peptide-channel complex was formed (5). We report here that (μ O \S -GVIIJ)₂ blocked rNav1.4 with a k_{off} of $0.0025 \pm 0.0009 \text{ min}^{-1}$, a value essentially the same as that of GVIIJ_{SSG}, which was $0.0016 \pm 0.0008 \text{ min}^{-1}$ (4) ($p = 0.25$). Thus, we expand to rNav1.4 our proposal that monomeric and dimeric GVIIJ (μ O \S -GVIIJ_{SSR} and (μ O \S -GVIIJ)₂, respectively) block by forming the same peptide-channel complex.

Table 6.4. Values of k_{obs} for the block by μ -GIIIA, μ O \S -GVIIJ or (μ O \S -GVIIJ)₂ of control I_{Na} and of rI_{Na} in presence of 33 μ M μ -PIIIA[R14Q]^a

Peptide	[Peptide] (μ M)	k_{obs} (min^{-1})	
		Control I_{Na} ^b	Residual I_{Na} ^c
μ -GIIIA	10	110.14 ± 8.7^d	0.81 ± 0.1 ($p < 0.001^e$)
μ O \S -GVIIJ _{SSG}	3.3	1.5 ± 0.1	1.12 ± 0.33 ($p = 0.18^e$)
(μ O \S -GVIIJ) ₂	33	1.367 ± 0.21	0.743 ± 0.05 ($p = 0.029^e$)

^aAverage \pm SD ($n \geq 3$ oocytes). ^bBlock by indicated peptide alone (see examples in insets of Figs. 6.8B-D). ^cBlock of rI_{Na} of oocytes pre-exposed to 33 μ M μ -PIIIA[R14Q] (see examples in Figs. 6.8B-D). ^d k_{obs} was too large to measure directly, so value shown was obtained using $k_{obs} = k_{on} + k_{off}$ with previously published k_{on} and k_{off} values of μ -GIIIA (107). ^eSignificance of the difference in k_{obs} for the block of control I_{Na} versus that of residual I_{Na} .

Combining our structural and functional results, it appears that μ O \S -GVIIJ may interact with two distinct sub-sites on the channel. Substitution of specific residues, predominantly located in a less well-defined region of the peptide (loop 2), had the greatest effects on k_{on} (Fig. 6.10A). Analogues containing substitutions of important residues in this loop were still very slowly reversible, but exhibited much slower on-rates and subsequently lower potency compared to GVIIJ_{SSEA}. Comparison of the activity of GVIIJ[C24S] with analogues containing a cysteine at position 24 showed that the identity of the residue at this position was important for k_{off} (Fig. 6.10B). The C24S replacement led to rapid reversibility of the peptide, but did not prevent VGSC inhibition. Presumably, this was because the peptide was no longer capable of undergoing covalent attachment to the channel, but, by retaining key residues, the analogues were still able to elicit VGSC

inhibition. Previous studies with the free-thiol form of $\mu\text{O}\xi\text{-GVIII}$ (GVIII_{SH}) showed similar results (93,132). The absence of a leaving group attached to Cys-24 prevented efficient disulfide bond formation between the channel and the peptide, which led to rapid reversibility of GVIII_{SH} upon washout. Likewise, the important residues in loop 2 (i.e. Lys-12, Arg-14 and Tyr-16) were retained in GVIII_{SH} , and therefore the peptide was still capable of block. Thus, our data suggest a ‘functionally bipartite’ mechanism of action where disulfide bond formation through Cys-24 and interactions between Lys-12, Arg-14 and Tyr-16 and the channel both contribute to VGSC blockade (Fig. 6.10).

$\mu\text{O}\xi\text{-GVIII}$ and its analogues present a unique opportunity to probe the structure and function of the newly-described site 8 on the sodium channel. In addition to the identification of residues that are important for VGSC blockade, SAR studies also identified potential sites for modification (i.e. residues that are noncritical for inhibition), such as residues near the C-terminus (e.g. Lys-30 and Asp-31) which could be replaced by residues with reporter groups (e.g., fluorescently-labeled amino acids) for the development of peptidic probes to identify the presence or absence of specific VGSC subtypes in different tissue preparations.

Given that $\mu\text{O}\xi\text{-GVIII}$ is the first conotoxin found to bind by the described ‘tethering’ mechanism, an untapped and significant opportunity now exists to identify additional ligands for site 8. Efforts are ongoing to improve the VGSC selectivity profile of $\mu\text{O}\xi\text{-GVIII}$. In addition, mining of venoms of closely-related *Conus* species is also underway to identify other members of this peptide family with improved selectivity

for pain-relevant VGSC subtypes (e.g. Nav1.3 and 1.7). From a therapeutic perspective, such efforts might prove useful in the identification and development of peptidic drug leads to combat disease states stemming from VGSC dysfunction, such as neuropathic pain, epilepsy, and multiple sclerosis (151,152).

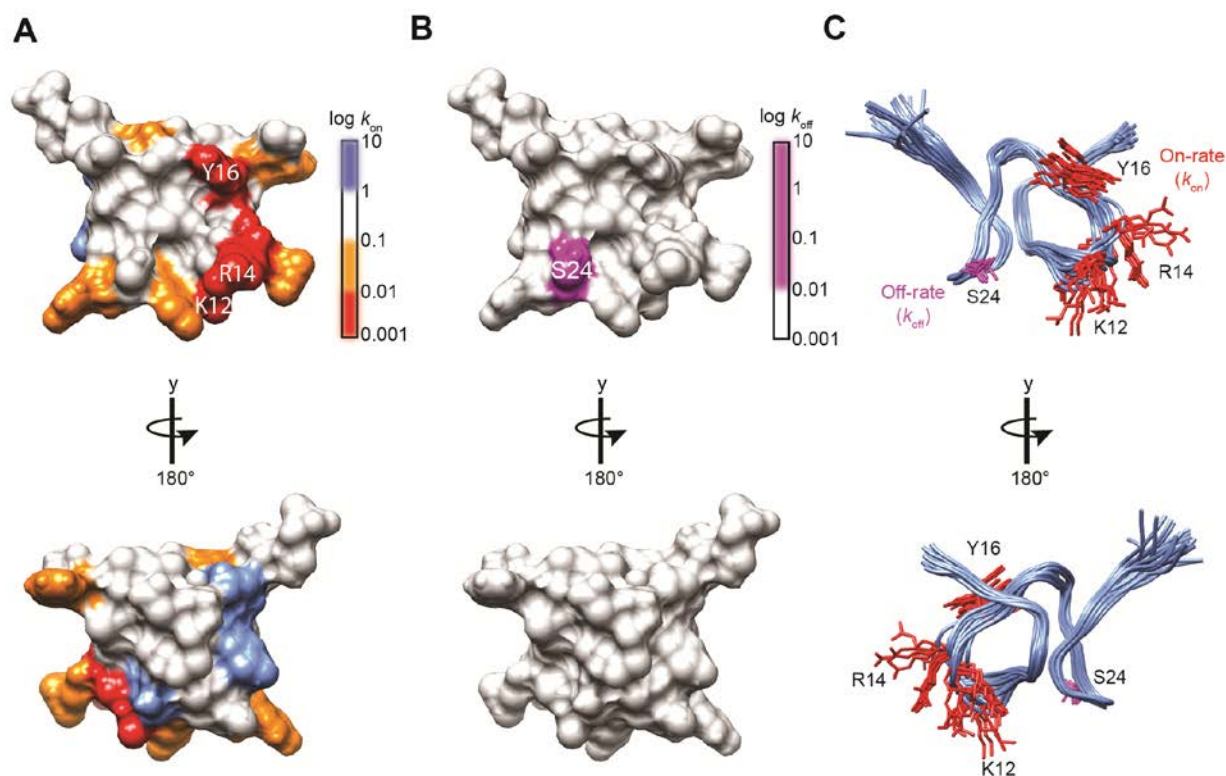


Figure 6.10. ‘Functionally bipartite’ mechanism of action for $\mu\text{O}\xi\text{-GVIIJ}$. (A) Locations of amino acid residues important for on-rates (k_{on}) of $\mu\text{O}\xi\text{-GVIIJ}$ against Nav1.2. Residues with the slowest k_{on} values are colored red. (B) Location of residue 24 (magenta) which is responsible for the covalent interactions with a free cysteine on the channel (Cys-910). Replacement of Cys-24 with serine prevented disulfide bridge formation between the peptide and the channel and led to rapid reversibility upon washout indicating that the identity of the residue in position 24 is critical for k_{off} . (C) Backbone representation of GVIIJ[C24S] which shows the locations of residues deemed particularly important for the activity of $\mu\text{O}\xi\text{-GVIIJ}$. Residues important for the on-rate (Lys-12, Arg-14 and Tyr-16) of the peptide are located in loop 2 (red), whereas that affecting the off-rate is located within the β -turn of loop 4 (magenta).

6.7 Acknowledgements

The authors thank Sam Robinson for review of the manuscript and for numerous helpful discussions related to this work. We also thank William Low for MS analysis of synthetic analogues, Alan Goldin for the Nav1.2 and Nav1.4 clones, and Layla Azam for preparation of rNav1.2 and rNav1.4 cRNA. This work was supported by National Institutes of Health Grants GM

048677, GM 099939, and GM 103362. R.S.N. acknowledges fellowship support from the Australian National Health and Medical Research Council.

6.8 Conflict of interest

The authors declare no conflicts of interest related to this work.

6.9 Author contribution

BRG designed, performed and analyzed experiments and drafted the paper. JG assisted with the synthesis, purification and oxidative folding of selected $\mu\text{O}\delta\text{-GVIII}$ analogues. SC and JS assisted with the collection and analysis of NMR spectra. MZ conducted electrophysiology experiments of selected $\mu\text{O}\delta\text{-GVIII}$ analogues and all experiments involving rNav1.4. JER synthesized $\mu\text{-GIIIA}$ and $\mu\text{-PIIIA[R14Q]}$. BRG, JG, GB, BMO, DY and RSN initiated the project and helped design experiments. All authors reviewed the results and assisted in preparing the manuscript.

Chapter 7

Conclusions and Future Directions

Over 50 million years of Cone snail evolution has resulted in the development of complex venom mixtures capable of paralysis and even death. However, it is the individual components of these deadly cocktails that when isolated, purified and characterised may lead to some of the most useful pharmacological tools to study and perhaps treat neuropathic pain. Peptides, such as conotoxins provide benefits of target specificity combined with high potency which is often lacking in small molecule drugs. Ongoing efforts to identify potent and selective analgesics have led to mining venoms of predatory organisms to discover potential drug leads. With over 500 species (Figure 7.1), each possessing a unique venom repertoire of 100 – 200 neuroactive peptides, the venoms of *Conus* remain largely unexplored (less than 0.1% of the *Conus* proteome has been studied to date).

In the experimental chapters of this thesis (Chapters 4 – 6), I focus on peptides isolated from the venoms of the fish-hunting snails *Conus bullatus* (the ‘bubble’ cone) and *Conus geographus* (the ‘geography’ cone), with an emphasis on identification of the structural features of these peptides that contribute to VGSC blockade. SAR studies of two distinct peptide classes of VGSC inhibiting peptides (μ - and $\mu\text{O}\delta$ -conotoxins) have demonstrated the importance of cysteine and non-cysteine amino acid residues for interactions with pain relevant VGSC subtypes. In the first part of this thesis (Chapters 3 – 4), SAR studies of μ -conotoxin BuIIIb were performed. Several VGSC subtypes play an important role in the transmission of pain signals. SAR studies in this thesis were conducted with the aim of improving the potency and/or subtype specificity of μ -BuIIIb against Nav1.3, which has been implicated in pain signal transmission following spinal cord injury. The role of Nav1.3 in neuropathic pain has been disputed thus potent and selective inhibitors of this subtype could be useful as pharmacological tools to determine if this subtype is relevant to the transmission of neuropathic pain signals.

To this end, I examined the roles of disulfide bridges and disulfide connectivity for Nav1.3 inhibition by μ -BuIIIb. The free-acid form of μ -BuIIIb for these studies was expressed in *E. coli* and no statistical significance was observed between the potency of the recombinant, carboxylated and synthetic, amidated forms of the peptide. It was shown that one isoform within the complex folding mixture (rBuIIIb^ Isoform 1) was more potent than the other major isoforms. Based on its activity and chromatographic mobility, it was hypothesised rBuIIIb^ Isoform 1 would possess the ‘canonical’ μ -conotoxin disulfide connectivity of [CysI-CysIV; CysII-CysV; CysIII-CysVI], though this has yet to be substantiated. Experiments are currently underway to unambiguously determine the disulfide connectivity of Isoform 1 to test this hypothesis. Perhaps less anticipated was that the remaining isoforms were also active, though to a lesser extent compared to Isoform 1. The disulfide connectivities for two of the less active isoforms (Isoforms 4 and 5) were established by CID-

MS/MS and, to the best of our knowledge, this was the first experimental evidence of the [CysI-CysV; CysII-CysIV; CysIII-CysV] and [CysI-CysII; CysIII-CysVI; CysIV-CysV] connectivities in oxidised peptides. Together these results point to a single disulfide connectivity being responsible for the potent block of Nav1.3 by μ -BuIII B. However, it also suggests some degree of flexibility in the disulfide framework for inhibition of the channel. Once the identities of all major isoforms are determined these peptides could be re-synthesised, either recombinantly as isotopically-labelled peptides, or synthetically to facilitate structural comparisons between active and less-active isoforms.

The studies described in Chapter 3 took a more holistic view of the roles of disulfide bridges for VGSC blockade. The importance of individual disulfide bridges was examined in Chapter 4. It was concluded that the disulfide bridge between Cys5 and Cys17 in μ -BuIII B was critical for activity of the peptide against Nav1.3. In contrast, the two remaining disulfide bridges (Cys6-Cys17 or Cys13-Cys24) could be removed without loss of activity. In light of the previous studies this is important because neither rBuIII B[^] Isoform 4 nor Isoform 5 retained this disulfide pairing. Loss of the Cys5-Cys17 bridge may help to explain the diminished activity of these isoforms against Nav1.3. These results suggested that, in addition to the contributions of individual amino acids, disulfide connectivity is also important for SAR studies to understand the functionality of μ -BuIII B.

SAR studies most often look at the effects of individual amino acid replacements on the biological activity of a peptide. Given that μ -BuIII B folds inefficiently, a strategy was implemented to simplify the oxidation pathway to reduce the possible number of folding isoforms. The ddSecBuIII B strategy was employed to carry out rapid SAR of all non-cysteine amino acid residues within the primary sequence. These results showed an accumulation of residues near the C-terminus that were important for activity which was largely consistent with studies of other three disulfide bridge containing μ -conotoxins. It was also demonstrated that amino acid substitutions made to the N-terminus of the peptide could improve the potency, but not the selectivity, of ddSecBuIII B. The exquisite selectivity of μ -conotoxins for VGSCs makes them ideal tools to study the structure and function of sodium channels generally. However, the difficulty in obtaining selectivity, due to similarities amongst VGSC subtypes at the TTX-binding site (Site 1) has limited their potential as viable drug leads. As such, interest has gravitated towards peptides that block through interactions at toxin binding sites distinct from Site 1.

SAR studies were performed on the recently discovered μ O ξ -GVIII which was found to be unique in that it tethers to the channel via disulfide bridge through an 'extra' cysteine residue at position 24 (Chapter 6). Pharmacological assessment of an analogue of μ O ξ -GVIII in which Cys24 was

replaced with serine (GVIIJ[C24S]) showed potent, but rapidly reversible block of the channel upon washout. NMR studies identified the location of Cys24 in a well-defined loop whereas those residues deemed important for biological activity were located on a separate and poorly defined loop. $\mu\text{O}\S$ -GVIIJ is the first member of a newly described family of conotoxins that tether to the sodium channel. There is a high probability, given the vast nature of the *Conus* pharmacopeia, several other members of this family could be isolated from the venoms of fish-hunting cone snails. Our unpublished data has identified numerous peptides with odd-numbered cysteine frameworks. Traditionally, these peptides were dismissed as read errors in the sequencing experiments. However, it remains to be seen if these peptides might actually present a unique opportunity to identify additional members of the $\mu\text{O}\S$ -conotoxin family, or perhaps new and novel peptide families that elicit their behaviors through a similar tethering event. SAR studies of VGSC modulating peptides will become increasingly important as additional members of the μ -, μO - or $\mu\text{O}\S$ -conotoxin families are discovered. These studies will function to identify important features of these peptides for interactions with the channel to better understand the structure and function of VGSCs in the absence of an accurate model of the mammalian sodium channel. Finally, studies such as those described in this thesis can help to identify areas within the peptide that could be modified for enhanced pharmacological properties for peptide drug development.



Figure 7.1 Diversity among *Conus* species. Photo illustrates some of the over 500 species of cone snails described to date. *Conus* venoms provide a rich resource for the discovery and development of potentially useful neuroactive peptides. SAR studies detailed in this thesis will serve as a starting point from which the intrinsic properties of VGSC inhibiting peptides can be improved upon.

Chapter 8

References

1. Goldberg, D. S., and McGee, S. J. (2011) Pain as a global public health priority. *BMC Public Health* **11**, 770-775
2. Bhattacharya, A., Wickenden, A. D., and Chaplan, S. R. (2009) Sodium channel blockers for the treatment of neuropathic pain. *Neurotherapeutics* **6**, 663-678
3. Kao, C. Y. (1966) Tetrodotoxin, saxitoxin and their significance in the study of excitation phenomena. *Pharmacol. Rev.* **18**, 997-1049
4. Dray, A. (2003) Novel molecular targets in pain control. *Curr. Opin. Anaesthesiol.* **16**, 521-525
5. Woolf, C. J. (2010) What is this thing called pain? *J. Clin. Invest.* **120**, 3742-3744
6. Campbell, J. N., and Meyer, R. A. (2006) Mechanisms of neuropathic pain. *Neuron.* **52**, 77-92
7. Woolf, C. J., and Mannion, R. J. (1999) Neuropathic pain: aetiology, symptoms, mechanisms, and management. *The Lancet* **353**, 1959-1964
8. Devor, M. (2013) *Wall and MelZack's Textbook of Pain: Sixth Edition*, Elsevier Saunders, Philadelphia, PA
9. Catterall, W. A. (2012) Voltage-gated sodium channels at 60: structure, function and pathophysiology. *J. Physiol.* **590**, 2577-2589
10. Catterall, W. A., Goldin, A. L., and Waxman, S. G. (2005) International Union of Pharmacology. XLVII. Nomenclature and structure-function relationships of voltage-gated sodium channels. *Pharmacol. Rev.* **57**, 397-409
11. Stevens, M., Peigneur, S., and Tytgat, J. (2011) Neurotoxins and their binding areas on voltage-gated sodium channels. *Front. Pharmacol.* **2**, 1-13
12. O'Malley, H. A., and Isom, L. L. (2015) Sodium channel β subunits: emerging targets in channelopathies. *Annu. Rev. Physiol.* **77**, 481-504
13. England, S., and de Groot, M. J. (2009) Subtype-selective targeting of voltage-gated sodium channels. *Br. J. Pharmacol.* **158**, 1413-1425
14. Catterall, W. A. (2001) Physiology. A one-domain voltage-gated sodium channel in bacteria. *Science* **294**, 2306-2308
15. Payandeh, J., Scheuer, T., Zheng, N., and Catterall, W. A. (2011) The crystal structure of a voltage-gated sodium channel. *Nature* **475**, 353-358
16. Korkosh, V. S., Zhorov, B. S., and Tikhonov, D. B. (2014) Folding similarity of the outer pore region in prokaryotic and eukaryotic sodium channels revealed by docking for conotoxins GIIIA, PIIIA and KIIIA in a NavAb-based model of Nav1.4. *J. Gen. Physiol.* **144**, 231-244
17. Ragsdale, D. S., McPhee, J. C., Scheuer, T., and Catterall, W. A. (1996) Common molecular determinants of local anesthetic, antiarrhythmic, and anticonvulsant block of voltage-gated Na⁺ channels. *Proc. Natl. Acad. Sci. USA* **93**, 9270-9275
18. Reusch, Y. A., Böni, T., and Borgeat, A. (2001) From cocaine to ropivacaine: The history of local anesthetic drugs. *Curr. Top. Med. Chem.* **1**, 175-182
19. Covino, B. G., and Giddon, D. B. (1981) Pharmacology of local anesthetic agents. *J. Dent. Res.* **60**, 1454-1459
20. Tremont-Lukats, I. W., Megeff, C., and Backonja, M. M. (2000) Anticonvulsants for neuropathic pain syndromes: mechanisms of action and place in therapy. *Drugs* **60**, 1029-1052
21. Vlieghe, P., Lisowski, V., Martinez, J., and Khrestchatisky, M. (2009) Synthetic therapeutic peptides: science and market. *Drug Discov. Today* **15**, 40-56
22. Wiese, M., D'Agostino, P. M., Mihali, T. K., Moffitt, M. C., and Neilan, B. A. (2010) Neurotoxic Alkaloids: saxitoxin and its analogs. *Mar. Drugs* **8**, 2185-2211
23. Narahashi, T., Moore, J. W., and Scott, W. R. (1964) Tetrodotoxin blockage of sodium conductance increase in lobster giant axons. *J. Gen. Physiol.* **47**, 965-974

24. Yotsu-Yamashita, M., Kim, Y. H., Samuel C. Dudley, J., Choudhary, G., Pfahnl, A., Oshima, Y., and Daly, J. W. (2004) The structure of zetekitoxin AB, a saxitoxin analog from the Panamanian golden frog *Atelopus zeteki*: A potent sodium-channel blocker. *Proc. Natl. Acad. Sci. USA* **101**, 4346-4351
25. (2008) *Modern Alkaloids: Structure, Isolation, Synthesis, and Biology*, Wiley-VCH Verlag GmbH & Co., Weinheim
26. Backx, P. H., Yue, D. T., Lawrence, J. H., Marban, E., and Tomaselli, G. F. (1992) Molecular localization of an ion-binding site within the pore of mammalian sodium channels. *Science* **257**, 248-251
27. Heinemann, S. H., Terlau, H., and Imoto, K. (1992) Molecular basis for pharmacological differences between brain and cardiac sodium channels. *Pflugers Arch.* **422**, 90-92
28. Satake, Y., Adachi, M., Tokoro, S., Yotsu-Yamashita, M., Isobe, M., and Nishikawa, T. (2014) Synthesis of 5- and 8-deoxytetrodotoxin. *Chem. Asian J.* **9**, 1922-1932
29. Fozzard, H. A., and Lipkind, G. M. (2010) The tetrodotoxin binding site is within the outer vestibule of the sodium channel. *Mar. Drugs* **8**, 219-234
30. Ménez, A. (2002) *Perspectives in Molecular Toxinology*, John Wiley & Sons, Ltd., West Sussex, England
31. Escoubas, P., Palma, M. F., and Nakajima, T. (1995) A microinjection technique using *Drosophila melanogaster* for bioassay-guided isolation of neurotoxins in arthropod venoms. *Toxicon* **33**, 1549-1555
32. Heghinian, M. D., Mejia, M., Adams, D. J., Godenschwege, T. A., and Marí, F. (2015) Inhibition of cholinergic pathways in *Drosophila melanogaster* by α -conotoxins. *FASEB J.* **29**, 1011-1018
33. Buczek, O., Bulaj, G., and Olivera, B. M. (2005) Conotoxins and the posttranslational modification of secreted gene products. *Cell Mol. Life Sci.* **62**, 3067-3079
34. Robinson, A. J., Safavi-Hemami, H., Raghuraman, S., Imperial, J. S., Papenfuss, A. T., Teichert, R. W., Purcell, A. W., Olivera, B. M., and Norton, R. S. (2015) Discovery by proteogenomics and characterization of an RF-amide neuropeptide from cone snail venom. *J. Proteomics* **114**, 38-47
35. Merrifield, R. B. (1963) Solid phase peptide synthesis. I. The synthesis of a tetrapeptide. *J. Am. Chem. Soc.* **85**, 2149-2154
36. Meienhofer, J. (1973) *Hormonal Proteins and Peptides*, Academic Press, New York
37. Atherton, E., and Sheppard, R. C. (1989) *Solid phase peptide synthesis. A practical approach*, IRL Press, Oxford
38. Wade, J. D. (2000) *Alpha amino protecting groups*, Marcel Dekker, Inc., New York, NY
39. Carpino, L. A., and Han, G. Y. (1972) 9-Fluorenylmethoxycarbonyl amino-protecting group. *J. Org. Chem.* **37**, 3404-3409
40. Quibell, M., Packman, L. C., and Johnson, T. (1995) Synthesis of the 3-repeat region of human Tau-2 by the solid phase assembly of backbone amide-protected segments. *J. Am. Chem. Soc.* **117**, 11656-11668
41. Klint, J. K., Senff, S., Saez, N. J., Seshadri, R., Lau, H. Y., Bende, N. S., Undheim, E. A. B., Rash, L. D., Mobli, M., and King, G. F. (2013) Production of recombinant disulfide-rich venom peptides for structural and functional analysis via expression in the periplasm of *E. coli*. *PLOS One* **8**, 1-12
42. Anangi, R., Koshy, S., Huq, R., Beeton, C., Chuang, W. J., and King, G. F. (2012) Recombinant expression of margatoxin and agitoxin-2 in *Pichia pastoris*: An efficient method for production of Kv1.3 channel blockers. *PLOS One* **7**, 1-9
43. Ul-Hasan, S., Burgess, D. M., Gajewiak, J., Li, Q., Hu, H., Yandell, M., Olivera, B. M., and Bandyopadhyay, P. K. (2013) Characterization of the peptidylglycine α -amidating

- monooxygenase (PAM) from the venom ducts of neogastropods, *Conus bullatus* and *Conus geographus*. *Toxicon* **74**, 215-224
44. Bandyopadhyay, P. K., Garret, R. P., Shetty, T., Keate, T., Walker, C. S., and Olivera, B. M. (2002) gamma-Glutamyl carboxylation: an extracellular posttranslational modification that antedates the divergence of molluscs, arthropods and chordates. *Proc. Natl. Acad. Sci. USA* **99**, 1264-1269
 45. (1996) *Natural Toxins 2: Structure, Mechanism of Action, and Detection*, Plenum Press, New York
 46. Woodward, S. R., Cruz, L. J., Olivera, B. M., and Hillyard, D. R. (1990) Constant and hypervariable regions in conotoxin propeptides. *EMBO J.* **1**, 1015-1020
 47. Bulaj, G., and Olivera, B. M. (2008) Folding of conotoxins: formation of the native disulfide bridges during chemical synthesis and biosynthesis of *Conus* peptides. *Antioxid. Redox. Signal.* **10**, 141-155
 48. Buczek, O., Olivera, B. M., and Bulaj, G. (2004) Propeptide does not act as an intramolecular chaperone but facilitates protein disulfide isomerase-assisted folding of a conotoxin precursor. *Biochemistry* **43**, 1093-1101
 49. Safavi-Hemami, H., Gorasia, D. G., Steiner, A. M., Williamson, N. A., Karas, J. A., Gajewiak, J., Olivera, B. M., Bulaj, G., and Purcell, A. W. (2012) Modulation of conotoxin structure and function is achieved through a multienzyme complex in the venom glands of cone snails. *J. Biol. Chem.* **287**, 34288-34303
 50. Hargittai, B., and Barany, G. (1999) Controlled syntheses of natural and disulfide-mispaired regioisomers of alpha-conotoxin SI. *J. Pept. Res.* **54**, 468-479
 51. Wingfield, P. T. (2001) Use of Protein Folding Reagents. in *Current Protocols in Protein Science*, John Wiley & Sons, Inc. pp
 52. Darlak, K., Wiegandt Long, D., Czerwinski, A., Darlak, M., Valenzuela, F., Spatola, A. F., and Barany, G. (2004) Facile preparation of disulfide-bridged peptides using the polymer-supported oxidant CLEAR-OX. *J. Pept. Res.* **63**, 303-312
 53. Besse, D., and Moroder, L. (1997) Synthesis of selenocysteine peptides and their oxidation to diselenide-bridged compounds. *J. Pept. Sci.* **3**, 442-453
 54. van Leirop, B. J., Robinson, S. D., Kompella, S. N., Belgi, A., McArthur, J. R., Hung, A., MacRaid, C. A., Adams, D. J., Norton, R. S., and Robinson, A. J. (2013) Dicarba α -conotoxin Vc1.1 analogues with differential selectivity for nicotinic acetylcholine and GABAB receptors. *ACS Chem. Biol.* **8**, 1815-1821
 55. Dekan, Z., Vetter, I., Daly, N. L., Craik, D. L., Lewis, R. J., and Alewood, P. F. (2011) α -Conotoxin ImI incorporating stable cystathionine bridges maintains full potency and identical three-dimensional structure. *J. Am. Chem. Soc.* **133**, 15866-15869
 56. Williamson, M. P. (1993) *Spectroscopic Methods and Analyses*, Humana Press
 57. Grant, M. A., Morelli, X. J., and Rigby, A. C. (2004) Conotoxins and structural biology: A prospective paradigm for drug discovery. *Curr. Protein Pept. Sci.* **5**, 235-248
 58. Stevens, M., Peigneur, S., Dyubankova, N., Lescrinier, E., Herdewijn, P., and Tytgat, J. (2012) Design of bioactive peptides from naturally occurring μ -conotoxin structures. *J. Biol. Chem.* **287**, 31382-31392
 59. Yao, S., Zhang, M. M., Yoshikami, D., Azam, L., Olivera, B. M., Bulaj, G., and Norton, R. S. (2008) Structure, dynamics, and selectivity of the sodium channel blocker μ -conotoxin SIIIA. *Biochemistry* **47**, 10940-10949
 60. Schroeder, C. I., Ekberg, J., Nielsen, K. J., Adams, D., Loughnan, M. L., Thomas, L., Adams, D. J., Alewood, P. F., and Lewis, R. J. (2008) Neuronally selective μ -conotoxins from *Conus striatus* utilize an α -helical motif to target mammalian sodium channels. *J. Biol. Chem.* **283**, 21621-21628

61. Sato, K., Ishida, Y., Wakamatsu, K., Kato, R., Honda, H., Ohizumi, Y., Nakamura, H., Ohya, M., Lancelin, J. M., Kohda, D., and Inagaki, F. (1991) Active site of μ -conotoxin GIIIA, a peptide blocker of muscle sodium channels. *J. Biol. Chem.* **266**, 16989-16991
62. Zhang, M. M., Green, B. R., Catlin, P., Fiedler, B., Azam, L., Chadwick, A., Terlau, H., McArthur, J. R., French, R. J., Guylas, J., Rivier, J. E., Smith, B. J., Norton, R. S., Olivera, B. M., Yoshikami, D., and Bulaj, G. (2007) Structure/function characterization of μ -conotoxin KIIIA, an analgesic, nearly irreversible blocker of mammalian neuronal sodium channels. *J. Biol. Chem.* **282**, 30699-30706
63. Zhang, M. M., Han, T. S., Olivera, B. M., Bulaj, G., and Yoshikami, D. (2010) μ -conotoxin KIIIA derivatives with divergent affinities versus efficacies in blocking voltage-gated sodium channels. *Biochemistry* **49**, 4804-4812
64. Khoo, K. K., Wilson, M. J., Smith, B. J., Zhang, M. M., Guylas, J., Yoshikami, D., Rivier, J. E., Bulaj, G., and Norton, R. S. (2011) Lactam-stabilized helical analogues of the analgesic μ -conotoxin KIIIA. *J. Med. Chem.* **54**, 7558-7566
65. Daly, N. L., Ekberg, J. A., Thomas, L., Adams, D. J., Lewis, R. J., and Craik, D. L. (2004) Structures of μ O-conotoxins from *Conus marmoreus*. Inhibitors of tetrodotoxin (TTX)-sensitive and TTX-resistant sodium channels in mammalian sensory neurons. *J. Biol. Chem.* **279**, 25774-25782
66. Norton, R. S., and Pallaghy, P. K. (1998) The cystine knot structure of ion channel toxins and related polypeptides. *Toxicon* **36**, 1573-1583
67. Guan, B., Chen, X., and Zhang, H. (2013) Two-electrode voltage clamp. *Methods Mol. Biol.* **998**, 79-89
68. Barnard, E. A., Miledi, R., and Sumikawa, K. (1982) Translation of exogenous messenger RNA coding for nicotinic acetylcholine receptors produces functional receptors in *Xenopus* oocytes. *Proc. R. Soc. Lond. B. Biol. Sci.* **215**, 241-246
69. Pi, C., Liu, J., Wang, L., Jiang, X., Liu, Y., Peng, C., Chen, S., and Xu, A. (2007) Soluble expression, purification and functional identification of a disulfide-rich conotoxin derived from *Conus litteratus*. *J. Biotechnol.* **128**, 184-193
70. Zhan, J., Chen, X., Wang, C., Qiu, J., Ma, F., Wang, F., and Zheng, S. (2003) A fusion protein of conotoxin MVIIA and thioredoxin expressed in *Escherichia coli* has significant analgesic activity. *Biophys. Res. Commun.* **311**, 495-500
71. Stewart, E. J., Aslund, F., and Beckwith, J. (1998) Disulfide bond formation in the *Escherichia coli* cytoplasm: an in vivo role reversal for the thioredoxins. *EMBO J.* **17**, 5543-5550
72. Done, J. N., Kennedy, G. J., and Knox, J. H. (1972) Revolution in liquid chromatography. *Nature* **237**, 77-81
73. Riley, C. M. (1996) *High Performance Liquid Chromatography: Fundamental principles and practise*, Blackie Academic and Professional, Glasgow
74. Pace, C. N., and Schmid, F. X. (1997) How to determine the molar absorption coefficient of a protein. in *Protein Structure: A Practical Approach* (Creighton, T. E. ed.), IRL Press, Oxford. pp 253
75. Bulaj, G., and Olivera, B. M. (2008) Folding of conotoxins: formation of the native disulfide bridges during chemical synthesis and biosynthesis of *Conus* peptides. *Antioxid. Redox Signal.* **10**, 141-155
76. Fuller, E., Green, B. R., Catlin, P., Buczek, O., Neilsen, J. S., Olivera, B. M., and Bulaj, G. (2005) Oxidative folding of conotoxins sharing an identical disulfide bridging framework. *FEBS J.* **272**, 1727-1738
77. Boisbouvier, J., Blackledge, M., Sollier, A., and Marion, D. (2000) Simultaneous determination of disulphide bridge topology and three-dimensional structure using

- ambiguous intersulphur distance restraints: possibilities and limitations. *J. Biomol. NMR* **16**, 197-208
78. Gray, W. R., Luque, F. A., Galyean, R., Atherton, E., Sheppard, R. C., Stone, B. L., Reyes, A., Alford, J., McIntosh, M., Olivera, B. M., and al, e. (1984) Conotoxin GI: disulfide bridges, synthesis, and preparation of iodinated derivatives. *Biochemistry* **23**, 2796-2802
 79. Gray, W. R. (1993) Disulfide structures of highly bridged peptides: a new strategy for analysis. *Protein Sci.* **2**, 1732-1748
 80. Khoo, K. K., Gupta, K., Green, B. R., Zhang, M. M., Watkins, M., Olivera, B. M., Balam, P., Yoshikami, D., Bulaj, G., and Norton, R. S. (2012) Distinct disulfide isomers of μ -conotoxins KIIIA and KIIIB block voltage-gated sodium channels. *Biochemistry* **51**, 9826-9835
 81. Bhattacharya, M., Gupta, K., Gowd, K. H., and Balam, P. (2013) Rapid mass spectrometric determination of disulfide connectivity in peptides and proteins. *Mol. Biosyst.* **9**, 1340-1350
 82. West, P. J., Bulaj, G., Garrett, J. E., Olivera, B. M., and Yoshikami, D. (2002) m-conotoxin SmIIIa, a potent inhibitor of tetrodotoxin-resistant sodium channels in amphibian sympathetic and sensory neurons. *Biochemistry* **41**, 15388-15393
 83. Wüthrich, K. (1986) *NMR of Proteins and Nucleic Acids*, John Wiley & Sons, Inc., New York
 84. Baxter, N. J., and Williamson, M. P. (1997) Temperature dependence of ¹H chemical shifts in proteins. *J. Biomol. NMR* **9**, 359-369
 85. Kuwajima, K., and Baldwin, R. L. (1983) Exchange behavior of the H-bonded amide protons in the 3 to 13 helix of ribonuclease S. *J. Mol. Biol.* **169**, 299-323
 86. Lala, A. K., Anteunis, M. J., and Lala, K. (1976) Conformational dependence on pH in tripeptides. *Biochim. Biophys. Acta.* **453**, 133-138
 87. Teng, Q. (2005) *Structural Biology: Practical NMR Applications*, Springer Science, New York
 88. Goddard, T. D., and Kneller, D. G. SPARKY 3. University of California, San Francisco
 89. Skinner, S. P., Goult, B. T., Fogh, R. H., Boucher, W., Stevens, T. J., Laue, E. D., and Vuister, G. W. (2015) Structure calculation, refinement and validation using CcpNmr Analysis. *Acta. Crystallogr. D. Biol. Crystallogr.* **71**, 154-161
 90. Wishart, D. S., Bigam, C. G., Holme, A., Hodges, R. S., and Sykes, B. D. (1995) ¹H, ¹³C and ¹⁵N random coil NMR chemical shifts of the common amino acids. I Investigations of the nearest-neighbor effects. *J. Biomol. NMR* **5**, 67-81
 91. Vuister, G. W., Tjandra, N., Shen, Y., Grishaev, A., and Grzesiek, S. (2011) *Measurement of Structural Restraints*, John Wiley & Sons, Ltd., Chichester, UK
 92. Shen, Y., and Bax, A. (2013) Protein backbone and sidechain torsion angles predicted from NMR chemical shifts using artificial neural networks. *J. Biomol. NMR* **56**, 227-241
 93. Gajewiak, J., Azam, L., Imperial, J., Walewska, A., Green, B. R., Bandyopadhyay, P. K., Raghuraman, S., Ueberheide, B., Bern, M., Zhou, H. M., Minassian, N. A., Hagan, R. A., Flinspach, M., Liu, Y., Bulaj, G., Wickenden, A. D., Olivera, B. M., Yoshikami, D., and Zhang, M. M. (2014) A disulfide tether stabilizes the block of sodium channels by the conotoxin μ O δ -GVIII. *Proc. Natl. Acad. Sci. U.S.A.* **111**, 2758-2763
 94. Güntert, P. (2004) Automated NMR structure calculation with CYANA. *Methods Mol. Biol.* **278**, 253-278
 95. Brünger, A. T., Adams, P. D., Clore, G. M., DeLano, W. L., Gros, P., Grosse-Kunstleve, R. W., Jiang, J. S., Kuszewski, J., Nilges, M., Pannu, N. S., Read, R. J., Rice, L. M., Simonson, T., and Warren, G. L. (1998) Crystallography & NMR system: a new software suite for macromolecular structure determination. *Acta. Crystallogr. D. Biol. Crystallogr.* **54**, 905-921

96. Laskowski, R. A., Rullmann, J. A., MacArthur, M. W., Kaptein, R., and Thornton, J. M. (1996) AQUA and PROCHECK-NMR: programs for checking the quality of protein structures solved by NMR. *J. Biomol. NMR* **8**, 477-486
97. Kabsch, W., and Sander, C. (1983) Dictionary of protein secondary structure: pattern recognition of hydrogen-bonded and geometrical features. *Biopolymers* **22**, 2577-2637
98. Hutchinson, E. G., and Thornton, J. M. (1996) PROMOTIF--a program to identify and analyze structural motifs in proteins. *Protein Sci.* **5**, 212-220
99. Wilmot, C. M., and Thornton, J. M. (1988) Analysis and prediction of the different types of β -turn in proteins. *J. Mol. Biol.* **203**, 221-232
100. Koradi, R., Billeter, M., and Wüthrich, K. (1996) MOLMOL: a program for display and analysis of macromolecular structures. *J. Mol. Graph.* **14**, 29-32
101. DeLano, W. L. The PyMOL Molecular Graphics System. 1.5.0.4 Ed., Schrödinger, LLC
102. Pettersen, E. F., Goddard, T. D., Huang, C. C., Couch, G. S., Greenblatt, D. M., Meng, E. C., and Ferrin, T. E. (2004) UCSF Chimera: a visualization system for exploratory research and analysis. *J. Comput. Chem.* **25**, 1605-1612
103. Holford, M., Zhang, M. M., Gowd, K. H., Azam, L., Green, B. R., Watkins, M., Ownby, J. P., Yoshikami, D., Bulaj, G., and Olivera, B. M. (2009) Pruning nature: biodiversity-derived discovery of novel sodium channel blocking conotoxins from *Conus bullatus*. *Toxicon* **53**, 90-98
104. Yanagawa, Y., Abe, T., and Satake, M. (1987) μ -Conotoxins share a common binding site with tetrodotoxin/saxitoxin on eel electroplax Na channels. *J. Neurosci.* **7**, 1498-1502
105. Kuang, Z., Zhang, M. M., Gupta, K., Gajewiak, J., Gulyas, J., Balaram, P., Rivier, J., Olivera, B. M., Yoshikami, D., Bulaj, G., and Norton, R. S. (2013) Mammalian neuronal sodium channel blocker μ -BuIIIIB has a structured N-terminus that influences potency. *ACS Chem. Biol.* **8**, 1344-1351
106. Green, B. R., Zhang, M. M., Chhabra, S., Robinson, S. D., Wilson, M. J., Redding, A., Olivera, B. M., Yoshikami, D., Bulaj, G., and Norton, R. S. (2014) Interactions of disulfide-deficient selenocysteine analogs of μ -conotoxin BuIIIIB with the α -subunit of the voltage-gated sodium channel subtype 1.3. *FEBS J.* **281**, 2885-2898
107. Wilson, M. J., Yoshikami, D., Azam, L., Gajewiak, J., Olivera, B. M., Bulaj, G., and Zhang, M. M. (2011) μ -Conotoxins that differentially block sodium channels Nav1.1 through 1.8 identify those responsible for action potentials in sciatic nerve. *Proc. Natl. Acad. Sci. U.S.A.* **108**, 10302-10307
108. Hains, B. C., Klein, J. P., Saab, C. Y., Craner, M. J., Black, J. A., and Waxman, S. G. (2003) Upregulation of sodium channel Nav1.3 and functional involvement in neuronal hyperexcitability associated with central neuropathic pain after spinal cord injury. *J. Neurosci.* **23**, 8881-8892
109. Samad, O. A., Tan, A. M., Cheng, X., Foster, E., Dib-Hajj, S. D., and Waxman, S. G. (2013) Virus-mediated shRNA knockdown of Na(v)1.3 in rat dorsal root ganglion attenuates nerve injury induced neuropathic pain. *Mol. Ther.* **21**, 49-56
110. Cummins, T. R., and Waxman, S. G. (1997) Downregulation of tetrodotoxin-resistant sodium currents and upregulation of a rapidly repriming tetrodotoxin-sensitive sodium current in small spinal sensory neurons after nerve injury. *J. Neurosci.* **17**, 3503-3514
111. Lindia, J. A., Köhler, M. G., Martin, W. J., and Abbadie, C. (2005) Relationship between sodium channel Nav1.3 expression and neuropathic pain behavior in rats. *Pain* **117**, 145-153
112. Nassar, M. A., Baker, M. D., Levato, A., Ingram, R., Mallucci, G., McMahan, S. B., and Wood, J. N. (2006) Nerve injury induces robust allodynia and ectopic discharges in Nav1.3 null mutant mice. *Mol. Pain* **2**, 33
113. Wakamatsu, K., Kohda, D., Hatanaka, H., Lancelin, J. M., Ishida, Y., Oya, M., Nakamura, H., Inagaki, F., and Sato, K. (1992) Structure-activity relationships of μ -conotoxin GIIIA:

- structure determination of active and inactive sodium channel blocker peptides by NMR and simulated annealing calculations. *Biochemistry* **31**, 12577-12584
114. Zhang, M. M., Green, B. R., Catlin, P., Fiedler, B., Azam, L., Chadwick, A., Terlau, H., McArthur, J. R., French, R. J., Guylas, J., Rivier, J., Smith, B. J., Norton, R. S., Olivera, B. M., and Yoshikami, D. (2007) Structure/function characterization of μ -conotoxin KIIIA, an analgesic nearly irreversible blocker of mammalian neuronal sodium channels. *J. Biol. Chem.* **282**, 30699-30706
 115. Lewis, R. J., Schroeder, C. I., Ekberg, J., Nielsen, K. J., Loughnan, M., Thomas, L., Adams, D. A., Drinkwater, R., Adams, D. J., and Alewood, P. F. (2007) Isolation and structure-activity of μ -conotoxin TIIIA, a potent inhibitor of tetrodotoxin-sensitive voltage-gated sodium channels. *Mol. Pharmacol.* **71**, 676-685
 116. Corpuz, G. P., Jacobsen, R. B., Jimenez, E. C., Watkins, M., Walker, C., Colledge, C., Garrett, J. E., McDougal, O., Li, W., Gray, W. R., Hillyard, D. R., Rivier, J., McIntosh, J. M., Cruz, L. J., and Olivera, B. M. (2005) Definition of the M-conotoxin superfamily: characterization of novel peptides from molluscivorous *Conus* venoms. *Biochemistry* **44**, 8176-8186
 117. Poppe, L., Hui, J. O., Liqutti, J., Murray, J. K., and Schnier, P. D. (2012) PADLOC: a powerful tool to assign disulfide bond connectivities in peptides and proteins by NMR spectroscopy. *Anal. Chem.* **84**, 262-266
 118. Tietze, A. A., Tietze, D., Ohlenschläger, O., Leipold, E., Ullrich, F., Kühl, T., Mischo, A., Buntkowsky, G., Görlach, M., Heinemann, S. H., and Imhof, D. (2012) Structurally diverse μ -conotoxin PIIIA isomers block sodium channel Nav1.4. *Angew. Chem. Int. Ed. Engl.* **51**, 4058-4061
 119. Johnson, I. S. (1983) Human insulin from recombinant DNA technology. *Science* **219**, 632-637
 120. Bosse-Doenecke, E., Weininger, U., Gopalswamy, M., Balbach, J., Knudsen, S. M., and Rudolph, R. (2008) High yield production of recombinant native and modified peptides exemplified by ligands for G-protein coupled receptors. *Protein Expr. Purif.* **58**, 114-121
 121. Kosana, R. R., Bajji, C., Kanumuri, R. M., Panati, K., Mangamoori, L. N., Tummuru, M. R., and Narala, V. R. (2014) Recombinant approach for the production of HIV fusion inhibitor Enfuvirtide using *Escherichia coli*. *Protein Expr. Purif.* **95**, 136-142
 122. West, P. J., Bulaj, G., Garrett, J. E., Olivera, B. M., and Yoshikami, D. (2002) μ -conotoxin SmIIIA, a potent inhibitor of tetrodotoxin-resistant sodium channels in amphibian sympathetic and sensory neurons. *Biochemistry* **41**, 15388-15393
 123. Kang, T. S., Vivekanandan, S., Jois, S. D., and Kini, R. M. (2005) Effect of C-terminal amidation on folding and disulfide-pairing of alpha-conotoxin ImI. *Angew. Chem. Int. Ed. Engl.* **44**, 6333-6337
 124. Kaas, Q., Yu, R., Jin, A. H., Dutertre, S., and Craik, D. J. (2012) Conoserver: updated content, knowledge, and discovery tools in the conopeptide database. *Nucleic Acids Res.* **40**, D325-D330
 125. Dutton, J. L., Paramjit, S. B., Hogg, R. C., Adams, D. A., Alewood, P. F., and Craik, D. J. (2002) A new level of conotoxin diversity, a non-native disulfide bond connectivity in alpha-conotoxin AuIB reduces structural definition but increases biological activity. *J. Biol. Chem.* **277**, 48849-48857
 126. Fuller, E., Green, B. R., Catlin, P., Buczek, O., Nielsen, J. S., Olivera, B. M., and Bulaj, G. (2005) Oxidative folding of conotoxins sharing an identical disulfide bridging framework. *FEBS J.* **272**, 1727-1738
 127. Chang, S. C., Galea, C. A., Leung, E. W., Tajhya, R. B., Beeton, C., Pennington, M. W., and Norton, R. S. (2012) Expression and isotopic labelling of the potassium channel blocker ShK toxin as a thioredoxin fusion protein in bacteria. *Toxicon* **60**, 840-850

128. Rosano, G. L., and Ceccarelli, E. A. (2014) Recombinant protein expression in *Escherichia coli*: advances and challenges. *Front. Microbiol.* **5**, 1-17
129. Robinson, S. D., and Norton, R. S. (2014) Conotoxin gene superfamilies. *Mar. Drugs* **12**, 6058-6101
130. Fiedler, B., Zhang, M. M., Buczek, O., Azam, L., Bulaj, G., Norton, R. S., Olivera, B. M., and Yoshikami, D. (2008) Specificity, affinity and efficacy of iota-conotoxin RxIA, an agonist of voltage-gated sodium channels Nav1.2, 1.6 and 1.7. *Biochem. Pharmacol.* **75**, 2334-2344
131. Leipold, E., DeBie, H., Zorn, S., Borges, A., Olivera, B. M., Terlau, H., and Heinemann, S. H. (2007) μ O-conotoxins inhibit NaV channels by interfering with their voltage sensors in domain-2. *Channels (Austin, Tex)* **1**, 253-262
132. Zhang, M. M., Gajewiak, J., Azam, L., Bulaj, G., Olivera, B. M., and Yoshikami, D. (2015) Probing the redox states of sodium channel cysteines at the binding site of μ O δ -conotoxin GVIIJ. *Biochemistry* **54**, 3911-3920
133. Pallaghy, P. K., Neilsen, K. J., Craik, D. J., and Norton, R. S. (1994) A common structural motif incorporating a cystine knot and a triple-stranded beta sheet in toxin and inhibitory polypeptides. *Protein Sci.* **3**, 1833-1839
134. Gracy, J., Le-Nguyen, D., Gelly, J.-C., Kaas, Q., Heitz, A., and Chiche, L. (2008) KNOTTIN: the knottin or inhibitor cysteine knot scaffold in 2007. *Nucleic Acids Res.* **36**, 314-319
135. Zhang, M. M., MacArthur, J. R., Azam, L., Bulaj, G., Olivera, B. M., French, J. R., and Yoshikami, D. (2009) Synergistic and antagonistic interactions between tetrodotoxin and μ -conotoxin in blocking voltage-gated sodium channels. *Channels (Austin)* **3**, 32-38
136. Zhang, M. M., Gruszczynski, P., Walewska, A., Bulaj, G., Olivera, B. M., and Yoshikami, D. (2010) Cooccupancy of the outer vestibule of voltage-gated sodium channels by μ -conotoxin KIIIA and saxitoxin or tetrodotoxin. *J. Neurophysiol.* **104**, 88-97
137. McArthur, J. R., Ostroumov, V., Al-Sabi, A., McMaster, D., and French, R. J. (2011) Multiple, distributed interactions of μ -conotoxin PIIIA associated with broad targeting among voltage-gated sodium channels. *Biochemistry* **50**, 116-124
138. Cruz, L. J., Gray, W. R., Olivera, B. M., Zeikus, R. D., Kerr, L., Yoshikami, D., and Moczydlowski, E. (1985) *Conus geographus* toxins that discriminate between neuronal and muscle sodium channels. *J. Biol. Chem.* **260**, 9280-9288
139. Shon, K. J., Olivera, B. M., Watkins, M., Jacobsen, R. B., Gray, W. R., Floresca, C. Z., Cruz, L. J., Hillyard, D. R., Brink, A., Terlau, H., and Yoshikami, D. (1998) μ -Conotoxin PIIIA, a new peptide for discriminating among tetrodotoxin-sensitive Na channel subtypes. *J. Neurosci.* **18**, 4473-4481
140. Ulrich, E. L., Akutsu, H., Doreleijers, J. F., Harano, Y., Ioannidis, Y. E., Lin, J., Livny, M., Mading, S., Maziuk, D., Miller, Z., Nakatani, E., Schulte, C. F., Tolmie, D. E., Kent, W. R., Yao, H., and Markley, J. L. (2008) BioMagResBank. *Nucleic Acids Res.* **36**, D402-D408
141. Seavey, B. R., Farr, E. A., Westler, W. M., and Markley, J. L. (1991) A relational database for sequence specific protein NMR data. *J. Biomol. NMR* **1**, 217-236
142. Zhang, M. M., Green, B. R., Catlin, P., Fiedler, B., Azam, L., Chadwick, A., Terlau, H., McArthur, J. R., French, J. R., Guylas, J., Rivier, J. E., Smith, B. J., Norton, R. S., Olivera, B. M., Yoshikami, D., and Bulaj, G. (2007) Structure/function characterization of μ -conotoxin KIIIA, an analgesic, nearly irreversible blocker of mammalian neuronal sodium channels. *J. Biol. Chem.* **282**, 30699-30706
143. Merutka, G., Dyson, H. J., and Wright, P. E. (1995) 'Random coil' ^1H chemical shifts obtained as a function of temperature and trifluoroethanol concentration for the peptide series GGXGG. *J. Biomol. NMR* **5**, 14-24

144. Wishart, D. S., Bigam, C. G., Holm, A., Hodges, R. S., and Sykes, B. D. (1995) ^1H , ^{13}C and ^{15}N random coil NMR chemical shifts of the common amino acids. I. Investigations of nearest-neighbor effects. *J. Biomol. NMR* **5**, 67-81
145. Sibanda, B. L., Blundell, T. L., and Thornton, J. M. (1989) Conformation of β -hairpins in protein structures. *J. Mol. Biol.* **206**, 759-777
146. Cestèle, S., and Catterall, W. A. (2000) Molecular mechanisms of neurotoxin action on voltage-gated sodium channels. *Biochimie* **82**, 883-892
147. Holm, A., and Rosenström, P. (2010) Dali server: conservation mapping in 3D. *Nucleic Acids Res.* **38**, W545-549
148. Chen, C., Calhoun, J. D., Zhang, Y., Lopez-Santiago, L., Zhou, N., Davis, T. H., Salzer, J. L., and Isom, L. L. (2012) Identification of the cysteine residue responsible for disulfide linkage of Na^+ channel α and $\beta 2$ subunits. *J. Biol. Chem.* **287**, 39061-39069
149. Gilchrist, J., Das, S., Van Petegem, R., and Bosmans, F. (2013) Crystallographic insights into sodium-channel modulation by the $\beta 4$ subunit. *Proc. Natl. Acad. Sci. U.S.A.* **110**, E5016-E5024
150. Becker, S., Prusak-Sochaczewski, E., Zamponi, G., Beck-Sickinger, A. G., Gordon, R. D., and French, R. J. (1992) Action of derivatives of μ -conotoxin GIIIA on sodium channels. Single amino acid substitutions in the toxin separately affect association and dissociation rates. *Biochemistry* **31**, 8229-8238
151. Chahine, M., Chatelier, A., Babich, O., and Krupp, J. J. (2008) Voltage-gated sodium channels in neurological disorders. *CNS Neurol. Disord. Drug Targets* **7**, 144-158
152. Waxman, S. G. (2002) Sodium channels as molecular targets in multiple sclerosis. *J. Rehabil. Res. Dev.* **39**, 233-242

Appendix I

Distinct Disulfide Isomers of μ -Conotoxins KIIIA and KIIIB Block Voltage-gated Sodium Channels

Similar to the results described in Chapter 3, Appendix I demonstrates the importance of disulfide connectivity for block of VGSCs using the μ -conotoxin KIIIA. Furthermore, these results show that 'non-canonical' connectivities can still inhibit channel activity.

Appendix I consists of the following publication:

Khoo, K. K.; Gupta, K.; **Green, B. R.**; Zhang, M. M.; Watkins, M.; Olivera, B. M.; Balaram, P.; Yoshikami, D.; Bulaj, G.; Norton, R. S. Distinct disulfide isomers of μ -conotoxins KIIIA and KIIIB block voltage-gated sodium channels. *Biochemistry*, 2012, 51: 9826-9635.

Distinct Disulfide Isomers of μ -Conotoxins KIIIA and KIIIB Block Voltage-Gated Sodium Channels

Keith K. Khoo,^{†,‡,§} Kallol Gupta,^{||} Brad R. Green,[†] Min-Min Zhang,[⊥] Maren Watkins,[⊥] Baldomero M. Olivera,[⊥] Padmanabhan Balaram,^{||} Doju Yoshikami,[⊥] Grzegorz Bulaj,[@] and Raymond S. Norton^{*,†}

[†]Medicinal Chemistry, Monash Institute of Pharmaceutical Sciences, Monash University, 381 Royal Parade, Parkville, VIC 3052, Australia

[‡]The Walter & Eliza Hall Institute of Medical Research, 1G Royal Parade, Parkville, VIC 3052, Australia

[§]The Department of Medical Biology, The University of Melbourne, Parkville, Victoria 3010, Australia

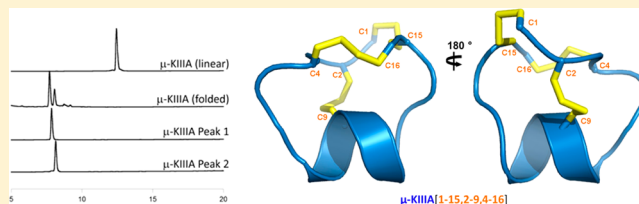
^{||}Molecular Biophysics Unit, Indian Institute of Science, Bangalore 560 012, India

[⊥]Department of Biology, University of Utah, Salt Lake City, Utah 84112, United States

[@]Department of Medicinal Chemistry, College of Pharmacy, University of Utah, Salt Lake City, Utah 84108, United States

S Supporting Information

ABSTRACT: In the preparation of synthetic conotoxins containing multiple disulfide bonds, oxidative folding can produce numerous permutations of disulfide bond connectivities. Establishing the native disulfide connectivities thus presents a significant challenge when the venom-derived peptide is not available, as is increasingly the case when conotoxins are identified from cDNA sequences. Here, we investigate the disulfide connectivity of μ -conotoxin KIIIA, which was predicted originally to have a [C1–C9,C2–C15,C4–C16] disulfide pattern based on homology with closely related μ -conotoxins. The two major isomers of synthetic μ -KIIIA formed during oxidative folding were purified and their disulfide connectivities mapped by direct mass spectrometric collision-induced dissociation fragmentation of the disulfide-bonded polypeptides. Our results show that the major oxidative folding product adopts a [C1–C15,C2–C9,C4–C16] disulfide connectivity, while the minor product adopts a [C1–C16,C2–C9,C4–C15] connectivity. Both of these peptides were potent blockers of Na_v1.2 (K_d values of 5 and 230 nM, respectively). The solution structure for μ -KIIIA based on nuclear magnetic resonance data was recalculated with the [C1–C15,C2–C9,C4–C16] disulfide pattern; its structure was very similar to the μ -KIIIA structure calculated with the incorrect [C1–C9,C2–C15,C4–C16] disulfide pattern, with an α -helix spanning residues 7–12. In addition, the major folding isomers of μ -KIIIB, an N-terminally extended isoform of μ -KIIIA identified from its cDNA sequence, were isolated. These folding products had the same disulfide connectivities as μ -KIIIA, and both blocked Na_v1.2 (K_d values of 470 and 26 nM, respectively). Our results establish that the preferred disulfide pattern of synthetic μ -KIIIA and μ -KIIIB folded in vitro is 1–5/2–4/3–6 but that other disulfide isomers are also potent sodium channel blockers. These findings raise questions about the disulfide pattern(s) of μ -KIIIA in the venom of *Conus kinoshitai*; indeed, the presence of multiple disulfide isomers in the venom could provide a means of further expanding the snail's repertoire of active peptides.



Disulfide bonds are a common feature of peptides and proteins that function outside the cell and are generally regarded as being essential for both the stability and the maintenance of the native structure.^{1,2} There is evidence, however, that they can be reduced and scrambled in vivo by agents such as glutathione, serum albumin, or redox enzymes,^{3–5} with possible losses of native structure and biological activity. Several strategies have been implemented to replace disulfide bridges with more stable linkages, including diselenides,^{6,7} thioethers such as lanthionine, in which one of the sulfur atoms of the disulfide bond is eliminated,⁸ cystathionine, in which one of the sulfur atoms is replaced with a methylene group,^{9,10} or dicarba bridges, in which the disulfide is replaced with a carbon–carbon bridge.^{11–13}

In peptides with multiple disulfide bonds, establishing the native disulfide connectivities can be challenging. Disulfide mapping methods have generally relied on selective reduction and alkylation of bonded thiol pairs, followed by sequencing using traditional Edman sequencing methods or mass spectrometry.^{14–16} This approach is limited by difficulties of selective reduction in the case of multiple disulfide-bonded peptides.¹⁷ Conventional two-dimensional ¹H nuclear magnetic resonance (NMR) spectroscopy can also identify these

Received: September 14, 2012

Revised: November 19, 2012

Published: November 20, 2012

connectivities in principle,¹⁶ but spectral overlap of resonances from multiple Cys spin systems often makes it difficult or impossible to decipher the native connectivities in peptides with multiple disulfide bonds.^{18,19} As such, alternative NMR-based strategies have been introduced to overcome this problem.^{20,21}

Recently, an alternative approach was proposed by Poppe et al.¹⁷ in which the disulfide connectivity was obtained by applying Bayesian rules of inference to the local topology of cysteine residues. This method was then applied to experimental NMR data for three exemplar peptides with complex disulfide connectivities: hepcidin, kalata-B1, and μ -conotoxin KIIIA. In the case of μ -KIIIA, the inferred [C1–C15, C2–C9, C4–C16] connectivity differed from the previously described pattern for this conotoxin, [C1–C9, C2–C15, C4–C16].²² The [C1–C9, C2–C15, C4–C16] pattern was consistent with the original NMR data set although not uniquely defined by it (for the reasons mentioned above), and the choice of that pattern was dictated predominantly by the ample precedent in the literature for the 1–4/2–5/3–6 disulfide pattern in numerous other μ -conotoxins.^{21,23–27} It was further supported by the observation that two-disulfide analogues of μ -KIIIA containing just the [C2–C15] and [C4–C16] bridges showed structures and activity profiles similar to those of μ -KIIIA itself.^{22,28,29}

In this paper, we have examined the two major isomers of synthetic μ -KIIIA (named μ -KIIIA-P1 and μ -KIIIA-P2) formed during oxidative folding. Their disulfide connectivities have been mapped by a newly developed mass spectrometry (MS) procedure that is based on the interpretation of the product ions produced upon direct gas-phase fragmentation of the native, disulfide-bonded intact peptides.^{15,30} NMR spectra of both the folding isoforms have also been analyzed. The results show that the more abundant product from oxidative folding has the [C1–C15, C2–C9, C4–C16] disulfide pattern observed by Poppe et al.¹⁷ while the minor product has a [C1–C16, C2–C9, C4–C15] pattern. Remarkably, both isomers exhibited blockade of sodium channels, raising questions about which, if either, is the “native” disulfide pattern in the venom of *Conus kinoshitai*, the *Conus* species from which the cDNA sequence encoding this peptide was first isolated.³¹ Upon further examination of the cDNA sequence of μ -KIIIA, it was determined that the mature peptide sequence of μ -KIIIA produced in the venom of *C. kinoshitai* possesses two additional residues preceding the N-terminus (Asn1 and Gly2). The N-terminally extended isoform of μ -KIIIA is named μ -KIIIB. The major oxidative isomers of this analogue (μ -KIIIB-P1 and μ -KIIIB-P2) have also been synthesized and their disulfide connectivities and sodium channel blocking activities compared with those of μ -KIIIA.

MATERIALS AND METHODS

Cloning of μ -KIIIB. μ -KIIIB was identified from a cDNA library prepared as described previously.³² Briefly, a cDNA library was created from the venom duct of an individual *C. kinoshitai* specimen. Total RNA was isolated from the venom duct with TRIzol reagent (TRIzol Total RNA Isolation, Life Technologies/Gibco BRL, Grand Island, NY), and cDNA was prepared using the SMART PCR cDNA Synthesis Kit (Clontech Laboratories, Palo Alto, CA). The cDNA was cloned into the pNEB206A vector (New England BioLabs, Inc., Beverly, MA), and sequences of individual clones were determined by standard automated sequencing.

Synthesis and Oxidative Folding. Peptides were synthesized on a 30 μ mol scale on preloaded Fmoc-Cys(Trt)-Rink Amide-MBHA resin (substitution of 0.32 mmol/g) using standard *N*-(9-fluorenyl)methoxycarbonyl (Fmoc) chemistry. The peptides were cleaved from the resin by a 3–4 h treatment with reagent K [82.5/5/2.5/5/5 (by volume) TFA/water/ethanedithiol/phenol/thioanisole mixture]. The cleaved peptides were filtered, precipitated with cold methyl *tert*-butyl ether (MTBE), and washed several times with cold MTBE. The reduced peptides were purified by reversed-phase high-performance liquid chromatography (HPLC) using a semipreparative C18 Vydac column (218TP510, 250 mm \times 10 mm, 5 μ m particle size) and eluted with a linear gradient from 5 to 35% solvent B over 35 min, where solvent A was 0.1% (v/v) TFA in water and solvent B was 0.1% (v/v) TFA in 90% aqueous acetonitrile. The flow rate was 4 mL/min, and the absorbance was monitored at 220 nm. Purified peptides were quantified by UV absorbance at 280 nm.

Oxidative folding of synthetic μ -KIIIA was accomplished via 2 h glutathione-assisted folding at room temperature under the following conditions: 20 μ M linear peptide, 0.1 M Tris-HCl (pH 7.5), 1 mM EDTA, and 1 mM reduced and 1 mM oxidized glutathione. Folding was quenched by acidification via addition of 8% (v/v) formic acid. Folded peptides were purified by reversed-phase HPLC using a semipreparative C18 column (218TP510, 250 mm \times 10 mm) over a linear gradient ranging from 5 to 35% solvent B over 35 min. Purities of the folded peptides were assessed by analytical HPLC using a linear gradient from 10 to 40% solvent B over 30 min. Quantities of the minor folding product were obtained by repurification using an analytical C18 column (218TP54, 250 mm \times 4.6 mm, 5 μ m particle size) using identical HPLC conditions. Amounts of the peptide were quantified by UV absorbance at 280 nm. Purified peptides were finally dried by lyophilization, and peptide masses were confirmed by matrix-assisted laser desorption/ionization time-of-flight (MALDI-ToF) mass spectrometry.

Mass Spectrometry. The mass spectrometric experiments were performed on an HCT Ultra ETDII ion trap mass spectrometer (Bruker Daltonics, Bremen, Germany). All experiments were performed through liquid chromatography–mass spectrometry (LC–MS) analysis of the samples by coupling the ion trap mass spectrometer with an Agilent 1100 HPLC system. The peptide samples were subjected to LC–MS using a reversed-phase C18 analytical column, with a H₂O/acetonitrile mixture (with 0.1% formic acid) as the solvent system, at a flow rate of 0.2 mL/min. The CID experiment was performed by selecting the precursor ion and subsequently fragmenting it through collision with He gas. The fragmentation amplitude (V_{p-p}) was kept between 1 and 3. The spectra were averaged over four scans.

NMR Spectroscopy. NMR spectra were recorded for μ -KIIIA-P1 (86 μ M) and μ -KIIIA-P2 (43 μ M) in a 95% H₂O/5% ²H₂O mixture at pH 4.8 and 5 °C on a Bruker DRX-600 spectrometer. Spectra were processed using TOPSPIN (version 1.3, Bruker Biospin). Spectra recorded as described by Khoo et al.²² were analyzed using XEASY (version 1.3.13).³³

Structure Calculations. Structure calculations were run using the original nuclear Overhauser effect (NOE) and dihedral restraint list as described by Khoo et al.²² (BioMagResBank entry 20048) but with the [C1–C15, C2–C9, C4–C16] disulfide connectivities. Additional structural calculations were run with six additional NOE distance restraints that were consistent with the [C1–C15, C2–

C9,C4–C16] disulfide connectivity but could not be unambiguously determined previously because of peak overlap. Structures were recalculated in XPLORE-NIH³⁴ using the simulated annealing script. Lowest-energy structures were subjected to energy minimization in water. Final families of the 20 lowest-energy structures were chosen for analysis using PROCHECK-NMR³⁵ and MOLMOL.³⁶ Final structures had no experimental distance violations greater than 0.2 Å or dihedral angle violations greater than 5°. Structural figures were prepared using MOLMOL³⁶ and PyMOL.⁵³ Final structures have been deposited in the Protein Data Bank as entry 2LXG.

Electrophysiology of the Rat Clones of Na_v1.2, 1.4 and 1.7 Expressed in *Xenopus* Oocytes. Oocytes expressing Na_v1.2, 1.4 and 1.7 α -subunits were prepared and two-electrode voltage clamped essentially as described previously.³⁷ Briefly, oocytes were placed in a 30 μ L chamber containing ND96 and two-electrode voltage clamped at a holding potential of –80 mV. To activate VGSCs, the membrane potential was stepped to –10 mV for a 50 ms period every 20 s. To apply toxin, the perfusion was halted, 3 μ L of the toxin solution (at 10 times the final concentration) was applied to the 30 μ L bath, and the bath was manually stirred for ~5 s by gently aspirating and expelling a few microliters of the bath fluid several times with a pipettor. Toxin exposures were in static baths to conserve material. On rate constants were obtained assuming the equation $k_{\text{obs}} = k_{\text{on}}[\text{peptide}] + k_{\text{off}}$,³⁸ where k_{obs} was determined from the single-exponential fit of the time course of block by a fixed peptide concentration of 10 μ M and k_{off} estimated from the level of recovery from block 20 min following toxin washout and assuming recovery followed a single-exponential time course; this procedure for determining k_{off} was adopted because recovery from block was too slow to measure by single-exponential fits.³⁷ All recordings were taken at room temperature (~21 °C).

RESULTS

Cloning of μ -KIIIB. The amino acid sequence of μ -KIIIB was deduced from cDNA derived from venom ducts of *C. kinoshitai*, as described previously.³² μ -KIIIB shared an identical amino acid sequence with μ -KIIIA but included two additional residues at the N-terminus (Asn-Gly).

Synthesis and Oxidative Folding. μ -KIIIA and μ -KIIIB were synthesized chemically using the Fmoc protocols described previously.³¹ After oxidation of the synthetic linear peptides, two distinct HPLC peaks for both μ -KIIIA and μ -KIIIB were obtained that yielded identical mass values (1882.6 Da for μ -KIIIA and 2055.4 Da for μ -KIIIB), corresponding to the respective native sequences with three disulfide bonds. Representative reversed-phase HPLC chromatograms of the oxidative folding of μ -KIIIA and μ -KIIIB are shown in Figure 1. The major isomer (μ -KIIIA-P1) elutes earlier than the minor isomer (μ -KIIIA-P2) for μ -KIIIA, while the major isomer (μ -KIIIB-P2) elutes later than the minor isomer (μ -KIIIB-P1) for μ -KIIIB.

Mass Spectrometric Determination of Disulfide Connectivities. Two distinct HPLC peaks of μ -KIIIA, obtained through the oxidation of the synthetic linear peptide, yielded identical mass values (1882.6 Da) corresponding to the native sequence with three disulfide bonds. In principle, 15 disulfide foldamers corresponding to distinct disulfide linkage patterns are possible (Figure S1 of the Supporting Information). Direct MS fragmentation of intact disulfide-bonded

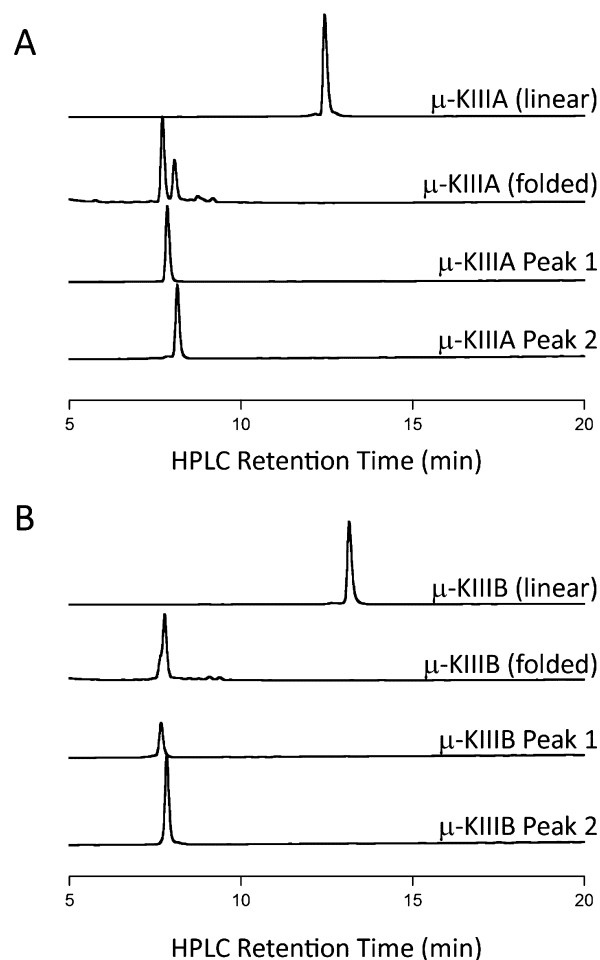


Figure 1. Representative reversed-phase HPLC chromatograms of the oxidative folding of (A) μ -KIIIA and (B) μ -KIIIB. μ -KIIIA peaks 1 and 2 represent the [C1–C15,C2–C9,C4–C16] and [C1–C16,C2–C9,C4–C15] connectivities, respectively (see the text). Folding was conducted in a buffered solution (pH 7.5) containing a mixture of 1 mM oxidized and 1 mM reduced glutathione for 2 h at room temperature.

peptides or proteolytically nicked peptides provides a route to de novo determination of disulfide connectivity in natural and synthetic peptides. This procedure relies on the interpretation of different modes of disulfide bond cleavage under ion trap mass spectrometric conditions. The structures of the ions are determined through a program, *DisConnect*, developed to analyze the CID MS/MS data of the native disulfide-bonded molecule. The key steps in establishing disulfide connectivity for the two μ -KIIIA and μ -KIIIB isomers (P1 and P2) are described below.

μ -KIIIA-P1. Upon trypsin digestion, the fraction shows a mass of 1423.6 Da (inset of Figure 2) that corresponds to a peptide in which the central tetrapeptide segment (DHRS) has been excised out by trypsin cleavage at the R–D and R–C15 peptide bonds. In addition, a proteolytic cleavage at the K–W bond is also observed. This means that the tryptic peptide consists of three individual peptide chains that are held together by three disulfide bonds. Foldamers F1, F4, and F7 (Figure S1 of the Supporting Information) cannot yield the observed tryptic peptide. In these cases, because of the C15–C16 connectivity, Arg14 is not inside a disulfide loop and thus would cause separation of the C15–C16 disulfide from the rest of the

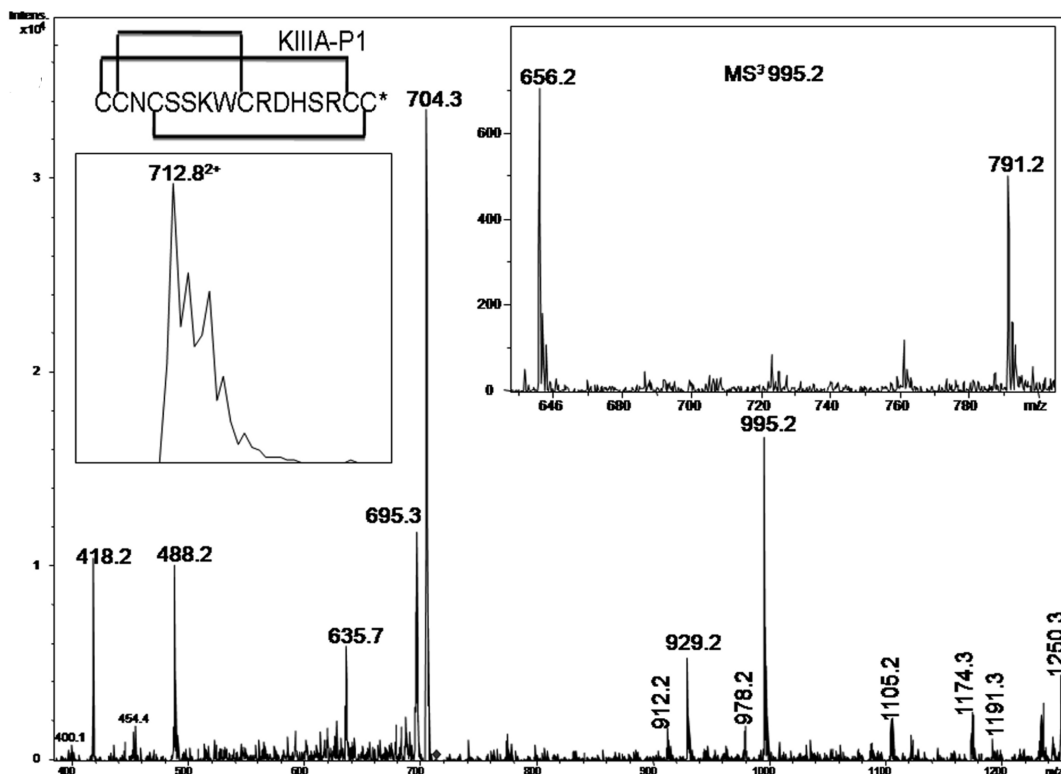


Figure 2. CID MS² spectrum of the peptide derived upon trypsin digestion of μ -KIIIA-P1 [m/z 712.8, (M + 2H)²⁺]. The inset shows the MS spectrum of the precursor ion and MS³ spectra of the ion at m/z 995.2.

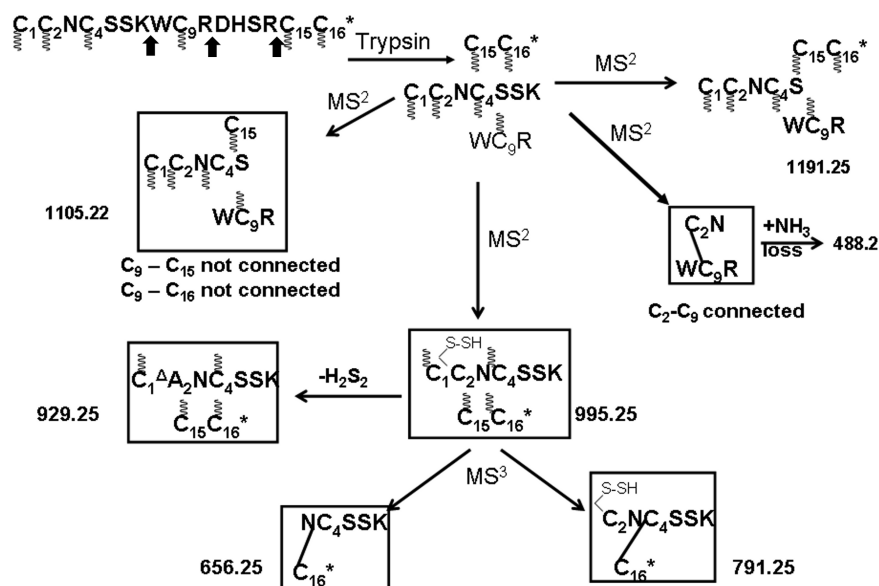


Figure 3. Assignments of the key MSⁿ fragment ions of tryptic μ -KIIIA-P1. The m/z values of each of the ions are indicated against the respective structures, and they correspond to the singly charged values, unless otherwise specified. For every structure, Cys residues with indeterminate connectivity are indicated with the wavy lines. Subsequently, in the structures from which a particular Cys connectivity is evident, the connected Cys residues are joined through a dashed line. The arrows indicate the site of proteolysis. The 2–4 connectivity is established by the product ion at m/z 488.2, while the ions at m/z 656.2 and 791.2 confirm the 3–6 connectivity.

peptide. Hence, 12 possible foldamers (Figure S2 of the Supporting Information) need to be considered. Figure 2 shows the CID MS/MS spectra of the tryptic peptide. The structures of the major fragment ions are determined through *DisConnect*. The chemical structures of the key ions, derived through the fragmentation of the disulfide-bonded molecule, are shown in Figure 3. The structures shown correspond uniquely to the

observed m/z values. A key ion is observed at m/z 488.2 that arises through the loss of NH₃ from an initial product ion, which necessarily must have C2 disulfide bonded to C9. This leaves only two probable foldamers, F11 and F14, to be considered further. A final distinction between these two foldamers is achieved by a subsequent MS³ fragmentation of the ion at m/z 995.2 (inset of Figure 2). The probable

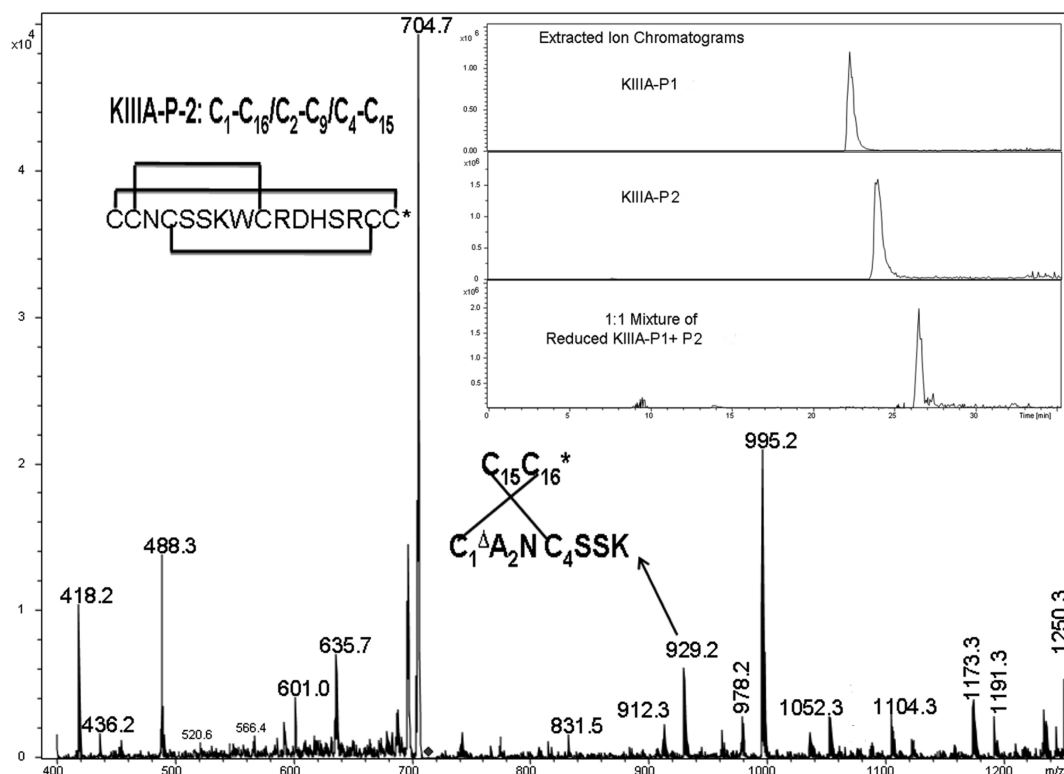


Figure 4. CID MS² spectrum of the peptide derived upon trypsin digestion of μ -KIIIA-P2 [m/z 712.8, $(M + 2H)^{2+}$]. The inset shows the extracted ion chromatogram from the LC–MS analysis of μ -KIIIA-P1, μ -KIIIA-P2, and a reduced equimolar mixture of both fractions.

Table 1. Structural Statistics for μ -KIIIA[C1–C15,C2–C9,C4–C16] and μ -KIIIA[C1–C9,C2–C15,C4–C16]

	μ -KIIIA[C1–C15,C2–C9,C4–C16]	μ -KIIIA[C1–C9,C2–C15,C4–C16] ^c
no. of distance restraints	231	225
intraresidue ($i = j$)	97	97
sequential ($ i - j = 1$)	70	70
short-range ($1 < i - j < 6$)	45	45
long-range	19	13
no. of dihedral restraints	8	8
energy E_{NOE} (kcal mol ⁻¹) ^a	1.7 ± 0.4	1.6 ± 0.3
deviations from ideal geometry ^b		
bonds (Å)	0.0015 ± 0.0001	0.0017 ± 0.0002
angles (deg)	0.503 ± 0.005	0.503 ± 0.013
impropers (deg)	0.379 ± 0.009	0.371 ± 0.009
mean global rmsd (Å) ^c		
backbone heavy atoms	0.51 ± 0.12	0.58 ± 0.11
all heavy atoms	1.39 ± 0.26	1.42 ± 0.28
Ramachandran plot ^d (%)		
most favored	81.1	78.9
allowed	18.9	21.1
additionally allowed	0	0
disallowed	0	0

^aThe values for E_{NOE} are calculated from a square well potential with force constants of 50 kcal mol⁻¹ Å⁻². ^bThe values for the bonds, angles, and impropers show the deviations from ideal values based on perfect stereochemistry. ^cThe pairwise rmsd over the indicated residues calculated with MOLMOL. ^dAs determined by PROCHECK-NMR for all residues except Gly and Pro. ^eStructural statistics for μ -KIIIA[C1–C9,C2–C15,C4–C16] from previously published data²² for comparison.

structures of the fragment ions at m/z 995.2 are shown in Figure 3. The ions at m/z 656.1 and 791.2, establish the C4–C16 connectivity unambiguously. The overall connectivity pattern is therefore that of foldamer F11 (1–5/2–4/3–6).

μ -KIIIA-P2. For μ -KIIIA-P2, an identical mass was obtained upon trypsin digestion. Fragmentation of the doubly charged

tryptic peptide yielded an identical MS/MS spectrum (Figure 4), which again leaves F11 and F14 as the two probable foldamers (as described previously for μ -KIIIA-P1). Unfortunately, the MS³ fragmentation of the ion at m/z 995.2 did not yield product ions with measurable intensities. However, assignment of the disulfide connectivity in μ -KIIIA-P2 to

foldamer F14 may be made through an alternative approach. As described above, the observation of the ion at m/z 995.2 is only compatible with foldamers F11 and F14. μ -KIIIA-P1 has already been assigned unambiguously, through mass spectral fragmentation, as F11. HPLC analysis of μ -KIIIA-P1 and -P2 reveals two distinct retention times, suggesting that they are indeed two distinct foldamers (inset of Figure 4). Upon reduction, the linearized product from the two foldamers must be identical. This is demonstrated by HPLC coelution of reduced products of both the μ -KIIIA foldamers (inset of Figure 4). Hence, the connectivity of μ -KIIIA-P2 is that of F14 (1-6/2-4/3-5) (Figure 4).

μ -KIIIB-P1 and -P2. Peptide μ -KIIIB, as mentioned previously, differs from μ -KIIIA by addition of an N-terminal Asn-Gly pair. In a similar way, described in the Supporting Information (Figures S3–S5 and the supplementary text), the disulfide connectivities of the μ -KIIIB isomers were determined. The disulfide connectivity of the major isomer, μ -KIIIB-P2, was determined to be 1-5/2-4/3-6, while that of μ -KIIIB-P1 was determined to be 1-6/2-4/3-5.

NMR of μ -KIIIA. Comparison of one-dimensional spectra at 5 °C of μ -KIIIA-P1 with that published originally for μ -KIIIA²² (Figure S6 of the Supporting Information) indicates that the original sample studied was identical to μ -KIIIA-P1, the major isomer obtained from oxidative folding. Spectra of μ -KIIIA-P2, on the other hand, displayed significant differences, indicating a different fold as a result of a different disulfide connectivity (Figure S6 of the Supporting Information).

Recalculated Solution Structure for μ -KIIIA-P1. The [C1–C15,C2–C9,C4–C16] disulfide connectivity was consistent with the original NOE and dihedral data set,²² with no major violations observed during the calculations, although there was a slight increase in the NOE energy function for the final structures calculated. A summary of experimental constraints and structural statistics for μ -KIIIA with the [C1–C15,C2–C9,C4–C16] disulfide connectivity (i.e., μ -KIIIA-P1) compared with the previously calculated structure for μ -KIIIA assuming the [C1–C9,C2–C15,C4–C16] disulfide connectivity is given in Table 1. The angular order parameters for φ and ψ in the final ensemble of 20 structures for μ -KIIIA[C1–C15,C2–C9,C4–C16] were both >0.8 over all residues (Figure S8 of the Supporting Information), indicating that the backbone dihedral angles are well-defined across the family of structures. The mean pairwise rmsd over the backbone heavy atoms over all residues for the family of structures of μ -KIIIA[C1–C15,C2–C9,C4–C16] was 0.51 Å. Comparisons of the calculated families of structures as well as closest-to-average structures of μ -KIIIA[C1–C9,C2–C15,C4–C16] and μ -KIIIA-[C1–C15,C2–C9,C4–C16] are shown in Figures 5 and 6. Similar to the findings of Poppe et al.,¹⁷ structures recalculated with the [C1–C15,C2–C9,C4–C16] disulfide connectivity had an overall topology resembling that of the previously published structure,²² with an α -helix spanning residues 7–12 in the closest-to-average structure. The backbones generally align well with a global rmsd of 0.57 ± 0.14 Å over residues 4–16. The main difference lies in the orientation of the N-terminus, with Cys2 now pulled closer to the α -helix and Cys1 oriented toward the C-terminal tail as a result of the C2–C9 and C1–C15 disulfide bonds, respectively. With the [C1–C15,C2–C9,C4–C16] disulfide connectivity, backbone φ and ψ angles of Cys2 correspond to the β -sheet region of the Ramachandran plot instead of the α -helix region, as observed

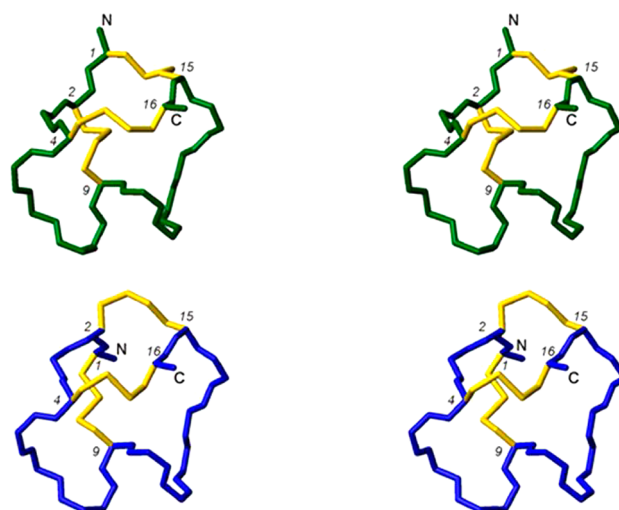


Figure 5. Stereoviews of backbone and closest-to-average structures of μ -KIIIA[C1–C15,C2–C9,C4–C16] (green) and μ -KIIIA[C1–C9,C2–C15,C4–C16]²² (blue). Disulfide bonds are colored yellow.

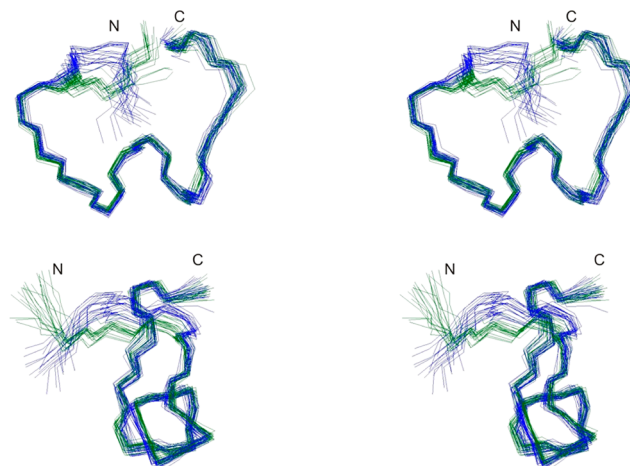


Figure 6. Stereoviews of the overlay of the ensemble of 20 NMR structures of μ -KIIIA[C1–C15,C2–C9,C4–C16] (green) and μ -KIIIA[C1–C9,C2–C15,C4–C16]²² (blue), superimposed over backbone heavy atoms of residues 4–16. Top and bottom panels are related by a 90° anticlockwise rotation about the vertical axis.

with the [C1–C9,C2–C15,C4–C16] disulfide connectivity (Figure S9 of the Supporting Information).

Electrophysiology Assays. The ability of the minor oxidative folding isomer of μ -KIIIA (μ -KIIIA-P2) and the two major oxidative folding isomers of μ -KIIIB (μ -KIIIB-P1 and μ -KIIIB-P2) to block $\text{Na}_v1.2$ expressed in oocytes was assessed by the voltage clamp protocol described in Materials and Methods. Table 2 summarizes the activity of 10 μM μ -KIIIA-P2, μ -KIIIB-P1, and μ -KIIIB-P2 on $\text{Na}_v1.2$ in comparison with that of the major oxidative folding isomer of μ -KIIIA (μ -KIIIA-P1) reported previously.³⁷ Representative sodium-current traces of the block by μ -KIIIB-P1 and μ -KIIIB-P2 of $\text{Na}_v1.2$ are shown in Figure S10 of the Supporting Information. Both μ -KIIIB isomers had slow off rates comparable to that of μ -KIIIA, indicating their almost irreversible binding to the $\text{Na}_v1.2$ channel. Of the two μ -KIIIB isomers, the major oxidative folding isomer, μ -KIIIB-P2, displayed a greater affinity ($K_d = 0.026 \mu\text{M}$) for $\text{Na}_v1.2$ than μ -KIIIB-P1 ($K_d = 0.47 \mu\text{M}$). Thus, μ -KIIIB-P2 was ~ 5 times less potent than μ -KIIIA-P1 ($K_d =$

Table 2. Block of Na_v1.2 by μ -KIIIA and μ -KIIIB^a

toxin	k_{off} (min ⁻¹)	k_{on} (μM^{-1} min ⁻¹)	K_{d} ^b (μM)
μ -KIIIA-P1 ^c	0.0016 \pm 0.0016	0.30 \pm 0.03	0.005 \pm 0.005
μ -KIIIA-P2	0.0044 \pm 0.0023	0.019 \pm 0.002 ^d	0.23 \pm 0.12
μ -KIIIB-P1	0.0052 \pm 0.0017	0.011 \pm 0.003 ^d	0.47 \pm 0.20
μ -KIIIB-P2	0.0034 \pm 0.0018	0.13 \pm 0.01 ^d	0.026 \pm 0.014

^aValues (mean \pm standard deviation; $n \geq 3$ oocytes) were obtained by two-electrode voltage clamp of *Xenopus* oocytes expressing rat Na_v1.2 channels as described in Methods and Materials. ^bFrom $k_{\text{off}}/k_{\text{on}}$. ^cValues for μ -KIIIA as determined previously.²² ^dFrom $(k_{\text{obs}} - k_{\text{off}})/10$ μM .

0.005 μM). Via comparison of the two μ -KIIIA isomers, the major oxidative folding isomer, μ -KIIIA-P1, was more potent than the minor isomer μ -KIIIA-P2, which had a K_{d} of 0.23 μM .

The minor isomer μ -KIIIA-P2 was also tested against the Na_v1.4 and Na_v1.7 subtypes, displaying K_{d} values of 0.83 and 1.57 μM , respectively (Table S4 of the Supporting Information). Among these three subtypes, therefore, the selectivity profile of μ -KIIIA-P2 remained the same as for the major μ -KIIIA isomer: Na_v1.2 > Na_v1.4 > Na_v1.7.³⁹

DISCUSSION

μ -Conotoxins belonging to the M-superfamily of conotoxins have the characteristic Cys framework (–CC–C–C–CC–) of this superfamily⁴⁰ and have been subdivided previously into five branches (M1–M5) based on the number of residues between the fourth and fifth half-cysteine residues. Interestingly, among known structures, different disulfide patterns can be found in the M1 (1–5/2–4/3–6), M2 (1–6/2–4/3–5), and M4 (1–4/2–5/3–6) branch conotoxins, suggesting that the number of residues in the last cysteine loop might determine the disulfide connectivity in this family.^{41,42} The first class of μ -conotoxins to be characterized (sequences in Table S1 of the Supporting Information) belonged to the M4 branch, which included μ -GIIIA, μ -GIIIB, μ -PIIIA, and μ -TIIIA, and the first of these to be characterized was μ -GIIIA from *Conus geographus*.⁴³ Typically, early characterization involved isolation and sequencing of the venom-derived peptide,⁴³ following which the peptide was synthesized chemically with the disulfide bonds formed by oxidative–reductive folding with glutathione.⁴⁴ HPLC coelution with the venom-derived toxin was then employed to confirm that the synthetic peptide had a fold identical to that of the native peptide and therefore possessed the same disulfide connectivity.^{23,44} Mass spectrometric methods have also been employed to elucidate disulfide connectivities.^{14,26,45} Disulfide mapping was previously conducted on synthetic μ -GIIIA, establishing the disulfide pattern as 1–4/2–5/3–6.⁴⁵ Disulfide mapping with other M4 branch μ -conotoxins μ -PIIIA and μ -SxIIIA also showed that the disulfide connectivity for this class of μ -conotoxins was consistent with that of μ -GIIIA.^{21,26}

Specific disulfide mapping for the newer class of μ -conotoxins belonging to the M5 branch, which includes μ -KIIIA (Table S1 of the Supporting Information), has, however, never been conducted. Disulfide connectivities were instead based on sequence alignment with the closely related μ -conotoxins in the M4 branch. Solution structures of μ -SmIIIA,²⁴ μ -SIIIA,²⁷ μ -KIIIA,²² and most recently μ -CnIIIC⁴⁶ were determined assuming those canonical disulfide connectivities. The results of our study on μ -KIIIA now confirm that the thermodynamically favored product of oxidative folding in vitro

has a disulfide connectivity pattern differing from the canonical pattern established for the M4 μ -conotoxins. The 1–5/2–4/3–6 disulfide connectivity pattern¹⁷ adopted by the major folding isomer, μ -KIIIA-P1, is similar to that observed in the M1 branch of conotoxins, while the 1–6/2–4/3–5 pattern of the minor isomer, μ -KIIIA-P2, is similar to that of the M2 branch. Similar studies of the other M5 μ -conotoxins will need to be conducted to determine whether all conotoxins in this class also adopt the 1–5/2–4/3–6 disulfide pattern, although we note that μ -KIIIA and μ -KIIIB have a shorter first loop compared with other M5 μ -conotoxins, with only one amino acid residue between the second and third cysteine residues (Table S1 of the Supporting Information), and this may also influence folding.

In addition to the two major disulfide isomers characterized in this paper, the biological activity and structure of the disulfide-deficient analogue μ -KIIIA[C1A,C9A], which has the [C2–C15,C4–C16] disulfide connectivity, were characterized previously.²² Intercysteine NOEs for μ -KIIIA[C1A,C9A]²² (Table S3 of the Supporting Information) were better resolved as only two disulfide bonds were present and confirmed the expected disulfide connectivity of μ -KIIIA[C1A,C9A]. It is intriguing that μ -KIIIA[C1A,C9A] showed potent blockade of Na_v1.2 (K_{d} of 8 nM, comparable to the value of 5 nM for μ -KIIIA) and Na_v1.4 (240 nM compared with 50 nM)²² even though it contained C2–C15 and C4–C16 disulfides rather than the C2–C9 and C4–C16 disulfides in the major product of in vitro folding of μ -KIIIA. Clearly, several distinct disulfide connectivities are compatible with a μ -KIIIA structure capable of potent sodium channel blockade.

The biological activities and structures of the major isomers of synthetic μ -PIIIA, an M4 branch μ -conotoxin, formed during oxidative folding were investigated recently.⁴⁷ Disulfide connectivity analysis by a combination of inter-cysteine NOE analysis and MALDI-ToF MS/MS revealed different disulfide connectivities for each of the three isomers investigated, with one adopting the canonical 1–4/2–5/3–6 connectivity. Consistent with our findings for μ -KIIIA, all three disulfide isomers of μ -PIIIA were able to block Na_v1.4 with considerable potency.⁴⁷ In contrast to μ -KIIIA, however, the different isomers adopted different overall folds, although the two most potent isomers did retain a common helical region between Phe7 and Arg12. Intriguingly, the disulfide isomer with a 1–5/2–6/3–4 connectivity was more than twice as potent as the 1–4/2–5/3–6 disulfide isomer,⁴⁷ which is the major form of this peptide in the venom gland.²⁶

These studies, together with the results presented here, highlight the different disulfide connectivities that can arise as a result of in vitro oxidative folding. The question this then poses is whether the disulfide connectivity in the major product of in vitro oxidative folding corresponds to the native disulfide pattern in the venom of the cone shell *C. kinoshitai*. Indeed, the mechanisms of oxidative folding in vivo that lead to the formation of the native toxin in the venom are still not well understood. In the biosynthesis of a conotoxin within the venom gland, several factors such as the propeptide precursor sequence, folding enzymes (protein disulfide isomerases), and molecular chaperones can play a role in directing folding and disulfide formation, allowing the efficient synthesis of the native disulfide pattern.⁴⁸ Recent work by Safavi-Hemami et al.⁴⁹ provided evidence of the presence of both the globular and ribbon forms of α -conotoxin ImI in the venom of *Conus imperialis*. Non-native disulfide isomers have also been reported

for other α -conotoxins such as α -GI and α -AuIB.^{50,51} In these α -conotoxins, two additional non-native disulfide bond isomers could be formed during oxidative folding, the “ribbon” isomer (1–4/2–3 disulfide connectivity) and the “bead” isomer (1–2/3–4). Each of these two isomers adopted a fold different from that of the native isomer (1–3/2–4), which had a globular fold. Pharmacological studies have traditionally focused on the activities of the globular form, assuming this form to be the native disulfide connectivity. However, in numerous cases (e.g., α -AuIB), it is actually the ribbon form that exhibits the greatest affinity and/or potency for the molecular target.⁵⁰ Taken together, these results suggest that multiple isoforms may have evolved, yielding even greater toxin diversity within *Conus* venoms. Although these studies emphasized the presence of multiple folding isoforms of α -conotoxins, it is conceivable that multiple “misfolded” isomers of μ -conotoxins are also present in the venom and should be explored for their biological activities.

In this study, we have also addressed the ambiguity regarding the mature peptide sequence of μ -KIIIA that was derived from the cDNA clone.³¹ Similar to μ -SmIIIA,³⁸ two putative proteolytic processing sites were identified, and to date, the shorter sequence lacking the Asn and Gly residues at the N-terminus has been taken to be the mature peptide sequence of μ -KIIIA. However, upon further examination of the cDNA sequence of μ -KIIIA, it was determined that, if cleavage occurs immediately after the putative “KR” proteolytic site in the propeptide sequence, as observed in several other μ -conotoxins (Table S2 of the Supporting Information), then the mature peptide sequence of μ -KIIIA produced in the venoms of *C. kinoshitai* would include the two additional residues preceding the N-terminus. The N-terminally extended isomer has been named μ -KIIIB, and its major folding isomer, μ -KIIIB-P2, has been shown to block Na_v1.2 with a K_d 5-fold greater than that of μ -KIIIA.

Our study shows that, for μ -KIIIA, both the [C1–C9,C2–C15,C4–C16] and [C1–C15,C2–C9,C4–C16] disulfide connectivities were consistent with the NMR data set, and interchanging between the two patterns altered the structure minimally, with the α -helix bearing the key residues for sodium channel blockade being preserved. This observation validates efforts to miniaturize μ -KIIIA²⁹ and mimic the pharmacophore in truncated, lactam-stabilized analogues of μ -KIIIA.⁵² Indeed, the uncertainty surrounding disulfide bond connectivities in synthetic conotoxins provides a compelling rationale for replacing them with more stable isosteres or removing them completely with the aim of designing more stable compounds for therapeutic use.

■ ASSOCIATED CONTENT

📄 Supporting Information

Ten figures and four tables. This material is available free of charge via the Internet at <http://pubs.acs.org>.

Accession Codes

Chemical shift assignments and the family of structures for μ -KIIIA-P1 have been deposited in the BioMagResBank and Protein Data Bank as entries 20048 and 2LXG, respectively.

■ AUTHOR INFORMATION

Corresponding Author

*E-mail: ray.norton@monash.edu. Telephone: (+61 3) 9903 9167. Fax: (+61 3) 9903 9582.

Funding

This work was supported in part by grants to R.S.N., G.B. and B.M.O. from the Australian Research Council (DP1094212) and National Institutes of Health Grant GM 48677 to G.B., B.M.O., and D.Y. K.G. acknowledges CSIR, Government of India, for a senior research fellowship. The work at Bangalore was supported by grants from Department of Biotechnology, Government of India. R.S.N. acknowledges fellowship support from the National Health and Medical Research Council of Australia.

Notes

The authors declare no competing financial interest.

■ ACKNOWLEDGMENTS

We thank Prof. Alan A. Goldin (University of California, Irvine, CA) for the Na_v1.2 and 1.4 clones, Prof. Gail Mandel (Howard Hughes Medical Institute, Portland, OR) for the Na_v1.7 clone, and Dr. Layla Azam (University of Utah) for preparing cRNA from these clones. We also thank Joanna Gajewiak and Konkallu H. Gowd for helpful discussions and suggestions.

■ ABBREVIATIONS

CID, collision-induced dissociation; μ -GIIIA and μ -GIIIB, μ -conotoxins GIIIA and GIIIB, respectively, from *C. geographus*; μ -KIIIA and μ -KIIIB, μ -conotoxins KIIIA and KIIIB, respectively, from *C. kinoshitai*; μ -KIIIA[C1A,C9A], μ -KIIIA with Cys1 and Cys9 replaced with Ala; MTBE, methyl *tert*-butyl ether; Na_v1.2, α -subunit of voltage-gated sodium channel subtype 1.2; μ -PIIIA, μ -conotoxin PIIIA from *Conus purpurascens*; μ -SIIIA, μ -conotoxin SIIIA from *Conus striatus*; μ -SmIIIA, μ -conotoxin SmIIIA from *Conus stercusmuscarum*; rmsd, root-mean-square deviation.

■ REFERENCES

- (1) Khoo, K. K., and Norton, R. S. (2012) Role of disulfide bonds in peptide and protein conformation. In *Amino Acids, Peptides and Proteins in Organic Chemistry* (Hughes, A. B., Ed.) pp 395–417, Wiley-VCH, Weinheim, Germany.
- (2) Trivedi, M. V., Laurence, J. S., and Siahaan, T. J. (2009) The role of thiols and disulfides on protein stability. *Curr. Protein Pept. Sci.* 10, 614–625.
- (3) Gilbert, H. F. (1995) Thiol/disulfide exchange equilibria and disulfide bond stability. *Methods Enzymol.* 251, 8–28.
- (4) Holmgren, A., and Bjornstedt, M. (1995) Thioredoxin and thioredoxin reductase. *Methods Enzymol.* 252, 199–208.
- (5) Buczek, O., Green, B. R., and Bulaj, G. (2007) Albumin is a redox-active crowding agent that promotes oxidative folding of cysteine-rich peptides. *Biopolymers* 88, 8–19.
- (6) Armishaw, C. J., Daly, N. L., Nevin, S. T., Adams, D. J., Craik, D. J., and Alewood, P. F. (2006) α -Selenoconotoxins, a new class of potent α 7 neuronal nicotinic receptor antagonists. *J. Biol. Chem.* 281, 14136–14143.
- (7) Walewska, A., Zhang, M. M., Skalicky, J. J., Yoshikami, D., Olivera, B. M., and Bulaj, G. (2009) Integrated oxidative folding of cysteine/selenocysteine containing peptides: Improving chemical synthesis of conotoxins. *Angew. Chem., Int. Ed.* 48, 2221–2224.
- (8) Paul, M., and Donk, W. A. v. d. (2005) Chemical and enzymatic synthesis of lanthionines. *Mini-Rev. Org. Chem.* 2, 23–37.
- (9) Knerr, P. J., Tzekou, A., Ricklin, D., Qu, H., Chen, H., van der Donk, W. A., and Lambris, J. D. (2011) Synthesis and activity of thioether-containing analogues of the complement inhibitor compstatin. *ACS Chem. Biol.* 6, 753–760.
- (10) Muttenthaler, M., Andersson, A., de Araujo, A. D., Dekan, Z., Lewis, R. J., and Alewood, P. F. (2010) Modulating oxytocin activity

and plasma stability by disulfide bond engineering. *J. Med. Chem.* 53, 8585–8596.

(11) Platt, R. J., Han, T. S., Green, B. R., Smith, M. D., Skalicky, J., Gruszczynski, P., White, H. S., Olivera, B., Bulaj, G., and Gajewiak, J. (2012) Stapling mimics noncovalent interactions of γ -carboxyglutamates in conantokins, Peptidic antagonists of N-methyl-D-aspartic acid receptors. *J. Biol. Chem.* 287, 20727–20736.

(12) MacRaild, C. A., Illesinghe, J., van Lierop, B. J., Townsend, A. L., Chebib, M., Livett, B. G., Robinson, A. J., and Norton, R. S. (2009) Structure and activity of (2,8)-dicarba-(3,12)-cystino α -ImI, an α -conotoxin containing a nonreducible cystine analogue. *J. Med. Chem.* 52, 755–762.

(13) Robinson, A. J., van Lierop, B. J., Garland, R. D., Teoh, E., Elaridi, J., Illesinghe, J. P., and Jackson, W. R. (2009) Regioselective formation of interlocked dicarba bridges in naturally occurring cyclic peptide toxins using olefin metathesis. *Chem. Commun.*, 4293–4295.

(14) Gray, W. R. (1993) Disulfide structures of highly bridged peptides: A new strategy for analysis. *Protein Sci.* 2, 1732–1748.

(15) Gupta, K., Kumar, M., and Balaram, P. (2010) Disulfide bond assignments by mass spectrometry of native natural peptides: Cysteine pairing in disulfide bonded conotoxins. *Anal. Chem.* 82, 8313–8319.

(16) Ye, M., Khoo, K. K., Xu, S., Zhou, M., Boonyalai, N., Perugini, M. A., Shao, X., Chi, C., Galea, C. A., Wang, C., and Norton, R. S. (2012) A helical conotoxin from *Conus imperialis* has a novel cysteine framework and defines a new superfamily. *J. Biol. Chem.* 287, 14973–14983.

(17) Poppe, L., Hui, J. O., Ligutti, J., Murray, J. K., and Schnier, P. D. (2012) PADLOC: A powerful tool to assign disulfide bond connectivities in peptides and proteins by NMR spectroscopy. *Anal. Chem.* 84, 262–266.

(18) Jordan, J. B., Poppe, L., Haniu, M., Arvedson, T., Syed, R., Li, V., Kohno, H., Kim, H., Schnier, P. D., Harvey, T. S., Miranda, L. P., Cheatham, J., and Sasu, B. J. (2009) Heptidin revisited, disulfide connectivity, dynamics, and structure. *J. Biol. Chem.* 284, 24155–24167.

(19) Lauth, X., Babon, J. J., Stannard, J. A., Singh, S., Nizet, V., Carlberg, J. M., Ostland, V. E., Pennington, M. W., Norton, R. S., and Westerman, M. E. (2005) Bass hepcidin synthesis, solution structure, antimicrobial activities and synergism, and *in vivo* hepatic response to bacterial infections. *J. Biol. Chem.* 280, 9272–9282.

(20) Mobli, M., and King, G. F. (2010) NMR methods for determining disulfide-bond connectivities. *Toxicon* 56, 849–854.

(21) Walewska, A., Skalicky, J. J., Davis, D. R., Zhang, M. M., Lopez-Vera, E., Watkins, M., Han, T. S., Yoshikami, D., Olivera, B. M., and Bulaj, G. (2008) NMR-based mapping of disulfide bridges in cysteine-rich peptides: Application to the μ -conotoxin SxIIIa. *J. Am. Chem. Soc.* 130, 14280–14286.

(22) Khoo, K. K., Feng, Z. P., Smith, B. J., Zhang, M. M., Yoshikami, D., Olivera, B. M., Bulaj, G., and Norton, R. S. (2009) Structure of the analgesic μ -conotoxin KIIIA and effects on the structure and function of disulfide deletion. *Biochemistry* 48, 1210–1219.

(23) Hill, J. M., Alewood, P. F., and Craik, D. J. (1996) Three-dimensional solution structure of μ -conotoxin GIIB, a specific blocker of skeletal muscle sodium channels. *Biochemistry* 35, 8824–8835.

(24) Keizer, D. W., West, P. J., Lee, E. F., Yoshikami, D., Olivera, B. M., Bulaj, G., and Norton, R. S. (2003) Structural basis for tetrodotoxin-resistant sodium channel binding by μ -conotoxin SmIIIa. *J. Biol. Chem.* 278, 46805–46813.

(25) Lancelin, J. M., Kohda, D., Tate, S., Yanagawa, Y., Abe, T., Satake, M., and Inagaki, F. (1991) Tertiary structure of conotoxin GIIIA in aqueous solution. *Biochemistry* 30, 6908–6916.

(26) Shon, K. J., Olivera, B. M., Watkins, M., Jacobsen, R. B., Gray, W. R., Floresca, C. Z., Cruz, L. J., Hillyard, D. R., Brink, A., Terlau, H., and Yoshikami, D. (1998) μ -Conotoxin PIIIA, a new peptide for discriminating among tetrodotoxin-sensitive Na channel subtypes. *J. Neurosci.* 18, 4473–4481.

(27) Yao, S., Zhang, M. M., Yoshikami, D., Azam, L., Olivera, B. M., Bulaj, G., and Norton, R. S. (2008) Structure, dynamics, and selectivity

of the sodium channel blocker μ -conotoxin SIIIA. *Biochemistry* 47, 10940–10949.

(28) Han, T. S., Zhang, M. M., Walewska, A., Gruszczynski, P., Robertson, C. R., Cheatham, T. E., III, Yoshikami, D., Olivera, B. M., and Bulaj, G. (2009) Structurally minimized μ -conotoxin analogues as sodium channel blockers: Implications for designing conopeptide-based therapeutics. *ChemMedChem* 4, 406–414.

(29) Stevens, M., Peigneur, S., Dyubankova, N., Lescrinier, E., Herdewijn, P., and Tytgat, J. (2012) Design of bioactive peptides from naturally occurring μ -conotoxin structures. *J. Biol. Chem.* 287, 31382–31392.

(30) Bhattacharyya, M., Gupta, K., Gowd, K. H., and Balaram, P. (2012) Rapid mass spectrometric determination of disulfide folds in peptides and proteins: A robust solution for a long standing problem in protein chemistry. *Mol. Biosyst.*, submitted.

(31) Bulaj, G., West, P. J., Garrett, J. E., Watkins, M., Zhang, M. M., Norton, R. S., Smith, B. J., Yoshikami, D., and Olivera, B. M. (2005) Novel conotoxins from *Conus striatus* and *Conus kinoshitai* selectively block TTX-resistant sodium channels. *Biochemistry* 44, 7259–7265.

(32) Biggs, J. S., Watkins, M., Puillandre, N., Ownby, J. P., Lopez-Vera, E., Christensen, S., Moreno, K. J., Bernaldez, J., Licea-Navarro, A., Corneli, P. S., and Olivera, B. M. (2010) Evolution of *Conus* peptide toxins: Analysis of *Conus californicus* Reeve, 1844. *Mol. Phylogenet. Evol.* 56, 1–12.

(33) Bartels, C., Xia, T. H., Billeter, M., Güntert, P., and Wüthrich, K. (1995) The program XEASY for computer-supported NMR spectral analysis of biological macromolecules. *J. Biomol. NMR* 6, 1–10.

(34) Schwieters, C. D., Kuszewski, J. J., Tjandra, N., and Clore, G. M. (2003) The Xplor-NIH NMR molecular structure determination package. *J. Magn. Reson.* 160, 65–73.

(35) Laskowski, R. A., Rullmann, J. A., MacArthur, M. W., Kaptein, R., and Thornton, J. M. (1996) AQUA and PROCHECK-NMR: Programs for checking the quality of protein structures solved by NMR. *J. Biomol. NMR* 8, 477–486.

(36) Koradi, R., Billeter, M., and Wüthrich, K. (1996) MOLMOL: A program for display and analysis of macromolecular structures. *J. Mol. Graphics* 14, 51–55, 29–32.

(37) Zhang, M. M., Green, B. R., Catlin, P., Fiedler, B., Azam, L., Chadwick, A., Terlau, H., McArthur, J. R., French, R. J., Gulyas, J., Rivier, J. E., Smith, B. J., Norton, R. S., Olivera, B. M., Yoshikami, D., and Bulaj, G. (2007) Structure/function characterization of μ -conotoxin KIIIA, an analgesic, nearly irreversible blocker of mammalian neuronal sodium channels. *J. Biol. Chem.* 282, 30699–30706.

(38) West, P. J., Bulaj, G., Garrett, J. E., Olivera, B. M., and Yoshikami, D. (2002) μ -Conotoxin SmIIIa, a potent inhibitor of tetrodotoxin-resistant sodium channels in amphibian sympathetic and sensory neurons. *Biochemistry* 41, 15388–15393.

(39) Wilson, M. J., Yoshikami, D., Azam, L., Gajewiak, J., Olivera, B. M., Bulaj, G., and Zhang, M. M. (2011) μ -Conotoxins that differentially block sodium channels Na_v1.1 through 1.8 identify those responsible for action potentials in sciatic nerve. *Proc. Natl. Acad. Sci. U.S.A.* 108, 10302–10307.

(40) Norton, R. S. (2010) μ -Conotoxins as leads in the development of new analgesics. *Molecules* 15, 2825–2844.

(41) Corpuz, G. P., Jacobsen, R. B., Jimenez, E. C., Watkins, M., Walker, C., Colledge, C., Garrett, J. E., McDougal, O., Li, W., Gray, W. R., Hillyard, D. R., Rivier, J., McIntosh, J. M., Cruz, L. J., and Olivera, B. M. (2005) Definition of the M-conotoxin superfamily: Characterization of novel peptides from molluscivorous *Conus* venoms. *Biochemistry* 44, 8176–8186.

(42) Jacob, R. B., and McDougal, O. M. (2010) The M-superfamily of conotoxins: A review. *Cell. Mol. Life Sci.* 67, 17–27.

(43) Yanagawa, Y., Abe, T., Satake, M., Odani, S., Suzuki, J., and Ishikawa, K. (1988) A novel sodium channel inhibitor from *Conus geographus*: Purification, structure, and pharmacological properties. *Biochemistry* 27, 6256–6262.

(44) Cruz, L. J., Kupryszewski, G., LeCheminant, G. W., Gray, W. R., Olivera, B. M., and Rivier, J. (1989) μ -Conotoxin GIIIA, a peptide

ligand for muscle sodium channels: Chemical synthesis, radiolabeling, and receptor characterization. *Biochemistry* 28, 3437–3442.

(45) Hidaka, Y., Sato, K., Nakamura, H., Kobayashi, J., Ohizumi, Y., and Shimonishi, Y. (1990) Disulfide pairings in geographutoxin I, a peptide neurotoxin from *Conus geographus*. *FEBS Lett.* 264, 29–32.

(46) Favreau, P., Benoit, E., Hocking, H. G., Carlier, L., D'hoedt, D., Leipold, E., Markgraf, R., Schlumberger, S., Córdova, M. A., Gaertner, H., Paolini-Bertrand, M., Hartley, O., Tytgat, J., Heinemann, S. H., Bertrand, D., Boelens, R., Stocklin, R., and Molgó, J. (2012) A novel μ -conopeptide, CnIIIC, exerts potent and preferential inhibition of $\text{Na}_v1.2/1.4$ channels and blocks neuronal nicotinic acetylcholine receptors. *Br. J. Pharmacol.* 166, 1654–1668.

(47) Tietze, A. A., Tietze, D., Ohlenschlager, O., Leipold, E., Ullrich, F., Kuhl, T., Mischo, A., Buntkowsky, G., Gorlach, M., Heinemann, S. H., and Imhof, D. (2012) Structurally diverse μ -conotoxin PIIIA isomers block sodium channel $\text{Na}_v1.4$. *Angew. Chem., Int. Ed.* 51, 4058–4061.

(48) Bulaj, G., and Olivera, B. M. (2008) Folding of conotoxins: Formation of the native disulfide bridges during chemical synthesis and biosynthesis of *Conus* peptides. *Antioxid. Redox Signaling* 10, 141–155.

(49) Safavi-Hemami, H., Gorasia, D. G., Steiner, A. M., Williamson, N. A., Karas, J. A., Gajewiak, J., Olivera, B. M., Bulaj, G., and Purcell, A. W. (2012) Modulation of conotoxin structure and function is achieved through a multienzyme complex in the venom glands of cone snails. *J. Biol. Chem.* 287, 34288–34303.

(50) Dutton, J. L., Bansal, P. S., Hogg, R. C., Adams, D. J., Alewood, P. F., and Craik, D. J. (2002) A new level of conotoxin diversity, a non-native disulfide bond connectivity in α -conotoxin AuIB reduces structural definition but increases biological activity. *J. Biol. Chem.* 277, 48849–48857.

(51) Gehrmann, J., Alewood, P. F., and Craik, D. J. (1998) Structure determination of the three disulfide bond isomers of α -conotoxin GI: A model for the role of disulfide bonds in structural stability. *J. Mol. Biol.* 278, 401–415.

(52) Khoo, K. K., Wilson, M. J., Smith, B. J., Zhang, M. M., Gulyas, J., Yoshikami, D., Rivier, J. E., Bulaj, G., and Norton, R. S. (2011) Lactam-stabilized helical analogues of the analgesic μ -conotoxin KIIIA. *J. Med. Chem.* 54, 7558–7566.

(53) DeLano, W. L. (2002) *The PyMOL Molecular Graphics System*, DeLano Scientific, San Carlos, CA.

Supplementary Material

Distinct disulfide isomers of μ -conotoxins KIIIA and KIIIB block voltage-gated sodium channels

Keith K. Khoo,^{†,‡,§} Kallol Gupta,^{||} Brad R. Green,[†] Min-Min Zhang,[±] Maren Watkins,[±] Baldomero M. Olivera,[±] Padmanabhan Balaram,^{||} Doju Yoshikami,[±] Grzegorz Bulaj,[@] and Raymond S. Norton^{†,*}

[†] Medicinal Chemistry, Monash Institute of Pharmaceutical Sciences, Monash University, 381 Royal Parade, Parkville VIC 3052, Australia

[‡] The Walter & Eliza Hall Institute of Medical Research, 1G Royal Parade, Parkville, VIC 3052, Australia

[§] The Department of Medical Biology, The University of Melbourne, Parkville, Victoria 3010, Australia

^{||} Molecular Biophysics Unit, Indian Institute of Science, Bangalore, 560 012, India

[±] Department of Biology, University of Utah, Salt Lake City, Utah 84112, USA

[@] Department of Medicinal Chemistry, College of Pharmacy, University of Utah, Salt Lake City, Utah 84108, USA

Table S1. Sequences of the M-4 and M-5 branches of the μ -conotoxin superfamily

Conotoxin	Sequence	Reference
M-4 branch		
μ -GIIIA	RD CC TOOKK- CK DR QC KOQR- CCA *	Cruz <i>et al.</i> (1985) (1)
μ -GIIIB	RD CC TOORK- CK DR RC KOMK- CCA *	Cruz <i>et al.</i> (1985) (1)
μ -TIIIA	RHG CC KGOKG- CSS RE CR OQH- CC *	Lewis <i>et al.</i> (2007) (2)
μ -PIIIA	ZRL CC GFOKS- CR SR QC KOHR- CC *	Safo <i>et al.</i> (2000) (3)
μ -SxIIIA	R CC TGKKGS CS GR AC KNLK- CCA *	Walewska <i>et al.</i> (2008) (4)
M-5 branch		
μ -KIIIA	CC -N---- CSS KW CR DHS RCC *	Bulaj <i>et al.</i> (2005) (5)
μ -KIIIB	NG CC -N---- CSS KW CR DHS RCC *	This work
μ -SIIIA	ZN CC -NG-- GCSS KW CR DH ARCC *	Bulaj <i>et al.</i> (2005) (5)
μ -SmIIIA	ZR CC -NGRR GCSS RW CR DHS RCC *	West <i>et al.</i> (2002) (6)
μ -CnIIIC	ZG CC -NGPK GCSS KW CR DH ARCC *	Favreau <i>et al.</i> (2012) (7)
μ -BuIIIB	VGER CC KNGKRG CG -RW CR DHS RCC *	Holford <i>et al.</i> (2009) (8)

Table S2. Prepropeptide sequences of μ -conotoxins determined from cDNA clones. □ indicates putative cleavage site to produce the mature conotoxin sequence, which is underlined.

Conotoxin	Sequence	Ref.
μ -PIIIA	MMSKLGVLLTTCLLLLFPITALPMDGDPADRLAERMQDNISSEHPF EKR □ <u>QRLLCCGFPKSCRSRQCKP</u> <u>HRCCGR</u>	Corpuz <i>et al.</i> (2005) (9)
μ -SIIIA	MMSKLGVLLTTCLLLLFPALTALPMDQPADQLEDRMQDDISSEQYPS FVRR □ <u>QKCCGEGSSCPKYFKNNFICGCC</u>	Wang <i>et al.</i> (2006) (10)
μ -BullIB	MMSKLGVLLTTCLLLLFPALFALPQDGPADRPAPERMQDDISSEQNP LLEKR □ <u>VGEFCCKNGKRGCGRWCRDHSRCCGRR</u>	Holford <i>et al.</i> (2009) (8)
μ -GIIIA	MMSKLGVLLTTCLLLLFPALTALPMDGDEFANRPVERMQDNISSEQYPL EKR □ <u>RDCCTPPKKCKDRQCKPQRCCAGR</u>	Corpuz <i>et al.</i> (2005) (9)
μ -KIIIB	-----KR□ <u>NGCCN</u> ----- <u>---CSSKWCARDHSRCCGR</u>	This work

In addition to the two major disulfide isomers characterized in this paper, the biological activity and structure of the disulfide-deficient analog μ -KIIIA[C1A,C9A], which has the [C2-C15,C4-C16] disulfide connectivity, were characterized previously.²² Intercysteine NOEs observed for the previously published structures of this analog and μ -KIIIA²² are summarized in Table S3. For μ -KIIIA, disulfide connectivities could not be determined unambiguously except for the [C4-C16] connectivity, with an NOE observed between C ^{α} H of Cys16 and C ^{β} H of Cys4. C ^{β} H-C ^{β} H NOEs from Cys2 to Cys9 could be overlapped with sequential NOEs between Arg10 C ^{α} H and Cys9 C ^{β} H. In contrast, intercysteine NOEs were more clearly defined for the μ -KIIIA[C1A,C9A] analog, in which only two disulfide bonds were present. In addition to intercysteine NOEs observed between Cys4 and Cys16, C ^{β} H-C ^{β} H NOEs between Cys2 and Cys15 were observed for this analog, thus defining its disulfide connectivity.

Table S3. Intercysteine NOEs observed for μ -KIIIA and μ -KIIIA[C1A,C9A]. * indicates undetermined intensity due to overlap with other cross peaks. + in parentheses indicates intensity of the NOE.

μ -KIIIA

Disulfide	HA-HA	HA-HB	HB-HB	HN-HB	Antidiagnostic HN-HA
C1-C15	-	-	HB2 1 – HB2 15 (*)	-	-
C2-C9	-	-	HB2 2 – HB2 9 (*) HB2 2 – HB3 9 (*)	-	-
C4-C16	-	HA 16 – HB3 4 (+)	HB2 16 – HB2 4 (*) HB2 16 – HB3 4 (*)	-	-

μ -KIIIA[C1A,C9A]

Disulfide	HA-HA	HA-HB	HB-HB	HN-HB	Antidiagnostic HN-HA
C2-C15	-	HA 2 – HB2 15 (*) HA 2 – HB3 15 (*)	HB2 15 – HB3 2 (++)	-	-
C4-C16	-	HA 16-HB3 4 (+)	HB2 16 – HB2 4 (++) HB2 16 – HB3 4 (+)	-	-

Table S4. Block of Nav1.2, 1.4 and 1.7 by μ -KIII A-P2.^a

Nav subtypes	k_{off} (min^{-1})	k_{on}^b ($\mu\text{M}\cdot\text{min}$)⁻¹	K_d^c (μM)
Nav1.2	0.0044 \pm 0.0023	0.019 \pm 0.002	0.23 \pm 0.12
Nav1.4	0.083 \pm 0.026	0.1 \pm 0.02	0.83 \pm 0.31
Nav1.7	0.011 \pm 0.001	0.007 \pm 0.004	1.57 \pm 0.91

^a Values (mean \pm S.D, $n \geq 3$ oocytes) were obtained by two-electrode voltage clamp of *Xenopus* oocytes expressing rat Nav1 channels as described in Methods and Materials. ^b From $[k_{\text{obs}} - k_{\text{off}}] / 10\mu\text{M}$. ^c From $k_{\text{off}}/k_{\text{on}}$.

Determination of disulfide connectivity of μ -KIIIB isomer.

The MS² spectrum of μ -KIIIB-P2 shows an identical spectrum to that of peak1 and peak2 of μ -KIIIA (Figure S3), with the exception of the ions containing the N-terminal Asn-Gly. In a similar manner, only two foldamers (F11, F14) fit all the MS² fragment ions. Subsequent MS³ fragmentation of 1100.5, which is identical in structure with 929.5 of μ -KIIIA (with the N-terminal extension), reveal the disulfide connectivity. Beside the N-terminal residue losses, giving rise to 986.3 and 929.3, ions at m/z 843.1 and 656.1 are observed, as in the MS³ spectrum of 929.3 in μ -KIIIA-P1. As in the case of μ -KIIIA-P1, the ion 656.1 clarifies the unambiguous assignment of the disulfide connectivity. In this case, ambiguity arising through the relatively low intensity of 656.1 is eliminated by the MS⁴ fragmentation of 843.1 that shows the presence of the same ion. The scheme of events is summarized in Figure S4. An identical MS² spectra for Peak-1 of μ -KIIIB (Figure S5), leaves again F11 and 14 as the two probable foldamers. As F11 has already been assigned to P2, the disulfide connectivity of μ -KIIIB-P1 is therefore assigned as F14.

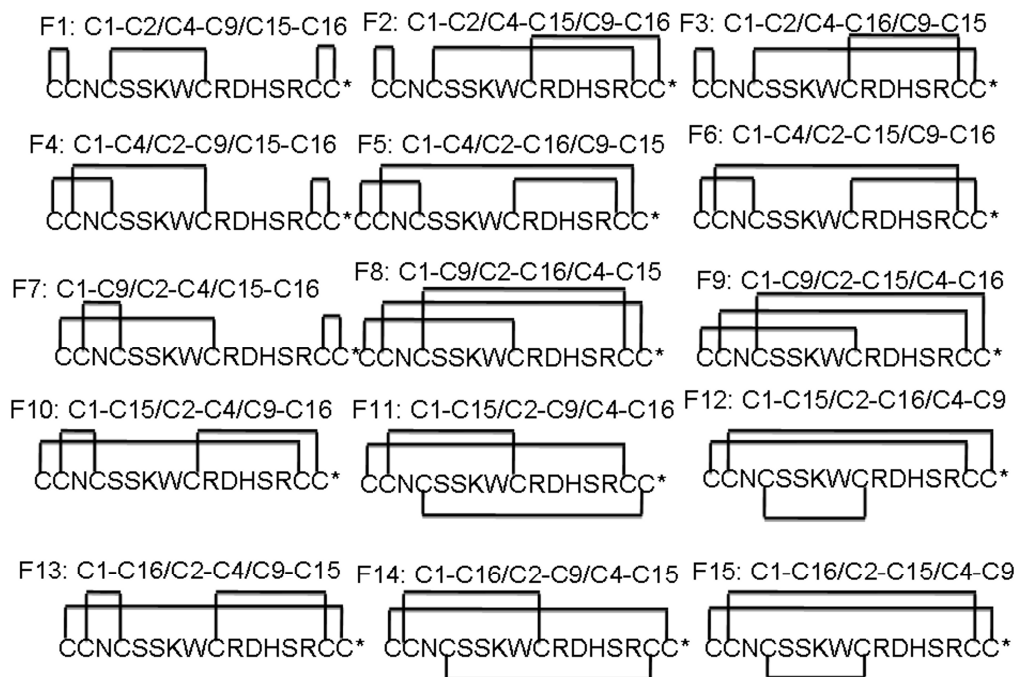


Figure S1. 15 possible foldamers of μ -KIIIA-P1

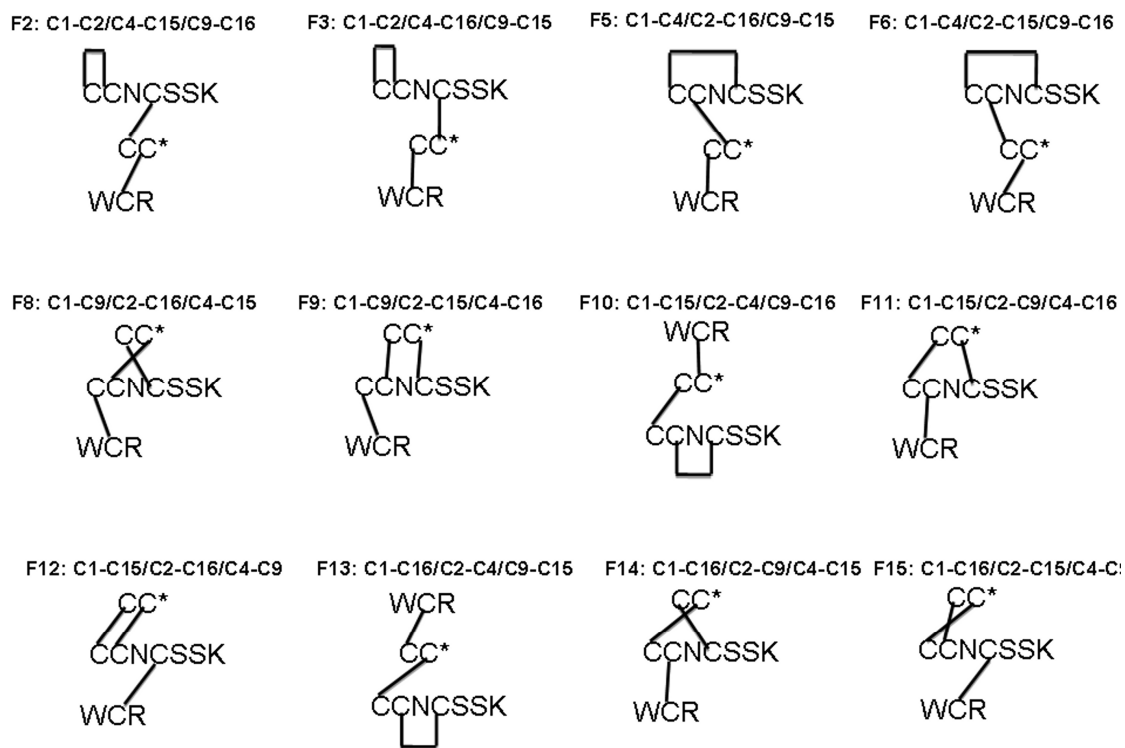


Figure S2. 12 possible foldamers of μ -KIIIA-P1 upon trypsin digestion

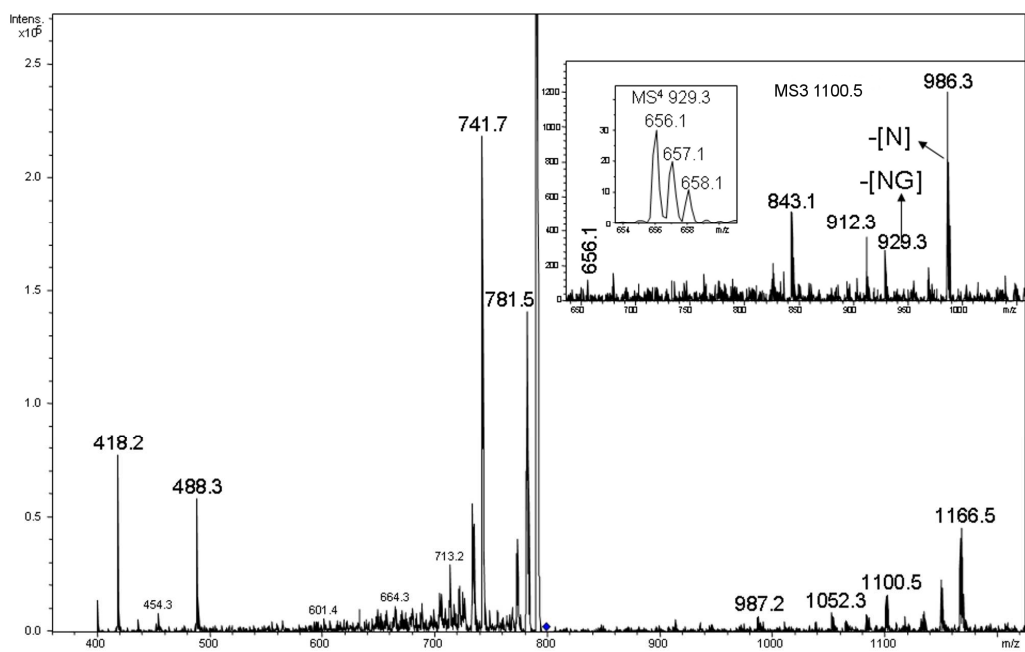


Figure S3. CID MS² spectrum of the peptide derived upon trypsin digestion of μ -KIIIB-P2. Inset shows the MS³ spectra of 1101.5 and MS⁴ of 843.1.

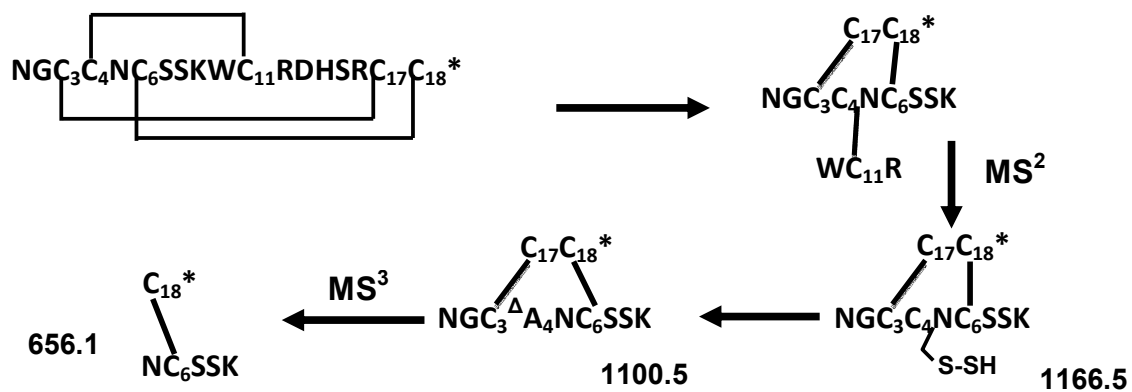


Figure S4. Assignments of the key MS^n fragment ions of tryptic μ -KIIIB-P2.

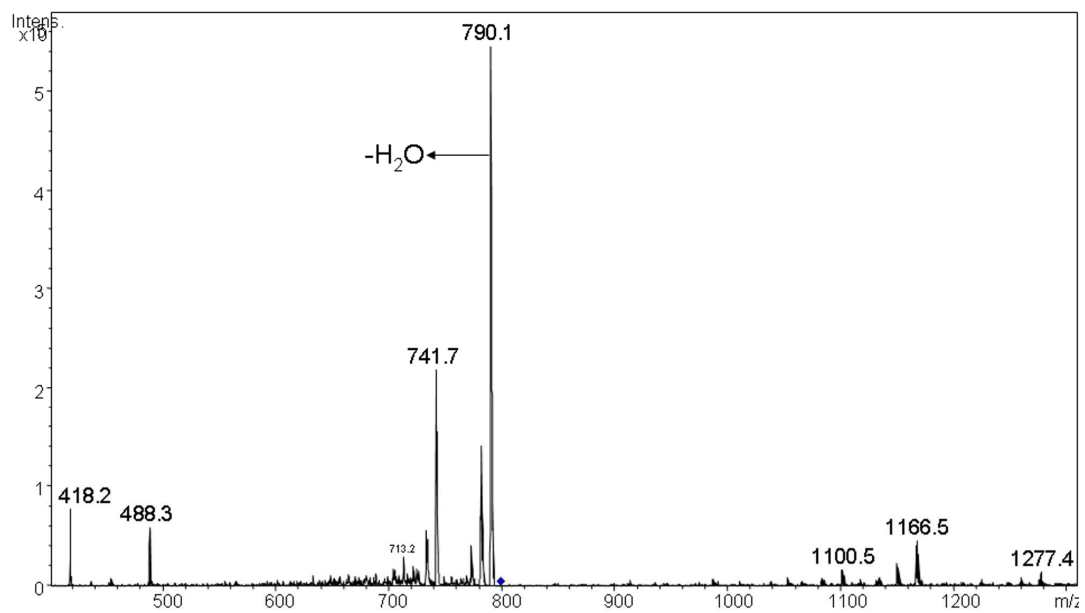


Figure S5. CID MS² spectrum of the peptide derived upon trypsin digestion of μ -KIIIB-P1.

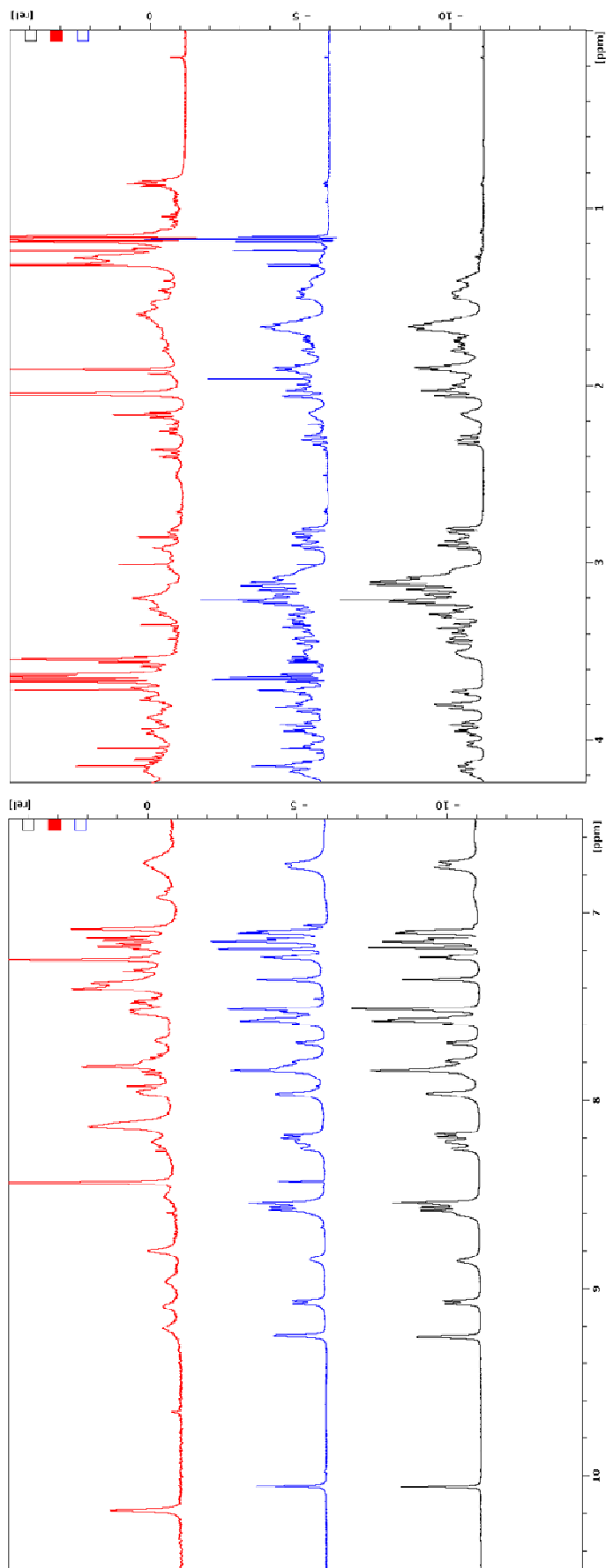


Figure S6. 1D ^1H NMR spectra of $\mu\text{-KIIIA-P1}$ (blue) and $\mu\text{-KIIIA-P2}$ (red) recorded at 5 $^\circ\text{C}$, pH 4.8 on a Bruker-DRX 600 spectrometer, compared with $\mu\text{-KIIIA}$ sample (black) for which solution structure was determined previously by Khoo *et al.* Left panel displays the amide region, right panel the aliphatic region.

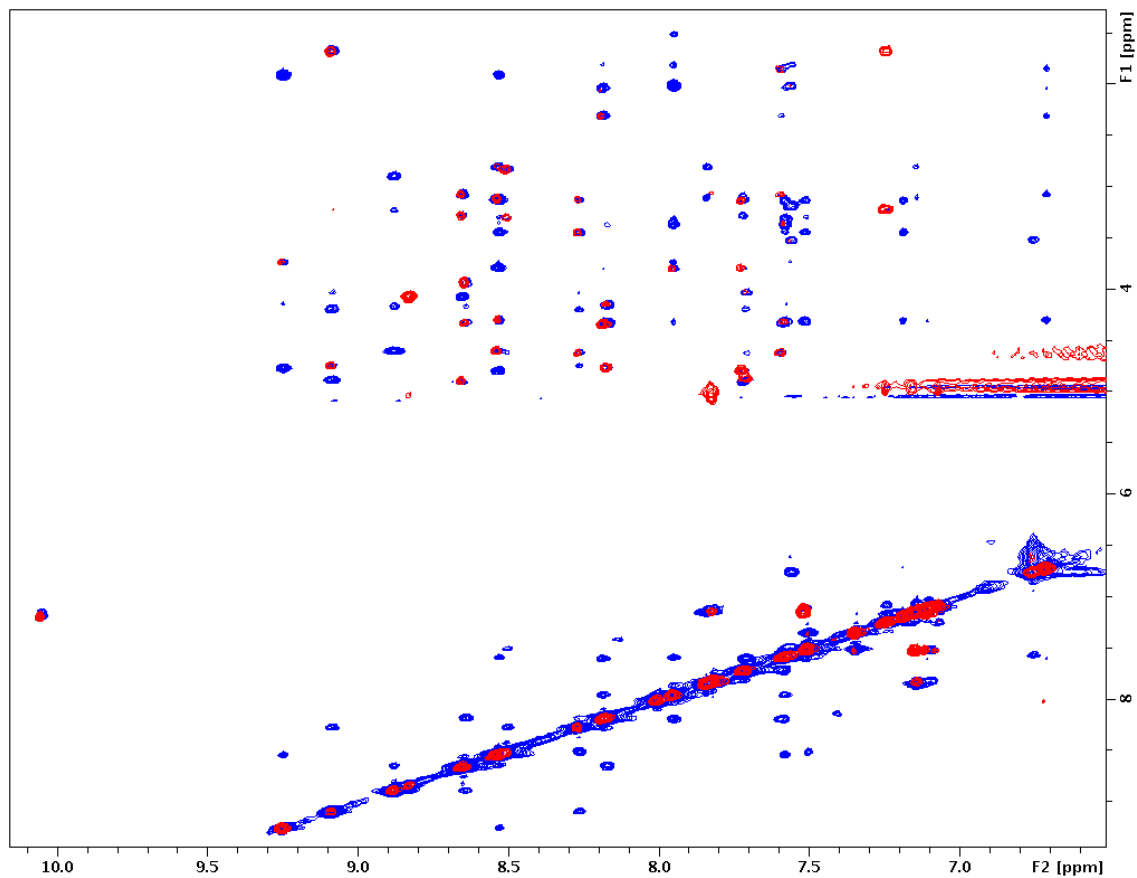


Figure S7. Amide and aromatic region of NOESY spectrum (blue) overlaid with TOCSY spectrum (red) for μ -KIIIB-P2 (at 5 °C and pH 4.8). NOESY (250 ms mixing time) and TOCSY (70 ms spin-lock time) spectra were acquired on a Bruker DRX-600 spectrometer.

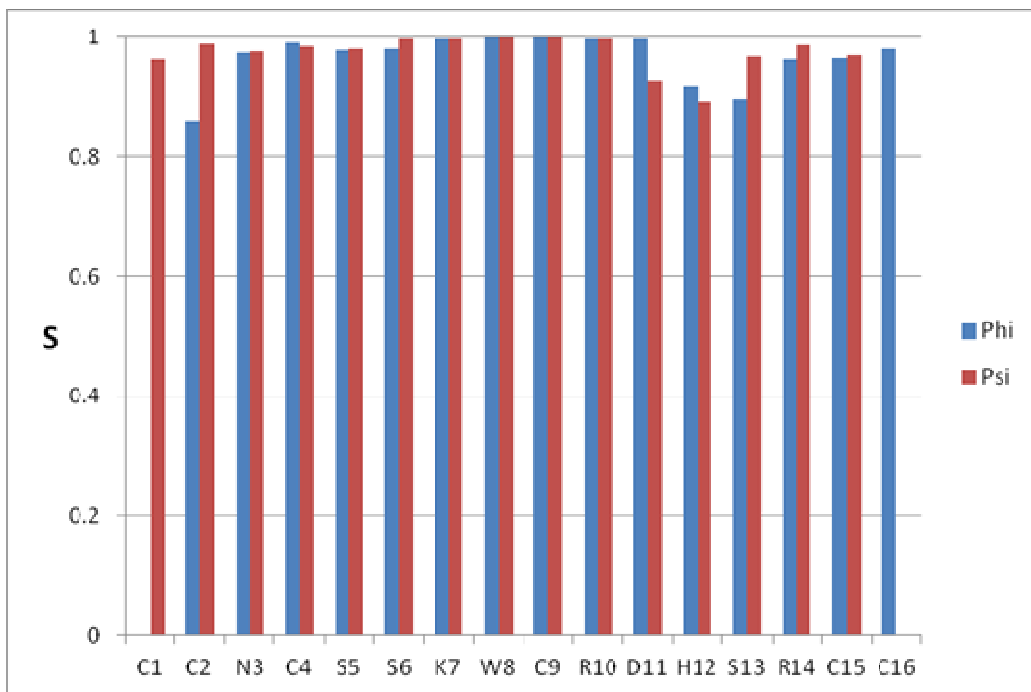


Figure S8. Angular order parameters (S) for the final 20 structures of μ -KIIIA[C1-C15,C2-C9,C4-C16] measured using MOLMOL for ϕ (blue) and ψ (red) backbone dihedral angles plotted as a function of residue.

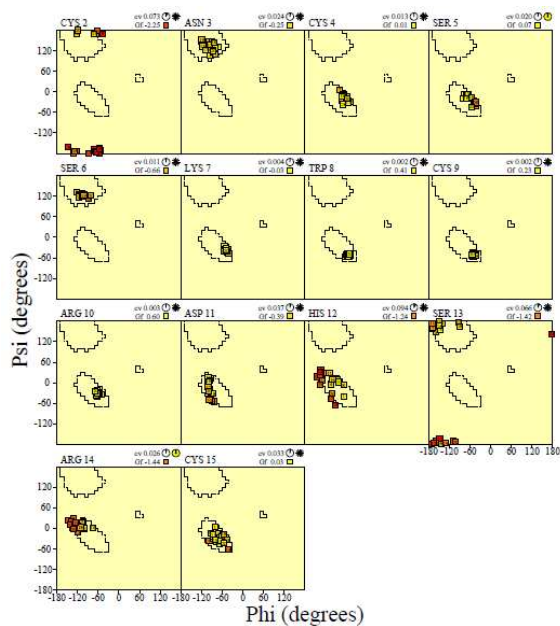
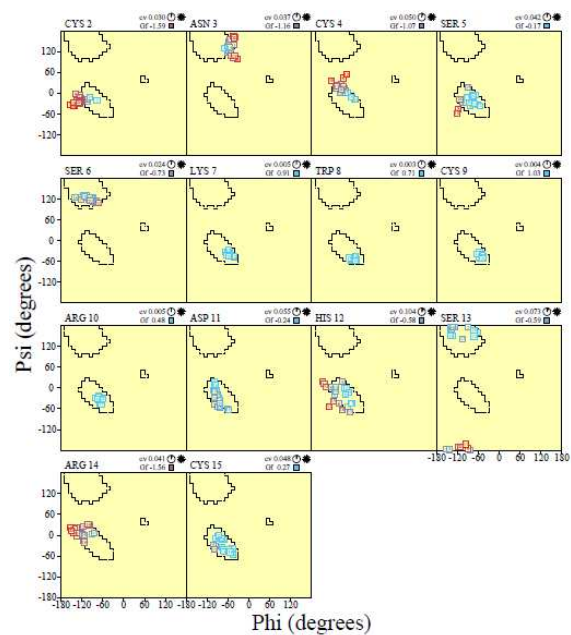


Figure S9. Residue Ramachandran plots of family of structures of μ -KIIIA[C1-C9,C2-C15,C4-C16] (top) and μ -KIIIA[C1-C15,C2-C9,C4-C16] (bottom)

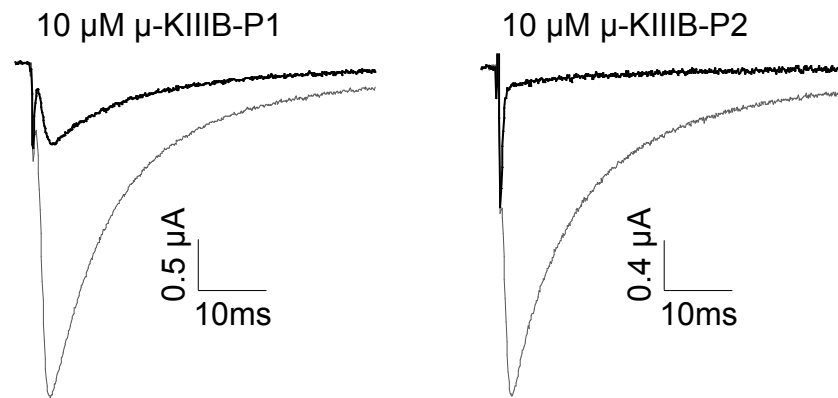


Figure S10. Representative sodium-current traces from voltage-clamped oocytes expressing rat Nav1.2. μ -KIIIB-P1 (left) and μ -KIIIB-P2 (right) were each tested at a concentration of 10 μ M. Each panel shows superimposed recordings before (control, *gray trace*) and after (*black trace*) 20-min exposure to the indicated peptide.

References

- (1) Cruz, L. J., Gray, W. R., Olivera, B. M., Zeikus, R. D., Kerr, L., Yoshikami, D., and Moczydlowski, E. (1985) *Conus geographus* toxins that discriminate between neuronal and muscle sodium channels, *J Biol Chem* 260, 9280-9288.
- (2) Lewis, R. J., Schroeder, C. I., Ekberg, J., Nielsen, K. J., Loughnan, M., Thomas, L., Adams, D. A., Drinkwater, R., Adams, D. J., and Alewood, P. F. (2007) Isolation and structure-activity of μ -conotoxin TIIIA, a potent inhibitor of tetrodotoxin-sensitive voltage-gated sodium channels, *Mol Pharmacol* 71, 676-685.
- (3) Safo, P., Rosenbaum, T., Shcherbatko, A., Choi, D. Y., Han, E., Toledo-Aral, J. J., Olivera, B. M., Brehm, P., and Mandel, G. (2000) Distinction among neuronal subtypes of voltage-activated sodium channels by μ -conotoxin PIIIA, *J Neurosci* 20, 76-80.
- (4) Walewska, A., Skalicky, J. J., Davis, D. R., Zhang, M. M., Lopez-Vera, E., Watkins, M., Han, T. S., Yoshikami, D., Olivera, B. M., and Bulaj, G. (2008) NMR-based mapping of disulfide bridges in cysteine-rich peptides: application to the μ -conotoxin SxIIIA, *J Am Chem Soc* 130, 14280-14286.
- (5) Bulaj, G., West, P. J., Garrett, J. E., Watkins, M., Zhang, M. M., Norton, R. S., Smith, B. J., Yoshikami, D., and Olivera, B. M. (2005) Novel conotoxins from *Conus striatus* and *Conus kinoshitai* selectively block TTX-resistant sodium channels, *Biochemistry* 44, 7259-7265.
- (6) West, P. J., Bulaj, G., Garrett, J. E., Olivera, B. M., and Yoshikami, D. (2002) μ -conotoxin SmIIIA, a potent inhibitor of tetrodotoxin-resistant sodium channels in amphibian sympathetic and sensory neurons, *Biochemistry* 41, 15388-15393.
- (7) Favreau, P., Benoit, E., Hocking, H. G., Carlier, L., D, D. H., Leipold, E., Markgraf, R., Schlumberger, S., Cordova, M. A., Gaertner, H., Paolini-Bertrand, M., Hartley, O., Tytgat, J., Heinemann, S. H., Bertrand, D., Boelens, R., Stocklin, R., and Molgo, J. (2012) A novel μ -conopeptide, CnIIIC, exerts potent and preferential inhibition of Na(V) 1.2/1.4 channels and blocks neuronal nicotinic acetylcholine receptors, *Br J Pharmacol* 166, 1654-1668.
- (8) Holford, M., Zhang, M. M., Gowd, K. H., Azam, L., Green, B. R., Watkins, M., Ownby, J. P., Yoshikami, D., Bulaj, G., and Olivera, B. M. (2009) Pruning nature: Biodiversity-derived discovery of novel sodium channel blocking conotoxins from *Conus bullatus*, *Toxicon* 53, 90-98.
- (9) Corpuz, G. P., Jacobsen, R. B., Jimenez, E. C., Watkins, M., Walker, C., Colledge, C., Garrett, J. E., McDougal, O., Li, W., Gray, W. R., Hillyard, D. R., Rivier, J., McIntosh, J. M., Cruz, L. J., and Olivera, B. M. (2005) Definition of the M-conotoxin superfamily: characterization of novel peptides from molluscivorous *Conus* venoms, *Biochemistry* 44, 8176-8186.
- (10) Wang, C. Z., Zhang, H., Jiang, H., Lu, W., Zhao, Z. Q., and Chi, C. W. (2006) A novel conotoxin from *Conus striatus*, μ -SIIIA, selectively blocking rat tetrodotoxin-resistant sodium channels, *Toxicon* 47, 122-132.

Appendix II

A Disulfide Tether Stabilizes the Block of Sodium Channels by the Conotoxin $\mu\text{O}\xi\text{-GVIII}$

Appendix II provides the historical context of the studies detailed in Chapter 6. The discovery and characterization of a recently identified inhibitor of VGSCs, $\mu\text{O}\xi\text{-conotoxin GVIII}$ are described in this section.

Appendix II consists of the following publication:

Gajewiak, J.; Azam, L.; Imperial, J.; Walewska, A.; **Green, B. R.**; Bandyopadhyay, P. K.; Raghuraman, S.; Ueberheide, B.; Bern, M.; Zhou, H. M.; Minassian, N. A.; Hagan, R. H.; Flinspach, M.; Liu, Y.; Bulaj, G.; Wickenden, A. D.; Olivera, B. M.; Yoshikami, D.; Zhang, M. M. A disulfide tether stabilizes the block of sodium channels by the conotoxin $\mu\text{O}\xi\text{-GVIII}$. *Proc. Natl. Acad. Sci. U.S.A.*, 2014, 111(7): 2758-2763.

A disulfide tether stabilizes the block of sodium channels by the conotoxin $\mu\text{O}\delta\text{-GVIIJ}$

Joanna Gajewiak^a, Layla Azam^a, Julita Imperial^a, Aleksandra Walewska^{a,1}, Brad R. Green^a, Pradip K. Bandyopadhyay^a, Shrinivasan Raghuraman^a, Beatrix Ueberheide^b, Marshall Bern^c, H. Mimi Zhou^d, Natali A. Minassian^d, Rebecca H. Hagan^d, Mack Flinspach^d, Yi Liu^d, Grzegorz Bulaj^e, Alan D. Wickenden^d, Baldomero M. Olivera^{a,2}, Doju Yoshikami^{a,2}, and Min-Min Zhang^a

^aDepartment of Biology and ^eDepartment of Medicinal Chemistry, L. S. Skaggs Pharmacy Institute, University of Utah, Salt Lake City, UT 84112; ^bNew York University Langone Medical Center, New York, NY 10016; ^cProtein Metrics Inc., San Carlos, CA 94070; and ^dJanssen Research and Development, LLC, San Diego, CA 92121

Contributed by Baldomero M. Olivera, December 31, 2013 (sent for review December 1, 2013)

A cone snail venom peptide, $\mu\text{O}\delta\text{-conotoxin GVIIJ}$ from *Conus geographus*, has a unique posttranslational modification, S-cysteinylation of cysteine, which makes possible formation of a covalent tether of peptide to its target Na channels at a distinct ligand-binding site. $\mu\text{O}\delta\text{-conotoxin GVIIJ}$ is a 35-aa peptide, with 7 cysteine residues; six of the cysteines form 3 disulfide cross-links, and one (Cys24) is S-cysteinylation. Due to limited availability of native GVIIJ, we primarily used a synthetic analog whose Cys24 was S-glutathionylated (abbreviated GVIIJ_{SSG}). The peptide-channel complex is stabilized by a disulfide tether between Cys24 of the peptide and Cys910 of rat (r) Na_v1.2. A mutant channel of rNa_v1.2 lacking a cysteine near the pore loop of domain II (C910L), was >10³-fold less sensitive to GVIIJ_{SSG} than was wild-type rNa_v1.2. In contrast, although rNa_v1.5 was >10⁴-fold less sensitive to GVIIJ_{SSG} than Na_v1.2, an rNa_v1.5 mutant with a cysteine in the homologous location, rNa_v1.5[L869C], was >10³-fold more sensitive than wild-type rNa_v1.5. The susceptibility of rNa_v1.2 to GVIIJ_{SSG} was significantly altered by treating the channels with thiol-oxidizing or disulfide-reducing agents. Furthermore, coexpression of rNa_vβ2 or rNa_vβ4, but not that of rNa_vβ1 or rNa_vβ3, protected rNa_v1.1 to -1.7 (excluding Na_v1.5) against block by GVIIJ_{SSG}. Thus, GVIIJ-related peptides may serve as probes for both the redox state of extracellular cysteines and for assessing which Na_vβ- and Na_vα-subunits are present in native neurons.

disulfide exchange | Na_vβ-subunit | tethered toxin | voltage-gated sodium channel | S-cysteinylation

Voltage-gated sodium channels (VGSCs) are responsible for the upstroke of action potentials in excitable tissues. Each VGSC is composed of a pore- and voltage sensor-bearing α-subunit and one or more auxiliary β-subunits. Mammals have nine α-subunit isoforms (Na_v1.1 to -1.9) and four β-subunit isoforms (Na_vβ1 to -β4) (1). An Na_v1 has about 2,000-aa residues arranged in four homologous domains, where each domain has six transmembrane spanning segments with an extracellular “pore” loop between segments 5 and 6 (1, 2); furthermore, each Na_v1 has about a dozen extracellular cysteine residues, all located in or near the pore loops. For the most part, not much is known about these cysteines (including whether they are disulfide bonded).

Na_vβ-subunits can affect the function and cellular localization of Na_v1s (1, 3–5). Each Na_vβ-subunit has some 200-aa residues and consists of a single transmembrane segment with a large extracellular domain and a smaller intracellular domain (1). Na_vβ2- and Na_vβ4-subunits, unlike Na_vβ1- and Na_vβ3-subunits, are disulfide bonded to α-subunits (1, 6). A given neuron can have multiple isoforms of these subunits whose identities are challenging to appraise pharmacologically (7).

Toxins that target VGSCs have been invaluable for probing the structure and function of these channels. Venoms are a rich source of such toxins. For example, in *Conus* snails, four families of neuroactive peptides have been characterized that target

VGSCs: μ-conotoxins and μO-conotoxins, which block VGSCs by plugging the ion-conductance pore and preventing channel activation, respectively; and ι-conotoxins and δ-conotoxins, which promote channel activation and block channel inactivation, respectively. Members within each conotoxin family have homologous structures (8–10). We have used μ-conotoxins to assess Na_v1-isoforms (7, 11) and both μ- and μO-conotoxins to examine the pharmacological impact of Na_vβ-subunit coexpression (12, 13).

Previously unidentified μOδ-conotoxin GVIIJ is the founding member of a fifth family of VGSC-targeting conotoxins. It is unusual among conopeptides in that it has an odd number of Cys residues in its primary amino acid sequence (Fig. 1). We present evidence that it potently blocks Na_v1-channels and that its “extra” cysteine residue, Cys24, is disulfide bonded to an extracellular Cys residue in the peptide’s binding site on the channel, which we call “site 8” and which is distinct from previously identified neurotoxin-receptor sites 1 through 7 (14, 15).

Results

Discovery of μOδ-GVIIJ, Its Sequence, and Its Synthesis and That of Its Analogs. We discovered μOδ-GVIIJ by fractionating crude venom from *Conus geographus* by HPLC and assaying the eluate for activity against rNa_v1.7 exogenously expressed in *Xenopus laevis* oocytes (Fig. 1A). A partial sequence of the peptide was obtained by conventional means, and the complete sequence was obtained

Significance

A biochemically unique cone snail venom peptide has been characterized that may be used to probe unexplored but important features of the diverse voltage-gated Na channel isoforms that underlie electrical signaling in the nervous system. This peptide has a unique posttranslational modification (S-cysteinylation of cysteine) and blocks sodium channels by forming a disulfide bond with the channel at a distinctive binding site. Because block by the peptide is prevented when specific β-subunits are coexpressed, this neurotoxin has potential for assessing which β-subunits are present in native Na channels. Peptide activity depends on the oxidation state of extracellular Cys residues on the channel. Thus, this peptide can also be used to monitor the oxidation state of the targeted Na channels.

Author contributions: J.G., M.F., Y.L., G.B., A.D.W., B.M.O., D.Y., and M.-M.Z. designed research; J.G., L.A., J.I., A.W., B.R.G., P.K.B., S.R., B.U., H.M.Z., N.A.M., R.H.H., M.F., Y.L., and M.-M.Z. performed research; J.G., L.A., B.U., and M.B. contributed new reagents/analytic tools; J.G., L.A., J.I., P.K.B., S.R., B.U., Y.L., G.B., A.D.W., D.Y., and M.-M.Z. analyzed data; and J.G., L.A., J.I., A.W., P.K.B., B.U., Y.L., B.M.O., D.Y., and M.-M.Z. wrote the paper. H.M.Z., N.A.M., R.H.H., M.F., Y.L., and A.D.W. are full-time employees of Janssen Research and Development, LLC. G.B. is a scientific co-founder of NeuroAdjuvants, Inc.

¹Present address: Faculty of Chemistry, University of Gdansk, 80-308, Gdansk, Poland.

²To whom correspondence may be addressed. E-mail: olivera@biology.utah.edu or yoshikami@bioscience.utah.edu.

This article contains supporting information online at www.pnas.org/lookup/suppl/doi:10.1073/pnas.1324189111/-DCSupplemental.

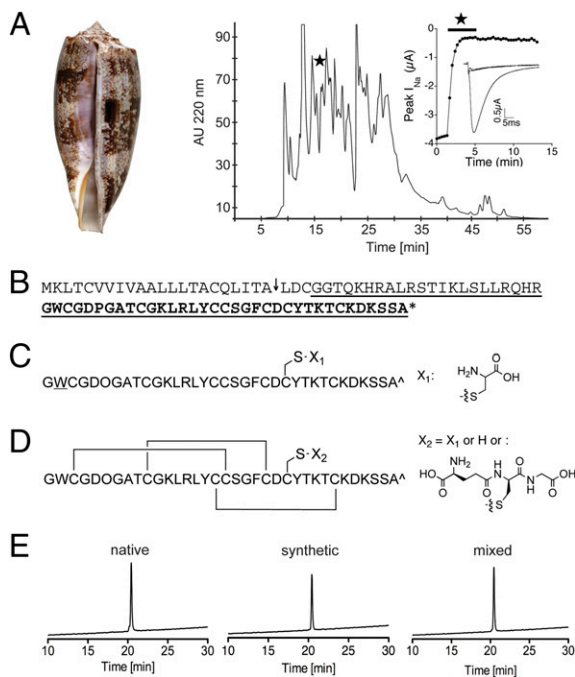


Fig. 1. Discovery of $\mu\text{O8-GVIIJ}$ from *Conus geographus*. (A) Photograph of *C. geographus* shell and RP-HPLC elution profile of *C. geographus* venom. The star indicates the area from where the native peptide was isolated. The *Inset* depicts the ability of the starred fraction to block sodium currents (I_{Na}) in an *X. laevis* oocyte expressing rNaV1.7 that was voltage clamped at -80 mV and I_{Na} evoked by a voltage step to -10 mV applied every 20 s (*Materials and Methods*): the major plot shows the time course of block (the bar represents when oocyte was exposed to the starred fraction)—note the very slow recovery from block when the fraction was washed out; the minor plot illustrates traces of I_{Na} before and during block (large and attenuated responses, respectively). The amount of material applied to oocyte (in a 30- μL bath) was an equivalent of 2 mg of starting crude venom. (B) The complete sequence of prepro GVIIJ from transcriptome. The arrow indicates the signal cleavage site predicted by Signal P; the underlined sequence was independently obtained from targeted PCR; the “LDC” sequence after the arrow is part of the propeptide; mature toxin is shown in bold; the asterisk indicates the stop codon. (C) Sequence and posttranslational modifications of native peptide determined by tandem mass spectrometry, where W is bromotryptophan (presumably L-6-bromoTrp, a residue also found in other *Conus* peptides) (35, 36), O is hydroxyproline, ^ indicates C-terminal free carboxyl group, and X_1 is cysteine (which is surmised to be disulfide bonded to the side-chain thiol of Cys24 based on the functional activities of synthetic analogs in D). (D) Synthetic analogs of GVIIJ with disulfide connectivities indicated by lines bridging Cys residues. X_2 represents glutathione (disulfide bonded to Cys24 in GVIIJ_{SSG}) or hydrogen (of the free thiol of Cys24 in GVIIJ_{SH}) or cysteine (disulfide bonded to Cys24 in GVIIJ_{SSG}). (E) RP-HPLC elution profiles of purified native GVIIJ (*Left*), synthetic GVIIJ (*Center*), and a mixture of both native and synthetic GVIIJ (*Right*) on an analytical C18 column with a gradient of 15–45% of solvent B (90% acetonitrile in 0.1% TFA) in 30 min at a flow rate of 1 mL/min. Methods and additional results are provided in *SI Materials and Methods*, Figs. S1–S3, Tables S1 and S2, and *SI Appendix*.

by searching the transcriptome of *C. geographus* (16) for sequences homologous to that of the peptide (Fig. 1B). Tandem mass spectrometry confirmed the sequence and identified three post-translationally modified residues: bromotryptophan, hydroxyproline, and S-cysteinylated cysteine (Fig. 1C and Figs. S2 and S3). Because of limited availability of the native peptide, most of the experiments were done with the two derivatives: GVIIJ[W2W; C24C(glutathione)] and GVIIJ[W2W; C24C(free thiol)], hereafter referred to as GVIIJ_{SSG} and GVIIJ_{SH}, respectively (Fig. 1D). Like the native peptide $\mu\text{O8-GVIIJ}$, the GVIIJ_{SSG} analog has Cys24 in a disulfide linkage whereas the GVIIJ_{SH} analog’s Cys24 is in the

free thiol form; thus, GVIIJ_{SH} served as a reference to help investigate the role of the disulfide-bonded modification of Cys24.

GVIIJ_{SSG} and GVIIJ_{SH} Readily Block Six of Eight Na_v1-Isoforms Tested.

GVIIJ_{SSG} blocked the voltage-gated currents (I_{Na}) of all tetrodotoxin-sensitive rNa_v1-subtypes (Na_v1.1 to -1.4, -1.6, and -1.7) with $K_{1/2}$ s ranging from 5 to 360 nM whereas the IC_{50} for rNa_v1.5 was >200 μM (Table S3). No block of rNa_v1.8 was observed at 100 μM , the highest concentration of the peptide tested. Similar results were obtained with human (h) Na_v1-subtypes stably expressed in human embryonic kidney (HEK) 293 or Chinese hamster ovary (CHO) cell lines (Table S4).

GVIIJ_{SSG} and GVIIJ_{SH} were extensively tested on oocytes expressing rNa_v1.2. The recovery from block by GVIIJ_{SSG} was invariably only very slowly reversible following washout of peptide (Fig. 2A and Table S3) whereas the recovery from block by GVIIJ_{SH} usually had two phases (Fig. 2B), a very rapid phase and a much slower phase ($k_{\text{off}} = 2.0 \pm 0.2$ s^{-1} and 0.004 ± 0.003 s^{-1} (mean \pm SD, $n = 6$ oocytes, respectively); the latter value is statistically the same as the k_{off} of GVIIJ_{SSG} (Table S3) ($P = 0.57$). The native $\mu\text{O8-GVIIJ}$ behaved like GVIIJ_{SSG} insofar as its block of Na_v1.7 reversed very slowly (Figs. 1A and 2A and Table S3).

Treating Channels with Thiol Oxidizing and Reducing Agents Has Reciprocal Effects on GVIIJ_{SSG} Versus GVIIJ_{SH}.

The structures and activities of GVIIJ_{SSG} and GVIIJ_{SH} suggested that they might interact, respectively, with a thiol and disulfide group on the channel. This possibility was explored by exposing oocytes expressing rNa_v1.2 to two reagents that induce free thiols to form disulfide bonds [MTSET and Cu^{2+} -phenanthroline (CuPhen); see last paragraph in this section] and one reagent (DTT) that reduces disulfides to free thiols.

The methanethiosulfonate (MTS) derivative $\text{CH}_3\text{SO}_2\text{SCH}_2\text{CH}_2\text{NMe}_3^+$ (or MTSET) oxidizes thiols upon disulfide-bond formation with $-\text{SCH}_2\text{CH}_2\text{NMe}_3^+$ (or ET) (17). Thus, MTSET treatment results in the attachment of an exogenous group, ET, to accessible free thiols on the channel via a disulfide bond. MTSET treatment completely protected the channel against block by GVIIJ_{SSG} (Fig. 2C). This protection was reversed by subsequent treatment of the oocytes with DTT (Fig. 2C). In contrast to the protection against GVIIJ_{SSG}, MTSET treatment of the oocytes converted the reversible block by GVIIJ_{SH} to one that was exclusively very slowly reversible (Fig. 2D), similar to that of GVIIJ_{SSG} on untreated oocytes (Fig. 2A).

At saturating concentrations, the level of block by GVIIJ_{SSG} was smaller and more variable than that by GVIIJ_{SH}; however, the block by GVIIJ_{SSG} was made less variable and increased to that by GVIIJ_{SH} by treatment of oocytes with DTT (Fig. 3B). The relative magnitude of the slow phase of recovery from block by GVIIJ_{SH} varied from oocyte to oocyte (e.g., Fig. 2B and D), and for a given oocyte it increased as the exposure time to GVIIJ_{SH} increased (Fig. S4).

When oocytes were exposed to CuPhen, which catalyzes air oxidation of thiols (18, 19), the magnitude of block by GVIIJ_{SSG} was decreased (Fig. 3A, b and B), and its off-rate accelerated (Fig. 3A, b). In stark contrast, the main effect of CuPhen treatment on the block by GVIIJ_{SH} was to make its off-rate very slow (Fig. 3A, b'), similar to that following treatment with MTSET shown in Fig. 2D. (Note, unlike MTSET treatment, which adds an exogenous group to the free thiol of channel Cys residues, CuPhen-catalyzed air oxidation is expected to result in a disulfide linkage of two free thiol groups, presumably those of channel Cys residues that are in close proximity to each other.) Furthermore, the effects of CuPhen on the block by both peptides were largely reversed by subsequent treatment of oocytes with DDT (Fig. 3A, c and c'). The interactions between the peptides and the channel, modifiable by thiol-oxidizing and disulfide-reducing agents, are summarized in the hypothetical reaction scheme in Fig. 3C, which is described in detail in *Discussion*.

Mutating VGSCs Pinpoint the Location of a Cys Residue in the Binding Site (Site 8). To help identify the cysteine(s) in the channel's active site, the amino acid sequences of rNav_v1.1 to -1.8 and those of hNav_v1.1 to -1.7 were aligned, and the locations of extracellular Cys residues were compared. The sequences of all Nav_v1s that were highly sensitive to GVIIJ_{SSG} have Cys residues at 14 extracellular locations (which are at identical homologous positions, except for rNav_v1.4, which has one fewer Cys residue). By comparison, Nav_v1.5, which was very poorly blocked by the peptides, lacks three Cys residues located in the N-terminal region near the pore loop of domain II in the other Nav_v1-isoforms. We constructed two complementary chimeras from hNav_v1.7 and 1.5: chimera 7577 (composed of domain II of hNav_v1.5 in an otherwise hNav_v1.7 background) and the reciprocal chimera 5755. The latter, like hNav_v1.7, was sensitive to GVIIJ_{SH} whereas chimera 7577, like hNav_v1.5, was significantly less sensitive (Fig. S5), suggesting that one or more of these three cysteines may be involved in the peptide binding to the channel.

For rNav_v1.2, the trio of Cys residues in domain II are Cys910, Cys912, and Cys918, and the mutant rNav_v1.2[C910L] was made and tested. (Leu was chosen to replace Cys because Leu869 is the residue found at the homologous location of rNav_v1.5.) rNav_v1.2[C910L] was poorly blocked by both peptides (Fig. 2E and F and Table S3). Treatment of oocytes expressing rNav_v1.2[C910L] with MTSET had essentially no effect on the activity of either peptide (Fig. 2G and H), suggesting that Cys910 alone was largely responsible for the consequences of MTSET treatment of the wild-type channel seen in Fig. 2C and D.

The rNav_v1.5 mutant with a Cys replacing Leu869 near the pore loop of domain II, rNav_v1.5[L869C], was expressed in oocytes and found to be significantly more sensitive than wild-type rNav_v1.5 to both GVIIJ_{SSG} and GVIIJ_{SH} (Fig. 4). GVIIJ_{SSG} had a >10³ higher affinity for the mutant over the wild-type channel (Table S3). Furthermore, in contrast to the rapidly reversible block of rNav_v1.5 by both peptides (Fig. 4A and B), the block of rNav_v1.5[L869C] was slowly reversible, with GVIIJ_{SSG} being more slowly reversible than GVIIJ_{SH} (Fig. 4C and D). These results further substantiate the importance of a cysteine near the pore loop of domain II in the active site, site 8, of the channel.

The Binding Site of GVIIJ_{SSG} (Site 8) on Rat Nav_v1.2 Does Not Overlap with Those of TTX and μ -KIIIA[K7A] (Site 1) or μ O-MrVIB (Site 4). Identification of Cys910 of rNav_v1.2 as a critical residue for both GVIIJ_{SSG} and GVIIJ_{SH} activity suggests that μ O δ -conotoxins act at a site different from those of members of the two other families of conotoxins that also block VGSCs: namely, μ -conotoxins and μ O-MrVIA/B. As previously mentioned, Cys910 in Nav_v1.2 is near the pore loop of domain II; in contrast, μ -conotoxins and TTX bind at site 1, closer to the channel's ion-selectivity filter (14, 20, 21), and the binding site of μ O-MrVIA/B is near the voltage sensor of domain II (22, 23) (for reviews of neurotoxin receptor binding site designations, see refs. 14 and 15). Thus, TTX and μ - and μ O-conotoxins might not be expected to compete with GVIIJ_{SSG}. Lack of competition was experimentally verified with oocytes expressing rNav_v1.2 using TTX, μ -KIIIA[K7A], and μ O-MrVIB (Fig. S6). KIIIA[K7A] was used because, like TTX, it blocks by plugging the pore of the channel, but the plug is "leaky" (20, 24) and, at saturating concentrations of KIIIA[K7A], an ~25% residual current (I_{Na}) persists with Nav_v1.2. This I_{Na} was readily blocked by 3 μ M GVIIJ_{SSG} (Fig. S6B), indicating that these two toxins occupy different sites on the channel. It should be noted that μ -KIIIA has 16 residues and is among the smallest μ -conotoxins; furthermore, KIIIA or KIIIA[K7A] can simultaneously occupy site 1 with TTX (20, 24). It is possible a larger μ -conotoxin, such as μ -GIIIA (with 22 aa), might intrude into GVIIJ's binding space, insofar as mutation of cysteines near the pore loop of domain II of Nav_v1.4 homologous to Cys912 and 918 of Nav_v1.2 does affect μ -GIIIA binding to Nav_v1.4 (25) (see also ref. 26).

To test for competition between GVIIJ_{SSG} and μ O-MrVIB, we took advantage of the observation that strong depolarizing pulses

accelerate the slow off-rate MrVIB (12) (Fig. S6C, *Inset*), but not that of GVIIJ_{SSG} (Fig. S6C and D). After sequential addition of these two peptides, regardless of their order of addition, the level of block that remained after strong depolarizing pulses (which "chased off" MrVIB) was similar and essentially that produced by exposure to GVIIJ_{SSG} alone (Fig. S6C and D), which indicates that the two toxins do not share a common binding site.

Coexpression of Nav β 2 or Nav β 4 Protects VGSCs Against GVIIJ_{SH} and GVIIJ_{SSG}. We examined whether coexpression of rNav_v β 1- β 4 with various rNav_v1s affected the activity of GVIIJ_{SSG}. rNav_v1.7 coexpressed with either rNav_v β 1 or rNav_v β 3 was readily blocked by GVIIJ_{SSG} (Fig. 5A, B, and E and Table S3); in contrast, when coexpressed with either rNav_v β 2 or rNav_v β 4, rNav_v1.7 was completely resistant to block (Fig. 5C-E). Coexpression of rNav_v1.7 with binary combinations of rNav_v β 1 + rNav_v β 4 and rNav_v β 3 + rNav_v β 4 showed that expression of rNav_v β 4 was dominant in inducing resistance to block by GVIIJ_{SSG} (Fig. 5E). Finally, to see which parts of rNav_v β 2 conferred resistance to GVIIJ_{SSG}, two β 1: β 2 chimeras were coexpressed with rNav_v1.7. Chimera β 112 has the extracellular and transmembrane domains of rNav_v β 1 and the intracellular domain of rNav_v β 2 whereas chimera β 211 has the extracellular domain of rNav_v β 2 on an otherwise rNav_v β 1 background (13). rNav_v1.7 coexpressed with the β 211, but not β 112, chimera was insensitive to GVIIJ_{SSG} (Fig. 5E); thus, the extracellular domain of rNav_v β 2 was responsible for conferring toxin resistance.

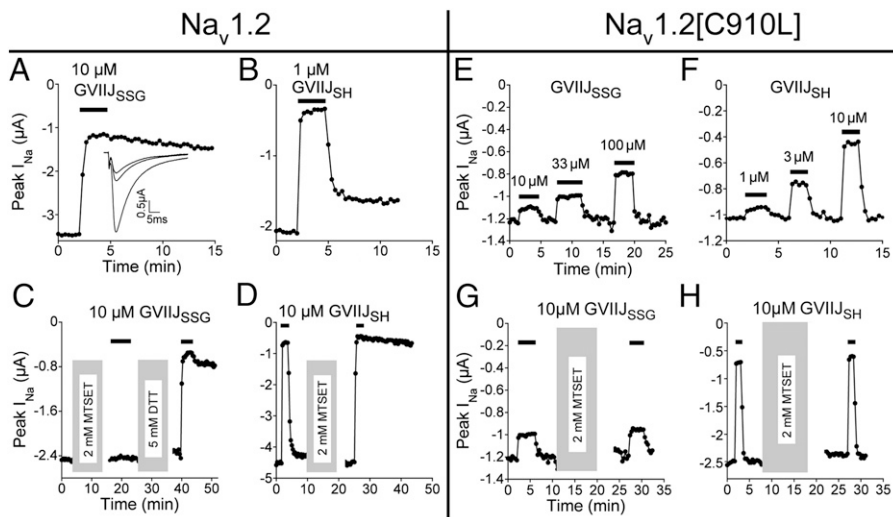
When coexpressed with rNav_v β 4, rNav_v1.1 through 1.6 were all rendered insensitive to 33 μ M GVIIJ_{SSG}, except rNav_v1.5, whose already-poor sensitivity was largely unaffected (Fig. 5F). Likewise, the poor sensitivity of rNav_v1.2[C910L] toward GVIIJ_{SSG} was minimally affected by rNav_v β 4 coexpression (Fig. 5F).

Functional Properties of GVIIJ_{SSG} and Synthetic μ O δ -GVIIJ. Only a limited number of experiments were performed with GVIIJ_{SSG} (Fig. 1D with Cys for X₂) and synthetic μ O δ -GVIIJ itself because the S-cysteinylation of a Cys residue and the presence of bromoTrp were identified only after the electrophysiological experiments described above had been completed. Tests with rNav_v1.2 and -1.7 showed that the k_{on} of GVIIJ_{SSG} was 3.5-fold larger (for both Nav_v1-isoforms) than that of GVIIJ_{SSG} (Table S3); the smaller size of cysteine, relative to that of glutathione, might account for the larger on-rate of GVIIJ_{SSG}. In contrast, the k_{off} values of both peptides were essentially the same (Table S3), which is expected; that is to say, for a given channel and peptide backbone, the identical peptide-channel complex is formed regardless of the SR-group disulfide bonded to Cys24 of the backbone because each peptide's respective SR group leaves when displaced by the thiol group of the channel cysteine during the process of disulfide exchange at site 8 (Fig. 3C).

Discussion

Binding Site of μ O δ -GVIIJ. Site 8 is distinct from those of members of the two other families of conotoxins that also block VGSCs, μ -conotoxins (14, 20) and μ O-conotoxins (22); consistent with this conclusion, μ -KIIIA and μ O-MrVIB do not compete with GVIIJ_{SSG} in blocking Nav_v1.2 (Fig. S6). Furthermore, site 8 can be modified by thiol-oxidizing and disulfide-reducing agents as summarized in Fig. 3C, which appears to be the most parsimonious scheme consistent with our results. The site exists in two basal states where, for one state (diagram a in Fig. 3C), the block by GVIIJ_{SSG} and GVIIJ_{SH} is slowly and rapidly reversible, respectively, whereas, for the other state (diagram b in Fig. 3C, where SX is a channel cysteine), the converse is true. However, when SX in diagram b in Fig. 3C is ET, then GVIIJ_{SSG} cannot block at all. These two interconvertible states can be driven by treatment with DTT in one direction and MTSET or CuPhen-catalyzed air oxidation in the other. Peptide binding results in three functionally blocked states; dissociation of the peptide occurs readily from two of the states (diagrams c and e in Fig. 3C) and slowly from the third,

Fig. 2. Block by GVIIJ_{SSG} and GVIIJ_{SH} of rNa_v1.2 and rNa_v1.2[C910L] and effects of thiol-oxidizing and disulfide-reducing agents. Oocytes expressing either native or mutant channels were voltage-clamped as described in Fig. 1A. (A–H) Representative plots of peak sodium currents (*I*_{Na}) as a function of time before, during (indicated by bar above each plot), and after exposure to toxin. (A) GVIIJ_{SSG} (10 μM) rapidly blocked *I*_{Na}, which very slowly recovered during toxin washout. (Inset) Averages of five *I*_{Na} traces obtained before, during, and after exposure to peptide (at *t* ~ 2, 4, and 15 min, respectively). (B) Block by GVIIJ_{SH} (1 μM) where recovery had fast and slow components. (C, D, G, and H) Vertical gray bars indicate when oocyte was exposed to 2 mM MTSET or 5 mM DTT, as indicated. Responses during washout of MTSET or DTT are not shown, accounting for blank area immediately following each vertical bar. (C) MTSET treatment prevented block by GVIIJ_{SSG}, whose block is restored by subsequent DDT treatment to produce a slowly reversible block like that in A. (D) Initial exposure to GVIIJ_{SH} produced a block that was essentially completely reversible, and MTSET treatment did not prevent block; on the contrary, the block was now only very slowly reversible, resembling that of GVIIJ_{SSG} in A. (E and F) Block of Na_v1.2[C910L] mutant channel by GVIIJ_{SSG} (E) and GVIIJ_{SH} (F) was attenuated and transient. (G and H) MTSET treatment of mutant channel affected the activities of neither GVIIJ_{SSG} (G) nor GVIIJ_{SH} (H); note that both magnitude and time course of block remained essentially unaltered.



disulfide-tethered state, which was achieved by disulfide exchange between peptide and channel (diagram d in Fig. 3C).

It might be noted that, although most of the GVIIJ-sensitive Na_v1-isoforms block with high potency (*K*_d = 5–50 nM), a standout is Na_v1.6 (*K*_d = 360 nM), whose poor potency is largely due to its relatively large *k*_{off} (Table S3). Presumably, the disulfide tether between GVIIJ and Na_v1.6 is more labile, and it would be interesting to examine this further.

Both MTSET Treatment and Coexpression of Na_vβ2 or -β4 Inhibit the Block by GVIIJ_{SSG}. Coexpression of Na_vβ2- and Na_vβ4-subunits, as well as MTSET treatment, produces the same effect; namely, the channels are protected against block by GVIIJ_{SSG}. Unlike Na_vβ1 and Na_vβ3, which are noncovalently attached to their Na_v1-subunit via a disulfide bond (1, 6). Thus, it is tempting to speculate that C910 of rNa_v1.2 might be disulfide-linked to its counterpart in

Fig. 3. Effects of CuPhen-catalyzed air oxidation of rNa_v1.2 on the block by GVIIJ_{SSG} and proposed reaction scheme accounting for the behavior of GVIIJ and its analogs on channels treated with oxidizing and reducing agents. Oocytes expressing rNa_v1.2 were voltage-clamped as described in Fig. 1A. (A) Representative time course of block by indicated peptide plotted as in Fig. 2. Treatment of oocytes with CuPhen (100 μM for 1 h) highly attenuated the block by GVIIJ_{SSG} and converted the slowly reversible block in control (a) to one that was mostly rapidly reversible (b). In contrast, CuPhen treatment converted the rapidly reversible block by GVIIJ_{SH} (a') to one that was largely slowly reversible (b'). These effects of CuPhen were largely reversed by subsequent DTT treatment of oocytes with 2 mM DTT for 1 h (c and c'). Each plot is from a different oocyte. (B) Relative to controls (white bars), DTT-treatment of oocytes (2 mM for 1 h, black bars) increased the maximum block by GVIIJ_{SSG} (33 μM) but not that by GVIIJ_{SH} (10 μM); furthermore, DTT treatment reduced the variability of block by GVIIJ_{SSG}. In contrast, the Cu²⁺-phenanthroline (CuPhen) treatment (gray bars) decreased the maximum block by GVIIJ_{SSG} whereas that by GVIIJ_{SH} was more modestly decreased. Bars represent mean ± SD (*n* ≥ 8 oocytes). *, The first bar is lower than the second bar, *P* < 0.0002; heights of the second, fourth, and fifth bars are not significantly different from each other (*P* > 0.5). (C) Hypothesized states of site 8, wherein P represents the peptide either as PSH (i.e., GVIIJ_{SH}) or as PS-SR where Cys24 is disulfide bonded to R, which is either cysteine (GVIIJ_{SSG} and native peptide) or glutathione (GVIIJ_{SSG}). (Diagrams a and b) Channel with Cys whose side chain has a free thiol (diagram a) or is disulfided bonded to X (diagram b), where SX is either another Cys residue of the channel or ET (-SCH₂CH₂NMe₃⁺), resulting, respectively, from CuPhen-catalyzed air oxidation or MTSET treatment. (Diagram c) Peptide noncovalently and readily reversibly bound to site 8. (Diagram d) Peptide tethered to channel via a disulfide bond and therefore only very slowly dissociable. Not shown are other possible thiol or disulfide groups at site 8, including those that may, for example, facilitate the c–d transition. (Diagrams e and f) When SX is a channel cysteine, then PS-SR binding is readily reversible (diagram e); however, when SX is ET, then PS-SR is unable to bind the channel (diagram f), possibly due to steric hindrance by ET.

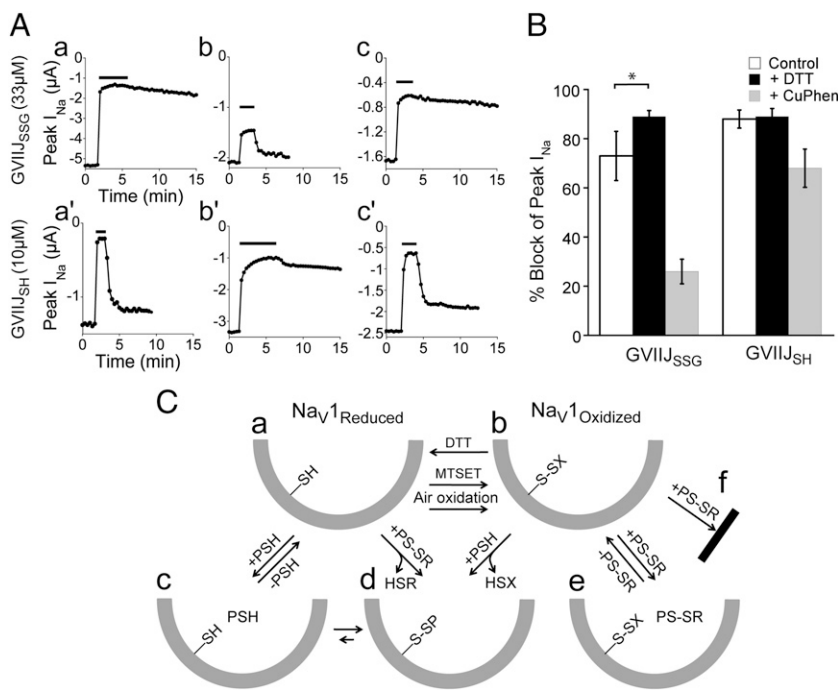
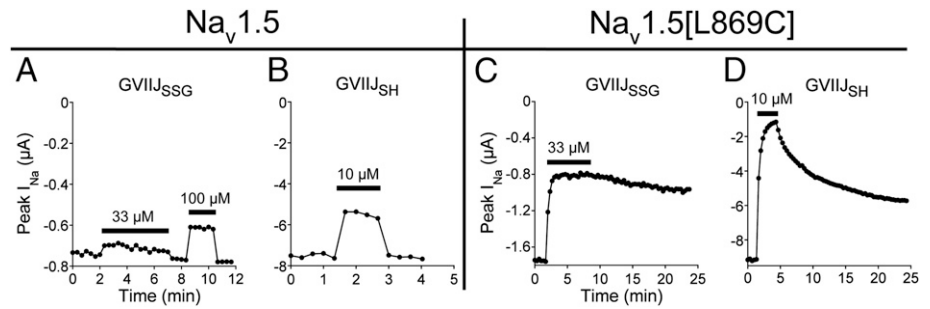


Fig. 4. Block of rNa_V1.5 and rNa_V1.5[L869C] by GVIIJ_{SSG} and GVIIJ_{SH}. Representative voltage-clamp records were acquired from oocytes as described in Fig. 1A. (A and B) GVIIJ_{SSG} (33 and 100 μM) and GVIIJ_{SH} (10 μM) poorly blocked I_{Na} of Na_V1.5, and, in each case, the time course of recovery upon peptide washout was too fast to accurately measure. (C and D) GVIIJ_{SSG} (33 μM) and GVIIJ_{SH} (10 μM) each blocked Na_V1.5[L869C] significantly greater than wild-type Na_V1.5. Furthermore, recovery of Na_V1.5[L869C] during peptide washout was slow ($k_{off} = 0.0039 \pm 0.0032 \text{ min}^{-1}$ for GVIIJ_{SSG}, and biphasic for GVIIJ_{SH} where $k_{off} = 1.2 \pm 0.6 \text{ min}^{-1}$ and $k'_{off} = 0.06 \pm 0.04 \text{ min}^{-1}$; mean \pm SD, $n \geq 3$ oocytes).



Na_Vβ2 or Na_Vβ4, a possibility also raised by Chen et al. for Na_Vβ2 based on other considerations (6).

Although Na_Vβ2- or Na_Vβ4-subunit coexpression protected against the block by both GVIIJ_{SH} and GVIIJ_{SSG}, MTSET treatment actually enhanced the block by GVIIJ_{SH} (i.e., rendered it less reversible) (Fig. 2D), an explanation for which is depicted in Fig. 3C. The difference between the consequences of Na_Vβ2- or Na_Vβ4-subunit coexpression and MTSET treatment could be explained by steric hindrance, in view of the large disparity in size between a β-subunit versus ET and that between a proton in GVIIJ_{SH} versus glutathione in GVIIJ_{SSG} (Fig. 1D).

It should be noted that coexpression versus association of α- and β-subunits per se are not synonymous; thus, for example, Na_Vβ1 coexpression can affect the glycosylation of the α-subunit (27), and the glycosylation state of the α-subunit, rather than its physical association with a β-subunit, could be responsible for the altered pharmacology of the VGSC.

It remains to be shown whether the effects of Na_Vβ-subunit coexpression in *X. laevis* oocytes is also manifested in mammalian expression systems and in neurons. Differences between VGSCs expressed in oocytes versus HEK cells with regard to Na_Vβ-subunit coexpression have been observed; for example, in oocytes, the rate of fast inactivation of Na_V1.7 coexpressed with either Na_Vβ1 or -β3 is faster than that of Na_V1.7 expressed alone (13, 28). This result was not observed when HEK 293 cells served as the expression system, where coexpression of any Na_Vβ isoform (Na_Vβ1 to -β4) had no effect on the kinetics of Na_V1.7 currents (29).

Other Unresolved Issues. The incomplete block of sodium current, i.e., the residual current (rI_{Na}), that persists in the presence of saturating concentrations of GVIIJ_{SSG} or GVIIJ_{SH} is not

understood. The maximum block produced by either peptide is about 90% (Fig. 3B). It could result from either (i) heterogeneity of the channel—i.e., ~10% of the channels are resistant to block, or (ii) incomplete, or partial, efficacy of block. Heterogeneity may play a role to some extent insofar as DDT treatment of oocytes can increase the efficacy of the block by GVIIJ_{SSG} (although not that by GVIIJ_{SH}). The rI_{Na} with GVIIJ_{SSG} is ~30% for Na_V1.2, -1.3, -1.4, -1.6, and -1.7 (Fig. 5E and F); however, that for Na_V1.1 is about twice as large (Fig. 5F). For all of these Na_V1-isoforms, DTT treatment reduces the residual current to about 10%, like that shown for Na_V1.2 in Fig. 3B.

The mechanism by which binding of GVIIJ results in block of the channel remains to be determined. GVIIJ_{SSG} is not a classical pore blocker. GVIIJ_{SSG} is able to block Na_V1.2 with the IFM→QQQ mutation (in the linker between domains III and IV) that removes fast inactivation (30) (Fig. S7), but the peptide may stabilize the channel in some other inactivated state, such as a slow-inactivated state that may involve conformational coupling between the pore and voltage-sensor domains (31). Alternatively, the GVIIJ peptides may inhibit channel activation by interfering with the channels' voltage sensors, similar to what gating modifiers such as μO-MrVIB, Protox II, and HwTx-IV do (22, 23, 32–34), but possibly allosterically. It might be noted that, at saturating toxin concentrations, the level (or efficacy) of block of Na_V1.7 by Protox II and of Na_V1.4 by HwTx-IV are 95% (32) and 41% (34), respectively, and they may represent precedents for the partial efficacy of block manifested by the GVIIJ peptides.

In conclusion, μO§-GVIIJ provides an exciting tool with which to explore the pharmacology, structure, and function of VGSCs.

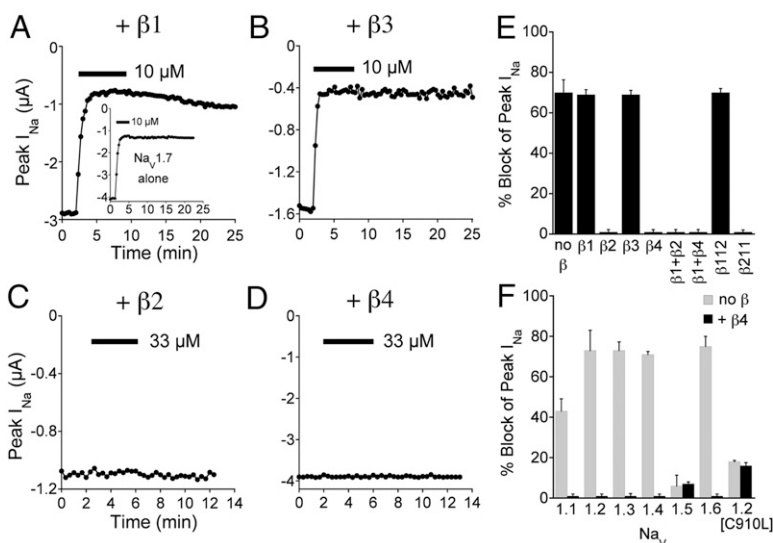


Fig. 5. Coexpression of rNa_Vβ2 or -β4, but not rNa_Vβ1 or -β3, prevented block by GVIIJ_{SSG} of all rNa_V1-isoforms except Na_V1.5 and Na_V1.2[C910L]. Records were acquired from oocytes as described in Fig. 1A. (A–D) Representative time course of block by GVIIJ_{SSG} of Na_V1.7 coexpressed with Na_Vβ1 to -β4 (the *Inset* in A shows Na_V1.7 expressed alone). (E and F) Levels of steady-state block (mean \pm SD, $n \geq 3$ oocytes). (E) Block by 33 μM GVIIJ_{SSG} of Na_V1.7 coexpressed with individual Na_Vβs, binary Na_Vβ combinations, and Na_Vβ1:β2 chimeras (β112 and β211). (F) Comparison of the block by GVIIJ_{SSG} of Na_V1.1 to -1.6 and Na_V1.2[C910L] without and with Na_Vβ4 coexpression. Peptide concentration was 33 μM throughout, except for Na_V1.3, -1.4, and -1.6 without Na_Vβ4 coexpression, where the concentration was 10 μM. The first gray bar is lower than second gray bar ($P < 0.001$), and the heights of the third, fourth, and sixth gray bars are not different from that of the second gray bar ($P > 0.05$) by *t* test.

Materials and Methods

The discovery of $\mu\text{O}\delta\text{-GVIIII}$ and its sequence determination are described in detail in *SI Materials and Methods*. The synthesis of $\mu\text{O}\delta\text{-GVIIII}$ and its analogs $\text{GVIIII}_{\text{SH}}$, $\text{GVIIII}_{\text{SSG}}$, and $\text{GVIIII}_{\text{SSC}}$, and disulfide-bond mapping of $\text{GVIIII}_{\text{SH}}$ are described in detail in *SI Materials and Methods*. Functional activities of peptides were assessed by two-electrode voltage clamp of *X. laevis* oocytes expressing rat channels and by patch clamp of HEK 293 or CHO cells expressing human channels as described in *SI Materials and Methods*.

- Catterall WA (2012) Voltage-gated sodium channels at 60: Structure, function and pathophysiology. *J Physiol* 590(Pt 11):2577–2589.
- Catterall WA, Goldin AL, Waxman SG (2005) International Union of Pharmacology. XLVII. Nomenclature and structure-function relationships of voltage-gated sodium channels. *Pharmacol Rev* 57(4):397–409.
- Brackenbury WJ, Isom LL (2011) Na channel β subunits: Overachievers of the ion channel family. *Front Pharmacol* 2:53.
- Chahine M, O'Leary ME (2011) Regulatory role of voltage-gated Na channel β subunits in sensory neurons. *Front Pharmacol* 2:70.
- Bant JS, Raman IM (2010) Control of transient, resurgent, and persistent current by open-channel block by Na channel beta4 in cultured cerebellar granule neurons. *Proc Natl Acad Sci USA* 107(27):12357–12362.
- Chen C, et al. (2012) Identification of the cysteine residue responsible for disulfide linkage of Na⁺ channel α and β 2 subunits. *J Biol Chem* 287(46):39061–39069.
- Zhang MM, et al. (2013) Pharmacological fractionation of tetrodotoxin-sensitive sodium currents in rat dorsal root ganglion neurons by μ -conotoxins. *Br J Pharmacol* 169(1):102–114.
- Fiedler B, et al. (2008) Specificity, affinity and efficacy of iota-conotoxin RXIA, an agonist of voltage-gated sodium channels Na(V)1.2, 1.6 and 1.7. *Biochem Pharmacol* 75(12):2334–2344.
- Terlau H, Olivera BM (2004) Conus venoms: A rich source of novel ion channel-targeted peptides. *Physiol Rev* 84(1):41–68.
- Lewis RJ, Dutertre S, Vetter I, Christie MJ (2012) Conus venom peptide pharmacology. *Pharmacol Rev* 64(2):259–298.
- Wilson MJ, et al. (2011) μ -Conotoxins that differentially block sodium channels Nav1.1 through 1.8 identify those responsible for action potentials in sciatic nerve. *Proc Natl Acad Sci USA* 108(25):10302–10307.
- Wilson MJ, et al. (2011) Nav β subunits modulate the inhibition of Nav1.8 by the analgesic gating modifier μ O-conotoxin MrVIB. *J Pharmacol Exp Ther* 338(2):687–693.
- Zhang MM, et al. (2013) Co-expression of Na(V) β subunits alters the kinetics of inhibition of voltage-gated sodium channels by pore-blocking μ -conotoxins. *Br J Pharmacol* 168(7):1597–1610.
- Cestèle S, Catterall WA (2000) Molecular mechanisms of neurotoxin action on voltage-gated sodium channels. *Biochimie* 82(9–10):883–892.
- Stevens M, Peigneur S, Tytgat J (2011) Neurotoxins and their binding areas on voltage-gated sodium channels. *Front Pharmacol* 2:71.
- Hu H, Bandyopadhyay PK, Olivera BM, Yandell M (2012) Elucidation of the molecular envenomation strategy of the cone snail *Conus geographus* through transcriptome sequencing of its venom duct. *BMC Genomics* 13:284.
- Akabas MH, Stauffer DA, Xu M, Karlin A (1992) Acetylcholine receptor channel structure probed in cysteine-substitution mutants. *Science* 258(5080):307–310.
- Kobashi K (1968) Catalytic oxidation of sulfhydryl groups by o-phenanthroline copper complex. *Biochim Biophys Acta* 158(2):239–245.
- Bénitah JP, et al. (1997) Molecular motions within the pore of voltage-dependent sodium channels. *Biophys J* 73(2):603–613.
- Zhang M-M, et al. (2010) Cooccupancy of the outer vestibule of voltage-gated sodium channels by micro-conotoxin KIIIA and saxitoxin or tetrodotoxin. *J Neurophysiol* 104(1):88–97.
- Santarelli VP, Eastwood AL, Dougherty DA, Horn R, Ahern CA (2007) A cation- π interaction discriminates among sodium channels that are either sensitive or resistant to tetrodotoxin block. *J Biol Chem* 282(11):8044–8051.
- Leipold E, et al. (2007) μ O conotoxins inhibit Nav channels by interfering with their voltage sensors in domain-2. *Channels (Austin)* 1(4):253–262.
- Heinemann SH, Leipold E (2007) Conotoxins of the O-superfamily affecting voltage-gated sodium channels. *Cell Mol Life Sci* 64(11):1329–1340.
- Zhang M-M, et al. (2009) Synergistic and antagonistic interactions between tetrodotoxin and μ -conotoxin in blocking voltage-gated sodium channels. *Channels (Austin)* 3(1):32–38.
- Li RA, et al. (2003) Molecular basis of isoform-specific micro-conotoxin block of cardiac, skeletal muscle, and brain Na⁺ channels. *J Biol Chem* 278(10):8717–8724.
- Chahine M, Sirois J, Marcotte P, Chen L, Kallen RG (1998) Extrapore residues of the S5-S6 loop of domain 2 of the voltage-gated skeletal muscle sodium channel (rSkM1) contribute to the μ -conotoxin GIIIA binding site. *Biophys J* 75(1):236–246.
- Laedermann CJ, Syam N, Pertin M, Decosterd I, Abriel H (2013) β 1- and β 3- voltage-gated sodium channel subunits modulate cell surface expression and glycosylation of Nav1.7 in HEK293 cells. *Front Cell Neurosci* 7:1–12.
- Vijayaragavan K, O'Leary ME, Chahine M (2001) Gating properties of Na(v)1.7 and Na(v)1.8 peripheral nerve sodium channels. *J Neurosci* 21(20):7909–7918.
- Ho C, Zhao J, Malinowski S, Chahine M, O'Leary ME (2012) Differential expression of sodium channel β subunits in dorsal root ganglion sensory neurons. *J Biol Chem* 287(18):15044–15053.
- West JW, et al. (1992) A cluster of hydrophobic amino acid residues required for fast Na⁺-channel inactivation. *Proc Natl Acad Sci USA* 89(22):10910–10914.
- Huang C-J, Schild L, Moczydlowski EG (2012) Use-dependent block of the voltage-gated Na⁺ channel by tetrodotoxin and saxitoxin: Effect of pore mutations that change ionic selectivity. *J Gen Physiol* 140(4):435–454.
- Xiao Y, Blumenthal K, Jackson JO, 2nd, Liang S, Cummins TR (2010) The tarantula toxins ProTx-II and huwentoxin-IV differentially interact with human Nav1.7 voltage sensors to inhibit channel activation and inactivation. *Mol Pharmacol* 78(6):1124–1134.
- Sokolov S, Kraus RL, Scheuer T, Catterall WA (2008) Inhibition of sodium channel gating by trapping the domain II voltage sensor with protoxin II. *Mol Pharmacol* 73(3):1020–1028.
- Xiao YY, et al. (2008) Tarantula huwentoxin-IV inhibits neuronal sodium channels by binding to receptor site 4 and trapping the domain ii voltage sensor in the closed configuration. *J Biol Chem* 283(40):27300–27313.
- Craig AG, et al. (1997) A novel post-translational modification involving bromination of tryptophan: Identification of the residue, L-6-bromotryptophan, in peptides from *Conus imperialis* and *Conus radiatus* venom. *J Biol Chem* 272(8):4689–4698.
- Jimenez EC, Watkins M, Olivera BM (2004) Multiple 6-bromotryptophan residues in a sleep-inducing peptide. *Biochemistry* 43(38):12343–12348.

Supporting Information

Gajewiak et al. 10.1073/pnas.1324189111

SI Materials and Methods

Isolation of the Native $\mu\text{O}\delta\text{-GVIII}$ and Characterization of Its Encoding cDNA. *Isolation of $\mu\text{O}\delta\text{-GVIII}$ from *Conus geographus* venom.* Lyophilized venom from *C. geographus* (840 mg) was suspended in 25 mL of aqueous 35% (vol/vol) acetonitrile-0.1% (vol/vol) trifluoroacetic acid (TFA) and homogenized at room temperature with a glass-Teflon tissue grinder for six cycles at 1,500 rpm. The homogenate was centrifuged in a Beckmann F0650 rotor at 10 °C for 15 min at 20,000 rpm. The supernatant was divided into two portions, and each was diluted threefold with aqueous 0.1% (vol/vol) TFA (gradient buffer A) before application on a Vydac preparative C_{18} HPLC column at a flow rate of 7 mL/min. Elution was performed using a multistep gradient of 10–50% of buffer B [aqueous 90% (vol/vol) acetonitrile-0.1% (vol/vol) TFA] for 40 min followed by 50–60% of buffer B for 5 min and 60–100% of buffer B for 5 min. The HPLC profile at 280 nm is shown in Fig. 1A of the main text. Pooled aliquots of fractions were assayed for activity on $\text{Na}_v1.7$ expressed in *Xenopus laevis* oocytes. Aliquots from each fraction in the active pool were subsequently assayed for activity, and the most active fraction is marked on the HPLC profile in Fig. 1A.

The most active preparative-HPLC fraction was subfractionated on a Vydac semipreparative C_{18} with a gradient of 0.2% per min change in the concentration of buffer B, at 45 °C; the active fraction from this semipreparative run was applied to a Vydac analytical monomeric C_{18} column. Elution from the monomeric C_{18} column was performed using buffers A' and B' [buffers A' and B' have 0.005% (vol/vol) TFA] over a gradient of 0.05% per min change in the concentration of buffer B'. The most active fraction was subjected to a final HPLC separation step using the monomeric C_{18} column and a gradient of buffers A'' and B'' (buffers A'' and B'' have TFA replaced with 0.2% formic acid) with a gradient of 0.05% of buffer B'' per min.

A sample of the purified native peptide, $\mu\text{O}\delta\text{-GVIII}$, was analyzed using matrix-assisted laser desorption ionization (MALDI) mass spectrometry at The Salk Institute for Biological Studies, and it had a mass of 3,934.49 Da [M+1].

Peptide sequencing. A small amount of the native $\mu\text{O}\delta\text{-GVIII}$ was linearized by treatment with DTT. The peptide sample was dissolved in 100 μL of 50% (vol/vol) acetonitrile, and the pH of the sample was adjusted to 8.0 using 0.5 M Tris base. A 50 mM solution of DTT was added to a final concentration of 10 mM, and the sample was incubated at 65 °C for 15 min for complete reduction of disulfide bridges. Following reduction, cysteine thiols were modified by addition of 0.8 μL of 4-vinylpyridine (VP; Sigma). The sample was incubated, in the dark, for 30 min at room temperature. Sequencing by Edman degradation of the fully reduced and alkylated peptide was done by R. Shackmann from the DNA/Peptide Synthesis Facility at the University of Utah. Sequencing efforts yielded a nearly complete toxin sequence, GxCGDOGATCGKLRLYCCSGFCDCYTKtxD, where x represents a cycle with an unreadable residue and residues marked in lowercase letters were not definitive. Due to ambiguities in the assignment of residues at the both N and C termini, the partial sequence was checked against the *C. geographus* transcriptome. A mature toxin sequence, with nearly 100% identity to the venom-derived peptide, was identified as described in *Venom-duct cDNA cloning and sequencing*.

Preparation of venom-duct RNA samples. Specimens of *C. geographus* were collected in the Philippines. Each specimen was dissected to isolate the venom duct, and the duct was immediately suspended in 1.0 mL of RNAlater (Ambion) at ambient temperature, and then

stored at -20 °C until used. Ducts were homogenized with a Tissue Tearor (Dremel model 985370), and total RNA isolated using a *mirVana* miRNA isolation kit (Ambion, Applied Biosystems) according to the manufacturer's recommendations.

Venom-duct cDNA cloning and sequencing. cDNA was prepared by reverse transcription of RNA isolated from the *C. geographus* venom duct. About 1 μg of total RNA was transcribed into cDNA using an In-Fusion SMARTer cDNA Library construction kit from Clontech. The resulting cDNA served as a template for PCR amplification. The 5' and 3' RACE experiments were carried out using a SMARTer RACE cDNA amplification kit (Clontech).

Based on the partial amino acid sequence of the peptide GVIII, we designed degenerate oligonucleotide primers, carried out 5' and 3' RACE experiments, and obtained a partial nucleotide sequence encoding GVIII. For 3' RACE, the forward primer (5' TAY TGY TGY TCN GGN TTY TGY GA 3', where Y = A/G and N = A/T/G/C) was designed corresponding to the region YCCSGFCD in peptide. For 5' ACE, the reverse primer (5' TGT AAC AAT CGC AAA ACC CCG 3') corresponding to the region SGFCDCY in the peptide was used. The nucleotide sequences obtained from the 5' and 3' RACE experiments were assembled, and additional PCR was carried out using the specific primers (forward primer) 5' GGA GGT ACG CAG AAG CAT CG 3' and (reverse primer) 5' ATG GAC TCG GGC AGA AAG GG 3' to obtain the complete mature toxin sequence. The PCR amplification profile consisted of an initial denaturation for 2 min at 94 °C followed by 39 cycles of 94 °C for 30 s, 62 °C for 30 s, 68 °C for 2 min, and a final extension at 68 °C for 10 min. PCR products were analyzed by electrophoresis on 1% agarose gels. One prominent PCR product band around 250 bp was observed. The band was excised from the gel and purified with a QIAquick gel extraction kit (Qiagen). The purified PCR product was ligated to a pGEM-T-Easy vector (Promega) and used to transform *Escherichia coli* DH10B. Plasmids were isolated from transformed colonies containing the insert, and their sequence was determined at the DNA sequencing facility at the University of Utah. The conceptual translation of the nucleotide sequence contained the partial sequence of the propeptide, the mature toxin sequence, and the 3' untranslated sequence. The complete sequence of $\mu\text{O}\delta\text{-GVIII}$ was, however, identified in the transcriptome of the venom duct from *C. geographus* (1). The nucleotide sequence of the transcript and the conceptual translation product is shown in Fig. S1A.

The sequence of the peptide, established by Edman degradation and completed by targeted PCR and transcriptome information, was chemically synthesized and folded (GVIII_{SH}; see *Chemical Synthesis of GVIII_{SH}, GVIII_{SSG}, GVIII_{SSC}, and $\mu\text{O}\delta\text{-GVIII}$*). A difference in mass between the native peptide and GVIII_{SH} was observed, and further mass spectrometry studies were carried out to identify the posttranslational modifications as described immediately below.

Tandem Mass Spectrometry of Native GVIII. An aliquot of the purified toxin was loaded onto a New Objectives 360- μm OD \times 75- μm ID column with an 8- μm integrated emitter and packed with 20 cm of HALO C_{18} , 2.7 μm , 90 Å material using the autosampler of an EASY-nLC 1000 (Thermo Scientific). The toxin was eluted from the column directly into an Orbitrap Elite mass spectrometer (Thermo Scientific) using a 30-min gradient from 2% to 50% solvent B [solvent A was 2% (vol/vol) acetonitrile in 0.5% acetic acid; solvent B was 90% (vol/vol) acetonitrile in

0.5% acetic acid]. To obtain the accurate mass of the native toxin, high-resolution full-scan spectra were acquired with a resolution of 240,000 at 400 m/z , an AGC target of 5e5 with a maximum ion injection time of 500 ms, scan range of 400–1,400 m/z and polysiloxane 445 m/z as lock mass ion. For the sequence determination, an aliquot of the purified toxin was incubated for 1 h at room temperature with 25 mM Tris(2-carboxyethyl) phosphine hydrochloride (TCEP) and 1 μ L of 2-methylaziridine in 500 mM triethylammonium bicarbonate (TEAB) buffer with 10% (vol/vol) acetonitrile. The mixture was acidified with TFA, and the toxin solution was desalted by adding a slurry of R2 20- μ m POROS beads (Life Technologies) in 5% (vol/vol) formic acid and 0.2% TFA. The beads were loaded onto an equilibrated C₁₈ ZipTip (Millipore) using a microcentrifuge for 30 s at 3,100 \times g. The POROS beads were rinsed three times with 0.1% TFA followed by further washes with 0.5% acetic acid. The toxin was eluted by the addition of 40% (vol/vol) acetonitrile in 0.5% acetic acid followed by the addition of 80% (vol/vol) acetonitrile in 0.5% acetic acid. The organic solvent was removed using a SpeedVac concentrator, and the sample was reconstituted in 0.5% acetic acid. An aliquot of the derivatized toxin was loaded on a New Objective HALO column as described at the beginning of this section, and spectra were acquired using the following instrument settings: The full scan was recorded with a resolution of 15,000 at 400 m/z , an AGC target value of 5e5 with a maximum ion injection time of 500 ms, and scan range of 300–1500 m/z and polysiloxane 445 m/z as lock mass ion. Following each full scan, the +6, +7, and +8 charge states of the derivatized toxin were subsequently fragmented using electron-transfer dissociation (ETD), and the resulting MS/MS spectra were acquired using the following instrument parameters: a resolution of 15,000 at 400 m/z and an AGC target value of 1e5 with a maximum ion injection time of 800 ms and 4 μ scans. The resulting MS/MS spectra were interpreted manually and analyzed using Conovo and Byonic optimized for peptide toxins of ~3,000 Da (Figs. S3 and S4). The observed N-terminal ions show a characteristic bromine isotope pattern, and the observed mass is consistent with a bromination on tryptophan. The c6 ion is observed 15.9949 Da higher, and the c5 ion is not observed, consistent with a hydroxyproline at the sixth position from the N terminus.

Chemical Synthesis of GVIIJ_{SH}, GVIIJ_{SSG}, GVIIJ_{SSC}, and μ O δ -GVIIJ. *Solid-phase peptide synthesis of the linear peptide with and without bromoTrp.* The linear GVIIJ with the sequence

GWCGDOGATCGKLRLYCCSGFCDCYTKTCKDKSSA ^

and the linear GVIIJ[W2W] with the sequence

GWCGDOGATCGKLRLYCCSGFCDCYTKTCKDKSSA ^

(where W, O, and ^ denote 6-Br-Trp, 4-hydroxyproline, and free carboxyl terminus, respectively) were synthesized on an Apex 396 automated peptide synthesizer (AAPPTec) applying standard solid-phase Fmoc (9-fluorenylmethyloxycarbonyl) protocols. The peptide was constructed on a preloaded Fmoc-L-Ala-Wang resin (substitution, 0.38 mmol·g⁻¹; Peptides International Inc.). All standard amino acids and pseudoproline dipeptide Fmoc-Tyr(tBu)-Thr($\psi^{Me,Me}$ pro)-OH were from AAPPTec. *N*- α -Fmoc-O-*t*-butyl-L-trans-4-hydroxyproline (Hyp) was from EMD Millipore, and Fmoc-D,L-6-Br-Trp-OH was provided by Jean Rivier (The Salk Institute for Biological Studies, La Jolla, CA). Side-chain protection for the following amino acids was as follows: Arg, 2,2,4,6,7-pentamethylidihydrobenzofuran-5-sulfonyl (Pbf); Asp and Glu, *O*-*tert*-butyl (OtBu); Lys and Trp, *tert*-butyloxycarbonyl (Boc); Hyp, Ser, Thr, and Tyr, *tert*-butyl (tBu); and Asn and Cys, trityl (Trt). Peptides were synthesized on a 50- μ mol scale. Coupling activation was achieved with 1 equivalent of 0.4 M benzotriazol-1-yl-oxytripyrrolidinophosphonium hexa-

fluorophosphate (PyBOP) and 2 equivalents of 2 M *N,N*-diisopropylethyl amine (DIPEA) using *N*-methyl-2-pyrrolidone (NMP) as the solvent. Ten-fold excess of standard amino acids was used except Hyp and 6-Br-Trp, which were used in fivefold excess. Double coupling, each in ten-fold excess, was used for every amino acid coupled after Cys and 6-Br-Trp. Standard amino acid coupling was conducted for 60 min except for Hyp and 6-Br-Trp, where the reaction was 90 min. Fmoc deprotection was carried out for 20 min with 20% (vol/vol) piperidine in dimethylformamide (DMF).

Cleavage and purification of the linear peptides. Peptides were cleaved from 50 to 100 mg of resin by a 3-h treatment with 1 mL of Reagent K (TFA/water/phenol/thioanisole/1,2-ethanedithiol 82.5/5/5/2.5 by volume) and subsequently filtered and precipitated with 12 mL of cold methyl-*tert*-butyl ether (MTBE). The crude peptides were then collected by centrifugation at 7,000 \times g for 6 min and washed once with 10 mL of cold MTBE. The washed peptide pellets were dissolved in 10% acetonitrile in 0.1% TFA in water and purified by reversed-phase (RP) HPLC using a semipreparative C₁₈ Vydac column (218TP510, 250 mm \times 10 mm, 5- μ m particle size) eluted with a linear gradient ranging from 15% to 45% of solvent B (GVIIJ[W2W]) and 25–55% of solvent B (GVIIJ) in 30 min at a flow rate of 4 mL/min. The HPLC solvents were 0.1% (vol/vol) TFA in water (solvent A) and 0.1% TFA (vol/vol) in 90% aqueous acetonitrile (solvent B). The absorbance of the eluent was monitored at 220/280 nm. Purity of the linear peptides was assessed using an analytical C₁₈ Vydac reversed-phase HPLC column (218TP54, 250 mm \times 4.6 mm, 5- μ m particle size) with a linear gradient ranging from 15% to 45% of solvent B (GVIIJ[W2W]) and 25–55% of solvent B (GVIIJ) in 30 min with a flow rate of 1 mL/min. Peptides were quantified by absorbance at 280 nm using an extinction coefficient (ϵ) value of 8,480 M⁻¹·cm⁻¹. On average, 1,200 nmol (4.49 mg) of pure linear GVIIJ[W2W] and 400 nmol (2.67 mg) of GVIIJ was obtained from 100 mg of cleaved resin.

Formation of GVIIJ_{SSG} by oxidative folding in the presence of oxidized and reduced glutathione. One hundred nanomoles of a linear GVIIJ[W2W] was resuspended in 0.5 mL of 0.01% TFA solution and added to a solution containing: 2.5 mL of 0.2 M Tris-HCl (pH 7.5) plus 0.2 mM EDTA, 0.25 mL of 20 mM reduced and 0.25 mL of 20 mM oxidized glutathione, and 1.5 mL of water. Final peptide concentration in the folding mixture was 20 μ M. The folding reaction was conducted for 6 h and quenched with formic acid to a final concentration of 8%. The quenched reaction mixture was then separated by RP-HPLC using a semipreparative C₁₈ column and a linear gradient ranging from 15% to 45% of solvent B in 30 min with a flow rate of 4 mL/min. The eluent was monitored by absorbance at 220/280 nm. Purity of the folded peptide was assessed by an analytical C₁₈ Vydac RP-HPLC using the gradient described above, with a flow rate 1 mL/min. Pure GVIIJ_{SSG} was quantified by absorbance at 280 nm as described for the linear peptide. On average, 36 nmol of GVIIJ_{SSG} was obtained from 100 nmol of linear peptide in the folding reaction. The molecular mass of GVIIJ_{SSG} was confirmed by MALDI MS (Table S1). The HPLC elution profile of the peptide is shown in Fig. S1B.

Formation of GVIIJ_{SH} by oxidative folding in the presence of CuCl₂. One hundred nanomoles of the linear GVIIJ[W2W] was suspended in 0.5 mL of 0.01% TFA solution and added to a solution containing 4 mL of 125 nM CuCl₂, 0.5 mL of 1 M Tris-HCl (pH 7.5) plus 10 nM EDTA. The final peptide concentration in the folding mixture was 20 μ M. The folding reaction was conducted for 7 h and quenched with formic acid to a final concentration of 8%. Peptides were purified as described for glutathione-assisted peptide folding. Pure GVIIJ_{SH} was quantified by measuring absorbance at 280 nm as described for the linear peptide. On average, 25 nmol of GVIIJ_{SH} was obtained from 100 nmol of linear peptide in the folding reaction. The molecular mass of GVIIJ_{SH} was confirmed by MALDI MS (Table S1). The HPLC elution profile of the peptide is shown in Fig. S1B.

Formation of GVII_{SSC} by oxidative folding in the presence of L-cystine.

One hundred nanomoles of the linear GVIIJ[W2W] was suspended in 0.5 mL of 0.01% TFA solution and added to a solution containing 2.5 mL of 0.2 M Tris-HCl (pH 7.5) plus 0.2 mM EDTA, 2 mL of L-Cystine solution [3 mg of L-Cystine suspended in 10 mL of 5% (vol/vol) acetonitrile in 0.01% TFA and sonicated for 1 h and vortexed before adding to the reaction mixture]. The final peptide concentration in the folding mixture was 20 μ M. The folding reaction was conducted for 22 h and quenched with formic acid to a final concentration of 8%. Peptides were purified as described for glutathione-assisted peptide folding. Pure GVII_{SSC} was quantified by measuring absorbance at 280 nm as described for the linear peptide. On average, 22 nmol of GVII_{SSC} was obtained from 100 nmol of linear peptide in the folding reaction. The molecular mass of GVII_{SSC} was confirmed by MALDI MS (Table S1). The HPLC elution profile of the peptide is shown in Fig. S1B.

Formation of synthetic μ O δ -GVIIJ by oxidative folding in the presence of L-cystine. The L-cystine assisted peptide folding protocol described for GVII_{SSC} was used to form, purify, and quantify μ O δ -GVIIJ from linear GVIIJ. On average, 8 nmol of μ O δ -GVIIJ was obtained from 100 nmol of linear peptide in the folding reaction. The molecular mass of μ O δ -GVIIJ was confirmed by MALDI MS (Table S1). The HPLC elution profile of the peptide is shown in Fig. S1B.

Determination of the Free Cys Residue in GVII_{SH}. Alkylation of free Cys residue of GVII_{SH}. Twelve nanomoles of GVII_{SH} was resuspended in 60 μ L of 100 mM TEAB, pH 8.5, and 2.4 μ L of VP was added [4% (vol/vol) solution]. The reaction was carried out for 30 min in the dark and quenched with 32 μ L of 0.01% TFA. The reaction mixture was purified by RP-HPLC on an analytical C18 column eluted over a linear gradient of 35–65% solvent B in 30 min with a flow rate of 1 mL/min and dried down using speed vac.

Reduction and alkylation of the remaining Cys residues. For complete reduction, ~12 nmol of alkylated GVII_{SH} was resuspended in 60 μ L of 100 mM TEAB buffer, mixed with 60 μ L of 10 mM TCEP, and incubated for 45 min at 45 $^{\circ}$ C. Next, 12 μ L of 125 mM iodoacetamide (IAM) was added to the solution and incubated at room temperature in the dark for 1 h, followed by quenching with 12 μ L of TCEP.

Endoproteinase Asp-N digestion. Without purification, the reduced and alkylated peptide was mixed with 8.75 μ L of endoproteinase Asp-N (1 μ g/100 μ L of water) at a ratio of 20:1 (wt/wt), incubated at room temperature for 3 h, and purified by RP-HPLC equipped with a C18 analytical column, using gradient of solvent B as follows: 5% for 10 min and then 5–65% in 30 min with a flow rate 1 mL/min. The peaks were isolated and analyzed by MALDI-TOF. The mass of one of the peaks [retention time (RT) = 17.16 min, [M+H]⁺ = 1123.56] was found to be the same as the expected mass ([M+H]⁺ = 1123.93) for the peptide fragment DC_(VP)YTKTC_(IAM)K of the digested GVII_{SH}. These results identified Cys24 as the location of either free thiol of glutathione adduct in the synthetic GVIIJ peptide.

Disulfide-Bond Mapping of the Synthetic GVII_{SH}. Alkylation of free Cys²⁴ residue of the synthetic, folded GVII_{SH}. The folded GVII_{SH} (30 nmol) was resuspended in 150 μ L of 100 mM TEAB buffer, pH 8.5, and then 6 μ L of VP, 4% (vol/vol) solution was added, and the mixture was left at room temperature in the dark for 30 min. The peptide was purified by RP-HPLC using an analytical C₁₈ column and a gradient of solvent B as follows: 5% for 10 min and then 5–65% in 30 min with a flow rate 1 mL/min.

Partial reduction and alkylation of the alkylated intermediate GVII_{SH}. Partial reduction was initiated by dissolving ~30 nmol of GVII_{SH} alkylated with VP in solvent B and adding 150 μ L of 30 mM TCEP in 100 mM sodium citrate buffer, pH 3.0. The reaction

was carried out at 37 $^{\circ}$ C for 45 min. Next, 30 μ L of 250 mM N-ethylmaleimide (NEM) in citrate buffer, pH 3.0, was added, and the mixture was left at room temperature for 1 h, followed by fractionation on the C₁₈ analytical column with a gradient of solvent B as described in *Alkylation of free Cys24 residue*. The masses of collected peaks (peak 1, peak 2, peak 3, peak 4, and peak 5) were analyzed by MALDI-TOF, and the results are shown in Table S2. The remaining material was dried and subjected to further reactions.

Reduction and alkylation of the remaining Cys residues in the intermediates.

The above intermediates (labeled as peak 2, peak 3, and peak 4) were each resuspended in 50 μ L of 1 M Tris-HCl, 10 mM EDTA, pH 7.5, and 30 μ L of 40 mM TCEP in 1 M Tris-HCl was added to each suspension. The mixtures were allowed to react for 1 h at 37 $^{\circ}$ C, and then 6 μ L of 200 mM IAM was added to each mixture, which then was incubated at room temperature for 1 h in the dark. The samples then were purified by RP-HPLC as described in *Alkylation of free Cys24 residue*.

Trypsin digestion. Reduced, alkylated, and purified peaks 2, 3, and 4 were each mixed with modified trypsin (1 μ g of trypsin was suspended in 100 μ L of 100 mM TEAB) at a ratio of 20:1 (wt/wt) and incubated at 37 $^{\circ}$ C for 3 h. The reaction was quenched with formic acid (8% final concentration) and analyzed by ESI-MS/MS, and the results are shown in *SI Appendix*.

Summary of the disulfide-mapping analysis of the synthetic GVII_{SH}. In the first step of the disulfide bond mapping, the free cysteine of the synthetic peptide GVII_{SH} was alkylated with VP and then reduced with TCEP and realkylated, this time with NEM. The HPLC profile of the reaction revealed five different peaks. Peak 1 and peak 5 had zero and three reduced and NEM-alkylated disulfide bonds, respectively. MALDI-TOF analysis of the collected peaks identified three intermediates: peak 2, peak 3, and peak 4. Peak 2 was found to have two disulfide bonds closed and one disulfide bond reduced and alkylated with NEM whereas both peak 3 and peak 4 were characterized as intermediates with one disulfide bond closed and two disulfide bridges reduced and alkylated with NEM (Table S2). In the next step, all three intermediates were reduced, and the remaining Cys residues were alkylated with IAM. Following HPLC purification, the intermediates were digested with trypsin and analyzed by ESI-MS/MS. For all three intermediates, MS analysis showed the presence of two peptide fragments (an identical set for each digested intermediate), in which Cys24 was modified with VP. Peak 2 (*SI Appendix*, Tables S1 and S2) was found to have Cys3 [*m/z* ions of 472.16 (*b*₃), 1,106.42 (*y*₁₀)] and Cys18 [*m/z* ion of 1,413.53 (*y*₁₀)] alkylated with NEM whereas four remaining Cys residues were modified with IAM. These findings implied the presence of the disulfide bond between Cys^I and Cys^{IV} (Cys3–Cys18). Cys17 in peak 3 (*SI Appendix*, Tables S3 and S4) was found to be the only one modified with IAM [*m/z* ion of 437.18 (*b*₃)], and the remaining Cys residues were alkylated with NEM. Cys29 was not identified by ESI-MS/MS analysis of the peptide fragments, which suggested the presence of a disulfide bridge between Cys^{III} and Cys^{VII} (Cys17–Cys29). The last intermediate (peak 4) (*SI Appendix*, Tables S5 and S6) contained Cys10 [*m/z* ions of 1,146.40 (*b*₁₀), 364.16 (*y*₃)] and Cys22 [*m/z* ion of 894.35 (*y*₆)] alkylated with IAM, and the rest of the Cys residues modified with NEM. The results suggested the presence of the disulfide bridge between Cys^{II} and Cys^V (Cys10–Cys22). The peptide fragments obtained from all intermediates show that the disulfide-bridging pattern of the synthetic GVII_{SH} was Cys^I–Cys^{IV}, Cys^{II}–Cys^V, and Cys^{III}–Cys^{VII}.

Oocyte Electrophysiology. rNa_v1 and rNa_v β clones. Clones for rNa_v1.1 (NM_030875), rNa_v1.2 (NM_012647), rNa_v1.3 (NM_013119), rNa_v1.4 (NM_013178), rNa_v1.5 (NM_013125), and rNa_v β 1 (NM_017288) and Na_v β 2 (NM_012877.1) were obtained from Alan Goldin (University of California, Irvine). Clones for

rNa_v1.7 (NM_133289) and rNa_v1.8 (NM_017247) were obtained from Gail Mandel (Vollum Institute) and John Wood (University College London), respectively. The clone for rNa_v1.6 (NM_019266.2) was prepared as previously described (2). Clones for rNa_vβ3 (NM_139097.3) and rNa_vβ4 (NM_001008880.1) were obtained from Lori Isom (University of Michigan). rNa_vβ1 and rNa_vβ2 DNA were linearized with NotI and transcribed with T7. rNa_vβ3 DNA was linearized with XbaI and transcribed with T7. rNa_vβ4 DNA was linearized with BamHI and transcribed with T7.

rNav1.2 and rNav1.5 mutant construction. The rNav1.2[C910L] and rNav1.5[L869C] mutants were prepared by PCR. Forward and reverse primers were designed with 18 base pairs flanking the desired mutation. Using the nonstrand displacing action of *Pfu Turbo* DNA polymerase, the mutagenic primers were extended and incorporated by PCR. The methylated, nonmutated parental cDNA was digested with DpnI. The mutated DNA was transformed into either DH5α electrocompetent (New England Biolabs) or XL-10 Gold ultracompetent (Agilent Technologies) cells. DNA was subsequently isolated using the Qiaprep mini prep kit (Qiagen) and sequenced to verify that the desired mutation had been produced. The DNA was linearized using either NotI (Nav1.2[C910L]) or AseI (Nav1.5[L869C]), and sense RNA was transcribed using T7 or SP6, respectively, RNA polymerase (mMessage mMachine RNA transcription kit; Ambion).

rNavβ chimera construction. All chimeras were made by PCR as previously described (2). Briefly, primers were designed to PCR amplify the desired area of one subunit, followed by an overhang belonging to the other subunit. In a subsequent PCR, the two DNA pieces were allowed to hybridize first at the overhangs, and then amplified using primers at the 5' and 3' ends, used to introduce restriction sites NotI and XhoI, respectively. The PCR product was gel-extracted and purified using Qiaquick PCR purification kit (Qiagen Sciences). The chimeras were subcloned into the pSGEM oocyte expression vector (which contains the 5' and 3' *Xenopus* globin regions) using the NotI and XhoI restriction sites, transformed into DH10B competent cells, and grown in ampicillin-containing LB. DNA was isolated using a Qiaprep Spin mini prep kit (Qiagen Sciences) and linearized. Sense RNA was transcribed using T7 polymerase (mMessage mMachine RNA transcription kit, Ambion).

Oocytes. Oocytes were harvested and prepared essentially as previously described (3). Briefly, freshly excised oocytes were treated with 2.5 mg/mL collagenase A (Roche Diagnostics) in OR-2 (82.5 mM NaCl, 2.0 mM KCl, 1.0 mM MgCl₂, and 5 mM Hepes, pH 7.3) for 1–2 h on a rotary shaker at room temperature. Half-way through the treatment, the solution was exchanged with fresh collagenase solution. The oocytes were then rinsed with OR-2 and incubated until used at 16 °C in ND96 (96 mM NaCl, 2 mM KCl, 1.8 mM CaCl₂, 1 mM MgCl₂, and 5 mM Hepes, pH 7.3) supplemented with the antibiotics penicillin (100 U/mL), streptomycin (0.1 mg/mL), Septra (0.2 mg/mL), and Amikacin (0.1 mg/mL). Use of *X. laevis* frogs, which provided oocytes for this study, followed protocols approved by the University of Utah Institutional Animal Care and Use Committee that conform to the National Institutes of Health Guide for the Care and Use of Laboratory Animals.

Injection of cRNA into oocytes. Injection of cRNA from rat Na_v1.1 to -1.8 and Na_vβ1 to -β4 clones into oocytes was done as previously described (2, 4). Briefly, a given oocyte was injected with 30–50 nL of cRNA in distilled water for one of the followings sodium channel isoforms: rNa_v1.1, rNa_v1.2, rNa_v1.3, rNa_v1.4, rNa_v1.5, rNa_v1.6, rNa_v1.7, or rNa_v1.8 (3, 1.5, 0.2, 0.6, 3, 30, 15, or 35 ng, respectively) without or with an equal weight of a rNa_vβ cRNA, except for coinjections of Na_v1.3 and Na_vβ, in which case 0.2 ng of Na_v1.3 and 0.6 ng of Na_vβ4 cRNAs were used. Oocytes

were incubated at 16 °C for 1–6 d in ND96 supplemented with antibiotics, as described in the preceding paragraph.

Two-electrode voltage clamping of oocytes. Oocytes were voltage clamped with a Warner OC-725C amplifier (Warner Instruments) using 3 M KCl-filled microelectrodes (<0.5 MW resistance) essentially as previously described (2). A holding potential of -80 mV was used, and voltage-gated sodium currents (*I*_{Na}) were induced every 20 s with a 50-ms depolarizing step to -20 mV (Na_v1.5), -10 mV (Na_v1.1, -1.2, -1.4, -1.6, and -1.7), 0 mV (Na_v1.3), or +20 mV (Na_v1.8). Current signals were filtered at 2 kHz, digitized at a sampling frequency of 10 kHz and leak-subtracted by a P/8 protocol using in-house software written in LabVIEW (National Instruments). The recording chamber was a 4-mm-diameter well (30 μL of total volume) sunk in the silicone elastomer, Sylgard (Dow Corning). Conopeptides were dissolved in ND96, and oocytes were exposed to toxin by applying 3 μL of peptide solution (at ten times the final concentration) to a static bath with a pipettor and manually stirring the bath for a few seconds by gently aspirating and expelling a few μL of bath fluid several times with the pipettor. A static bath was used to conserve peptide. Peptides were washed out by continuous perfusion with ND96, initially at a rate of 1.5 mL/min for 20 s, then at a steady rate of 0.5 mL/min. Exposures of oocytes while in the recording chamber to DTT (Sigma-Aldrich) or MTSET (Toronto Research Chemicals) were performed in a static bath, just as for toxin exposures. Exposures to DTT or copper phenanthroline (CuPhe) before introducing the oocytes into the recording chamber were done in 35-mm-diameter plastic culture dishes followed by rinsing with ND96. CuPhe was prepared from CuSO₄ and 1–10 phenanthroline (Sigma-Aldrich) as described by Bénitah, et al. (5).

All experiments were done at room temperature.

Analysis of oocyte data. Percentage block of peak *I*_{Na} by peptide was determined by obtaining the average peak of ≥3 control traces and the average peak of ≥3 traces acquired at steady state in the presence of peptide, then dividing the latter by the former and multiplying by 100. Fitting of time-course data to a single-exponential function was done with homemade software written with LabVIEW. The interaction of toxin with channel was assumed to be that of a simple bimolecular reaction whose kinetics are described by the equation, $k_{obs} = k_{on}[toxin] + k_{off}$ where [toxin] is toxin concentration. The time course of peak *I*_{Na} was plotted before, during, and after exposure to toxin. The on-rate constant was determined as follows: The onset of block at a given peptide concentration was fit to a single-exponential function to yield the observed rate constant, *k*_{obs}, following which *k*_{on} was obtained from the linear-regression slope of a *k*_{obs} versus peptide concentration plot for at least three different peptide concentrations (where each concentration was tested on ≥3 oocytes), as previously described (2, 6). The off-rate constant was determined by fitting the toxin-washout curve to a single-exponential function; however, when recovery from block was very slow (less than 50% recovery after 20 min; i.e., *k*_{off} < 0.035·min⁻¹), *k*_{off} was estimated from the level of recovery observed after 20 min of washing and assuming recovery followed a single-exponential time course (2, 4). Times longer than 20 min were not used to avoid error due to possible baseline drift. Each *k*_{off} value was the average of ≥9 oocytes.

All oocyte data are presented as mean ± SD. Statistical comparisons were performed by two-tailed unpaired *t* tests.

Mammalian Cell-Line Electrophysiology. Culture of cell lines expressing hNav1s. Human embryonic kidney (HEK) 293 cells stably expressing human Na_v1.2 (supplied by H. A. Hartmann, University of Maryland Biotechnology Institute), Na_v1.4, Na_v1.5, or Na_v1.7 (Millipore) were cultured in DMEM/F-12 media (1:1), supplemented with 10% (vol/vol) FBS, 1% penicillin/streptomycin, 400 μg/mL G418 (Geneticin), and 100 μM Non Essential Amino

Acids (NEAAs) (all reagents from Invitrogen). Chinese hamster ovary (CHO) cells stably expressing human $\text{Na}_V1.3$ were cultured in IMDM (Iscove's media with L-Glutamine), supplemented with 10% (vol/vol) dialyzed FBS, 1% HT supplement (a mixture of 10 mM hypoxanthine and 1.6 mM thymidine), 1% NEAAs, and 400 $\mu\text{g}/\text{mL}$ G418. Tetracycline-inducible CHO cells stably expressing human $\text{Na}_V1.1$ or $\text{Na}_V1.6$ were cultured in Ham's F-12 media (Mediatech), supplemented with 10% (vol/vol) FBS, 100 units/mL penicillin/streptomycin, 10 $\mu\text{g}/\text{mL}$ blasticidin, and 400 $\mu\text{g}/\text{mL}$ zeocin (Invitrogen) and induced with 1 $\mu\text{g}/\text{mL}$ tetracycline at least 24 h before use. Cells were maintained at 37 °C and in 5% CO_2 and harvested for QPatch experiments upon reaching ~50–90% confluency.

Preparation of cells for, and their use with, QPatch. Cell preparation for assay with QPatch HT (Sophion) was performed essentially as previously described (7). Briefly, cells were dissociated using 0.05% trypsin (5 min at 37 °C), centrifuged, resuspended in CHO-S-SFM media (Life Technologies), and gently triturated to break up cell clumps. Cell density was adjusted to $1\text{--}2 \times 10^6/\text{mL}$ with the same media, and cells were transferred to a cell "hotel" in QPatch and used in experiments for several hours. For gigaohm seal formation and whole-cell patch clamp recording, the extracellular solution contained 137 mM NaCl (except for $\text{Na}_V1.5$), 5.4 mM KCl, 1 mM MgCl_2 , 2 mM CaCl_2 , 5 mM glucose, and 10 mM Hepes, pH 7.4, and an osmolarity of 315 mOsm. For $\text{Na}_V1.5$, the 137 mM NaCl was replaced by 27.4 mM NaCl and 109.6 mM choline chloride. The intracellular solution contained 135 mM CsF, 10 mM CsCl, 5 mM EGTA, 5 mM NaCl, and 10 mM Hepes, pH 7.3, and an osmolarity of 290 mOsm.

Voltage protocol. From a holding potential that corresponds to $\sim V_{1/2}$ value for steady-state inactivation for each Na_V1 isoform (i.e., -60 mV for $\text{Na}_V1.1$, $\text{Na}_V1.3$, and $\text{Na}_V1.6$, -65 mV for $\text{Na}_V1.2$, -75 mV for $\text{Na}_V1.4$ and $\text{Na}_V1.7$, and -105 mV for $\text{Na}_V1.5$), cells were first hyperpolarized to -120 mV for 2 s and then depolarized to 0 mV for 5 ms before returning to the holding potential. This protocol was repeated once every 60 s during applications of control or test-compound solutions. The series resistance compensation level was set at 80%, and currents were filtered at 5 kHz with an 8-pole Bessel filter and sampled at 25 kHz. Cells were held at the holding potential when the above voltage protocol was not being executed.

Application of test compounds and determination of isochronal IC_{50} values. The volume of the QPatch's recording chamber is $\sim 1 \mu\text{L}$. Following establishment of the whole-cell recording configuration, cells were exposed to a total of five applications of the extracellular solution [all containing 0.1% BSA each with or without test compound, except for the last application, which contained either 1 μM TTX (for all Na_V1 isoforms except $\text{Na}_V1.5$) or 10 mM lidocaine (for $\text{Na}_V1.5$ only) without BSA]. The first solution applied contained only the control buffer (5 μL). The voltage protocol was executed 10 times (for a total duration of 10 min), starting 5 s after the application. The next three applications (5 μL each) were of a solution with a test compound (same compound and concentration for all three applications) or control buffer (for control cells only). Five seconds after each of these applications, the voltage protocol was again executed 10 times (also once per min). The last application was that of 1 μM TTX or 10 mM lidocaine (in three 10- μL boluses, each separated by 2 s), five seconds after which the voltage protocol was executed twice to obtain the baseline (TTX- or lidocaine-insensitive) current. For each cell, the peak of the last current trace obtained in the presence of TTX (or lidocaine) was subtracted away from the peak of each of the current traces obtained during the preceding four solution applications to obtain the peak values of the (TTX- or lidocaine-sensitive) sodium currents (I_{Na}). These I_{Na} values were normalized to the I_{Na} of the last trace in the first (control buffer) application. To correct for current rundown (or drift), the I_{Na} values for each cell in the

presence of a test compound were further normalized to the (temporally corresponding) average values for control (typically four to six) cells in the same experiment. The mean of the last two such values in the last test-compound application (i.e., the normalized and drift-corrected I_{Na} value obtained ~ 30 min following the initial application of a test compound), f , was used to calculate the percentage inhibition for each cell at the particular test-compound concentration tested, as follows: % inhibition = $100 \times (1 - f)$. The average of the percentage inhibition values for all cells tested at each test-compound concentration was used in concentration-response calculations. Isochronal IC_{50} values were determined from fits of the concentration-response data to a logistic function of the form, % inhibition = $100/[1 + (\text{IC}_{50}/c)^p]$, where p is the Hill coefficient and c is the test-compound concentration, using Origin 7.0 (OriginLab). Data are expressed as mean \pm SD. All experiments were performed at room temperature (~ 22 °C).

Production and patch-clamp recording of HEK cells expressing chimeras of human $\text{Na}_V1.5$ and -1.7 . cDNAs encoding human $\text{Na}_V1.5$ (NM_198056.1) and human $\text{Na}_V1.7$ (NM_002977.1) were obtained from Origene. To create the chimera 7577 (composed of domain II S1–S6 of hNav1.5 in an otherwise hNav1.7 background), the amino acid sequence FIVMDPFVDL.....LVVLNLFALLL of human $\text{Na}_V1.7$ (corresponding to amino acids 739–968 of Q15858-1) was replaced with the amino acid sequence LVVMDPFTD....LVVLNLFALLL of human $\text{Na}_V1.5$ (corresponding to amino acids 712–939 of Q14524-1). The reciprocal chimera, 5755 (composed of domain II S1–S6 of hNav1.7 in an otherwise hNav1.5 background), was constructed by replacing the amino acid sequence LVVMDPFTD....LVVLNLFALLL of human $\text{Na}_V1.5$ (corresponding to amino acids 712–939 of Q14524-1) with the amino acid sequence FIVMDPFVDL.....LVVLNLFALLL of human $\text{Na}_V1.7$ (corresponding to amino acids 739–968 of Q15858-1). The DNA sequences encoding the donor and recipient channel fragments plus the mammalian expression vector pcDNA4/TO (Invitrogen/Life Technologies) were amplified by PCR using Prime Star GXL polymerase (Takara/Clontech). The donor and recipient cDNA fragments (plus the vector) were cloned together using the In-Fusion technology (Clontech).

HEK293 cells were transiently transfected with cDNA encoding either chimera channel using FuGENE HD at a ratio of 3 μL :1 μg FuGENE HD:DNA. Channel DNA was cotransfected with CD4 at a ratio of 10:1. Cells were grown to 70–80% confluency and tested experimentally using manual patch-clamp 3–5 d posttransfection. Before conducting patch-clamp experiments, cells were incubated with paramagnetic CD4 beads (Dynabeads; Invitrogen; 11331D) to aid in detection of transfected cells.

Whole-cell patch-clamp recordings were carried out at room temperature using an AxoPatch 200B amplifier (Molecular Devices). Electrodes were made from thin-wall capillary glass (Cat. no. TW150F-4; WPI) using a P-97 puller from Sutter. The intra- and extracellular solutions were those used for QPatch. The resistances of the filled pipettes were $\sim 2 \text{M}\Omega$. Voltage errors were minimized using 80% series resistance compensation. Membrane currents were filtered at 5 kHz and sampled at 25 kHz.

To elicit sodium currents, cells were first hyperpolarized from the holding potential (-75 mV for chimera 7577, and -100 mV for chimera 5755) to -120 mV for 2 s and then depolarized to 0 mV for 5 ms before returning to the holding potential. This voltage protocol was executed once every 60 s. Non-TTX- or non-lidocaine-sensitive currents (for chimeras 5755 and 7577, respectively) were subtracted from total currents to obtain voltage-gated sodium currents as described for QPatch measurements. A stock solution of GVILJ_{SH} in deionized water was freshly made on the day of the experiment. The stock solution was introduced into the recording chamber (volume of 550 μL) and mixed gently and repeatedly to achieve a final peptide concentration of 1 μM (Fig. S5).

- Hu H, Bandyopadhyay PK, Olivera BM, Yandell M (2012) Elucidation of the molecular envenomation strategy of the cone snail *Conus geographus* through transcriptome sequencing of its venom duct. *BMC Genomics* 13:284.
- Zhang MM, et al. (2013) Co-expression of Na(V) β subunits alters the kinetics of inhibition of voltage-gated sodium channels by pore-blocking μ -conotoxins. *Br J Pharmacol* 168(7):1597–1610.
- Cartier GE, et al. (1996) A new alpha-conotoxin which targets alpha3beta2 nicotinic acetylcholine receptors. *J Biol Chem* 271(13):7522–7528.
- Wilson MJ, et al. (2011) μ -Conotoxins that differentially block sodium channels Nav1.1 through 1.8 identify those responsible for action potentials in sciatic nerve. *Proc Natl Acad Sci USA* 108(25):10302–10307.
- Bénitah JP, et al. (1997) Molecular motions within the pore of voltage-dependent sodium channels. *Biophys J* 73(2):603–613.
- West PJ, Bulaj G, Garrett JE, Olivera BM, Yoshikami D (2002) μ -conotoxin SmIIIA, a potent inhibitor of tetrodotoxin-resistant sodium channels in amphibian sympathetic and sensory neurons. *Biochemistry* 41(51):15388–15393.
- Liu Y, Beck EJ, Flores CM (2011) Validation of a patch clamp screening protocol that simultaneously measures compound activity in multiple states of the voltage-gated sodium channel Nav1.2. *Assay Drug Dev Technol* 9(6):628–634.

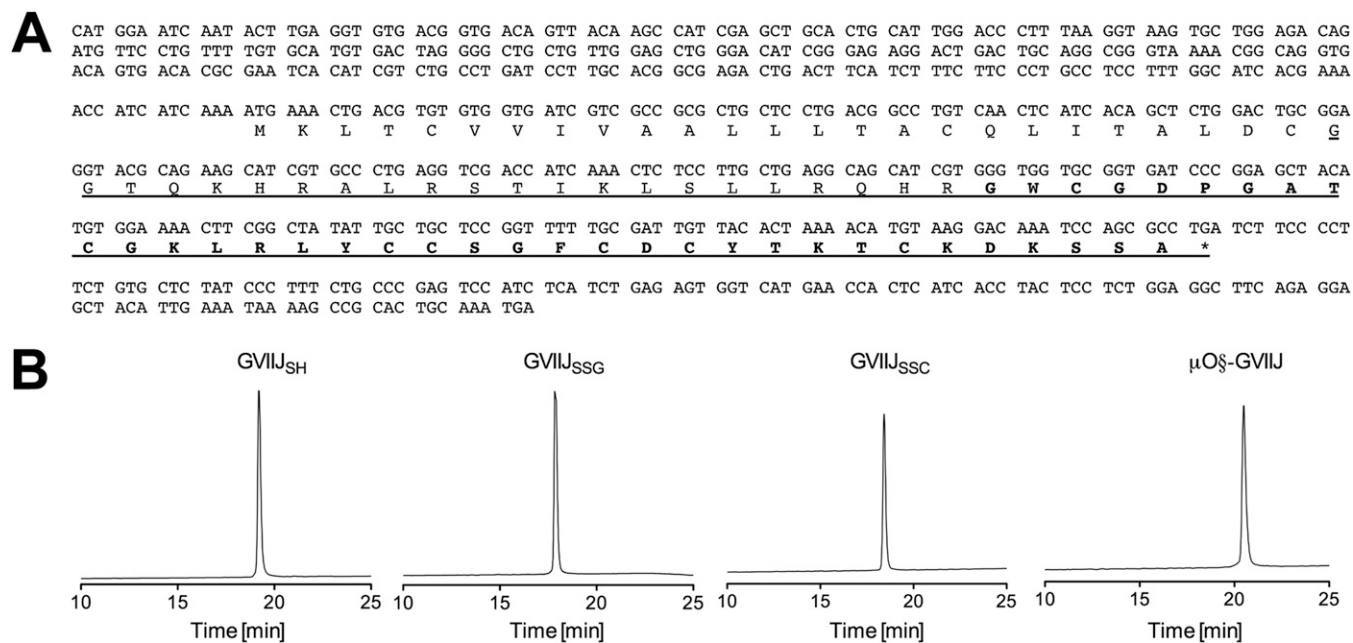


Fig. S1. Nucleotide and conceptual translation product obtained from analysis of *Conus geographus* transcriptome, and HPLC elution profiles of GVII_{SH}, GVII_{SSG}, GVII_{SSC}, and synthetic μ O₅-GVIIJ. (A) Underlined are propeptide and the mature toxin obtained from the targeted PCR; mature toxin is shown in bold. The signal sequence and the remaining segment of the propeptide were inferred from the transcriptome sequence. The partial sequences of the 5' and 3' untranslated regions are also shown. (B) An analytical C₁₈ column was used with a flow rate of 1 mL/min and a gradient ranging from 15% to 45% of solvent B in 30 min. Absorbance was monitored at 220 nm.

G W C G D O G A T C G K L R L R L Y C C S G F C D C Y T K T C K D K S S A

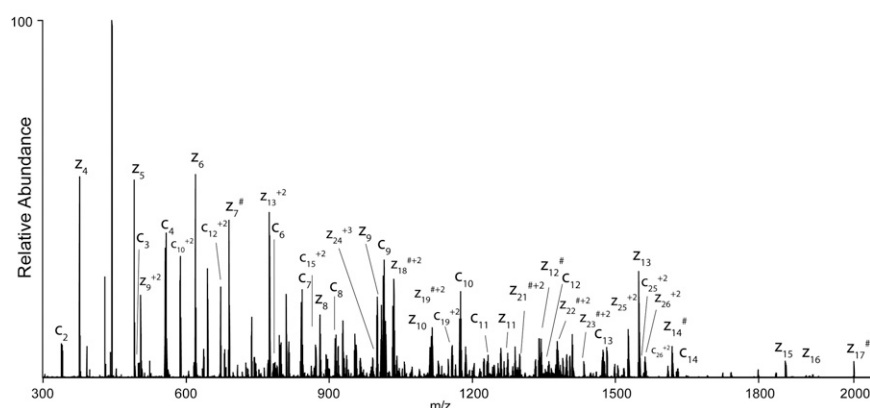


Fig. S2. MS/MS spectrum of native $\mu\text{O5-GVII}$. MS/MS ETD spectrum of the $(M + 5H)^{+5}$ ion of $\text{GWCGDOGATCGKLRLYCCSGFCDCYTKTKDKSSA}$ after reduction and alkylation with 2-methylaziridine acquired on the Orbitrap Elite with 15,000 resolution (at 400 m/z). N-terminal fragment ions (c) are indicated by], and C-terminal fragment ions (z) are indicated by [. Doubly charged ions are indicated with +2, and z ions resulting from cleavage at cysteine and loss of the cysteine side chain are indicated with # (1). Due to space limitations, different charge states of already labeled peptide bond cleavages are not all labeled. W is a brominated tryptophan and O is a hydroxylated proline. Eleven scans were averaged for this spectrum. The mass accuracy for all fragment ions is better than 15 ppm.

1. Chalkley RJ, Brinkworth CS, Burlingame AL (2006) Side-chain fragmentation of alkylated cysteine residues in electron capture dissociation mass spectrometry. *J Am Soc Mass Spectrom* 17(9):1271–1274.

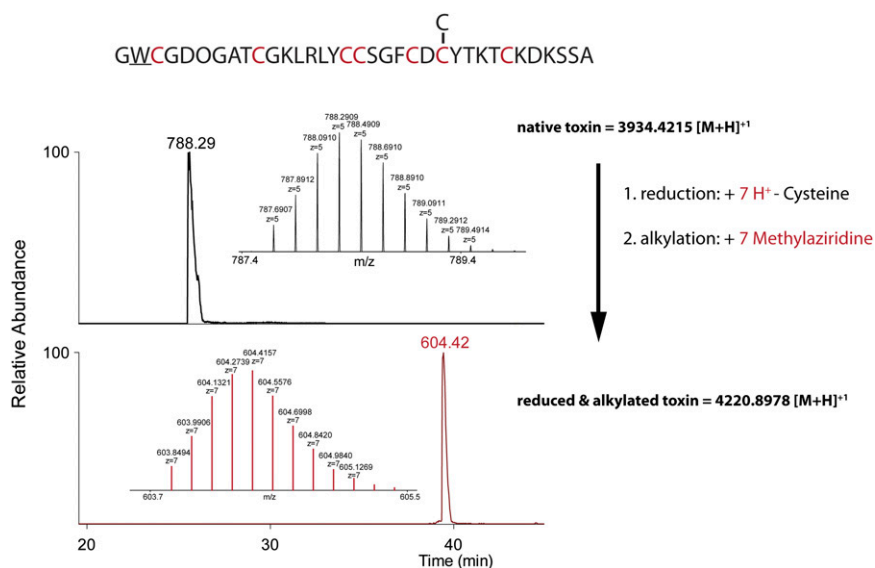


Fig. S3. Detection of cysteinylolation in native $\mu\text{O5-GVII}$. Shown are the extracted ion chromatograms for the +5 ion of the native toxin (*Upper*) and the +7 ion of the reduced and 2-methylaziridine alkylated toxin (*Lower*). The *Insets* show the isotopic distribution of each charge state. The observed shift in mass from the native to the reduced and alkylated toxin is consistent with a cysteinylolated toxin. Reduction results in breakage of all disulfide bonds and leading to the addition of one proton ($H^+ = 1.008$ Da) per cysteine that took part in a disulfide bond. The reduction also leads to the loss of the cysteine (deprotonated cysteine = 120.0121) that was attached to one of the cysteines via a disulfide bond. Subsequent alkylation with 2-methylaziridine leads to a mass increase of 54.0578 Da per cysteine residue. The measured mass of the native toxin was 3,934.4215 $[M+H]^+1$, which is within 0.25 ppm of the theoretical mass of 3,934.4214 $[M+H]^+1$. The measured mass of the reduced and alkylated toxin was 4,220.8978 $[M+H]^+1$, which is within 6.6 ppm of the theoretical mass of 4,220.8699 $[M+H]^+1$. Note that cysteinylolation of Cys at position 24 (in the amino acid sequence above the plots) is assumed based on the structure and activity of the synthetic GVII_{5H} (see "Determination of the free Cys residue in GVII_{5H} " in *SI Materials and Methods* and Table S3).

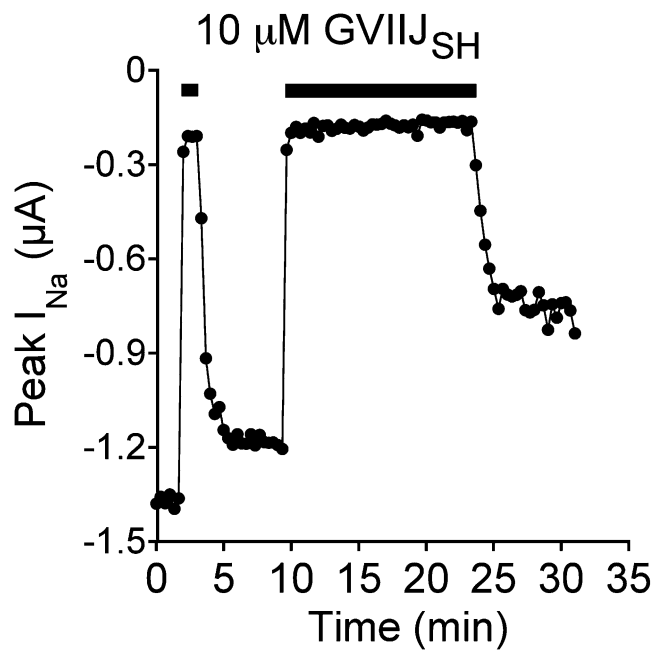


Fig. S4. The magnitude of the slow component of the biphasic recovery of $\text{Na}_v1.2$ following washout of GVIIJ_{SH} increased as toxin-exposure time was increased. The first exposure to $10 \mu\text{M GVIIJ}_{\text{SH}}$ was for 1.3 min (first horizontal bar) whereas the second was for 13 min (second horizontal bar). The level of block with slow off-rate was larger with longer time-of-exposure to peptide.

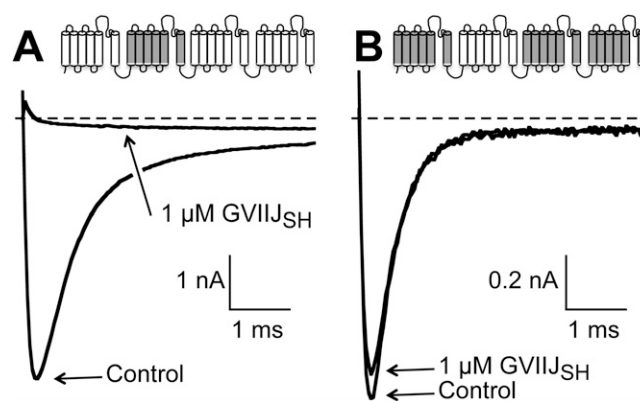


Fig. S5. GVIIJ_{SH} blocks human $\text{Na}_v1.5:\text{Na}_v1.7$ chimera 5755 but not chimera 7577. (Upper) Shown are diagrams depicting the channel's four domains, illustrating that chimera 5755 (A) consisted of domain II of $\text{Na}_v1.7$ (gray) with the remaining three domains those of $\text{Na}_v1.5$ (white), whereas chimera 7577 (B) had the reciprocal composition of domains. (A and B, Lower) Representative I_{Na} traces of patch-clamped HEK 293 cells (SI Materials and Methods) expressing each chimera before and after exposure to $1 \mu\text{M GVIIJ}_{\text{SH}}$. The peptide largely blocked I_{Na} of chimera 5755 (A) but not that of chimera 7577 (B). Chimera 5755 was inhibited by $81.1 \pm 3.5\%$ (mean \pm SD, $n = 5$) whereas chimera 7577 was inhibited by only $12.6 \pm 4.5\%$ ($n = 5$).

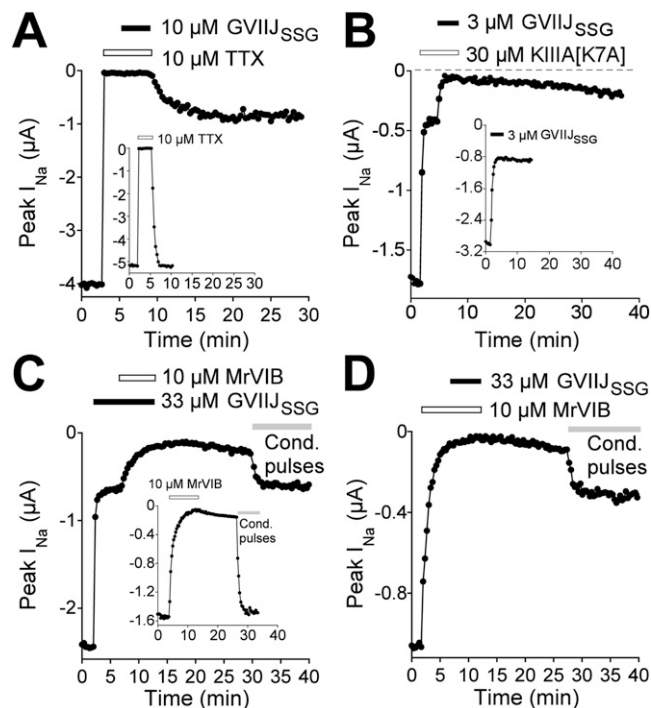


Fig. S6. GVIIJ_{SSG} competes with neither TTX, μ -KIIIA[K7A], nor μ O-MrVIB for their sites on rNa_v1.2. (A–D) Oocytes expressing rat Na_v1.2 were voltage clamped as in Fig. 1A. (A) Oocyte was exposed first to a saturating TTX concentration (10 μ M) (white bar) and then additionally to a saturating concentration of 10 μ M GVIIJ_{SSG} (black bar), following which both toxins were washed out. *Inset* shows the readily reversible block by 1 μ M TTX alone (white bar). TTX did not reduce the level of slowly reversible block produced by GVIIJ_{SSG} that persisted after both toxins were washed out (compare levels of block following washout of both toxins here with that during washout following exposure to GVIIJ_{SSG} alone in *Inset* of B). (B) Saturating concentration (30 μ M) of μ -KIIIA[K7A] was added first (at the time and duration shown by the white bar) leaving a residual current of \sim 25%. This exposure was followed by 3 μ M GVIIJ_{SSG} (black bar), which blocked a large fraction of μ -KIIIA[K7A]'s residual current. Finally, both toxins were washed out at the same time. This result shows that GVIIJ_{SSG}'s block was not impeded by the presence μ -KIIIA[K7A], as evident by comparison with the block produced by the 3 μ M GVIIJ_{SSG} alone (*Inset*). (C) Saturating concentration (33 μ M) of GVIIJ_{SSG} was added first (black bar) followed by 10 μ M μ O-MrVIB (white bar), and then both peptides were washed out; after several minutes, conditioning-depolarizing pulses (300-ms rectangular steps to 120 mV that preceded each test pulse by 3.3 s) were applied (gray bar), which accelerated the washout of μ O-MrVIB to a steady-state level expected of that if GVIIJ_{SSG} had been added alone. The *Inset* shows that exposure to 10 μ M μ O-MrVIB (white bar) largely blocks I_{Na} , which slowly recovers following washout, but rapidly recovers during depolarizing-conditioning pulses (gray bar) essentially completely. (D) μ O-MrVIB (10 μ M) was added first (white bar) followed by 33 μ M GVIIJ_{SSG} (black bar), and then both toxins were washed out; after several minutes, conditioning-depolarizing pulses were applied (gray bar), which accelerated the washout of μ O-MrVIB to a steady-state level similar to that arrived at in C. A more detailed description of these results is as follows. TTX blocked in a readily reversible manner (A, *Inset*). A saturating concentration of TTX present before and during exposure to GVIIJ_{SSG} did not prevent the peptide from producing its slowly reversible block (A), and we conclude that the two toxins don't compete for the same site on the channel. Like TTX, μ -KIIIA[K7A] also blocks by plugging the pore of the channel, but the plug is leaky (1, 2); thus, at saturating concentrations of μ -KIIIA[K7A], a \sim 25% residual current (I_{Na}) persists with Na_v1.2. When μ -KIIIA[K7A] was added first, this I_{Na} was readily evident (B), and when 3 μ M GVIIJ_{SSG} was added to the bath already containing μ -KIIIA[K7A], most of the I_{Na} was readily blocked (B), which indicates that the presence of μ -KIIIA[K7A] did not impede the block by GVIIJ_{SSG}; therefore, these two toxins occupy mutually exclusive sites on the channel. A protocol similar to the preceding was used to see whether GVIIJ_{SSG} and μ O-MrVIB competed for a common site on rat Na_v1.2. The off-rate of μ O-MrVIB can be accelerated with strong depolarizing-conditioning pulses: i.e., 300-ms rectangular steps to 120 mV that preceded each test pulse by 3.3 s (3) (C, *Inset*). When 30 μ M GVIIJ_{SSG} was added first, its residual current was readily and largely blocked when the bath was supplemented with 10 μ M μ O-MrVIB (Fig. S6C). When both toxins were washed out, recovery from block was slow but could be accelerated by strong depolarizing pulses to a steady-state level of block that was essentially the same as the level of block initially produced by GVIIJ_{SSG} alone, before μ O-MrVIB was added. Because at least part of GVIIJ_{SSG}'s residual current is likely due to heterogeneity of channels (*Discussion*), this result was not unexpected. To more rigorously test for competition, the order of addition of the toxins was reversed: that is, 10 μ M μ O-MrVIB was added first, which blocked most of the current; then, the bath was supplemented with 30 μ M GVIIJ_{SSG}, and then both toxins were washed out, following which slow recovery from block ensued that could be accelerated by strong depolarizing pulses to a steady-state level of block (D). Because the final level of steady-state block was similar to the level of block produced by GVIIJ_{SSG} alone (e.g., see C), it appears that prior exposure to μ O-MrVIB did not protect the channel against occupation by GVIIJ_{SSG}, which indicates that the two toxins do not share a common binding site.

- Zhang M-M, et al. (2009) Synergistic and antagonistic interactions between tetrodotoxin and mu-conotoxin in blocking voltage-gated sodium channels. *Channels (Austin)* 3(1):32–38.
- Zhang M-M, et al. (2010) Cooccupancy of the outer vestibule of voltage-gated sodium channels by micro-conotoxin KIIIA and saxitoxin or tetrodotoxin. *J Neurophysiol* 104(1):88–97.
- Wilson MJ, et al. (2011) Nav β subunits modulate the inhibition of Nav1.8 by the analgesic gating modifier μ O-conotoxin MrVIB. *J Pharmacol Exp Ther* 338(2):687–693.

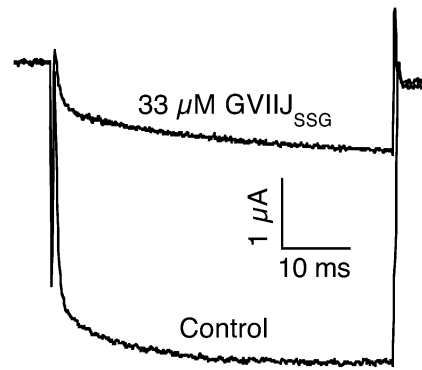


Fig. S7. GVIIJ_{SSG} is able to block an Na_v1.2 channel that is deficient in fast inactivation. Oocytes were used that expressed the rNa_v1.2 mutant where the IFM sequence of residues in the intracellular link between domains III and IV were replaced by QQQ to remove fast inactivation (1). Oocytes were voltage clamped as described in Fig. 1A. Both traces, before (control) and after 2-min exposure to 33 μM GVIIJ_{SSG}, showed impairment of fast inactivation (compare time course of these traces with those shown in Fig. 2A). The attenuated trace obtained in the presence of GVIIJ_{SSG} illustrates that the mutant channel can be blocked by the peptide.

1. West JW, et al. (1992) A cluster of hydrophobic amino acid residues required for fast Na⁽⁺⁾-channel inactivation. *Proc Natl Acad Sci USA* 89(22):10910–10914.

Table S1. HPLC retention times, purity, and MS data for GVIIJ_{SH} and GVIIJ_{SSG}

Peptide	HPLC RT*, min	Purity, %	[M] + (Da, calc.)	[M+H] + (Da, found)
GVIIJ _{SH}	19.13	99	3,736.54	3,737.58
GVIIJ _{SSG}	17.50	99	4,041.61	4,042.44
GVIIJ _{SSC}	18.31	99	3,855.70	3,856.90
μOS-GVIIJ	20.43	99	3,933.46	3,934.40

*Retention time (RT) was assessed by RP-HPLC using an analytical C₁₈ column and an elution gradient ranging from 15% to 45% of solvent B in 30 min.

Table S2. Fragments identified by MS after partial reduction and alkylation of GVIIJ_{SH}

Peak	Mass [M+H] ⁺ found	Disulfide bonds closed	NEM-alkylated disulfide bonds
1	3,842.37	3	0
2	4,093.56	2	1
3	4,345.69	1	2
4	4,345.66	1	2
5	4,598.60	0	3

Table S3. Kinetics of block by GVIIJ_{SSG} of rNa_v1.1 to -1.8 (top 10 rows), of rNa_v1.7 + β1 or β3 (rows 11 and 12), and of rNa_v1.2 and -1.7 by GVIIJ_{SSC} or μOS-GVIIJ (bottom four rows)

Peptide	Na _v	k _{on} [*] , μM ⁻¹ .min ⁻¹	k _{off} [†] , min ⁻¹	K _d [‡] or IC ₅₀ [§] , μM
GVIIJ _{SSG}	1.1	0.41 ± 0.05	0.0047 ± 0.0006	0.011 ± 0.002 [‡]
GVIIJ _{SSG}	1.2	0.48 ± 0.04	0.0051 ± 0.0026	0.011 ± 0.006 [‡]
GVIIJ _{SSG}	1.2[C910L]	NA	3.1 ± 1.3	88 ± 2 (160 ± 2) [§]
GVIIJ _{SSG}	1.3	0.32 ± 0.02	0.0047 ± 0.002	0.015 ± 0.006 [‡]
GVIIJ _{SSG}	1.4	0.34 ± 0.02	0.0016 ± 0.0008	0.0047 ± 0.0024 [‡]
GVIIJ _{SSG}	1.5	NA	3.7 ± 2.2	207 ± 12 (579 ± 8) [§]
GVIIJ _{SSG}	1.5[L869C]	0.035 ± 0.004	0.0046 ± 0.0032	0.13 ± 0.09 [‡]
GVIIJ _{SSG}	1.6	0.33 ± 0.02	0.12 ± 0.016	0.36 ± 0.05 [‡]
GVIIJ _{SSG}	1.7	0.12 ± 0.02	0.0049 ± 0.0032	0.041 ± 0.027 [‡]
GVIIJ _{SSG}	1.8	NA	NA	>1,000 [¶]
GVIIJ _{SSG}	1.7 + β1	0.1 ± 0.02	0.0045 ± 0.0037	0.045 ± 0.038 [‡]
GVIIJ _{SSG}	1.7 + β3	0.11 ± 0.012	0.005 ± 0.0025	0.05 ± 0.023 [‡]
GVIIJ _{SSC} **	1.2	1.66 ± 0.05	0.0057 ± 0.0022 ^{††}	0.0034 ± 0.0013 [‡]
μOS-GVIIJ**	1.2	2.60 ± 0.12	0.0075 ± 0.0010	0.0029 ± 0.0004 [‡]
GVIIJ _{SSC} **	1.7	0.42 ± 0.06	0.0055 ± 0.0025 ^{††}	0.013 ± 0.006 [‡]
μOS-GVIIJ**	1.7	2.00 ± 0.22	0.0064 ± 0.0026	0.0032 ± 0.0013 [‡]

Values represent mean ± SD (n ≥ 3 oocytes for each of ≥3 different concentrations of peptide).

*On-rate constants were determined from onsets of block at different [peptide] as described in *SI Materials and Methods*.

†Off-rate constants were determined from toxin-washout curves as described in *SI Materials and Methods*.

‡K_d was determined from the ratio of k_{off}/k_{on}. When rates were too fast to measure, steady-state IC₅₀ was obtained as a measure of affinity instead of K_d.

§Steady-state IC₅₀s were determined by fitting % block versus peptide concentration ([peptide]) curves to the equation (using GraphPad Prism or KaleidaGraph software): % block = % maximum block/(1 + IC₅₀/[peptide]) for ≥3 different [peptide]; % maximum predicted block was 66 ± 0.2% and 42 ± 2% for Na_v1.2[C910L] and Na_v1.5 [L869C], respectively. The value in parentheses indicates the IC₅₀ obtained when % maximum block was fixed at 100%.

¶Less than 5% block of Na_v1.8 was observed with 100 μM peptide, the highest concentration tested.

||k_{on} and k_{off} values with β1- or β3-subunit coexpression not significantly different from those of Na_v1.7 without β-subunit coexpression (P > 0.6).

**GVIIJ_{SSC} is synthetic peptide of Fig. 1D where X₂ is cysteine, and μOS-GVIIJ is synthetic native peptide (i.e., GVIIJ_{SSC} with brominated Trp2).

††Value not different from k_{off} of GVIIJ_{SSG} with Na_v1.2 (P = 0.63).

‡‡Value not different from k_{off} of GVIIJ_{SSG} with Na_v1.7 (P = 0.70). Two-tailed unpaired t tests were used for these statistical comparisons.

Table S4. Isochronal IC₅₀s for the block by GVIIJ_{SSG} and GVIIJ_{SH} of human Na_v1.1 to -1.7 expressed in HEK 293 or CHO cells

hNa _v	GVIIJ _{SSG}			GVIIJ _{SH}		
	IC ₅₀ , nM	SD	N	IC ₅₀ , nM	SD	N
1.1*	NA	NA	NA	23	10	4–10
1.2 [†]	1,110	372	5–6	55	23	2–5
1.3*	NA	NA	NA	139	38	2–7
1.4 [†]	812	515	2–6	14	4	6–13
1.5 [†]	19 ± 2% at 10 μM [‡]		7	0.3 ± 6.4% at 10 μM [§]		3
1.6*	756	62	3–7	14	11	2–6
1.7 [†]	783	110	11–15	78	21	4–10

Values were determined as described in *SI Materials and Methods*. NA, not available.

*Expressed in CHO cells.

[†]Expressed in HEK 293 cells.

[‡]Percentage block of hNa_v1.5 by 10 μM GVIIJ_{SSG} was 19 ± 2%.

[§]Percentage block of hNa_v1.5 by 10 μM GVIIJ_{SH} was 0.3 ± 6.5%.

Other Supporting Information Files

[SI Appendix \(DOC\)](#)